Unlocking the therapeutic potential of RARRES-1: innovative treatment strategy for liver fibrosis through bioenergetics regulation

Iram Irshad

A thesis submitted in fulfilment of the requirements for the degree of

Doctor of Philosophy

Faculty of medicine and Health

The University of Sydney

NSW, Australia

2024

This research supported in this thesis was supported by the award of a

Research Training Program scholarship to the PhD candidate

Statement of Originality

The work in this thesis was performed towards a degree under the supervision of Professor Mohammed Eslam at the Storr Liver Centre, Westmead Institute for Medical Research, University of Sydney. I certify that to the best of my knowledge; the content of this thesis is my own work. This thesis has not been submitted towards any other degree or purpose. I certify that the intellectual content of this thesis is the product of my own work and that all the assistance received in preparing this thesis and sources have been acknowledged.

Iram Irshad

31/08/24

Abstract

Background and aims: Liver disease is the 5th common cause of deaths in Australia, with a financial burden account for $5.4 billion annually. Liver fibrosis is ultimate outcome of virtually all untreated liver-related diseases that can progress to cirrhosis, cancer and liver failure. Our epigenome-wide-association study suggested increased methylation at the RARRES-1 locus in metabolic dysfunction associated fatty liver disease (MAFLD) patients with advanced fibrosis. Hypermethylation of RARRES-1 causes transcriptional silencing in various cancers. The functional status of RARRES-1 in liver fibrosis is unknown.

Methods: The changes of RARRES-1 expression in liver fibrosis were investigated. Expression of RARRES-1 was restored by genome editing and pharmacological activation. The impact of RARRES1 on hepatic stellate cells activation and fibrosis was investigated at mRNA and protein levels using RTqPCR and immunofluorescence for the expression of fibrotic markers. Structural changes in mitochondria and autophagosomes with RARRES-1 activation were visualized using electron microscopy. Impact of ROS and autophagy modulation was evaluated on antifibrotic effect of RARRES-1 using immunofluorescence.

Results: The mRNA expression of RARRES-1 by RTqPCR was found to be downregulated in human in-vitro culture model ($p < 0.01$), multiple mouse fibrotic models ((bile duct ligation (BDL), carbon tetra chloride model (CCL4) & methionine and choline deficient diet (MCD) $p < 0.05$, for all) and in two cohorts of patients with hepatitis C virus (HCV) ($p < 0.01$) and MAFLD ($p < 0.0001$). Genetic and pharmacological activation of RARRES-1 significantly reduced the mRNA expression of fibrotic markers, namely alpha-smooth muscle actin (alpha SMA), alpha-1-type I collagen (COL1A1), connective tissue growth factor (CTGF) & transforming growth factor-β (TGF-β) ($p < 0.05$, for all). Mechanistically I found that RARRES-1 reduces energy release during myofibroblast activation via regulating autophagy

initiation, mitochondrial function and preserving lipid droplets. Notably, both ROS and autophagy inhibitors had synergistic anti-fibrotic effect with RARRES-1 activation ($p < 0.05$).

Discussion and conclusion: The data presented in this thesis indicates that the silencing of RARRES-1 is involved in liver fibrosis. Activation of RARRES-1 has the potential to reverse liver fibrosis by regulating ROS generation, autophagy, and lipid preservation. The next step is to develop a CRISPR Cas9 epigenome editing tool to investigate if these findings can be translated to treat fibrosis in vivo. In conclusion, my findings highlight that regulating RARRES-1 may offer therapeutic benefits for treating liver fibrosis.

Acknowledgements

First and foremost, I would like to pay my gratitude to the almighty, "**Allah, the Most Gracious and the Most Merciful",** His showers of blessings, opportunities, knowledge, enabled me to accomplish my thesis.

The past 3.5 years of my PhD journey have been life-changing and transformative. This period has been both enriching and enlightening, characterized by significant skill development and intellectual growth, despite the numerous challenges and hardships encountered. As a mother of special need child, navigating this path presented additional difficulties. Throughout this journey, I have found solace in a verse from my Holy Book: "Verily, that along with every hardship is relief." This has been vividly demonstrated in my experience, as I have been blessed to be part of this remarkable group.

On this challenging journey, I have been profoundly fortunate to have the guidance of my supervisor, **Professor Mohammed Eslam**. I am deeply grateful for his invaluable advice, encouragement, and steadfast support. One of the most remarkable aspects of his supervision was his consistent availability for mentoring, guidance, and discussion. He offered me numerous opportunities to acquire diverse techniques, engage in critical thinking, and develop strong analytical skills. The training I received under his mentorship will not only benefit my professional career but will also have lasting positive impacts. I am truly indebted to Professor Eslam for his exceptional support and mentorship throughout this process.

I would also like to extend my gratitude to Dr. Myada Metwally, Dr. Jawaher Alharti, and Dr. Ziyan Pan from genomics group, for their invaluable expertise. Their guidance in familiarizing me with various techniques has been instrumental to my research.

I would like to thank to the Storr Liver Centre for your invaluable help, support, and friendship throughout my PhD journey.

I would like to offer special thanks to my husband, **Aftab Ahmed**, for standing by me through both the highs and lows of this journey. Without his cooperation and unwavering encouragement, this achievement would not have been possible.

I am also deeply grateful to my parents **(Irshad Ahmed** & **Rehana Irshad)** and mother-in-law for their prayers and support. You have proven that we need support from our parents at every stage of life. I would like to extend my heartfelt thanks to my brothers and sisters for their unwavering emotional support. Your encouragement and understanding have been a source of immense strength, and I am deeply grateful for your presence in my life.

Lastly, I extend my special thanks to my daughters, **Areesha** and **Inaya**, for their patience and understanding throughout this process. Your cooperation has been crucial in allowing me to complete my thesis. While I know that this journey has presented its challenges, I hope you can take pride in the accomplishment of your mother.

Contents table

i. Originality statement----ii
ii. Abstract----iii
iii. Acknowledgement----v
iv. Contents table----vii
v. Figure list----xii
vi. Tables list----xvii
vii. Abbreviation list----xviii

Chapter 1: Literature Review----1

1. Liver Fibrosis----2
1.1 Burden of liver disease----2
1.2 Causes of liver fibrosis----3
1.3 Diagnosis of liver fibrosis----4
1.3.1 Liver biopsy and histological assessment ----4
1.3.2 Non-invasive biomarkers----4
1.4 Pathogenesis of Liver fibrosis----7
1.5 Cell types implicated in liver fibrosis----9
1.5.1 Hepatic stellate cells----9
1.5.2 Hepatocyte----11
1.5.3 Liver sinusoidal endothelial cells (LSECs) ----13
1.5.4 Other cell types and hepatic macrophages----13
1.6 Cell signaling in liver fibrosis----15
1.7 TGF-β signaling in HSC activation and liver fibrosis----16
1.7.1 SMAD (small worm phenotype) dependent signaling----16
1.7.2 Non-SMAD (Drosophila MAD or Mothers against decapentaplegic) dependent signaling----17
1.8 Regression of liver fibrosis----18
1.9 Energy metabolism and liver fibrosis----18
1.10 Mitochondrial function and energy production----20
1.11 Autophagy----26
1.12 Epigenetic and liver fibrosis----27

1.13 Antifibrotic drug development: Novel approach ----------29

1.14 Identification of RARRES1 as a potential therapeutic target----------29

1.15 Hypothesis----------33

1.16 Aims----------33

Chapter Two: Material and Methods----------34

2.1 Materials----------35

2.2 Methods----------40

2.2.1 Cell Culture & Experimental Plan----------40

2.2.1.1 RARRES-1 activation----------40

2.2.1.2 Pharmacological activation of RARRES-1----------40

2.2.1.3 Genetic activation of RASSES-1----------40

2.2.1.4 Treatment with TGF-β----------41

2.2.2 mRNA Expression----------41

2.2.2.1 RNA Extraction----------41

2.2.2.2 cDNA synthesis----------42

2.2.2.3 Real-Time Quantitative PCR (RTqPCR) ----------43

2.2.3 Western Blot Analysis ----------43

2.2.3.1 Extraction of protein Lysates----------43

2.2.3.2 Western Blot ----------43

2.2.4 ELISA----------44

2.2.5 Immunofluorescence Assay----------44

2.2.6 Cellular reactive oxygen species (ROS) assay----------44

2.2.7 TMRE Mitochondrial membrane potential ----------45

2.2.8 Autophagic flux----------45

2.8.9 Electron microscopy----------45

2.8.10 Data Analysis and Statistics----------46

Chapter Three: RARRES-1 attenuates liver fibrosis in activated hepatic stellate cells----------47

3.1 Introduction----------48

3.2 Results----------50

3.2.1 RARRES-1 is expressed in different human tissues and liver Cells----------50
3.2.2 RARRES-1 expression is downregulated in patients with viral and non-viral liver diseases----------52
3.2.3 RARRES-1 expression is downregulated in fibrotic mouse models ----------53
3.2.4 Expression of RARRES-1 mRNA is downregulated with the activation of human hepatic stellate cells----------57
3.2.5 Expression of RARRES-1 is downregulated in *in-vitro* fibrotic models ----------58
3.2.6 RARRES-1 expression attenuates fibrosis in myofibroblasts ----------60
3.2.6.1 Pharmacological activation of RARRES-1 attenuates fibrosis in myofibroblasts----------60
3.2.6.2 Genetic activation of RARRES-1 and effect on fibrosis----------64
3.2.7 RARRES-1 activation has antifibrotic effect in murine hepatic stellate cells----------68
3.3 Discussion----------70
Chapter Four: RARRES-1 regulates fibrosis by regulating mitochondrial Function----------72
4.1 Introduction----------73
4.2 Results----------75
4.2.1 RARRES-1 activation modulates mitochondrial morphology----------75
4.2.2 RARRES-1 activation reduces the expression of mitochondrial importer protein----------78
4.2.3 RARRES-1 activation regulates the expression of ATP synthase beta and metabolic reprogramming----------81
4.2.4 RARRES-1 activation reduces the expression of fusion protein----------84
4.2.5 RARRES-1 activation reduces mitochondrial membrane potential----------87
4.2.6 RARRES-1 activation along with CCCP synergistically reduces the mitochondrial membrane potential----------89
4.2.7 RARRES-1 activation along with CCCP synergistically reduces the generation of ROS----------94

4.2.8 RARRES-1 activation along with CCCP synergistically reduces the expression of fibrotic markers----------99

4.3 Discussion----------104

Chapter Five: RARRES-1 regulates fibrosis by regulating ROS generation----------107

5.1 Introduction ----------108

5.2 Results----------110

5.2.1 TGF-β induced ROS generation----------110

5.2.2 RARRES-1 activation modulates the generation of ROS----------111

5.2.2.1 RARRES-1 modulates cytosolic ROS----------111

5.2.2.2 RARRES-1 activation modulates the generation of mitochondrial ROS----------114

5.2.3 ROS inducers reverse the antifibrotic effect of RARRES-1----------117

5.2.4 ROS inhibitors synergize the antifibrotic effect of RARRES-1----------127

5.2.5 NOX4 siRNA synergises the antifibrotic effect of RARRES-1----------153

5.3 Discussion----------163

Chapter Six: RARRES-1 regulates fibrosis by regulating autophagy----------165

6.1 Introduction ----------166

6.2 Results----------169

6.2.1 RARRES-1 activation modulates autophagosomal morphology----------169

6.2.2 RARRES-1 activation reduces the autophagy initiation in HSCs----------172

6.2.3 RARRES-1 activation reduces the autophagic flux----------177

6.2.4 RARRES-1 activation reduces the formation of lysosomes----------181

6.2.5 RARRES-1 activation regulates the formation of lysosomes and autophagy----------183

6.2.6 RARRES-1 activation preserves cell lipids----------186

6.2.7 RARRES-1 activation preserves cell lipids and reduce autophagy----------189

6.2.8 Effects of autophagy modulation on antifibrotic effect of RARRES-1----------192

6.2.8.1 Autophagy inducers reverse the antifibrotic effect of RARRES-1----192

6.2.8.1.1 LC3 plasmid reverses the antifibrotic effect of RARRES-1--------193

6.2.8.1.2 ATG-12 plasmid will reverse the antifibrotic effect of RARRES-1----198

6.2.8.2 Autophagy inhibitors synergise the antifibrotic effect of RARRES-1-----203

6.2.8.2.1 Chemical Inhibitors----204

6.2.8.2.2 Autophagy genetic inhibitors----230

6.3 Discussion----240

Chapter Seven: Summary and Future direction----242

7.1 Summary of future challenges and open questions----243

7.2 Summary of findings----244

7.3 Significance of the findings----245

7.4 Future directions----246

7.4.1 Determine if RARRES-1 activation limits fibrosis progression *in-vivo*-----246

7.4.2 Determine if RARRES-1 activation accelerates fibrosis resolution *in-vivo*----247

7.4.3 Develop CRISPR Cas9 epigenetic editing tool----247

7.5 Conclusion----247

References----248

List of Figures

Figure 1.1 Pathogenesis of liver fibrosis----------8

Figure 1.2 Activation of hepatic stellate cells----------10

Figure 1.3 Hepatocyte structure in normal and fibrotic liver----------12

Figure 1.4 Cell types in liver fibrosis and release of fibrogenic factors----------14

Figure 1.5 Schematic representation of liver damage and activation of various signaling pathways contributing to fibrosis----------15

Figure 1.6 SMAD and non-SMAD-dependent TGF-β signaling----------17

Figure 1.7 Mitochondrial dynamics; the process of fission and fusion----------22

Figure 1.8 Role of ROS in the development of fibrosis----------24

Figure 1.9 Schematic representation for mitophagy and mitochondrial quality control----------25

Figure 1.10 Relationship between autophagy and liver fibrosis----------26

Figure 1.11 Epigenetics and gene environment interaction in MAFLD----------28

Figure 1.12 Genomic location for RARRES-1 gene----------30

Figure 1.13 Three-dimensional structure for RARRES-1 gene----------30

Figure 1.14 Overview of vitamin A, uptake, metabolism and transport----------32

Figure 2.1 Genetic activation of RARRES-1 with RARRES-1 transfection in HSCs----------41

Figure 3.1 RARRES1 expression in various human tissues and cells----------51

Figure 3.2 RARRSE-1 mRNA expression in cohort of human liver diseases----------52

Figure 3.3 RARRES-1 expression is downregulated in fibrotic mouse models----------54

Figure 3.4 RARRES-1 protein expression in multiple fibrotic mouse models----------55

Figure 3.5 RARRES-1 expression at protein level in multiple fibrotic mouse models----------56

Figure 3.6 Transcriptional silencing of RARRES-1 expression during the course of culture-dependent activation of human primary stellate cells----------57

Figure 3.7 Relative Expression of RARRES-1 mRNA in LX-2 *in-vitro* models----------59

Figure 3.8 Retinoic acid treatment increases the expression of RARRES-1 in LX-2 cells----------61

Figure 3.9 Pharmacological activation of RARRES-1 produces antifibrotic effect in LX-2 cells----63

Figure 3.10 RARRES-1 transfection increased the expression of RARRES-1 in LX-2 cells----64

Figure 3.11 Genetic activation of RARRES-1 produces antifibrotic effect in LX-2 cells----65

Figure 3.12 Expression of α-SMA in RARRES-1 transfected cells using immunofluorescence in human hepatic stellate cell line----67

Figure 3.13 Expression of α-SMA in RARRES-1 transfected cells using immunofluorescence in mouse cell line----69

Figure 4.1 RARRES-1 activation regulates mitochondrial morphology in TGF-β stimulated HSCs----77

Figure 4.2 RARRES-1 activation reduces the expression of mitochondrial importer protein Tomm20----79

Figure 4.3 RARRES-1 activation reduces the expression of ATP synthase beta----82

Figure 4.4 RARRES-1 activation reduces the expression of mitofusion protein----85

Figure 4.5 RARRES-1 activation reduces the mitochondrial membrane potential----88

Figure 4.6 RARRES-1 activation along with CCCP synergistically reduces mitochondrial membrane potential in unstimulated HSCs----90

Figure 4.7 RARRES-1 activation along with CCCP synergistically reduce mitochondrial membrane potential in stimulated HSCs----92

Figure 4.8 RARRES-1 activation along with CCCP synergistically reduce ROS generation in unstimulated HSCs----95

Figure 4.9 RARRES-1 activation along with CCCP synergistically reduce ROS generation in stimulated HSCs----97

Figure 4.10 RARRES-1 activation along with CCCP synergistically reduces expression of fibrotic marker in unstimulated HSCs----100

Figure 4.11 RARRES-1 activation along with CCCP synergistically reduce expression of fibrotic markers in stimulated HSCs----102

Figure 5.1 TGF-β induced ROS generation model in LX-2 cells----110

Figure 5.2 RARRES-1 activation regulates the generation of ROS----112

Figure 5.3 RARRES-1 activation regulates the generation of mitochondrial ROS----115

Figure 5.4 ROS inducers reverse the antifibrotic effect of RARRES-1 in unstimulated HSCs----118

Figure 5.5 ROS inducers reverse the antifibrotic effect of RARRES-1 in TGF-β stimulated HSCs----------120

Figure 5.6 ROS inducers reverse the antifibrotic effect of RARRES-1 in unstimulated HSCs----------123

Figure 5.7 ROS inducers reverse the antifibrotic effect of in TGF-β stimulated HSCs----------125

Figure 5.8 ROS inhibitors synergise the antifibrotic effect of RARRES-1 in unstimulated HSCs----------128

Figure 5.9 ROS inhibitors synergise the antifibrotic effect of RARRES-1 in TGF-β stimulated HSC----------130

Figure 5.10 ROS inhibitors synergise the antifibrotic effect of RARRES-1 in unstimulated HSCs----------132

Figure 5.11 ROS inhibitors synergise the antifibrotic effect of RARRES-1 in TGF-β stimulated HSCs----------134

Figure 5.12 ROS inhibitors synergise the antifibrotic effect of RARRES-1 in unstimulated HSCs----------136

Figure 5.13 ROS inhibitors synergise the antifibrotic effect of RARRES-1 in TGF-β stimulated HSCs----------138

Figure 5.14 ROS inhibitors synergise the antifibrotic effect of RARRES-1 in unstimulated HSCs----------141

Figure 5.15 ROS inhibitors synergise the antifibrotic effect of RARRES-1 in TGF-β stimulated HSCs----------143

Figure 5.16 ROS inhibitors synergise the antifibrotic effect of RARRES-1 in unstimulated HSCs----------145

Figure 5.17 ROS inhibitors synergise the antifibrotic effect of RARRES-1 in TGF-β stimulated HSCs----------147

Figure 5.18 ROS inhibitors synergise the antifibrotic effect of RARRES-1in unstimulated HSCs----------149

Figure 5.19 ROS inhibitors synergise the antifibrotic effect of RARRES-1 in TGF-β stimulated HSCs----------151

Figure 5.20 NOX4 silencing synergizes the antifibrotic effect of RARRES-1 in unstimulated HSCs----------154

Figure 5.21 NOX4 silencing synergizes the antifibrotic effect of RARRES-1 in TGF-β stimulated HSCs----------

Figure 5.22 NOX4 siRNA synergizes the antifibrotic effect of RARRES-1 in unstimulated HSCs----------159

Figure 5.23 NOX4 siRNA synergizes the antifibrotic effect of RARRES-1 in TGF-β stimulated HSCs----------161

Figure 6.1 Schematic model of the design of experiments in this chapter exploring the effect of RARRES1 on the different stages of autophagy----------168

Figure 6.2 RARRES-1 activation preserves autophagosomal morphology in TGF-β stimulated HSCs----------171

Figure 6.3 RARRES-1 activation reduces the expression of ATG-5----------173

Figure 6.4 RARRES-1 activation reduces the expression of ATG-12----------174

Figure 6.5 RARRES-1 activation reduces the expression of LC3----------175

Figure 6.6 RARRES-1 activation reduces the expression of Beclin----------176

Figure: 6.7 RARRES-1 activation preserves p62 protein----------177

Figure 6.8 RARRES-1 modulates autophagic flux in HSCs----------180

Figure 6.9 RARRES-1 activation reduces the formation of lysosomes----------182

Figure 6.10 RARRES-1 activation reduces the formation of lysosomes and autophagy in unstimulated HSCs----------184

Figure 6.11 RARRES-1 activation reduces the formation of lysosomes and autophagy in TGF-β stimulated HSCs----------185

Figure 6.12 RARRES-1 activation preserves the expression of Bodipy----------187

Figure 6.13 RARRES-1 activation preserves the expression of oil red----------188

Figure 6.14 RARRES-1 activation attenuates the expression of cell lipids and LC3 in unstimulated HSCs----------190

Figure 6.15 RARRES-1 activation attenuates the expression of cell lipids and LC3 in TGF-β stimulated HSCs----------191

Figure 6.16 Schematic diagram of the autophagy inducers experiments----------192

Figure 6.17 LC3 plasmid reverse the antifibrotic effect of RARRES-1 in unstimulated HSCs----------194

Figure 6.18 LC3 plasmid reverse the antifibrotic effect of RARRES-1 in TGF-β stimulated HSCs----------196

Figure 6.19 ATG-12 plasmid reverses the antifibrotic effect of RARRES-1 in unstimulated HSCs----------199

Figure 6.20 ATG-12 plasmid reverses the antifibrotic effect of RARRES-1 in TGF-β stimulated HSCs----------201

Figure 6.21 Schematic diagram of the autophagy inhibitors experiments----------203

Figure 6.22 Chloroquine diphosphate synergises the antifibrotic effect of RARRES-1 in unstimulated HSCs----------205

Figure 6.23 Chloroquine diphosphate synergises the antifibrotic effect of RARRES-1 in stimulated HSCs----------207

Figure 6.24 MRT68921 dihydrochloride synergises the antifibrotic effect of RARRES-1 in unstimulated HSCs----------209

Figure 6.25 MRT68921 dihydrochloride synergises the antifibrotic effect of RARRES-1 in stimulated HSCs----------211

Figure 6.26 Bafilomycin synergises the antifibrotic effect of RARRES-1 in unstimulated HSCs----------213

Figure 6.27 Bafilomycin synergises the antifibrotic effect of RARRES-1 in stimulated HSCs---------- 215

Figure 6.28 Chloroquine diphosphate synergises the antifibrotic effect of RARRES-1 in unstimulated HSCs----------218

Figure 6.29 Chloroquine diphosphate synergises the antifibrotic effect of RARRES-1 in stimulated HSCs----------220

Figure 6.30 MRT68921 dihydrochloride synergises the antifibrotic effect of RARRES-1 in unstimulated HSCs ----------222

Figure 6.31 MRT68921 dihydrochloride synergises the antifibrotic effect of RARRES-1 in stimulated HSCs----------224

Figure 6.32 Bafilomycin synergises the antifibrotic effect of RARRES-1 in unstimulated HSCs----------226

Figure 6.33 Bafilomycin synergises the antifibrotic effect of RARRES-1 in stimulated HSCs----------228

Figure 6.34 LC3 silencing synergizes the antifibrotic effect of RARRES-1 in unstimulated HSCs----------231

Figure 6.35 LC3 silencing synergizes the antifibrotic effect of RARRES-1 in TGF-β stimulated HSCs----------233

Figure 6.36 ATG-12 silencing synergizes the antifibrotic effect of RARRES-1 in unstimulated HSCs----------236

Figure 6.37 ATG-12 silencing synergizes the antifibrotic effect of RARRES-1 in TGF-β stimulated HSCs----------238

Figure 7.1 Model of RARRES-1 mechanisms for regulation of TGF-β induced fibrotic pathways in liver fibrosis----------246

List of Tables

Table 1.1: A list of some of the most commonly used blood biomarkers and scoring system for noninvasive assessment of liver fibrosis----------6

Table 2.1 The origins of the commercial kits used in this investigation----------35

Table 2.2 The source of the primers and probes used in this thesis ----------35

Table 2.3 Primers sequences----------36

Table 2.4 The source of the reagents used in this thesis----------37

Table 2.5 The source of the antibodies used in this thesis----------38

Table 2.6 Softwares----------39

List of Abbreviations

Name	Abbreviations
MAFLD	Metabolic dysfunction associated fatty liver disease
ECM	Extracellular matrix
ASIR	Age-standardized death rate
CLD	Chronic liver disease
GGT	Gamma-glutamyl transferase
AST	Aspartate aminotransferase
ALT	Aspartate aminotransferase
MMP	Matrix metalloproteinase
IGF	Insulin-like growth factor
TIMP	Tissue inhibitor of metalloproteinase
α_2M	α-2-macroglobulin
HA	Hyaluronic acid
PIIINP	Pro-collagen III N-terminal pro-peptide
HSCs	Hepatic stellate cells
EMT	Epithelial-to-mesenchymal transition
LSECs	Liver sinusoidal endothelial cells
eNOS	Endothelial-NO-synthase
NO	Nitric oxide
TNF-α	Tumor necrotic factor α
PDGF	Platelet growth factor
SHH	Sonic hedgehog
IGFs	Insulin like growth factors
IL-6	Interleukin-6
TGF-β	Tumor growth factor beta
MAPK	Mitogen-activated protein kinase
JNK	c-jun-N terminal kinase
TCA	Tri-carboxylic acid
ETC	Electron transport chain
Pal-1	Pro-fibrogenic mediators
mPTP	Permeability transition pore

Name	Abbreviations
CCL4	Carbon tetrachloride
EWAS	Epigenome wide association study
ROS	Reactive oxygen species
DMEM	Dulbecco's Modified Eagle Medium
µl	Microliter
PVDF	Polyvinylidene difluoride
CCCP	Carbonyl cyanide3-chlorophenyl hydrazone
GAPDH	Glyceraldehyde-3-phosphate dehydrogenase
RTqPCR	Polymerase chain reaction
HHSTEC	Human hepatic stellate cells
HH	Human hepatocytes
BDL	Bile duct ligation
MCD	Methionine and choline deficient
α-SMA	Alpha-smooth muscle actin
COL1A1	Alpha-1-type I Collagen
CTGF	Connective tissue growth factor
mPTP	Mitochondrial-permeability–transition-pore
TEM	Transmission electron microscope
TOM20	Outer mitochondrial membrane 20
MFN1	Mitofusin protein 1
TMRE	Tetramethylrhodamine, ethyl ester
DCFDA	2'7'-dichlorofluorescin diacetate
mROS	Mitochondrial ROS
ELISA	Enzyme linked immunosorbent Assay
GFP	Green fluorescent protein
RFP	Red fluorescent protein
RARRES-1	Retinoic acid receptor responder 1
NADPH	Nicotinamide adenine dinucleotide phosphate
mRNA	Messenger RNA

Chapter One: Literature review

1. Liver Fibrosis

1.1 Burden of liver disease

Liver fibrosis is the outcome of virtually all liver diseases [1]. It involves the accumulation of fibrillary extracellular matrix (ECM) in and around the liver tissue, causing damage to liver tissues that leads to scarring, cirrhosis, and eventually liver failure [2].

Liver disease is responsible for 2 million deaths annually and accounts for 1 of 25 deaths worldwide [3]. Liver cirrhosis is the primary cause of death due to liver disease. In 2019, liver cirrhosis contributed to 1.5 million deaths in patients with liver disease [4], with Central Asia having the highest liver cirrhosis-related age-standardized death rate (ASIR) of 59.06 and Central Latin America having the 2nd highest ASIR of approximately 40.76 per 100,000 population [4].

In Australia, almost 6 million people suffer from chronic liver disease (CLD), which accounts for 7000 deaths annually. Liver disease is considered the 5th most common cause of death in Australia, with a financial burden of almost $5.4 billion [5]. The prevalence of CLD is estimated to increase to 8 million by 2030 [5, 6]. In 2015, liver disease was responsible for 2.05% of deaths in Australia and 1.33% in New Zealand [7]. In 2021, liver cancer was the 7th most common cause of death in Australia, accounting for 2290 deaths [8].

Unfortunately, despite this soaring health and economic burden, few drugs are available for liver fibrosis, and liver transplantation remains the main option for treatment. Therefore, the development of antifibrotic drugs is urgently needed.

1.2 Causes of liver fibrosis

Liver fibrosis is the consequence of all liver-related diseases, including metabolic dysfunction-associated fatty liver disease (MAFLD), viral hepatitis B and C, alcohol-related liver diseases and other less common liver diseases, including autoimmune liver disease and hereditary diseases such as haemochromatosis, alpha1-antitrypsin deficiency and Wilson's disease [9]. Cholestatic (biliary excretory system-related) and hepatotoxic (hepatocyte-related) injuries are the two main categories leading to liver fibrosis.

MAFLD (previously called non-alcoholic fatty liver disease (NAFLD)) is currently the most common chronic liver disease, that affects nearly one-third of Australians and 20–30% of people globally [10]. This growing burden parallels the global increases in obesity, diabetes and lack of metabolic health. MAFLD is diagnosed based on the presence of hepatic steatosis and one of the following criteria: obesity/overweight, type II diabetes mellitus or metabolic dysregulation [11].

Metabolic dysfunction-associated steatohepatitis (MASH) is a severe form of the disease that is characterized by hepatic steatosis and inflammation. After developing steatohepatitis, almost 20–50% of patients will develop cirrhosis within 10 years [12-14]. The outcomes of MAFLD extend beyond the liver to multiple extrahepatic diseases, including diabetes, cardiovascular disease, and cancer [15].

MAFLD can be best explained as a multifactorial condition shaped by the combined and dynamic interactions of various environmental factors and genetic susceptibility, with a pivotal role for epigenetic modifiers in mediating this interaction. Understanding the genetic and epigenetic factors associated with disease pathogenesis is important for informing the process of developing novel therapeutic strategies [16].

1.3 Diagnosis of liver fibrosis

1.3.1 Liver biopsy and histological assessment

Liver biopsy is considered the "gold standard" method for assessing the severity of liver injury [17]. It is typically recommended when more information is needed to diagnose, predict the outcome, and plan treatment for chronic liver diseases. Liver biopsy provides information about the degree of necroinflammation, steatosis, histological staging, morphometry (distribution of liver fibrosis), cirrhosis, classification of tumours, and investigations of adverse drug reactions [18].

Different scoring systems are used to evaluate liver fibrosis histologically. These include the METAVIR, Knodell, and Ishak scores for viral hepatitis, as well as the SAF (steatosis, activity, and fibrosis) score, fatty liver inhibition score, and NAFLD activity score for assessing MAFLD [19-21].

Stages of liver fibrosis can be defined based on the microscopic changes in the structure of liver tissues and the hepatic venous pressure gradient (HVPG). Fibrosis is classified into 5 stages from F0 to F4 as follows: F0 (no fibrosis), F1 (portal fibrosis), F2 (periportal fibrosis), F3 (bridging fibrosis) and F4 (cirrhosis).

However, several disadvantages are associated with liver biopsy. It is invasive, painful, and time-consuming. Additionally, sampling errors and inter/intra observer agreement have led to incorrect diagnoses in 20% of cases [22-24].

1.3.2 Non-invasive biomarkers

Interest in the use of non-invasive biomarkers and scoring systems to stage liver fibrosis is increasing. Serum biomarkers can be classified into three categories: direct biomarkers (which directly measure ECM turnover), indirect biomarkers (which measure markers in the

blood released due to hepatic dysfunction), and combinatorial biomarkers (where direct and indirect markers are combined to produce composite scores) [25, 26]. The various combinatorial biomarkers used are listed in **Table 1.1** [27].

Additionally, the progression of liver fibrosis is usually evaluated in the clinic with imaging techniques. The different imaging techniques used are magnetic resonance imaging (MRI), ultrasound (US), US elastography (USE), and computed tomography (CT).

Table 1.1: A list of some of the most used blood biomarkers and scoring system for non-invasive assessment of liver fibrosis.

Score	Components	Liver conditions
HepaScore [28]	Age, gender, α_2M, total bilirubin, HA	Predicting stages of liver fibrosis in hepatitis C patients [29]
Fibroindex [30]	AST, platelet count & γ-globulin	Predicting significant fibrosis in chronic hepatitis C patients [30]
Forns index [28]	Age, platelet count, GGT and cholesterol	Rule out patients without significant hepatic fibrosis in HCV patients [31]
APRI [28]	AST to platelet ratio	HCV related fibrosis and cirrhosis [32]
Euorpean liver fibrosis test [33]	Collagen IV & VI, PIIINP, HA, tenascin, laminin, MMP2, MMP9 & TIMP 1	Diagnose advanced fibrosis in MAFLD patients [34]
ADAPT algorithm [35]	Age, platelet count, PRO-C3 & diabetes	Used to diagnose patients with MAFLD and advanced fibrosis [36]
FIBROSpect II [37]	α_2M, HA, TIMP-1	Used to differentiate chronic HCV patients with/without fibrosis [38]
Fibrosis score 4 (FIB-4) [28]	Age, Platelet, AST & ALT	Identify HCV/HIV co-infection related fibrosis [39]
NAFLD fibrosis score (NFS) [35]	Age, Platelets, albumin, BMI, AST, ALT & AGF/ diabetes	Identify advanced fibrosis in patients with MAFLD [40]
AAR [22]	AST/ALT ratio	Predictor of cirrhosis in various liver diseases [41]
ELF test [42]	TIMP-1, HA & PIIINP	Predict advanced liver fibrosis for chronic liver disease [43]

Gamma-glutamyl transferase (GGT), Aspartate aminotransferase (AST), Alanine aminotransferase (ALT), Matrix metalloproteinase (MMP), Insulin-like growth factor (IGF) and tissue inhibitor of metalloproteinase (TIMP). α-2-macroglobulin (α_2M), hyaluronic acid (HA), pro-collagen III N-terminal pro-peptide (PIIINP).

1.4 Pathogenesis of liver fibrosis

Liver fibrosis is a complex process that involves various cellular and extracellular signalling [44]. Regardless of the aetiology, the development of liver fibrosis involves different molecular mechanisms, including the activation of hepatic stellate cells (HSCs), disruption of the endothelial and epithelial barriers, release of cytokines, chronic inflammation, and hepatocyte death. These mechanisms work in concert, leading to liver fibrosis.

After liver injury, hepatocytes undergo inflammation and generate apoptotic bodies, which lead to the activation of HSCs. In addition, macrophages and other inflammatory cells, such as T cells, natural killer cells and Kupffer cells, are also activated. These inflammatory cells release various cytokines and chemokines that further activate HSCs.

Additionally, the injury disrupts the normal microenvironment of cells, contributing to HSCs activation. Once activated, HSCs release various vasoactive peptides, growth factors and cytokines that further aggravate fibrosis. This process results in the accumulation of ECM proteins, such as collagen types I and III, leading to the development of fibrous scar tissues in the liver and ultimately affecting normal liver function [44, 45]. A simplified scheme of events occurring during liver fibrosis is depicted in **Figure 1.1**. If the liver injury is resolved, fibrosis can be reversed. This resolution is achieved by either the apoptosis of activated HSCs or their reprogramming to the deactivated state, along with regeneration of hepatocytes [46].

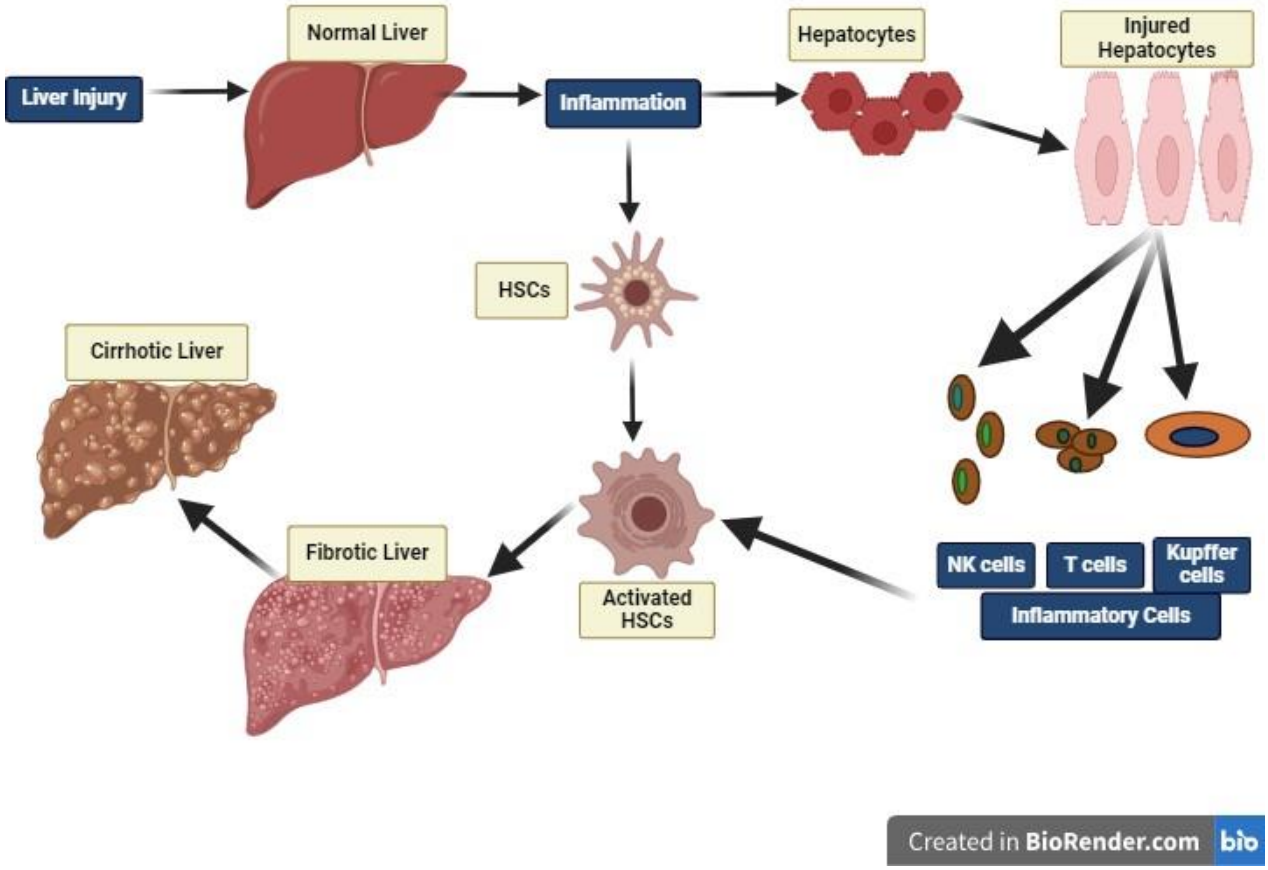

Figure 1.1: Pathogenesis of liver fibrosis. *A cascade of events involved in the pathogenesis of liver fibrosis. After liver injury, hepatocytes undergo inflammation. Inflammation activates HSCs and inflammatory cells (T cells, Kupffer cells & NK cells). These inflammatory cells release various factors that further activate HSCs. Additionally, HSCs after activation produce various vasoactive peptides, growth factors and cytokines that further perpetuate fibrosis.*

1.5 Cell types implicated in liver fibrosis

Different types of cells integrate and coordinate to produce liver fibrosis. The main types of cells involved in the pathogenesis of liver fibrosis are described below.

1.5.1 Hepatic stellate cells

HSCs are the primary cells involved in hepatic fibrosis. Normally, HSCs are quiescent cells located in the space of Disse (the space between the liver epithelium and sinusoidal endothelium), where they act as liver pericytes that support vitamin A storage and various liver functions [6, 47].

However, continuous liver injury causes HSCs to transform into myofibroblasts. These activated myofibroblasts express genes related to fibrosis, lose lipid droplets and secrete extracellular matrix (ECM). They also release growth factors and chemokines that contribute to the proliferation and migration of HSCs [48-50].

HSCs activation involves two main steps: initiation and perpetuation. Initiation is the early phase in which cells become responsive to extracellular signals, mainly due to paracrine stimulation from neighbouring cells [51]. This phase involves the production of growth factors, the formation of a contractile phenotype, and changes in growth factor signalling. After initiation, HSCs enter the perpetuation phase, in which they respond to different cytokines and growth factors. This phase amplifies the activated phenotype of HSCs and leads to scar formation through increased cell proliferation, contractility, fibrogenesis, matrix degradation, chemotaxis, and inflammatory signalling [52-56].

Under conditions of chronic liver injury, several processes, such as cell contractility, proliferation, the secretion of pro-inflammatory signalling molecules, alter matrix degradation and the production of the ECM to maintain the activated phenotype of HSCs **(Figure 1.2)**[57].

If the injury is resolved, HSCs can be reversed to the resolution phase. During this phase, activated HSCs can either revert to a quiescent state or be eliminated through apoptosis [52].

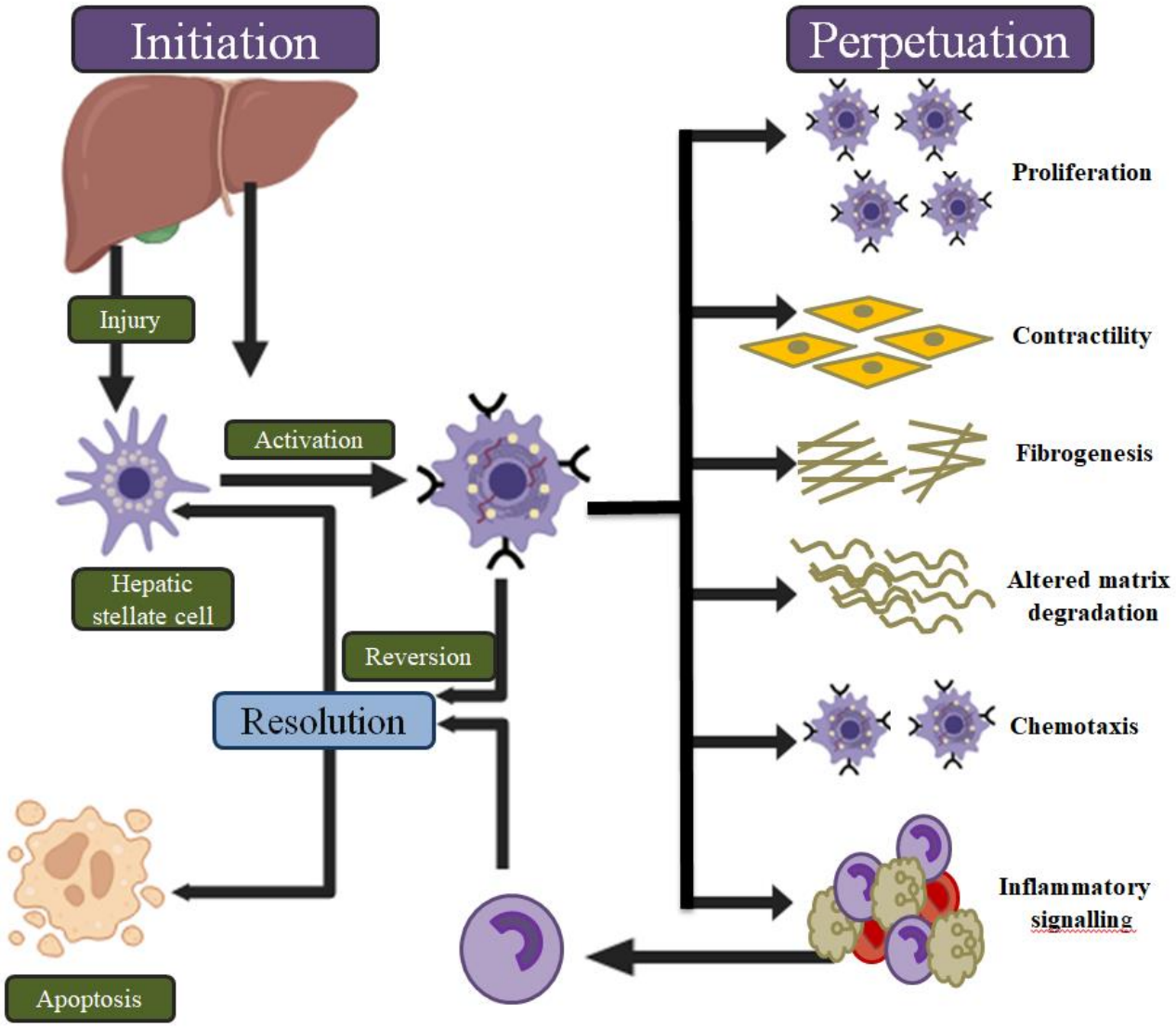

Figure 1.2: Activation of hepatic stellate cells [50]. 1) *Initiation phase activates quiescent HSCs to activated HSC. 2) Perpetuation phase maintains activated HSCs under proliferation, contractility, Fibrogenesis, altered matrix degradation and chemotaxis and inflammatory signaling. If resolution happens, activated HSCs are cleared by apoptosis or get reversed to inactivated HSCs phenotype.*

1.5.2 Hepatocytes

Hepatocytes, which comprise approximately 80% of the liver mass, are epithelial cells. They perform vital functions, including the synthesis of proteins, carbohydrate/lipid metabolism, biotransformation/detoxification of foreign compounds and bile synthesis [58]. Injured hepatocytes contribute to the development of liver fibrosis by acquiring myofibroblastic features through the epithelial–mesenchymal transition (EMT) [59]. During the EMT, cells lose their epithelial characteristics, cell–cell adhesion features, and apical–basal polarity and instead acquire mesenchymal characteristics such as ECM production [60].

Injured hepatocytes start producing fibrogenic mediators that promote inflammation and fibrosis. These mediators lead to the necrosis and apoptosis of liver cells. As a result of apoptosis, apoptotic bodies are released. HSCs engulf these apoptotic bodies and undergo transdifferentiation into myofibroblasts, which further contributes to fibrosis [61]. In addition, injured hepatocytes augment the release of inflammatory cytokines from inflammatory cells, which further stimulates HSCs activation, leading to fibrosis [52]. The morphology of normal and fibrotic liver tissues is shown in **Figure 1.3**.

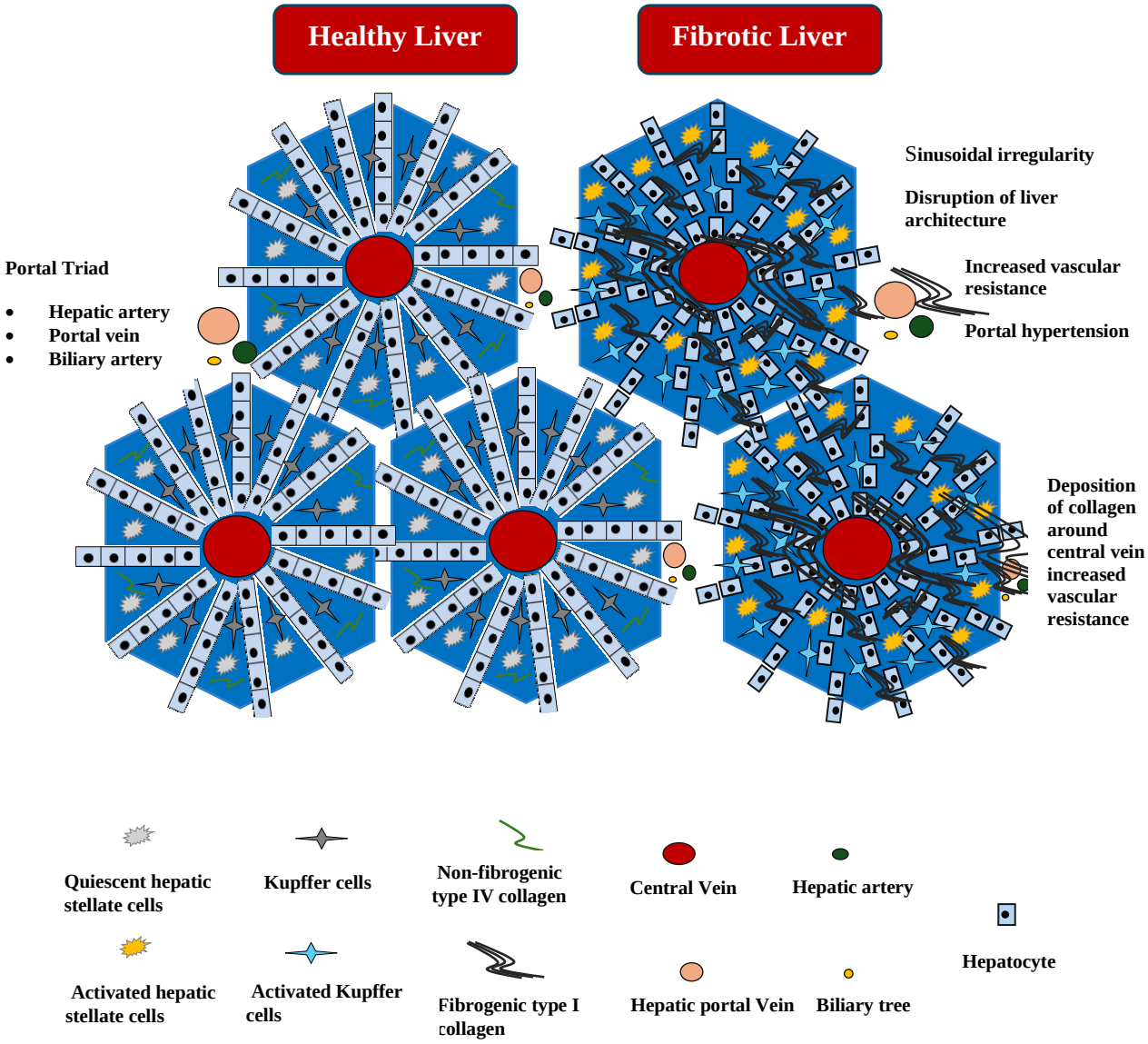

Figure 1.3: Hepatocyte structure in normal and fibrotic liver [62]. *(A) In normal liver hepatocytes are arranged in rows radiating towards the edge. The gaps between hepatocytes are known as sinusoids, lined with HSCs, endothelial cells, Kupffer cells and non-fibrogenic collagen (type IV collagen). Three vessels naming hepatic artery, biliary tree and hepatic portal vein are supplied in sinusoids and are responsible for exchange of nutrients, signalling molecules and blood gases. (B) In chronic liver injury, fibrogenic pathway is activated. Fibrogenic type I collagen is deposited with in the sinusoids, which will increase vascular resistance and portal hypertension. Compensatory mechanisms are activated e.g., formation of esophageal varices and ascites.*

1.5.3 Liver sinusoidal endothelial cells (LSECs)

In the normal liver, liver sinusoidal endothelial cells (LSECs) possess normal fenestrations and maintain HSCs in the quiescent phase **(Figure 1.4)**. LSECs produce nitric oxide (NO) through endothelial NO synthase (eNOS), which helps maintain the normal function of LSECs and promotes the reversal of activated HSCs to a quiescent state [63]. However, in the case of chronic liver injury, LSECs undergo capillarization, lose their fenestrations, and decrease eNOS activity and NO production. This loss of function impedes the reversion of HSCs to a quiescent state. Additionally, LSECs also secrete interleukins, PDGF*β*, tumour necrosis factor α (TNF-α), VEGF, and TGF-$\beta_{1,}$ which are fibrogenic cytokines [44, 64] and can recruit inflammatory cells to the site of injury and activate HSCs [64].

1.5.4 Other cell types and hepatic macrophages

During acute liver injury, inflammation can be beneficial for liver regeneration, and sustained inflammation due to chronic liver injury is detrimental and plays a critical role in the pathogenesis of liver fibrosis. Immune cells such as monocytes (bone marrow-derived), neutrophils, Th-17 cells, and Kupffer cells (liver macrophages) amplify inflammation, which in turn activate HSCs by secreting growth factors and cytokines, interferons, TNFα, interleukin-1 and interleukin-6 [44, 65]. Kupffer cells are the primary source of transforming growth factor-β (TGF-β), which is a key promoter of fibrogenesis [66]. Various mediators, such as TNFα, interleukin-1, interleukin-6, CCL2, and PDGF, are released by liver macrophages and contribute to HSCs activation and fibrosis. Neutrophils and activated Kupffer cells release reactive oxygen species (ROS) that further activate HSCs during liver injury.

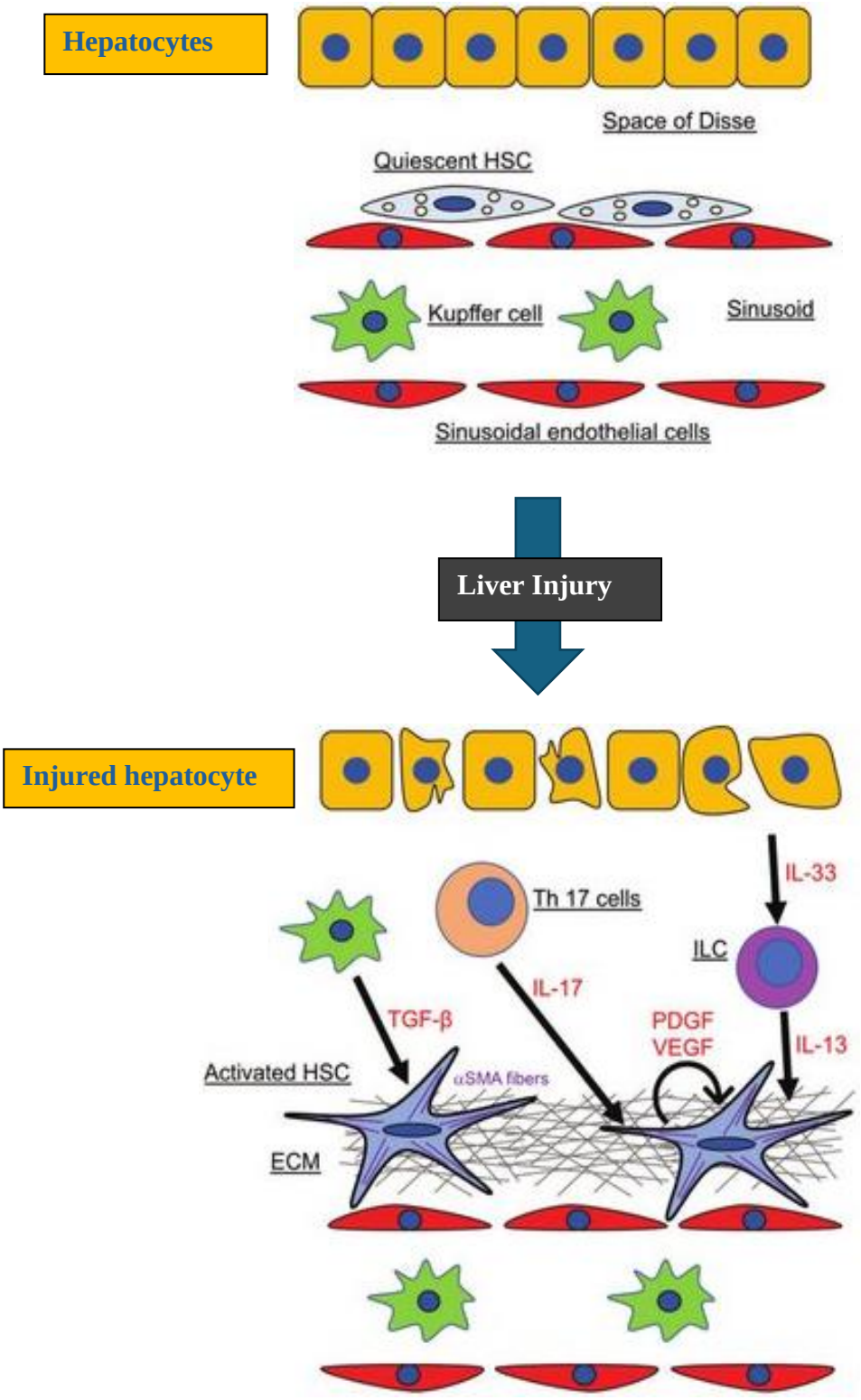

Figure 1.4: Cell types in liver fibrosis and release of fibrogenic factors [67]. *After chronic injury, hepatocytes, Kupffer cells and immune cells (Th 17 cells & IL-33) release pro-fibrogenic factors which stimulates HSCs activation. Activated HSCs increase the secretion of α-SMA, growth factors and ECM.*

1.6 Cell signalling in liver fibrosis

Liver fibrosis and HSCs activation are complicated processes involving several events that are regulated at the transcriptional, translational, and post- transcriptional levels. Various signalling pathways, including those involving connective tissue growth factor (CTGF), inflammatory cytokines (leptin, IFN-ɣ and reduced adiponectin levels), TGF-β, VEGF, and PDGF, are implicated in this process **(Figure 1.5)** [67, 68].

In particular, TGF-β is the archetypal profibrotic cytokine and its expression is elevated in all fibrotic diseases. The next section discusses this pathway in more detail, given its relevance to my thesis.

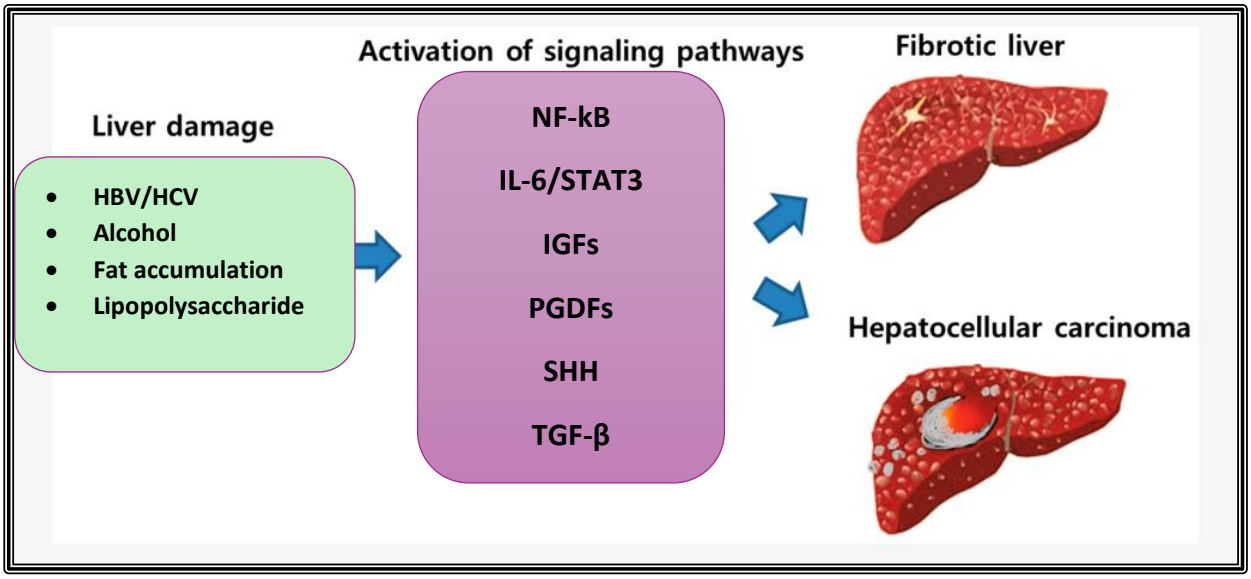

Figure 1.5: Schematic representation of liver damage and activation of various signaling pathways contributing to fibrosis [69]. *In response to liver injury, various signaling pathways are activated namely: Transcription factor (NF-kB), interleukin-6 (IL-6) and activator of transcription 3(Stat3), insulin like growth factors (IGFs), platelet growth factor (PDGF), sonic hedgehog (SHH) and tumor growth factor beta (TGF-β). These pathways ultimately develop liver fibrosis and hence hepatocellular carcinoma.*

1.7 TGF-β signalling in HSCs activation and liver fibrosis

The TGF-β family, which comprises 33 members, including TGF-β (1, 2, and 3), activins, and bone morphogenetic proteins (BMPs), regulates various processes, such as homeostasis, repair, the immune response, and ECM deposition in liver cells, by influencing differentiation, proliferation, migration, and cell death [70-72]. The TGF-β signalling pathway involves the SMAD and non-SMAD pathways **(Figure 1.6)**.

Under normal physiological conditions, TGF-β1 regulates tissue remodelling, apoptosis, and homeostasis. Macrophages, Kupffer cells, platelets, hepatocytes, HSCs, and endothelial cells are sources of TGF-β in the liver [73, 74]. Following liver injury, TGF-β plays a central role in the function and phenotype of fibroblasts by mediating different cellular subsets to promote fibrosis.

Therefore, not surprisingly, TGF-β inhibition has been extensively investigated as an antifibrotic strategy, with approaches including blocking circulating TGF-β1, antagonizing TGF-β receptors, and blocking TGF-β activation at the cell surface. However, due to the pleotropic function of TGF-β, the efficacy of these therapeutic approaches is hindered by adverse effects, such as on-target cardiovascular toxic effects and the development of benign tumours [66, 75-80]. Thus, novel therapeutic approaches for the selective targeting of the fibrotic effect of TGF-β signalling are needed.

1.7.1 SMAD (small worm phenotype)-dependent signalling

TGF-β mediates its function by SMAD-dependent signalling pathway. After activation, TGF-β binds to the transmembrane receptor type 1 TGF-β receptor (TβRI), as shown in **Figure 1.6**. After binding, TGF-β phosphorylates SMAD2 and SMAD3 (crucial mediators)[81]. Afterwards, phosphorylated SMAD2/3 forms a complex with SMAD4 and accumulates in the

nucleus. The SMAD protein activates several transcription factors that will lead to genes transcription. This process ultimately increases collagen production [82].

1.7.2 Non-SMAD (Drosophila MAD or Mothers against decapentaplegic) dependent signaling

TGF-β also activates MAPK (mitogen-activated protein kinase), which involves the activation of ERK (extracellular signal regulated-kinase), P38, JNK (c-jun N-terminal kinase), PI3K/AKT, c-ab1, JAK2/STAT3 and Rho-associated coiled-coil protein kinases, as shown in **Figure 1.6** [83].

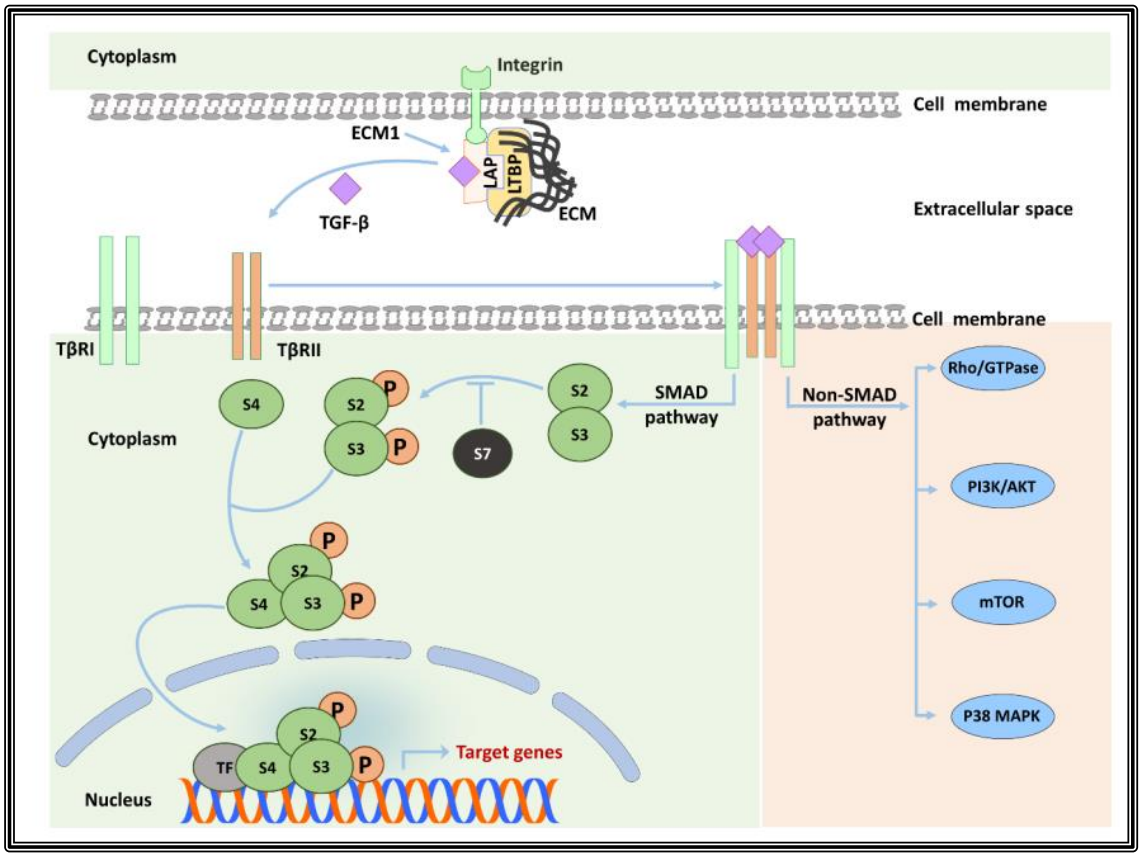

Figure 1.6: SMAD and non-SMAD-dependent TGF-β signaling [84]. *After the liver injury, TGF-β is released from the large latent complex. This release involves the interaction of integrins with latent association protein (LAP). TGF-β then binds to receptors TβRII. It forms heterotetramer with TβRI and initiates signaling pathways by phosphorylating R-SMADs i.e. S2 (SMAD2) and S3 (SMAD3). TGF-β also activates SMAD-independent pathways, which includes MAPK, mTOR, P13K/AKT and Rho/GTPase pathways [83].*

1.8 Regression of liver fibrosis

Research using experimental models and data from human patients has suggested that liver fibrosis can be reversed if the liver injury is resolved. Once the causative factor is eliminated, myofibroblasts can undergo apoptosis or become inactive, leading to the regression of fibrosis [49, 85]. After the depletion of fibrogenic signals, HSCs increase the expression of TNF receptor 1 and Fas receptor, which are death-mediated genes. They also upregulate p^{53}, caspase 9 and Bax (pro-apoptotic proteins) and downregulate BCL_2 (anti-apoptotic factors). In addition, interferon-γ-activated natural killer cells eliminate HSCs, thus resolving liver fibrosis. In addition to undergoing apoptosis, myofibroblasts can also revert to an inactive phenotype during the regression phase of liver fibrosis. These inactivated HSCs are more prone to fibrogenic injuries than are the original quiescent HSCs.

1.9 Energy metabolism and liver fibrosis

Energy metabolism (the process of generating energy from nutrients) is crucial for maintaining balance within an organism's cells and ensuring proper functionality [86]. The transformation of quiescent stellate cells into fibrous matrix-secreting cells is an energy-dependent process. As a result, the overall energy demand of cells increases during liver fibrosis. Disruptions in energy metabolism have been linked to the development of liver fibrosis and can potentially be targeted for anti-fibrotic drug development [87]. Therefore, instead of solely focusing on cell signalling, a novel strategy to reverse fibrosis could involve targeting the energy demand of fibrotic cells, thus minimizing the impact on quiescent stellate cells. This approach has not yet been fully explored.

This energy is produced by oxidative phosphorylation (mitochondrial metabolism) and the oxidation of fatty acids [88-91]. Altered mitochondrial activity has been observed in cirrhotic patients and in activated HSCs [92, 93], and mitochondrial oxidation has been found to be increased in patients with MAFLD [94]. In support of the concept of targeting energy metabolism to treat liver fibrosis, the use of 3-bromopyruvate, an alkylating/anticancer agent, has been shown to restrict liver fibrosis by inhibiting energy production in mice [95].

The other source of energy is autophagy. Mitochondria and autophagy are interconnected in their regulation of each other; autophagy is responsible for degrading defective mitochondria, while mitochondria regulate various aspects of autophagy, such as the production of autophagosomes and the overall autophagic process [96, 97]. Autophagy is closely linked to mitochondrial metabolism and serves as a source of fuel for energy production [85, 98]. Furthermore, mitochondria-generated ROS can stimulate autophagy, and autophagy in turn regulates lipid droplet turnover in HSCs through a ROS-dependent pathway [98-100]. During fibrosis, activated HSCs consume intracellular lipid droplets, which are also broken down by autophagy to produce free fatty acids. These free fatty acids are then utilized by mitochondria to produce ATP through the process of mitochondrial β-oxidation [101-103].

TGF-β is implicated in regulating HSCs energy metabolism [104]. TGF-β induces autophagy, stimulates the loss of lipid droplets in HSCs, releases energy and increases energy release to promote fibrosis [105, 106]. Additionally, TGF-β regulates energy metabolism by directly controlling mitochondrial metabolism. It also leads to increased ROS generation, which causes mitochondrial damage [107]. This increased energy release supports HSCs activation and proliferation and hence liver fibrosis [108]. Therefore, therapeutic approaches that can reduce energy release can be used to reverse liver fibrosis.

1.10 Mitochondrial function and energy production

Mitochondria, often referred to as “the powerhouse of the cell,” play crucial roles in the energy metabolism of cells. They are semi-autonomous organelles involved in ATP synthesis, ROS generation, cell differentiation modulation, signal transduction maintenance, and apoptosis [109, 110].

The inner membrane of the mitochondria contains enzymes that participate in the electron transport chain, ATP production, and the maintenance of an electrochemical gradient. These enzymes are responsible for oxidative phosphorylation [111, 112]. Mitochondria produce energy from glucose and fatty acids through the tricarboxylic acid (TCA) cycle and electron transport chain (ETC), respectively. These metabolic pathways (TCA cycle and ETC) release the energy stored in food (glucose and fatty acids) in the form of high-energy electrons.

Nicotinamide adenine dinucleotide (NAD) and flavin adenine dinucleotide (FAD) capture these electrons and form NADH and $FADH_2$. NADH and $FADH_2$ transfer these electrons to the ETC. The ETC is the primary site for ATP generation and consists of 5 complexes (complexes I to V). As an electron moves across the complexes, a proton gradient is established. The energy released from proton transfer is used to generate ATP from ADP [113]. Approximately 2% of electrons are released from the ETC while travelling through different complexes. These electrons combine with oxygen and generate superoxide radicals (ROS). Dysfunction of the ETC may lead to the excessive generation of ROS, resulting in cellular injury [114].

Mitochondrial homeostasis is maintained through processes such as mitochondrial fission, mitochondrial fusion, mitophagy, and mitochondrial biogenesis. Mitochondrial fission and fusion are important processes that regulate mitochondrial morphology, quantity, and function **(Figure 1.7)**.

Mitochondrial fission separates damaged mitochondria from healthy mitochondria and is regulated by dynamin-related protein 1 (Drp1) and mitochondrial fission protein 1 (FiS1). Mitochondrial fusion combines neighbouring, depolarized mitochondria to form a healthy mitochondrion [115] and is stimulated by the energy demand of the cells. Mitochondrial fusion is regulated by mitofusin protein 1 (Mfn1), mitofusin protein 2 (Mfn2) and optic atrophy 1 (Opal 1). Any changes in the expression of Drp1, Mfn1, Mfn2, and optic atrophy 1 will affect mitochondrial fission and fusion processes [116]. In response to liver injury, changes in mitochondrial structure and function occur. Defective mitochondria stimulate mitochondrial fission and fusion processes and hence disturb mitochondrial homeostasis [117]. Under conditions of increased oxidative stress, mitochondrial fusion is increased, which leads to increased HSCs activation. Hence, the inhibition of mitochondrial fusion can alleviate liver fibrosis [118].

Mitochondrial biogenesis regulates mitochondrial turnover through the expression of peroxisome proliferator-activated receptor-gamma coactivator (PGC-1α), which is a transcriptional coactivator [119].

Mitochondrial dysfunction may occur due to damage in the structure of mitochondria, defects in the respiratory chain, biogenic dysfunction, a reduction in the number of mitochondria, gene damage and may be due to changes in the activity of oxidative protein [120].

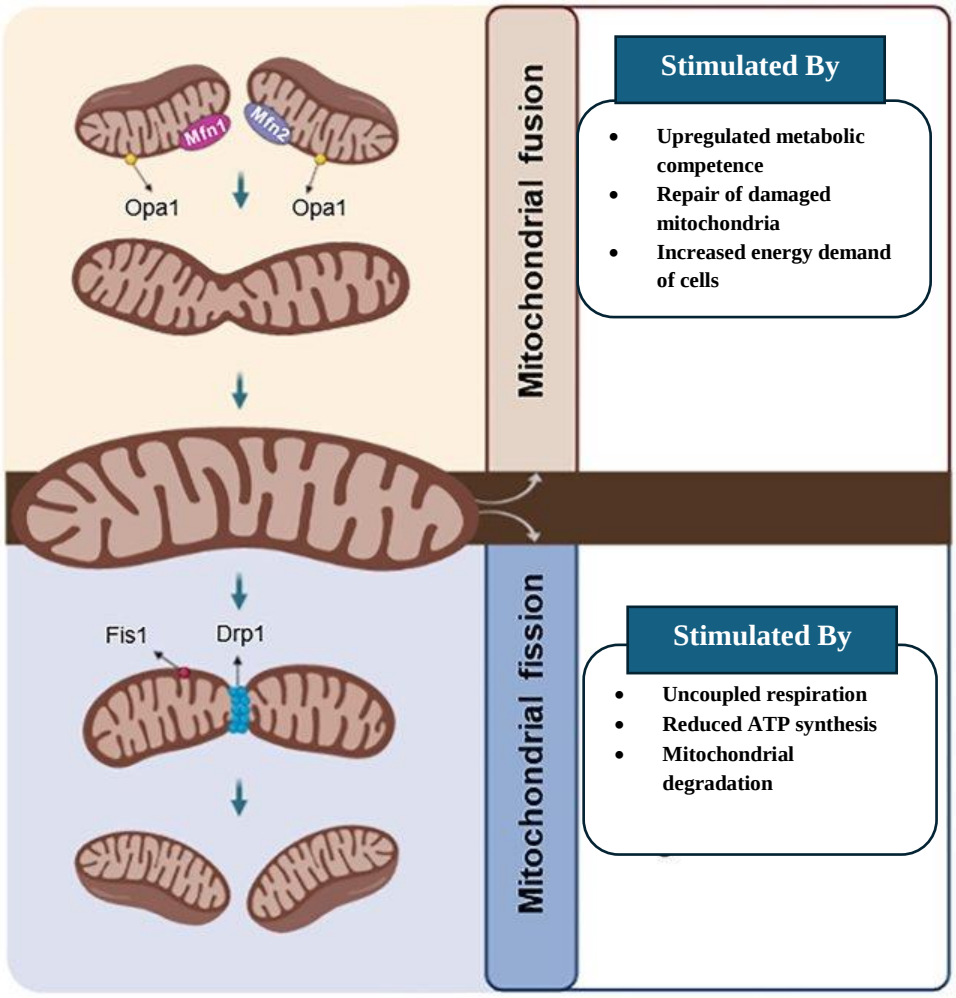

Figure 1.7: Mitochondrial dynamics; the process of fission and fusion [121]. *Drp1 & FiS1 facilitate the mitochondrial fission by compressing from the middle and separating it into two mitochondria. Fission is stimulated under the condition of low energy demand and hence results in reduced ATP synthesis. While fusion is stimulated under increased energy demands and it upregulates metabolic competence. During fusion process, Mfn1, Mfn2 & OPA1 integrates outer mitochondrial and inner mitochondrial membrane and forms one functional mitochondria.*

ROS regulates myofibroblasts differentiation, epithelial cell apoptosis, and the expression of pro-fibrogenic mediators (Pal-1), which suppresses the degradation of the ECM **(Figure 1.8)**. All these processes promote the accumulation of ECM and liver fibrosis [122]. An imbalance between the production and removal of ROS creates an imbalance that results in increased oxidative damage to mitochondrial lipids, proteins, and DNA.

Increased ROS production can also open the mitochondrial permeability transition pore (mPTP) and can induce mitochondrial depolarization and swelling. It will reduce ETC activity and the levels of apoptotic factors. Additionally, histones bound to mitochondrial DNA are sensitive to oxidative stress caused by the increased generation of ROS. It causes defects in the respiratory chain and biogenesis of mitochondria [123].

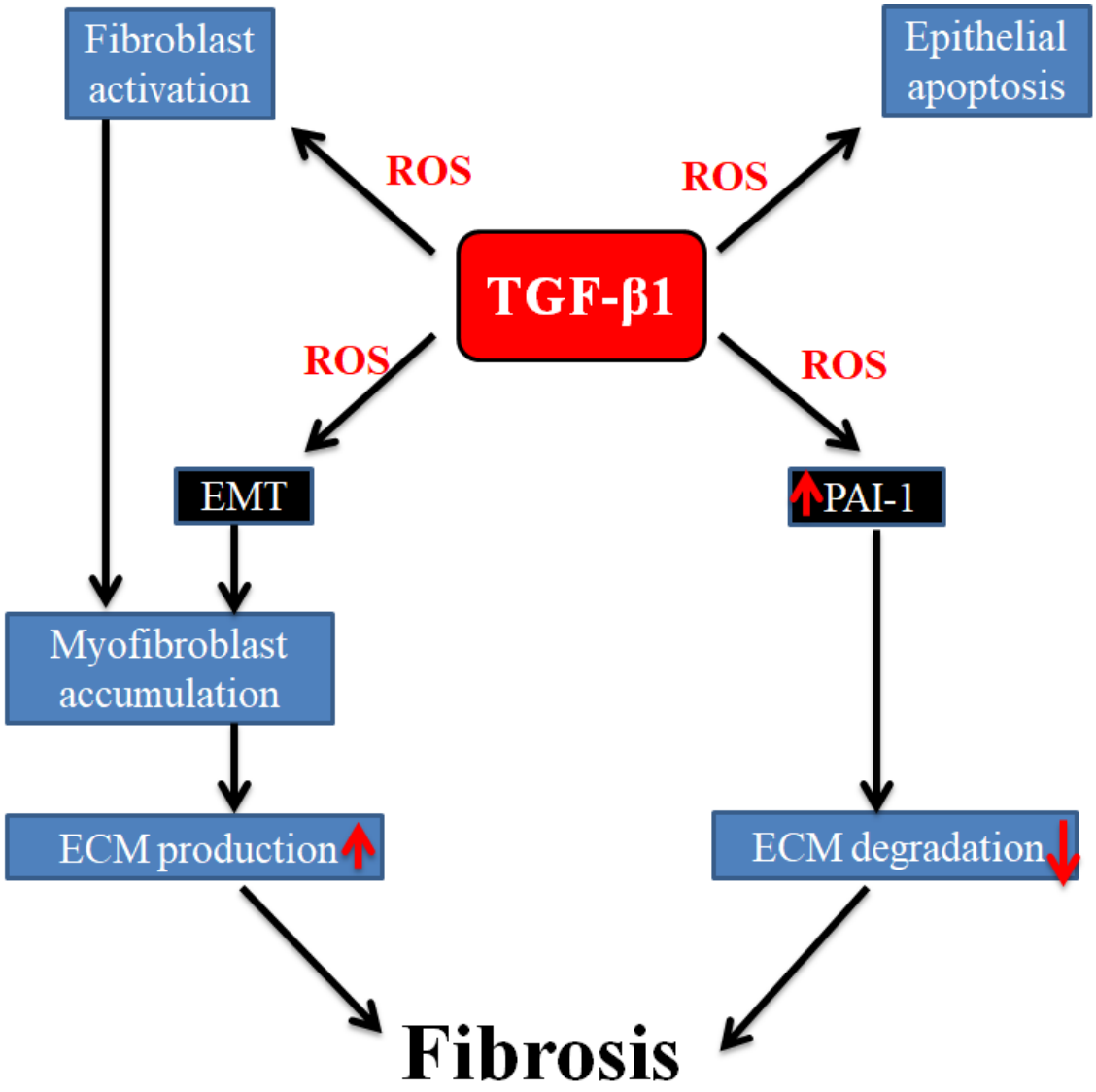

Figure 1.8: Role of ROS in the development of fibrosis [122]. *ROS mediates TGF-β induced profibrotic effects including fibroblast activation and accumulation, epithelial apoptosis, expression of profibrogenic mediators (PAI-1), mesenchymal transition, ECM production and degradation.*

Mitophagy is the process of removing damaged mitochondria **(Figure 1.9)**. Alterations in the expression of components of the PINK1/Parkin pathway (Ser/Thr kinase/ubiquitin-protein ligase) will attenuate mitophagy and lead to the accumulation of damaged mitochondria [124].

Different evidence suggests that inhibitors of mitochondrial functions can alleviate the energy demand of cells and hence reverse liver fibrosis. Mitochondrial electron transfer involves proton flux and is coupled with a redox proton pump. Mitochondrial complexes (CI, CIII and CIV) mediate this coupling. Mitochondrial uncouplers can transfer energy (generated by electron transfer) in the respiratory chain. Therefore, energy cannot be used for the phosphorylation of ADP and hence is emitted as heat. Recently, mitochondrial uncouplers have been shown to reduce ATP and ROS generation and hence inhibit HSC activation [125].

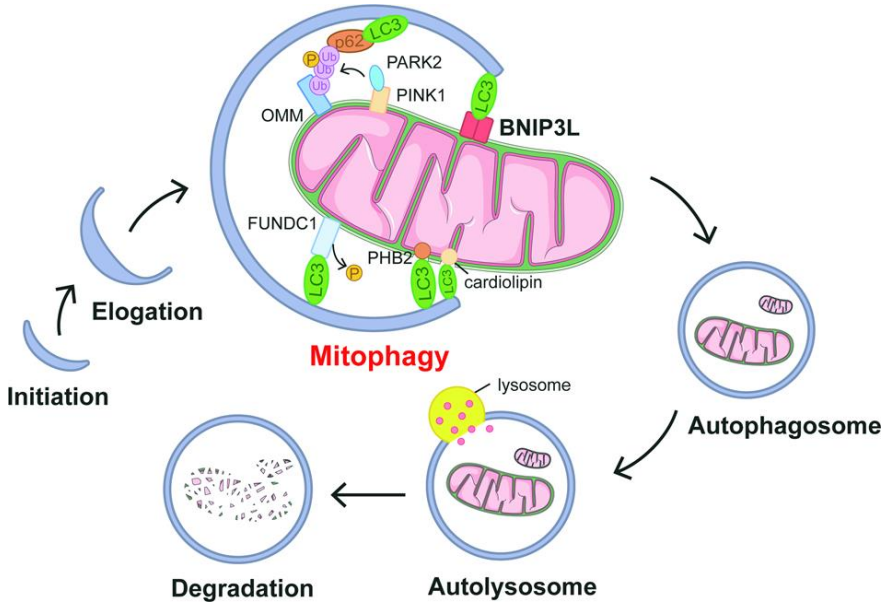

Figure 1.9: Schematic representation for mitophagy and mitochondrial quality control [126]. *Mitophagy related protein (PINK1/PARK2) senses the defective mitochondria. PINK1/PARK2 phosphorylates ubiquitin that link p62 to LC3 to engulf mitochondria. Various mitophagy receptors (BNIP3L, FUNDC1, PHB2, cardiolipin and BNIP3recruit autophagosomes by binding with Atg8s and LC3.These pathways ensure mitochondrial quality control through elimination of damaged bacteria by lysosomes.*

1.11 Autophagy

Autophagy is a process in which liver cells recycle materials to provide energy and maintain essential metabolites for growth and maintenance [127]. Autophagy stores glycogen during starvation and breaks down lipid droplets [128]. Starvation activates autophagy, whereas insulin, free fatty acids, obesity, and ageing inhibit it [129]. Impaired autophagy leads to metabolic problems in the liver, causing lipid droplet accumulation and increased reactive oxygen species (ROS) generation. It also promotes fibrosis by providing energy to activate HSCs [130].

Autophagy is crucial for activating HSCs **(Figure 1.10)**. Quiescent HSCs contain lipids in the form of triglycerides and retinyl esters [101]. HSCs consume lipid droplets to become activated into myofibroblasts during liver injury [131, 132]. Autophagy mobilizes lipid droplets, releasing free fatty acids that are used for energy production by the mitochondria through β-oxidation to meet the energy needs of activated HSCs during proliferation and fibrosis [101, 133].

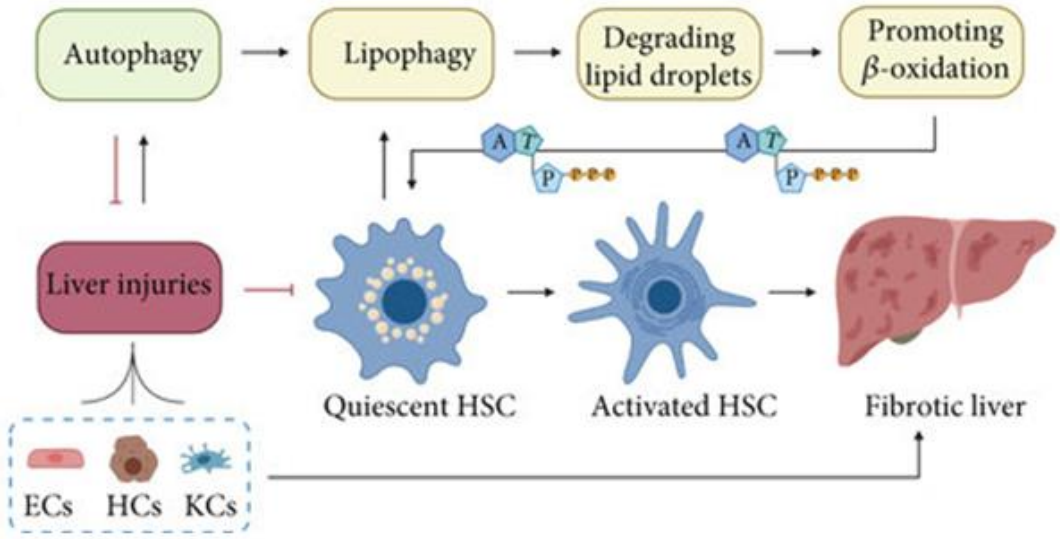

Figure 1.10: Relationship between autophagy and liver fibrosis [134]. *ECs: Endotheliocytes; HCs: Hepatocytes; KCs: Kupffer cells. Autophagy plays dual role in liver fibrosis. On one hand it promotes fibrosis by providing energy to active HSCs. On the other*

hand it ameliorates fibrosis by improving the function of other hepatic cells like ECs, HCs & KCs.

The P62/SQSTM1 protein, a key substrate for autophagy, acts as a link between LC3 and ubiquitinated substrates. It delivers ubiquitinated cargoes for degradation through autophagy, is itself consumed during the process and is used as a marker to measure autophagy flux [135, 136]. Lipotoxic stimuli phosphorylate P62/SQSTM1 and promote its accumulation, leading to defects in autophagy [137].

TGF-β1 can induce autophagy in HSCs and increase the expression of the autophagy-related protein LC3II/I in HSCs, which could lead to the activation of HSCs and reduce apoptosis [138-140].

In vivo studies in mice have shown that the specific deletion of Atg7 in HSCs reduces liver fibrosis. Additionally, inhibition of HSCs in mice by bafilomycin A1, decreased the activation and proliferation of HSCs through the attenuation of autophagy [141]. Chloroquine-mediated inhibition of autophagy improved CCL4-induced liver fibrosis by reducing HSCs activation [142]. Therefore, inhibiting autophagy reduces HSC activation, preserves lipid droplets [143, 144] and ameliorates fibrosis [145]. Hence, exploring the reduction in autophagy to decrease the energy demand of the cells could be a potential therapeutic target for curing liver fibrosis.

1.12 Epigenetic and liver fibrosis

In the study of disease pathogenesis, the epigenome provides a missing connection between genes and the environment. The epigenome is highly adaptive to environmental cues such as stress, diet and toxins. These cues can change the expression and function of genes in the body **(Figure 1.11)**.

A recent study revealed that both genes and the environment equally contribute to the heritability of complex human traits [146]. Another study of monozygotic twins indicated the presence of identical genomes and epigenomes in early life, but their epigenomes underwent significant changes later in life [147]. Recent evidence has shown that MAFLD is an epigenome-driven disease [148]. A recent review indicated that various epigenetic processes are involved in the development of MAFLD and that various epigenome editing tools can be developed as promising methods to restore the healthy epigenetic landscape [149]. Epigenetic modifications, especially DNA methylation, promote fibrosis and impact myofibroblast fate and activation [150, 151].

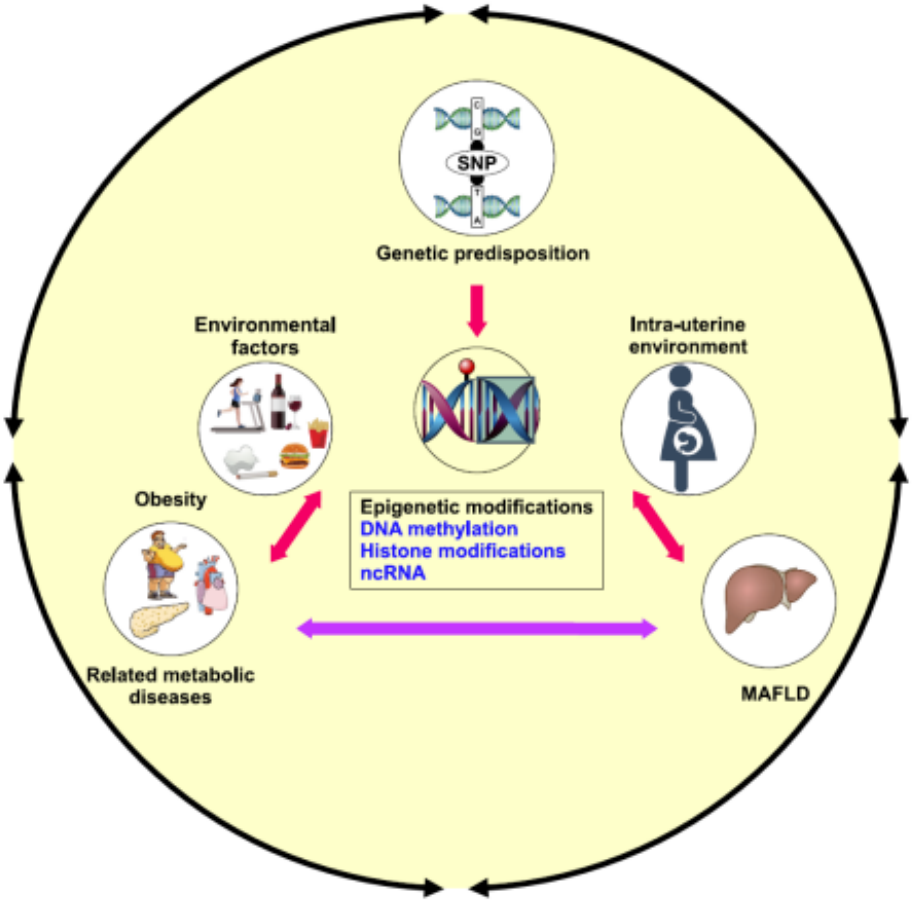

Figure 1.11: Epigenetics and gene environment interaction in MAFLD [152]. *Various genetics and epigenetics factors are involved in the development of MAFLD. Various environmental factors such as ageing, smoking, alcohol, diet, exercise, intrauterine environment with the genetics to develop MAFLD. Abbreviation: ncRNA (noncoding RNA).*

1.13 Antifibrotic drug development: Novel approaches

Currently, limited therapeutic options are available to cure liver fibrosis. Liver transplantation is the main option for survival in patients with end-stage liver diseases. Hence, the development of new therapeutic approaches to cure liver fibrosis is urgently needed. Recent findings from non-liver systems revealed that the epigenome tightly regulates energy metabolism. When energy metabolism is altered, it contributes to cancers. Conversely, metabolites can alter the epigenome, and these changes can regulate the expression of metabolic genes [153-156]. We surmise that restoring the homeostatic balance between the epigenome and metabolism should lead to a first-in-class treatment strategy for fibrosis.

Epigenetics can be an avenue to identify novel therapeutic targets for liver diseases. Epigenome-wide association studies (EWASs) could provide excellent insights into the mechanistic pathways involved in liver fibrosis. Thus, the application of epigenome-based tools may help identify new therapeutic targets to cure liver fibrosis.

1.14 Identification of RARRES1 as a potential therapeutic target

Our group employed an EWAS and identified an association between RARRES-1 and liver fibrosis (unpublished data). The basis of this association is that the RARRES-1 promoter is consistently hypermethylated, which silences the expression of RARRES-1 during liver fibrosis. Therefore, specific DNA demethylation of RARRES-1 can activate RARRES-1 expression and hence reverse liver fibrosis.

RARRES-1 is retinoic acid receptor responder element 1, also known as tazarotene-induced gene 1, encoding the RARRES-1 protein and was initially identified in psoriatic skin cultures [157].

RARRES-1 is cytogenetically located on chromosome *3q25.32* [158]. A sequence analysis revealed that the RARRES-1 protein is composed of 228 amino acids. It is a transmembrane protein with three regions, including an intracellular region with a small N-terminal region, a hydrophobic region containing a single spanning membrane and an extracellular region with the C-terminal region containing a glycosylation signal and a hyaluronic acid-building motif [159]. The genomic location of RARRES-1 is shown in **Figure 1.12,** and the three-dimensional structure of RARRES-1 is shown in **Figure 1.13**.

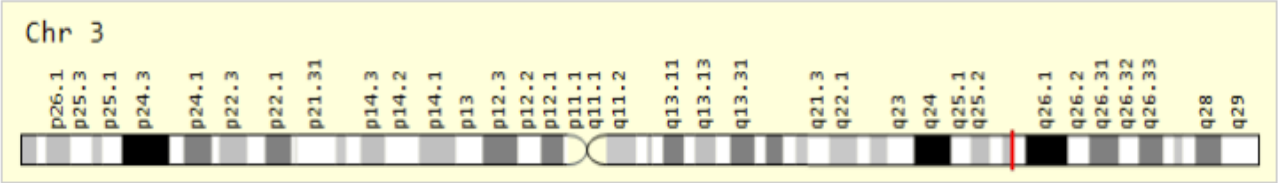

Figure 1.12 : Genomic location for RARRES-1 gene [158]
(Bands according to Ensemble, locations according to GeneLoc)

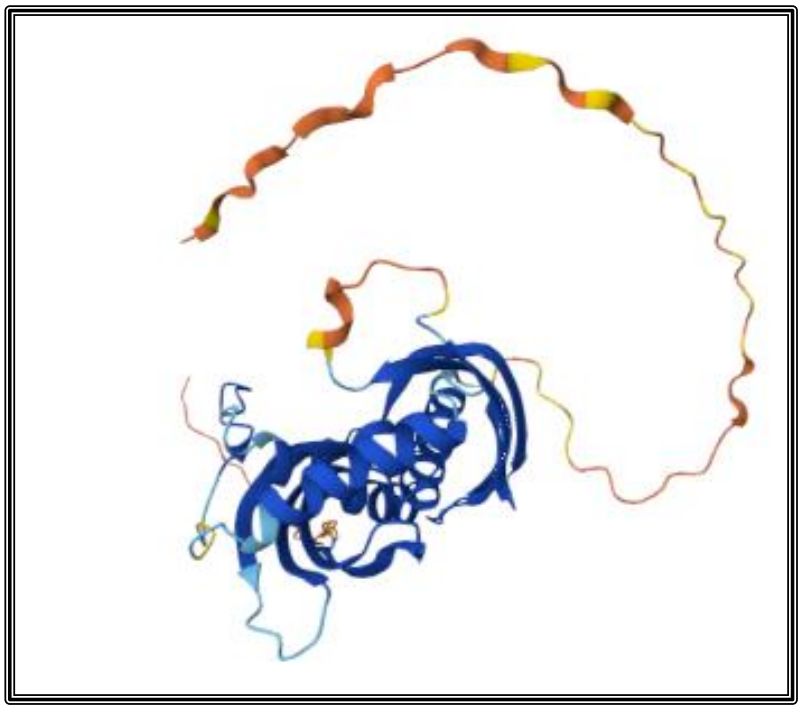

Figure 1.13: Three-dimensional structure for RARRES-1 gene [158]

RARRES-1 is expressed in various normal tissues, including the heart, liver, lungs, prostate and small intestine. The expression of this gene is increased by tazarotene and retinoic acid receptors. Retinoic acid is an active metabolite of vitamin A (retinol).

Enterocytes (cells in the intestinal lumen) absorb dietary retinyl esters and carotenoids. After esterification, they are packed (lipoprotein complexes) into chylomicrons. These complexes are released into the circulation and form chylomicron remnants. Liver and peripheral cells readily absorb chylomicron remnants **(Figure 1.14)**.

In the liver, most vitamin A is stored as retinyl esters in HSCs. This stored vitamin A can be converted to retinol by hydrolysis. This retinol can be transported to target organs via the formation of a complex with retinol binding protein 4 (RBP4) and transthyretin (TTR). In the liver, retinol circulates between hepatocytes and HSCs [160]. Retinoic acid is involved in the regulation of various physiological processes through retinoid X receptors (RXRs) and retinoic acid receptors (RARs) [161].

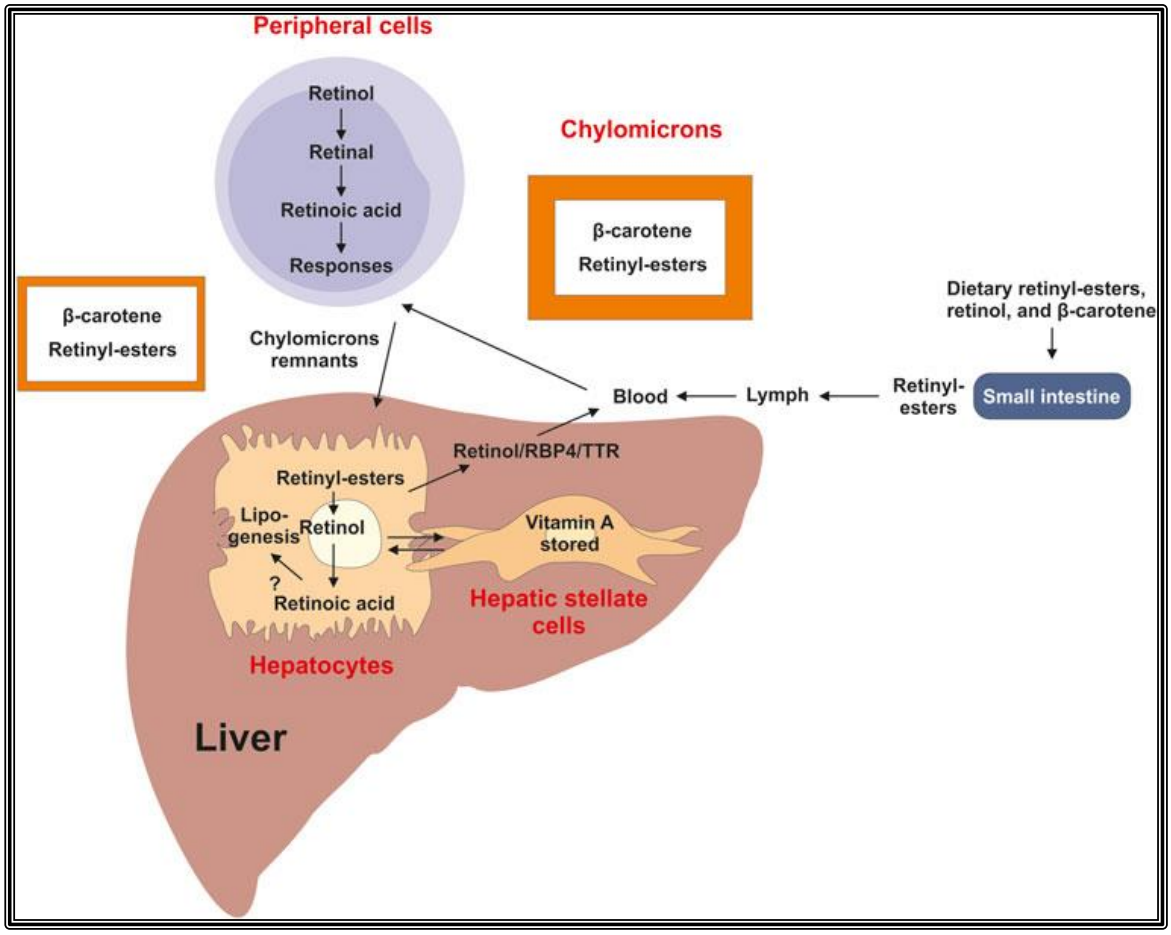

Figure 1.14: Overview of vitamin A, uptake, metabolism and transport [160]. *Retinyl esters are absorbed by intestine lumen and are packed into chylomicron after esterification. Later these chylomicrons are converted into chylomicron remnants. These chylomicrons are absorbed by liver and other peripheral tissues for processing.*

Retinol, its precursors and metabolites are important for normal cell growth [162], vision [163] and prevent developmental defects [164]. A decrease in RARRES-1 expression has been observed in several types of cancers, including prostate, nasopharyngeal, breast, colon and leukaemia [174]. RARRES-1 is among the most methylated loci in various cancers [180] and is recognized as a tumour suppressor gene [181, 182]. Restoring the expression of RARRES-1 has been linked to hypomethylation of the gene, indicating the potential role of hypermethylation of RARRES-1 in cancer development [174].

In prostate cancer, RARRES-1 induces autophagy, reduces the level of rapamycin, and increases the level of sirtuin 1, which regulates the energy balance [183]. Additionally, RARRES-1 has been implicated in autophagy in cervical cancer and is noted as one of the most methylated genes [184, 185]. The specific role of RARRES-1 in liver fibrosis remains unclear and is an area I aim to explore in my project.

1.15 Hypothesis

During liver injury, the levels of TGF-β increase, leading to RARRES-1 silencing in stellate cells. This process initiates a cascade of events, including mitochondrial dysfunction, the generation of reactive oxygen species (ROS), autophagy and energy release. All these processes activate HSCs and increase matrix deposition that leads to fibrosis.

In this study, I investigated the effect of RARRES-1 activation as a treatment option for liver fibrosis. While investigating this phenomenon in detail, I hypothesized that restoring RARRES-1 expression would reverse liver fibrosis through the downregulation of energy release.

1.16 Aims

I test my hypothesis through four aims.

Aim 1: To explore whether RARRES-1 attenuates liver fibrosis in activated hepatic stellate cells.

Aim 2: To explore whether RARRES-1 regulates fibrosis by regulating mitochondrial function.

Aim 3: To explore whether RARRES-1 regulates fibrosis by regulating ROS generation.

Aim 4: To explore whether RARRES-1 regulates fibrosis by regulating autophagy.

Chapter Two: Material and Methods

2.2 Materials

The materials used in this thesis were obtained from the sources listed in **Tables (2.1-2.6)**.

Table 2.1: The origins of the commercial kits used in this investigation

REAGENTS or RESOURCE	Source / Identifier
QIAGEN Plasmid Maxi Kit	QIAGEN (12163)
FavorPrep Tissue Total RNA Purification Mini Kit	Favorgen Biotech Corp (FATRK001-2)
DCFDA Cellular ROS Detection Assay Kit	Abcam (ab113851)
TMRE-Mitochondrial membrane potential kit	Abcam (ab113852)
Premo Autophagy Tandem Sensor RFP-GFP-LC3B	Thermofisher (P36239)
MitoSOX™ Mitochondrial Superoxide Indicators	Thermofisher (M36008)
MitoTEMPO	Sigma-Aldrich SML0737
QuantiNova™ SYBR Green PCR Kit	QIAGEN (208152)

Table 2.2: The source of the primers and probes used in this thesis

Primers and Probes	Source / Identifier
GAPDH (VIC)	Thermofisher scientific (4448489)
RARRES1 (FAM)	Thermofisher scientific (4331182)
Human CTGF(R)	IDT (817704)
Human CTGF (F)	IDT (817703)
Hu COL1A1 (R)	IDT (103321564)
Hu COL1A1 (F)	IDT (103321563)

Human Alpha-SMA (R)	IDT (103285469)
Human Alpha-SMA (F)	IDT (103285468)
Human GAPDH (R)	IDT (103285473)
Human GAPDH (F)	IDT (103285472)
Hu-RARRES1 (R)	IDT (99633348)
Hu-RARRES-1 (F)	IDT (99633347)

Table 2.3: Primers sequences

Primers	Sequence
Human CTGF(R)	5`-GCTCGGTATGTCTTCATGCTG
Human CTGF (F)	5`-AGCTGACCTGGAAGAGAACAT
Hu COL1A1 (R)	5`-TCATCTCCATTCTTTCCAGG-3
Hu COL1A1 (F)	5`-GCTATGATGAGAAATCAACCG-3
Human Alpha-SMA (R)	5`-ATGCCATG TCTATCGGGTACTT-3
Human Alpha-SMA (F)	5`-GACAATGGCTCTGGGCTCTGTAA-3
Human GAPDH (R)	5`-GGCCATCCACAGTCTTCTGAG-3
Human GAPDH (F)	5`-CCTGCACCACCAACTGCTTA-3
Hu-RARRES1 (R)	5`-CTTCTTCTGCTGTCTGTA-5
Hu-RARRES-1 (F)	5`-CATTCACTTGGTCTGGTA-3

Table 2.4: The source of the reagents used in this thesis

REAGENTS or RESOURCE	Quantity	Source / Identifier
Bafilomycin A1 from streptomyces	2uG	Sigma (B1793)
rmTGF-B1	5uG	R & D systems (B1793)
rhTGF-B1	5uG	R & D Systems (7754-BH)
MAP1LC3A Plasmid	10uG	Origene (RC220473)
ATG-12 Plasmid	10uG	Origene (RC202012)
Carbonyl cyanide 3-chlorophenyl hydrazone	100mg	Merck (C2759)
MRT68921 dihydrochloride	5MG	Sigma Aldrich (SML 1644-5 MG)
Chloroquine diphosphate salt	25G	Sigma Aldrich (C6628)
siRNA human NOX4	20UG	Sigma Aldrich (EHU064361)
L-Glutathione reduced	5g	Sigma Aldrich (G6013)
Prolong™ Glod antifade reagent with DAPI	10mL	Thermofisher (P36931)
Hoechst	5mL	Thermoscientific (33342)
Triton X-100	500mL	Sigma (9002-93-1)
Retinoic acid	5mg	Sigma (H7779)
Tween® 20	500mL	Sigma (P1379)
RARRES1 Plasmid	10µg	Origene (RC205143)
pCMV6-Entry Vector	10µg	Origene (PS100001)

Table 2.5: The source of the antibodies/stains used in this thesis

REAGENTS or RESOURCE	Quantity	Source / Identifier
Anti-mRARRES1	100 µg	R & D systems (AF4657)
Anti-hRARRES1	100 µg	R & D systems (AF4255)
Tomm20	100 µl	abcam (Ab186735)
Lysotracker red DND-99	20 X 50 µl	Thermofisher (L7528)
Bodipy	10 mg	Invitrogen (D3922)
Goat anti-Rabbit IgG (H+L) cross-adsorbed Secondary antibody, Alexafluor 546	1 mg	Thermofisher scientific (A-11010)
Mitofusion (MFN1)	0.1 mL	Thermofisher (MA524789)
ATP- Synthase beta Polyclonal	100 µl	Thermofisher (PA581952)
Anti-Collagen I	100 µl	abcam (ab34710)
Anti-Alpha-Smooth Muscle Actin	100 µl	Invitrogen (MA5-11547)
Anti-LC3B	100 µl	abcam (ab192890)
Anti-APG5L/ATG5	100µl	abcam (ab108327)
Anti-ATG-12	100 µl	abcam (ab155589)
Anti-Beclin 1	100 µl	abcam (Ab62557)

Table 2.6: Software

NAME	LINK
ImageJ	BD https://imagej.nih.gov/ij/
GraphPad Prism 7	http:www.graphpad.com/scientificsoftware/prism/
StepOne Software v2.3	Applied Biosystems

2.2 Methods:

2.2.1 Cell Culture & Experimental Plan

The human hepatic stellate (HSC) immortalised cell line, LX-2 were kindly provided by Dr Scott L. Friedman, Icahn School of Medicine, Mount Sinai, New York, USA. The mouse hepatic stellate cells (HSC) immortalised cell line, JS-1 were supplied by Kerafast Inc.

According to the previously described protocol [165], cell cultures were maintained in incubator where temperature was maintained at 37°C and CO_2 concentration was maintained at 5%. Cells were maintained by changing media every 2 days. When cells were 80-90% confluent, splitting was done in 1:2-1:3 ratio. Dulbecco's Modified Eagle Medium (DMEM) with 10% heat inactivated fetal bovine serum (10% FBS DMEM) was used to grow the cells. For passaging cells, washing with PBS was done twice and then 1.5mL of TrypLE was added and cells were incubated in the incubator. After trypsinisation HSCs were resuspended in media (4 mL). 3 X 10^5 HSCs were seeded in 12 well plate in 1000µL of growth media (10% FBS DMEM). Starvation was done with FBS free DMEM medium for 14-18 hours. The following experiments were undertaken.

2.2.1.1 RARRES-1 activation

Expression of RARRES-1 was increased using genetic and pharmacological activation.

2.2.1.2 Pharmacological activation of RARRES-1

Pharmacological expression of RARRES-1 was done by treating HSCs with all trans-retinoic acid at treatment dose of 1 µM/ml.

2.2.1.3 Genetic activation of RASSES-1

Genetic activation of RARRES-1 was done by transfecting HSCs cells with RARRES-1 plasmid, FuGENE and optimum, as detailed below **(Figure 2.1)**. Transfection was done according to the previously described protocol [165]. Briefly, cells were transfected with

either RARRES1 plasmid or empty vector using FuGENE HD (Promega) for 24 hours **(Figure 2.2)**.

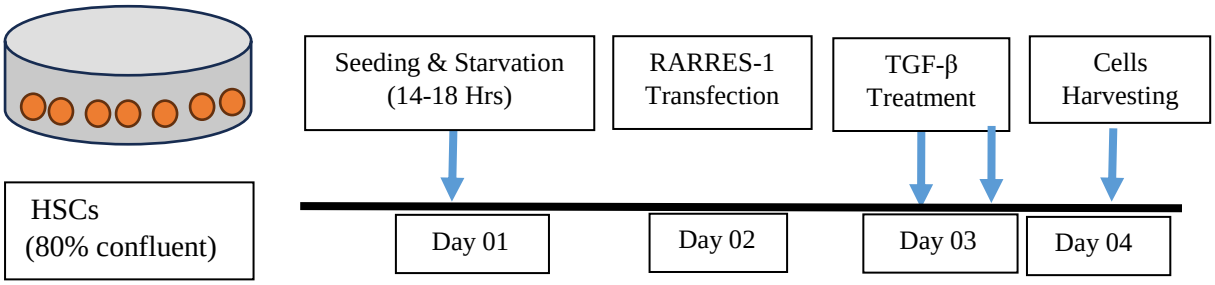

Figure 2.1: Genetic activation of RARRES-1 with RARRES-1 transfection in HSCs

2.2.1.4 Treatment with TGF-β

After 24 hours of transfection step or the pharmacological activation of RARRES-1, media was changed and TGF-β or vehicle was added at the treatment dose of 5 ng/ml. Harvesting was done after 24 hours of TGF-β treatment **(Figure 2.2)**. HSCs were harvested for further experiment [166].

2.2.2 mRNA Expression

2.2.2.1 RNA Extraction

The extraction of RNA was performed according to previously described method [165, 167, 168]. To extract RNA, sterile PBS was used to wash (2X) HSCs. FARB Buffer (350µl) plus β-Mercaptoethanol (3.5µl) was added to HSCs and incubation was done at RT (5 min). HSCs were separated from the well using cell scraper. Cells were vortexed vigorously for 1 min for resuspension. Filter column was placed on collection tube. The mixture was transferred to it (filter column + collection tube). Centrifugation was done at 16,000 Xg for 2 min. Supernatant was transferred to another microcentrifuge tube. 70% ethanol (350µl) was added to the tube (Filter column + collection tube). The mixture was then transferred to FARB mini

column. Centrifugation (@14,000 rpm) was done for 1 min. The pass-through liquid was discarded. Then final washing was done.

First wash was done with wash buffer 1 (500 µl), followed by centrifugation was done @ 16,000 Xg (1 min). Liquid (pass-through) was discarded. Another washing was done with buffer 2 (750 µl). Then centrifugation (@16,000 Xg) was done for 1 min. Another centrifugation (3 min) was done to dry the FARB mini column. The columns were transferred to the new collection tubes for elution step. For elution of RNA, RNase free water (50 µl) was added to the centre of mini column. Incubation (1 min) and then centrifugation (@14,000 rpm) was done for 1 min. RNA concentration was determined by using NanoDrop (spectrophotometer) that measures optical density at 260nm and 280nm. The purity of the samples was confirmed along with RNA measurement.

2.2.2.2 cDNA synthesis

The synthesis of cDNA was done according to the previously described protocol [167]. RNA extracted in the previous experiment was utilized to synthesize cDNA using enzyme M-MLV reverse transcriptase kit by Promega. RNA yield was high >200 ng/ul, RNA concentration was normalized in all samples to > 50 ng/ul with 20 ul final volume.

About 0.5 µl of dNTPs, 0.5 µl random primers and 6.5 µl of RNA sample were added to the 500 µl of microcentrifuge tube. RNA Samples were melted by incubating on thermocycler at 70ºC (5 min). Samples were then cooled directly on ice. Reaction premix was prepared by adding 2.0 µl 5X buffer and 0.5 µl RT enzyme. Then 2.5 µl reaction premix was added to priming premix. Further incubation was done at 25ºC and then at 37ºC (for 10 min and 1 hr respectively). cDNA samples were chilled on ice and diluted by 1:10 in Accu H_2O. The storage of cDNA was done at -20ºC.

2.2.2.3 Real-Time Quantitative PCR (RTqPCR)

The Real time quantitative PCR was performed according to the previously described protocol [167, 169]. Experiments were done in three replicates. CT values were used to measure the expression of mRNA. Samples were normalized to GAPDH by calculating ΔCT = CT for GAPDH – CT for Sample cDNA and then expressed as $2^{-\Delta CT}$. RTqPCR was done using QIAGEN PCR kit. Master mix was prepared for all wells by adding Syber Green (10 µl), 2 µl of ROX, forward (0.3 µl) and reverse (0.3 µl) primes and H_2O (4.4 µl). Master mix (17 µl) + cDNA (3 µl) was added to PCR plate. Melting temperature was set at 95°C (10 min) for all primers and reactions were run for 40 cycles.

2.2.3 Western Blot Analysis

2.2.3.1 Extraction of protein Lysates

The extraction of protein was undertaken according to the previously described protocol [165]. For extraction of protein lysates, HSCs were washed with 2 times with ice-cold PBS. Next, cells were treated with RIPA buffer (100 µl). Further incubation of cells was done on ice (15 min). Cell scrapper was used to remove and collect the lysate on one side of the plate. Using 200 µl pipette, the lysate was moved to a microcentrifuge tube. The lysate was centrifuged @ 13000rpm at 4ºC for 10 min. The supernatant was moved to another tube. The concentration of proteins was determined using Bio-Rad, DC protein Assay Kit. Bovine serum albumin (BSA) was used as a standard. The storage of protein was done at -80ºC.

2.2.3.2 Western Blot

The protocol was previously prescribed [169]. Proteins were fractionated by SDS-PAGE. Proteins were transferred to a membrane called polyvinylidene difluoride membrane (PVDF membranes). After that, PVDF membranes were blocked with the blocking agent ((5% skim milk in TBST (150mM NaCl, 50 mM Tris, 0.05% Tween 20, pH 7.4)) for 1 hour at RT. PVDF membranes were washed 2X with TBST. Then incubation of PVDF membrane was

done with the primary antibodies overnight at 4ºC. Antibodies were diluted in 5% skim milk in TBST. After incubation, PVDF membrane was washed three times for (10 min each wash) with TBST. Following washing step, PVDF membrane was incubated in the dark with secondary antibodies for 1 hour at RT. Further TBST washing of blots was done 3X. Finally, blots were developed with SuperSignal West Pico PLUS Chemiluminescent and SuperSignal West Femto Maximum Sensitivity Substrates (Life Technologies, Australia). ChemiDoc touch imaging system by Bio-Rad, Herculs, CA was used to scan the membranes.

2.2.4 ELISA

p62 protein levels were measured by using Enzyme-Linked-Immunosorbent Assay, as described by manufacturer (Abcam).

2.2.5 Immunofluorescence Assay

The protocol was previously described in [169]. After the fixation and permeabilization of cells, as a blocking step, cells were incubated in Cas-Block for 1h at RT. Then, the primary antibody was incubated to the cells. Cells were then incubated with the secondary antibody. Examination of coverslips was undertaken using the florescence microscope (with 20X, 40 X and 60 X objectives).

2.2.6 Cellular reactive oxygen species (ROS) assay

The protocol was previously prescribed in [169]. Cellular ROS Assay kit (Abcam, ab113851) using Redox sensitive dye DCFDA/H2DFDA was used to measure intracellular ROS. Fluorescence intensities were measured using Deltavision microscope. Fluorescence was quantified using Image J software.

2.2.7 TMRE Mitochondrial membrane potential

Live cell imaging was performed according to previously prescribed protocol (Abcam, 113852). HSCs were transfected of with RARRES-1 plasmid and EV for 24 Hrs. TGF-β was further administered to HSCs (24 hours). Effect of mitochondrial membrane potential inhibitor was also observed by treating cells with Carbonyl cyanide3-chlorophenyl hydrazone (CCCP) by adding 2 hours before TGF-β. Last day, LX-2 cells were treated with TMRE stain for about 30 min. Nucleus was stained using Hoechst dye and were observed under Deltavision microscope. Fluorescence intensities were measured by live cell imaging using confocal and Deltavison microscope.

2.2.8 Autophagic flux

Effect of RARRES-1 plasmid was evaluated by the following method prescribed by the manufacturer (Thermofisher (P36239)). HSCs were seeded in 4 chambered slides in 10 % FBS+DMEM media. Next day, Transduction was done by adding 25 µl of BecMam to each well. On Day3, Transfection with RARRES-1 plasmid and EV for 24 hours in serum free media to do starvation. On Day 4, profibrotic drug TGF-β was further administered to HSCs (24 hours). On Day 5, live cell imaging was done using Deltavision microscope to measure autophagic flux according to manufacturer's protocol.

2.2.9 Electron microscopy

The protocol was previously prescribed in [169]. Cells were fixed in Karnovsky's fixative for 4Hrs and were then cute into sections (90nm) using Leica UC6 ultramicrotome using Leica microsystems. Sections were further stained for 10 min in mixture of 2% uranyl acetate and 50% ethanol. Sections were further stained for 4 min in Reynold's lead citrate. Jeol 1400 plus Transmission-Electron-microscope was used at 80KV to examine the grids. Flash camera called Digital sCMOS with "Limitless Panorama" wide area automontage software was used

to collect the images. Mitochondrial and autophagosomal measurements of perimeter, area and length were manually done using image viewer software (Jeol SightX), using free hand tool.

2.2.10 Data Analysis and Statistics

Statistical analysis was undertaken using GraphPad Prism. Comparison was done using student's t-test (for two groups) and One-way analysis of variance (for multiple groups). Statistically significant difference was presumed for p values (****$p \leq 0.0001$, ***$p \leq 0.001$, **$p \leq 0.01$, *$p \leq 0.05$).

Chapter Three:

RARRES-1 attenuates liver fibrosis in activated hepatic stellate cells

3.1 Introduction

Liver fibrosis is a global health problem. Regardless of the aetiology, the progression of nearly every chronic liver condition eventually results in the development of fibrosis, which accounts for more than 90% of liver-related morbidity and mortality [170, 171]. Chronic liver diseases are responsible for approximately 2 million deaths every year and are the 5th most common cause of death in Australia [172]. Unfortunately, no effective drugs are available to treat liver fibrosis [173].

Liver fibrosis is a complex, reversible, and coordinated response to chronic injury, and HSCs are the master cell type responsible for the elaboration of excess matrix during liver fibrosis. The reversal of liver fibrosis has been documented in patients and experimental models [174-176]. Since antifibrotic drugs are unavailable, novel approaches to identify targets that are likely to translate to clinical benefits are urgently needed.

Epigenetics can be avenue to identify novel therapeutic targets for liver fibrosis. Epigenetics refers to heritable phenotype changes that do not involve alterations in the DNA sequence. Epigenetic processes, including DNA methylation, histone modification, noncoding RNAs and chromatin remodelling, occur at various levels. All these epigenetic processes can modulate the access of DNA to the transcriptional machinery of cells; hence, aberrant epigenetic changes lead to the expression of disease-related genes [177], including those involved in the development of chronic liver disease and liver fibrosis [151]. Notably, conventional drugs do not reverse epigenetic modifications. Thus, we require treatment approaches that can specifically target the epigenome to restore the balance of the "Epigenetic Landscape"[178].

DNA methylation is an important epigenetic process. Aberrant DNA methylation causes transcriptional silencing of genes that ultimately affects the cellular pathways implicated in

fibrosis [179]. DNA methylation also plays a major role in HSC differentiation and extracellular matrix accumulation during the liver fibrotic disease process [177].

Epigenome-wide association studies (EWASs) help researchers investigate the associations between a particular phenotype and DNA methylation in a systematic and hypothesis-free manner. Therefore, these studies have contributed to advancing our understanding of the epigenetic basis of various complex diseases [180, 181]. However, the application of EWASs to explore epigenetic changes in liver fibrosis is still limited.

Therefore, we conducted an EWAS to systematically explore epigenetic changes in liver fibrosis. Approximately 88 Northern European patients with metabolic-associated fatty liver disease (MAFLD) with or without advanced fibrosis (stage 3–4) were included. DNA was extracted from blood, and EWAS was performed. Increased methylation of the retinoic acid receptor responder protein 1 gene (RARRES-1) locus was found to be the top hit associated with advanced fibrosis.

Aberrant DNA hypermethylation of the RARRES-1 promoter results in transcriptional silencing of RAARES-1 expression in multiple cancers, including oesophageal cancer, gastric cancer, hepatocellular carcinoma (HCC), and endometrial, breast and prostate cancers [182]. However, the role of RARRES-1 in fibrosis is still largely unknown. Therefore, I opted to investigate its role.

In this chapter, I start by measuring the expression of RARRES-1 in different human tissues and hepatic cells. If RARRES-1 is expressed in the liver, I will explore whether the hepatic expression of RARRES1 is correlated with fibrosis in human, mouse, and *in vitro* fibrotic models. Finally, if this result is confirmed, I will investigate whether RARRES-1 can attenuate liver fibrosis in activated hepatic stellate cells.

3.2 Results

3.2.1 RARRES-1 is expressed in different human tissues and liver cells.

I first assessed the expression of RARRES-1 across panels of human tissues and cells. Although I can identify RARRES1 ubiquitously, RARRES-1 shows different expression levels across various human tissues **(Figure 3.1A)**. Within the liver, RARRES-1 is most strongly expressed in hepatic stellate cells, with approximately 4 and 5 times higher expression compared to different subsets of liver cells namely, Kupffer cells and hepatocytes, respectively **(Figure 3.1B)**.

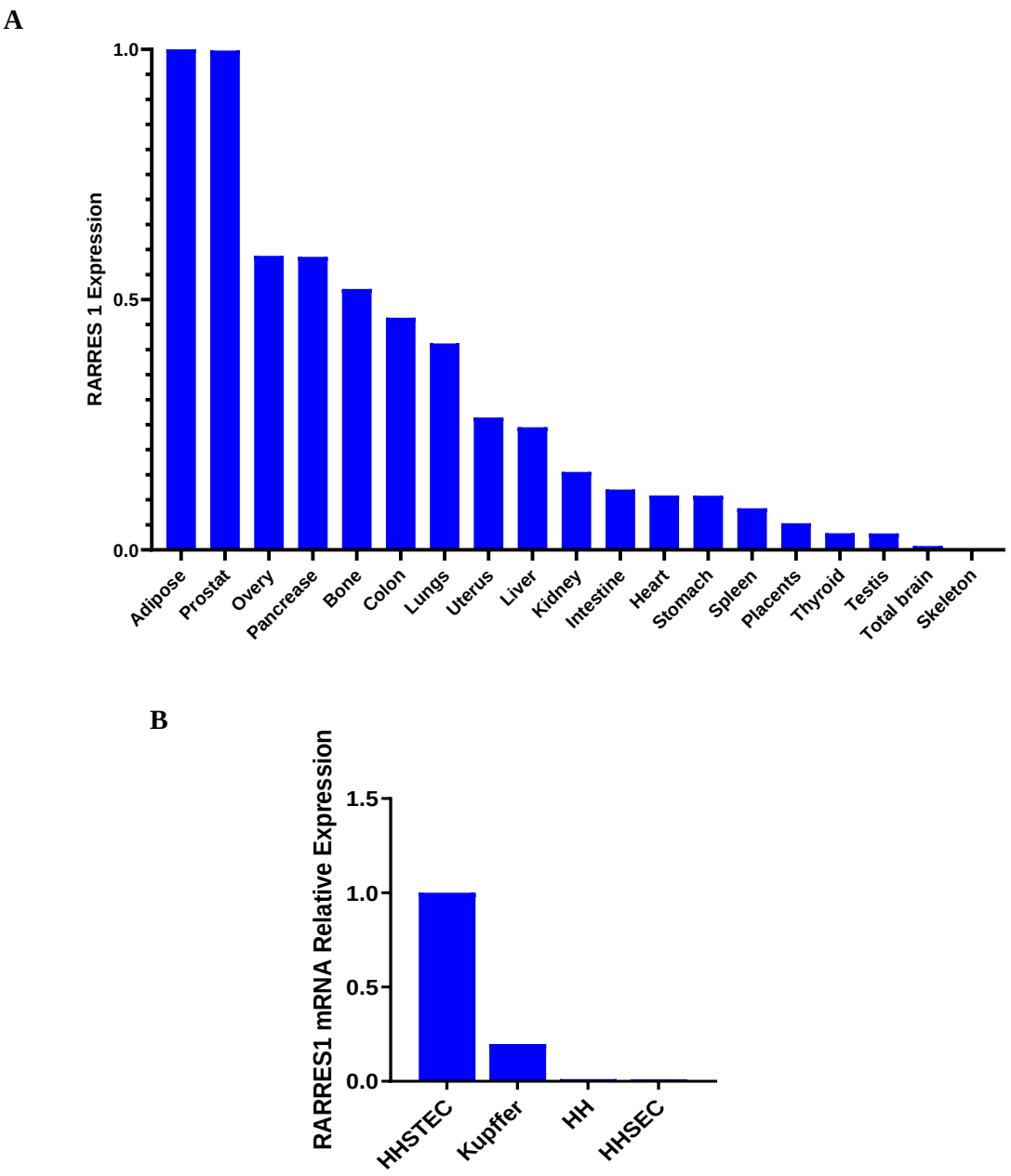

Figure 3.1: RARRES1 expression in various human tissues and cells. mRNA expression in **A)** different human tissues and **B)** human primary hepatic cell types. RARRES-1 mRNA expression levels were assessed by real time polymerase chain reaction (RTqPCR). Glyceraldehyde-3-phosphate dehydrogenase (GAPDH) was used for normalization. The highest CT value was designated as value of 1 for the tissue or cell line. *HHSTEC, human hepatic stellate cells; HH, human hepatocytes; HHSEC, human hepatic sinusoidal endothelial cells.*

3.2.2 RARRES-1 expression is downregulated in patients with viral and non-viral liver diseases

To investigate if the hepatic expression of RARRES-1 is correlated with liver fibrosis. I compared the mRNA expression of RARRES1 in liver samples of 19 patients with hepatitis C and 46 patients of MAFLD related fibrosis with mRNA expression of RARRES-1 in liver samples of 7 healthy individuals. RARRES-1 mRNA was downregulated in HCV and MAFLD patients as compared to healthy control **(Figure 3.2)**.

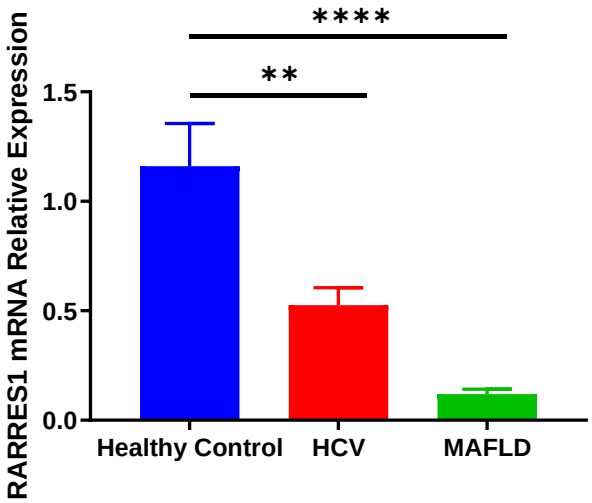

Figure 3.2: RARRSE-1 mRNA expression in cohort of human liver diseases. RARRES-1 mRNA expression was significantly reduced in HCV (n=19) and MAFLD (n=46) patients as compared to healthy individuals (n=7). Values are represented as mean ± SEM. Statistical difference between the groups was measured by 2- tailed Student's t test. *$p \leq 0.05$, **$p \leq 0.01$, ***$p \leq 0.001$, ****$p \leq 0.0001$.

3.2.3 RARRES-1 expression is downregulated in fibrotic mouse models

After confirming RARRES-1 expression is downregulated in cohort of HCV and MAFLD patients, I further investigated, if the expression of RARRES-1 is similarly altered in fibrotic mouse models. Three liver fibrotic mouse models were created in our Lab and utilised for this analysis. These models are CCL4 (Carbon tetrachloride), BDL (Bile duct ligation) and MCD (methionine and choline deficient) mouse models. As depicted in **Figure 3.3A- C,** RARRES-1 hepatic mRNA expression was found to be downregulated consistently with fibrosis across all three models.

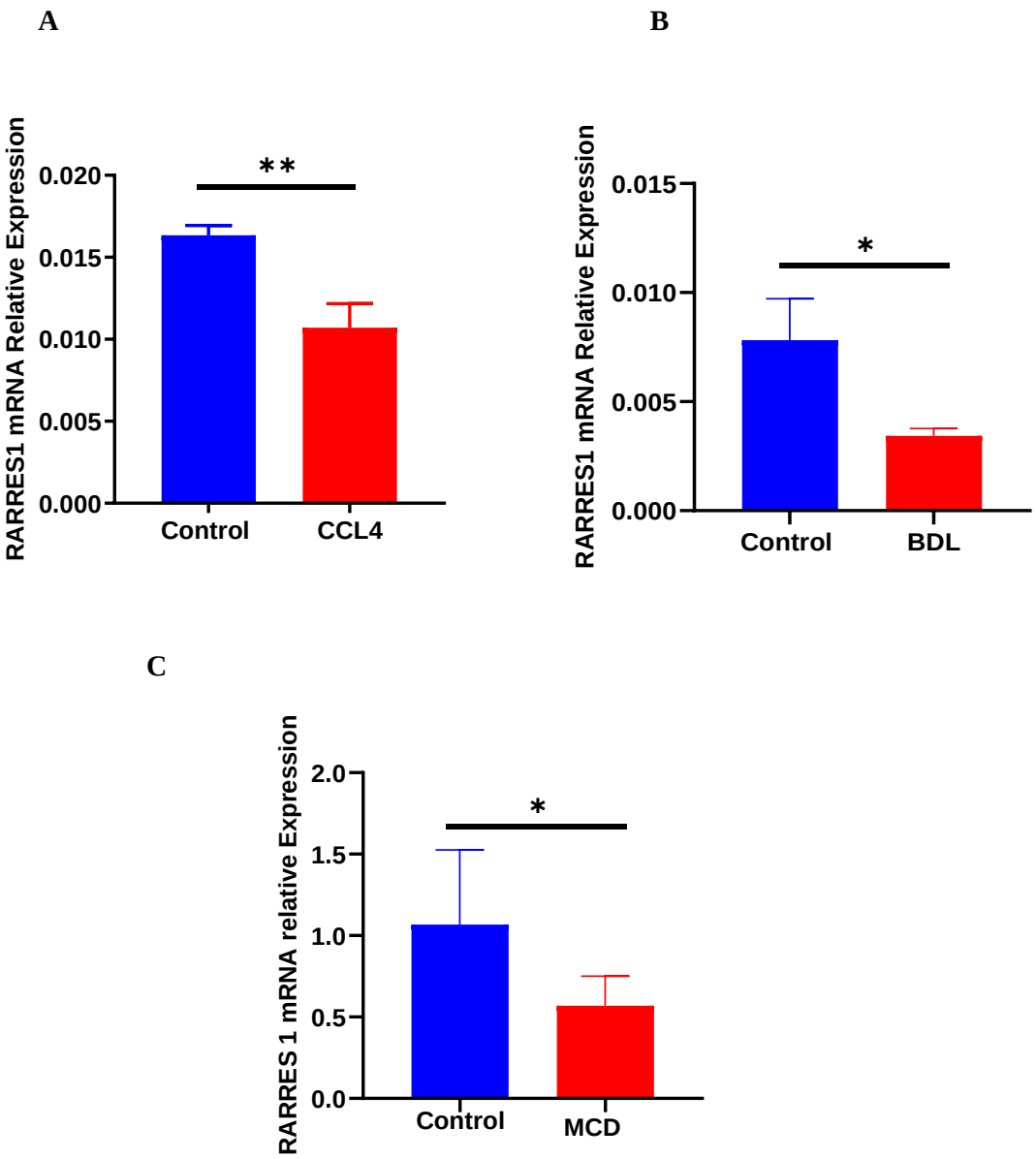

Figure 3.3: RARRES-1 expression is downregulated in fibrotic mouse models. Relative expression of hepatic RARRES-1 mRNA in multiple fibrotic mouse models **A)** in CCL4 model, **B**) in BDL model and **C)** in MCD model (n=3, per each group). Expression of RARRES-1 was analysed by RTqPCR and normalized to GAPDH. Values are represented as mean ± SEM. Statistical difference was measured by 2- tailed Student's t test. *$p \leq 0.05$, **$p \leq 0.01$, ***$p \leq 0.001$A, ****$p \leq 0.0001$.

To further confirm the changes in the expression of RARRES-1 in fibrotic mouse models, the expression of RARRES-1 at protein levels was evaluated in the same three models using Western blot. This analysis has consistently shown a significant reduction in the expression of hepatic RARRES-1 expression in all three models **(Figure 3.4)**.

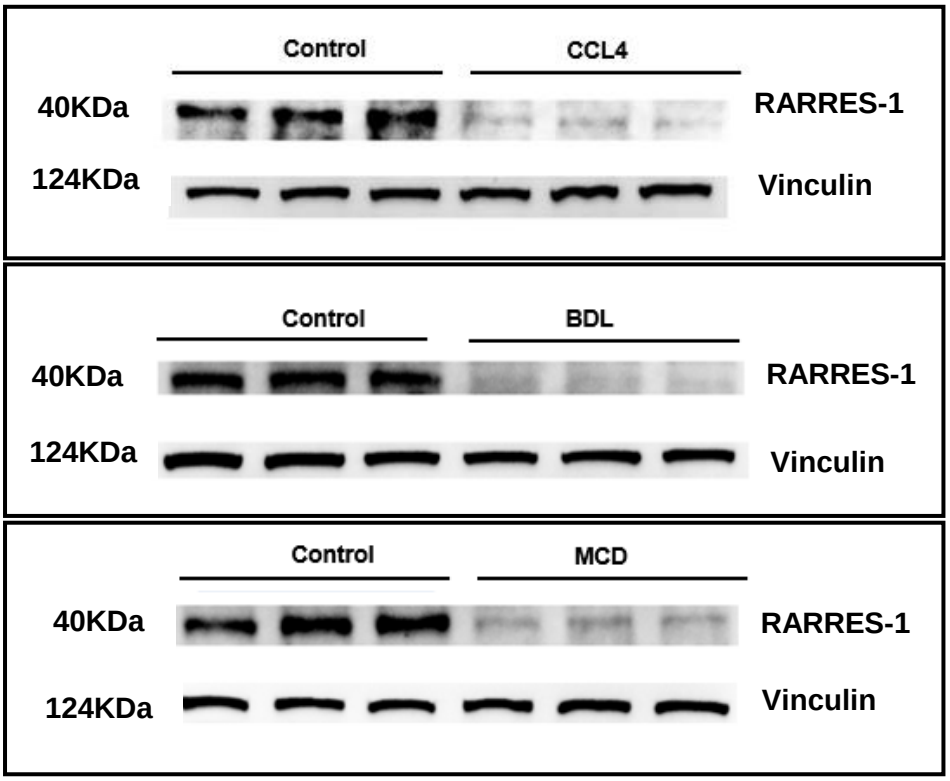

Figure 3.4: RARRES-1 protein expression in multiple fibrotic mouse models (CCL4, BDL & MCD). Western blot analysis has shown reduction in the expression of RARRES-1 in CCL4, BDL and MCD fibrotic mouse models. Expression of RARRES-1 was normalized to vinculin.

Lastly, for further confirmation, the expression of RARRES-1 was determined using immunohistochemistry in CCL4 and BDL mice. IHC images and subsequent quantification using image J have demonstrated reduction in the expression of RARRES-1 protein in both models as compared to control (**Figure 3.5A- C)**.

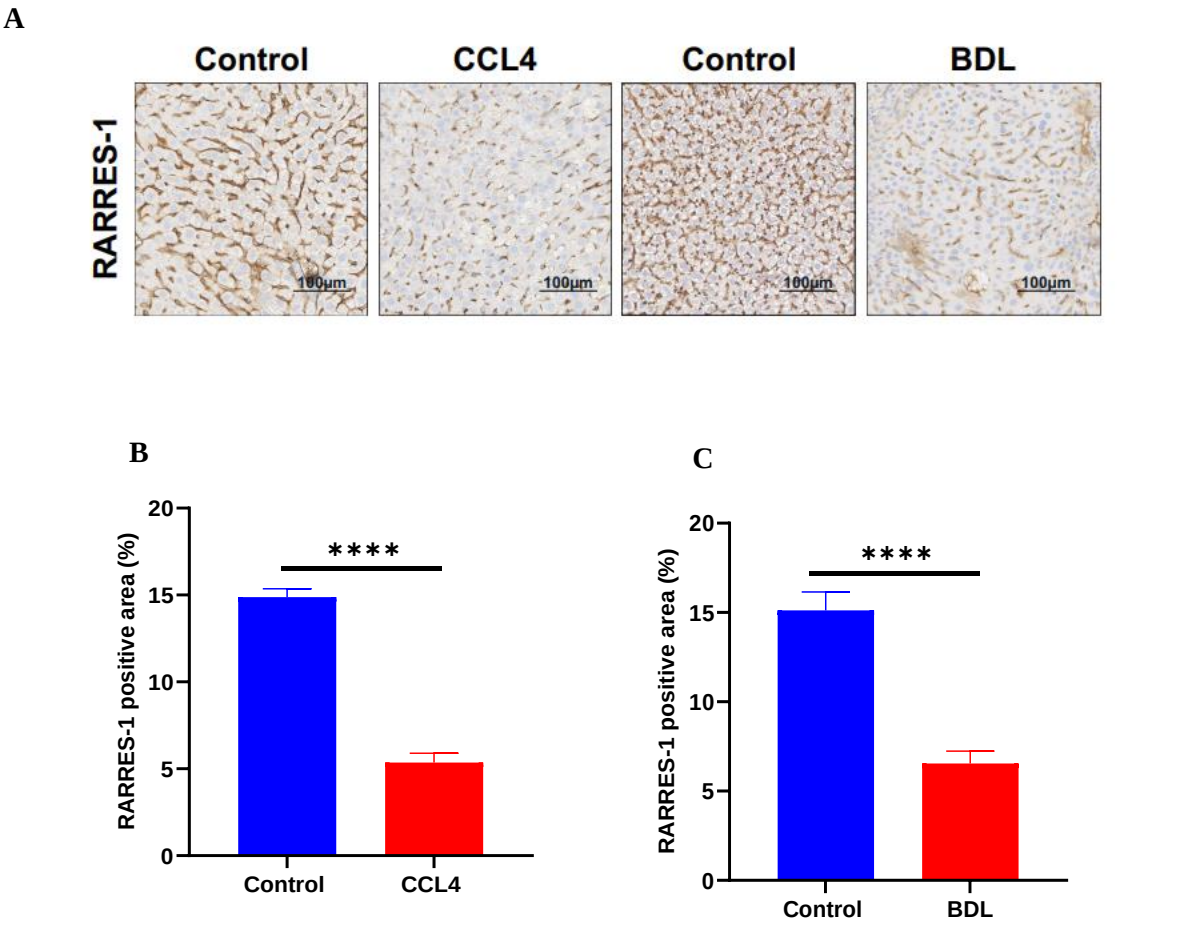

Figure 3.5: RARRES-1 expression at protein level in multiple fibrotic mouse models. A) RARRES-1 immunohistochemistry staining was assessed in liver sections in CCL4 and BDL mice (n=3, per each group). Expression data was derived from average of all animals. RARRES-1 positive area was quantified by image J in **B)** CCL4 and **C)** in BDL mouse models. Expression of RARRES-1 was significantly reduced in both CCL4 & BDL. Values are represented as mean ± SEM. Statistical difference between the groups was measured by 2- tailed Student's t test. *$p \leq 0.05$, **$p \leq 0.01$, ***$p \leq 0.001$A, ****$p \leq 0.0001$.

3.2.4 Expression of RARRES-1 mRNA is downregulated with the activation of human hepatic stellate cells

As I demonstrated that RARRES-1 is highly expressed in hepatic stellate cells (HSCs). I then thought to explore the dynamic of RARRES-1 expression during the course of culture-dependent activation of human primary stellate cells (HSCs). RARRES-1 mRNA expression was found to be reduced with activation of human primary HSCs, further implying a potential role for RARRES-1 in fibrosis **(Figure 3.6)**.

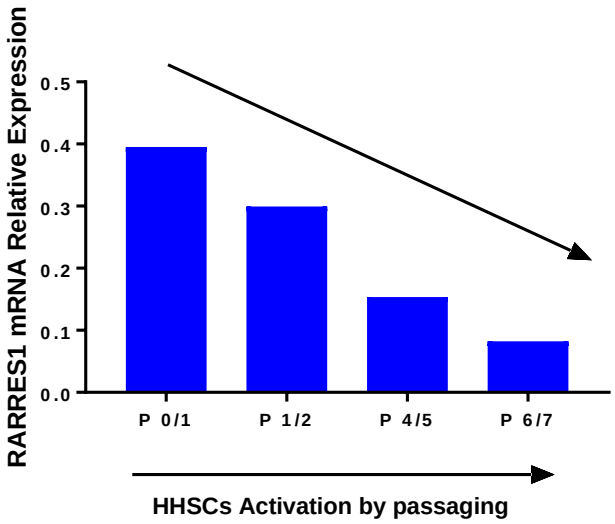

Figure 3.6: Transcriptional silencing of RARRES-1 expression during the course of culture-dependent activation of human primary stellate cells. HHSC cells were cultured and harvested according to the indicated passage number and RARRES-1mRNA expression was quantified using RTqPCR.

3.2.5 Expression of RARRES-1 is downregulated in *in-vitro* fibrotic models

Further, I investigated the changes of expression of RARRES-1 in *in-vitro* fibrotic model induced by TGF-β, a classical profibrotic cytokine that triggers the expression of fibrogenic characteristics of HSC. Human HSC (LX-2 cells) were treated with TGF-β for 24 hours with or without TGF-β inhibitor (LY2109761, a specific inhibitor of TGF-β receptor type I/II).

This experiment has shown that the RARRES-1 expression was repressed in LX-2 cells treated with TGF-β, an effect which was reversed by TGF-β inhibitor, indicating the specificity of the effect **(Figure 3.7)**.

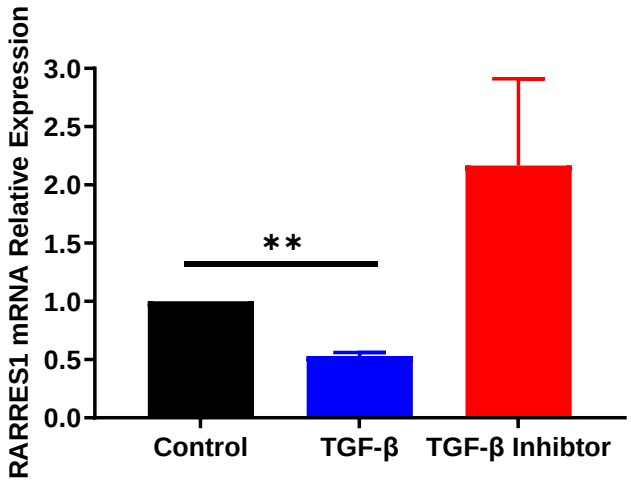

Figure 3.7: Relative Expression of RARRES-1 mRNA in LX-2 *in-vitro* models. RARRES-1 mRNA expression in TGF-β and TGF-β inhibitor treated LX-2 cells (n=2, per each group). Expression of RARRES-1 was normalized to GAPDH. Values are represented as mean ± SEM. Statistical difference between the groups was measured by 2-tailed Student's t test. *$p \leq 0.05$, **$p \leq 0.01$, ***$p \leq 0.001$A, ****$p \leq 0.0001$.

3.2.6 RARRES-1 expression attenuates fibrosis in myofibroblasts

After confirmation that RARRES-1 correlates fibrosis, I then moved on to investigate if RARRES-1 could attenuate fibrosis. To address this, I increased the expression of RARRES-1 using two different approaches, pharmacological and genetic activation.

3.2.6.1 Pharmacological activation of RARRES-1 attenuates fibrosis in myofibroblasts

Pharmacological activation was done by treating LX-2 cells with retinoic acid p-hydroxyanilide. Retinoic acid is vitamin A acid analogue, that increases the expression of RARRES-1 among multiple other effects [183].

Firstly, I confirmed that retinoic acid increases the expression of RARRES-1 in LX-2 cells using RTqPCR **(Figure 3.8)**.

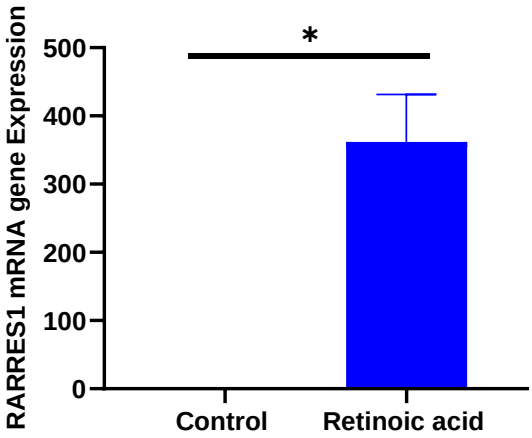

Figure 3.8: Retinoic acid treatment increases the expression of RARRES-1 in LX-2 cells. LX-2 cells were treated with retinoic acid and RTqPCR, for the measurement of RARRES-1 mRNA was undertaken according to standard protocol (n=2). Expression of RARRES-1 mRNA was normalized to GAPDH. Values are represented as mean ± SEM. Statistical difference between the groups was measured by 2- tailed Student's t test. *$p \leq 0.05$, **$p \leq 0.01$, ***$p \leq 0.001$A, ****$p \leq 0.0001$.

After confirmation that retinoic acid treatment increases the expression of RARRES-1, I further moved to investigate if this overexpression of RARRES-1 modulates the expression of fibrotic markers. To evaluate this, I treated the cells with retinoic acid for 48 hours, with and without stimulation with TGF-β for another 24 hours. Cells were harvested and RTqPCR was performed. Results of the experiment has shown that RARRES-1 activation has significantly repressed the expression of fibrotic markers, namely alpha-smooth muscle actin (α-SMA), alpha-1-type I Collagen (COL1A1), transforming growth factor-β (TGF-β) and connective tissue growth factor (CTGF) **(Figure 3.9A-D)**. These results suggest that RARRES-1 activation have antifibrotic effect.

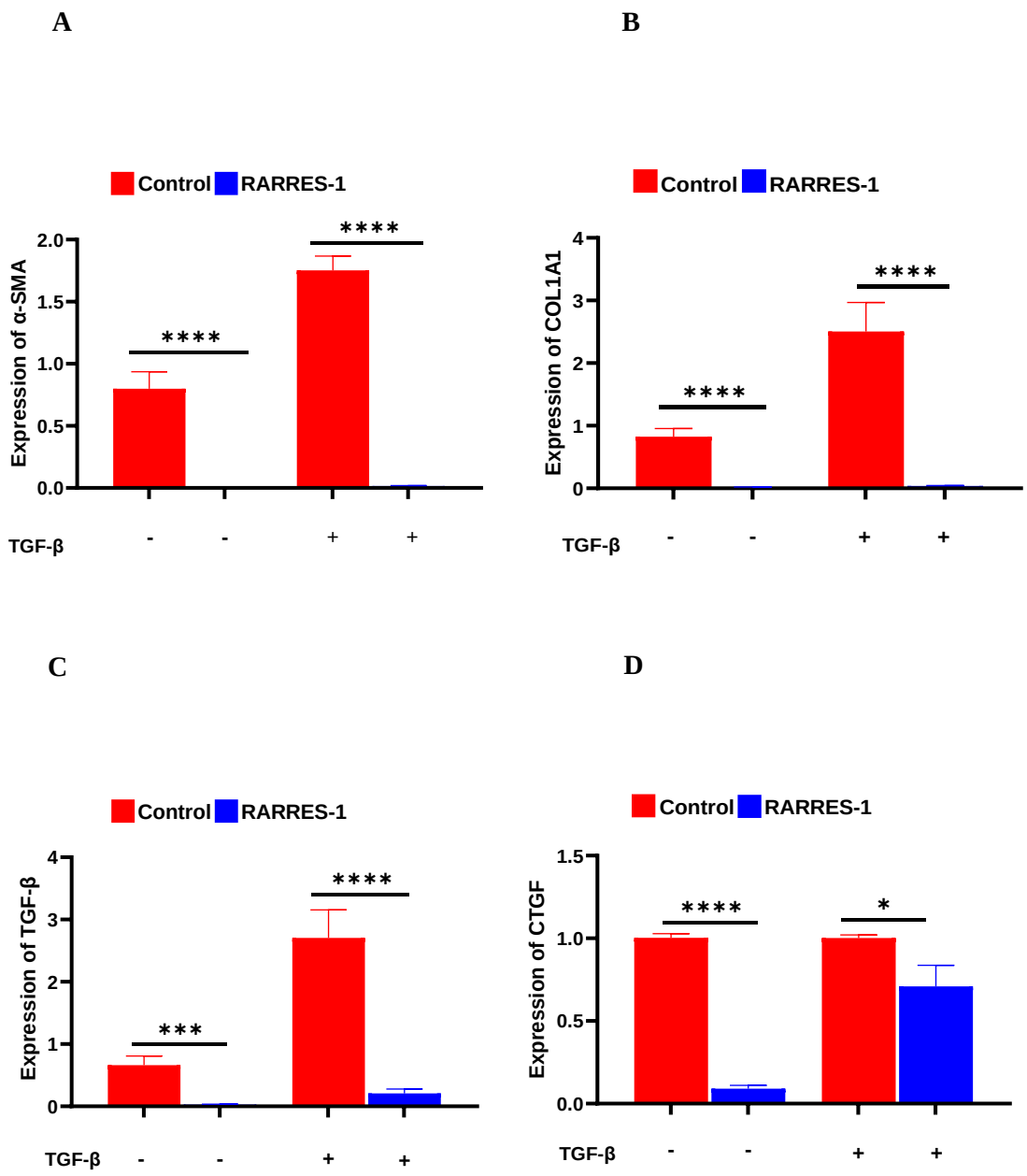

Figure 3.9: Pharmacological activation of RARRES-1 produces antifibrotic effect in LX-2 cells. RARRES-1 activation reduces the mRNA expression of **A)** α-SMA, **B)** COL1A1, **C)** TGF-β and **D)** CTGF (n=3, per each group) using RTqPCR. Expression of RARRES-1 mRNA was normalized to GAPDH. Values are represented as mean ± SEM. Statistical difference between the groups was measured by 2- tailed Student's t test. *$p \leq 0.05$, **$p \leq 0.01$, ***$p \leq 0.001$, ****$p \leq 0.0001$.

3.2.6.2 Genetic activation of RARRES-1 and effect on fibrosis

To confirm that these results are specifically attributed to RARRES1 activation, I then undertook another approach for activation of RARRES-1 in LX-2 cells using RARRES-1 specific plasmid. To this end, LX-2 cells were transfected with RARRES-1 plasmid or empty vector as a control for 48 hours and the efficacy of the transfection was confirmed using Western blot that showed a significant upregulation of RARRES1 compared to control **(Figure 3.10)**.

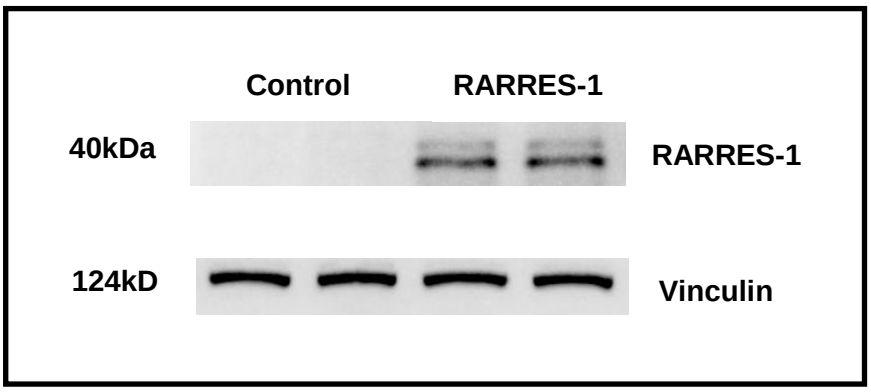

Figure 3.10: RARRES-1 transfection increased the expression of RARRES-1 in LX-2 cells. The expression of RARRES-1 protein was evaluated by Western blot analysis in both RARRES-1 plasmid transfection and control after 48 hours. RARRES-1 protein expression was normalized to vinculin.

Next, I investigated the impact of RARRES-1 on TGF-β induced fibrotic effect. Consistently, RARRES-1 activation was demonstrated to repress the expression of TGF-β induced fibrotic markers, α-SMA (**Figure 3.11A)**, COL1A1 **(Figure 3.11B)** and TGF-β **(Figure 3.11C)**.

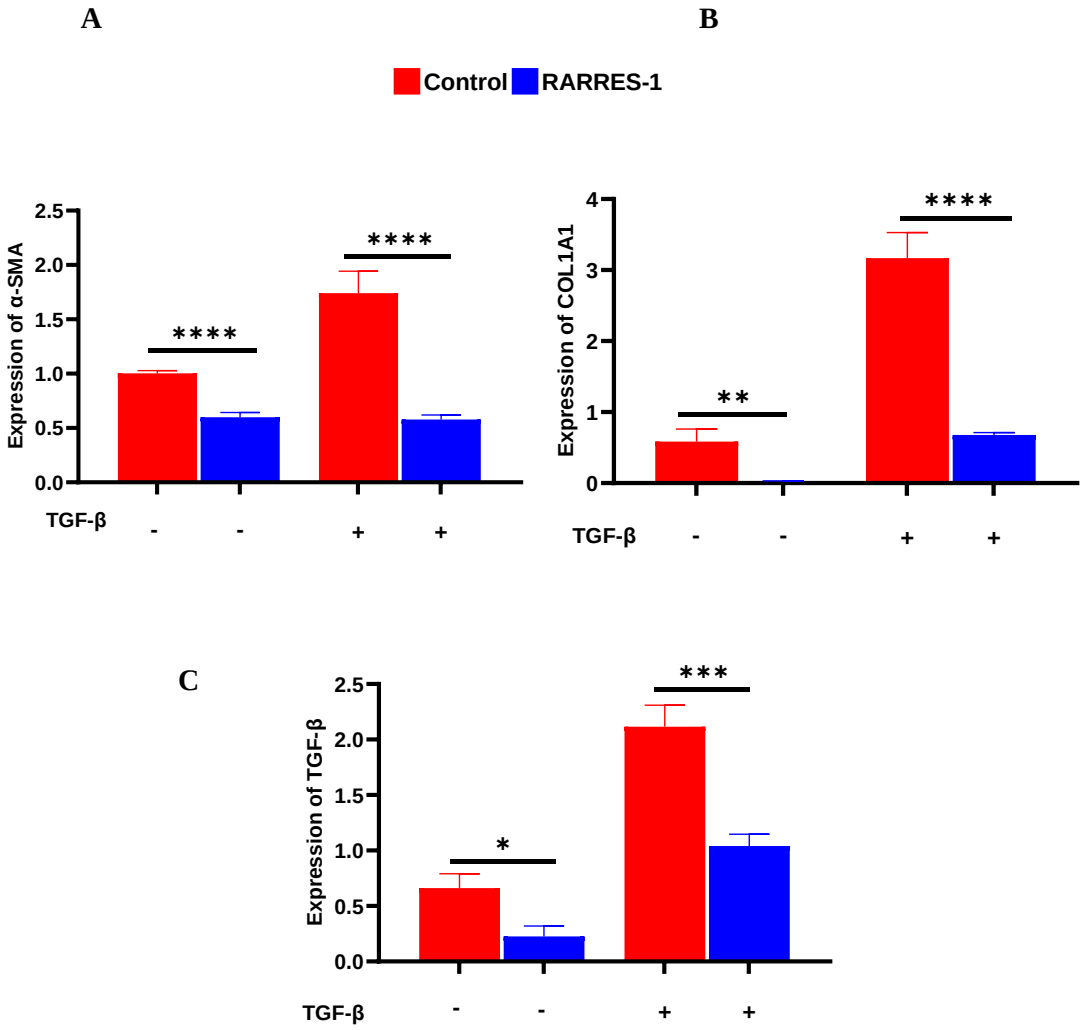

Figure 3.11: Genetic activation of RARRES-1 produces antifibrotic effect in LX-2 cells. RARRES-1 activation reduces the expression of **A)** α-SMA, **B)** COL1A1, and **C)** TGF-β (n=3, per each group) using RTqPCR. RARRES-1 mRNA expression was normalized to GAPDH. Values are represented as mean ± SEM. Statistical difference between the groups was measured by 2- tailed Student's t test. *$p \leq 0.05$, **$p \leq 0.01$, ***$p \leq 0.001$A, ****$p \leq 0.0001$.

For further confirmation, the impact of RARRES1 activation on the expression of α-SMA in LX-2 upon TGF-β treatment was determined by immunofluorescence. Images analysis has shown significant reduction in the expression of α-SMA protein with RARRES1 activation (**Figure 3.12 A-B)**.

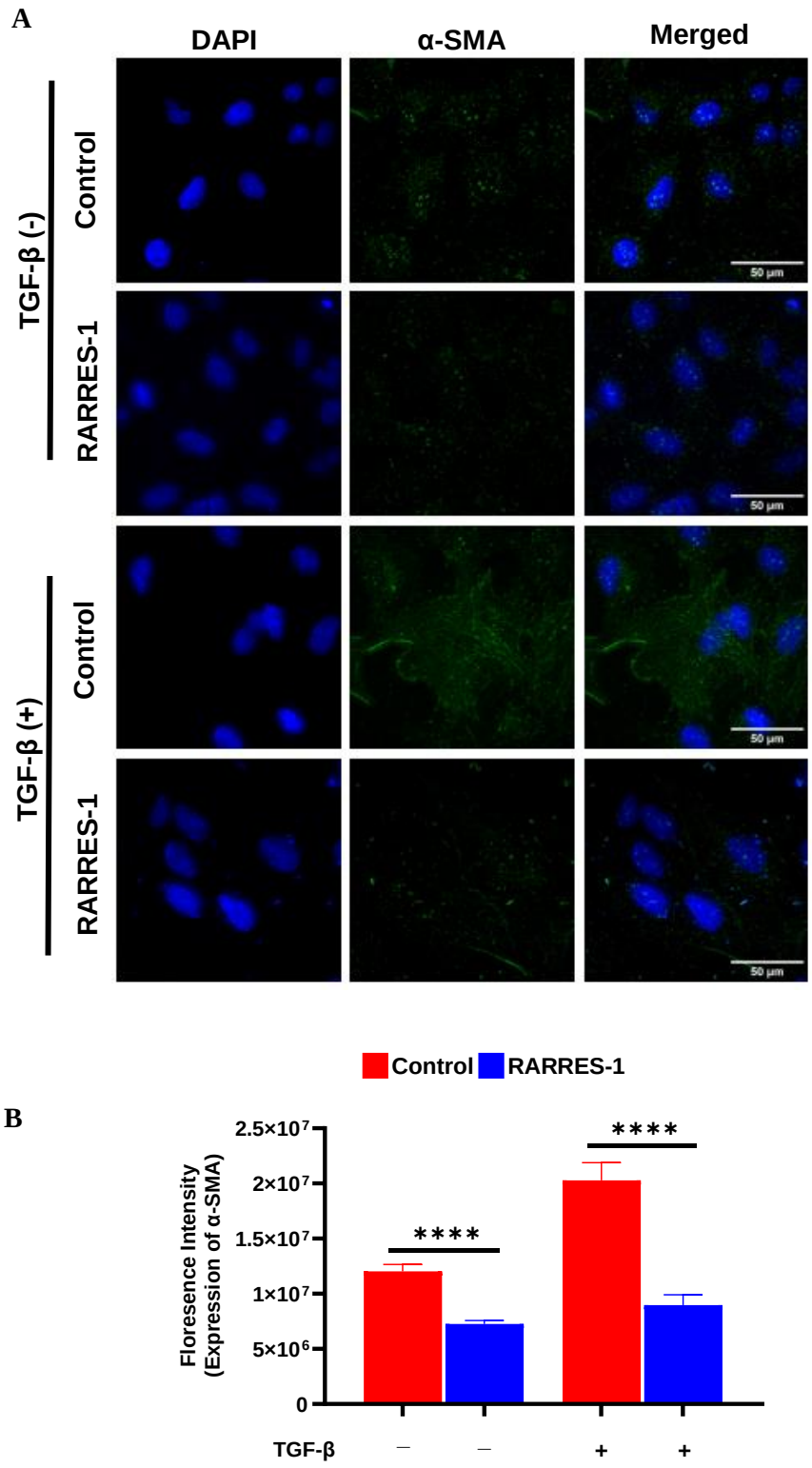

Figure 3.12: Expression of α-SMA in RARRES-1 transfected cells using immunofluorescence in human hepatic stellate cell line. A) Representative images for the expression of α-SMA (n=2). **B)** Quantification of α-SMA protein. Values are represented as mean ± SEM. Statistical difference between the groups was measured by 2- tailed Student's t test. *$p \leq 0.05$, **$p \leq 0.01$, ***$p \leq 0.001$A, ****$p \leq 0.0001$.

3.2.7 RARRES-1 activation has antifibrotic effect in murine hepatic stellate cells

To further confirm that the antifibrotic effect of RARRES-1 is not species dependent. I further extended my study in mice using mouse HSCs cell line (JS-1cell line). JS-1 cells were transfected with RARRES-1 plasmid and stimulated with TGF-β. Immunofluorescence staining for α-SMA was done using Deltavision microscope. Images analysis has shown a significant reduction in the expression of TGF-β induced α-SMA expression in JS-1 cells upon RARRES1 activation (**Figure 3.13 A-B)**. Collectively, these results confirm the antifibrotic effect of RARRES1 in human and mouse models.

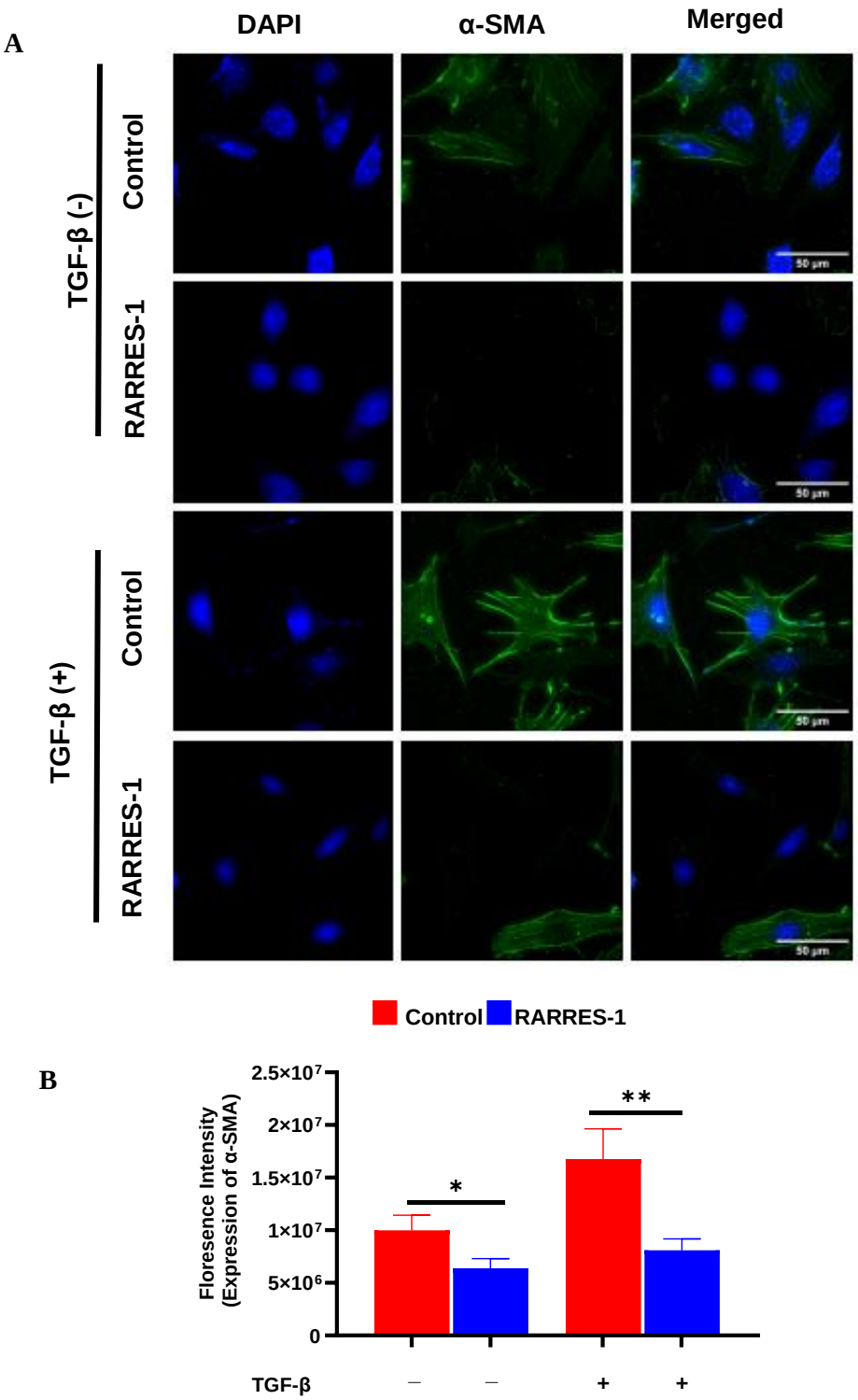

Figure 3.13: Expression of α-SMA in RARRES-1 transfected cells using immunofluorescence in mouse cell line. A) Representative images for the expression of α-SMA (n=2). **B)** Quantification of α-SMA protein. Values are represented as mean ± SEM. Statistical difference between the groups was measured by 2- tailed Student's t test. *$p \leq 0.05$, **$p \leq 0.01$, ***$p \leq 0.001$A, ****$p \leq 0.0001$.

3.3 Discussion

The work presented in this chapter identified the RARRES-1 gene as a novel gene that possibly affects the risk of hepatic fibrosis. Hepatic RARRES-1 gene expression is attenuated with the progression of fibrosis or HSCs activation. However, restoring RARRES-1 expression reversed the TGF-β-induced fibrotic response in HSCs.

Specifically, the results presented in this chapter revealed that the RARRES-1 gene is expressed in various human tissues and liver cell subsets. Compared with that in other liver cells, RARRES-1 was expressed at higher levels in HSCs. These findings point to the potential involvement of RARRES1 in liver fibrosis. Furthermore, a comprehensive analysis confirmed that RARRES-1 expression was downregulated in a cohort of patients with liver diseases, including HCV and MAFLD patients, and similar findings were obtained in fibrotic mouse models. Consistent with these findings, RARRES-1 mRNA expression was repressed with the activation of HSCs either during the course of culture-dependent activation or after stimulation with TGF-β.

After confirming that RARRES-1 expression correlated with fibrosis, I conducted a series of *in vitro* tests to investigate whether RARRES-1 expression attenuates fibrosis. The results of pharmacological and genetic activation confirmed that the overexpression of RARRES-1 reduced fibrosis in human and murine HSCs.

TGF-β is a fibrogenic cytokine that plays a central role in the development of liver fibrosis and has been shown to promote fibrosis by activating HSCs to myofibroblasts [184]. Activated HSCs proliferate and produce extracellular matrix proteins to form fibrous scars [185]. However, deactivation of HSCs has been implicated in the regression of liver fibrosis [186]. Thus, approaches that regulate the TGF-β signalling pathway have been widely investigated for the treatment of liver fibrosis [187, 188]. In addition to promoting fibrosis, TGF-β is involved in regulating many other physiological processes. Therefore, ubiquitous

inhibition of TGF-β is not favourable, as it can lead to unwanted systemic side effects. As shown in the present study, RARRES-1 activation inhibits HSCs activation and regulates the TGF-β fibrogenic response. RARRES-1 might provide a way to selectively target the fibrotic effect of the TGF-β signalling pathway.

In conclusion, the results presented in this chapter suggest that RARRES-1 expression is attenuated with fibrosis, whereas restoring RARRES-1 expression has antifibrotic effects. RARRES-1 is a promising therapeutic target that can be extrapolated to treat liver fibrosis, but the mechanism underlying its antifibrotic effect remains unclear. Therefore, in the next chapter, I investigate the underlying mechanism of the antifibrotic effect of RARRES-1.

Chapter Four:

RARRES-1 regulates fibrosis by regulating mitochondrial function

4.1 Introduction

The activation of hepatic stellate cells (HSCs) is an energy-dependent process, and mitochondria are the “power house” of the cells responsible for producing ATP and maintaining energy metabolism in cells [189]. During fibrosis, changes in mitochondrial metabolism, mitophagy, fission, fusion, and biogenesis occur to meet the energy demand, which ultimately leads to mitochondrial dysfunction [190]. This altered mitochondrial activity results in increased generation of reactive oxygen species (ROS) [90, 91]. Uncontrolled activation of ROS leads to the constant expression of extracellular matrix proteins and, consequently, fibrosis [191].

On the other hand, excessive ROS can damage the normal structure and function of mitochondria. This process can lead to the release of ROS due to mitochondrial permeability transition pore (mPTP) opening, causing changes in mitochondrial structure, increased mitochondrial membrane potential, and damage to mitochondrial DNA that ultimately exacerbate ROS generation, creating a vicious cycle [192].

In the previous chapter, I demonstrated that RARRES-1 is downregulated with the progression of liver fibrosis. However, RARRES-1 activation can reduce HSCs activation and subsequent fibrosis, suggesting that it could be exploited as a potential therapeutic target. However, the underlying mechanism by which RARRES-1 produces antifibrotic effects is still unknown. Thus, I hypothesize that RARRES-1 may also regulate mitochondrial activity and mitochondrial morphology and thereby the generation of ROS, ultimately attenuating the energy demand of activated HSCs and fibrosis.

Hence, in this chapter, I investigate whether RARRES-1 activation regulates mitochondrial structure and activity during fibrosis. I will focus on the effects of RARRES-1 activation on the regulation of mitochondrial morphology; the expression of ATP synthase beta protein,

fusion protein, and mitochondrial importer protein; the mitochondrial membrane potential; the generation of ROS; and the expression of fibrotic markers.

4.2 Results

4.2.1 RARRES-1 activation modulates mitochondrial morphology

To support the increase of energy demand during fibrosis, mitochondrial activity is altered that lead to changes in mitochondrial morphology [193]. Additionally, increased ROS production can damage mitochondrial proteins, membranes, and DNA [194].

To investigate the impact of RARRES-1 activation on mitochondrial morphology, LX-2 cells were transfected with RARRES-1 plasmid for 48 hours and stimulated with TGF-β for 24 hours. Analysis was then undertaken using transmission electron microscope (TEM) for mitochondrial morphology.

Results have shown that RARRES1 reversed the TGF-β induced increase in mitochondrial perimeter, area, and length, implying that RARRES-1 regulates mitochondrial morphology **(Figure 4.1A-D)**.

A

Control
(Mitochondrial measurement)

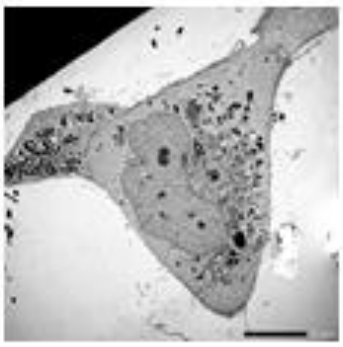

ER-22-240-C1-EVTGFB
Pub Images_6_500X

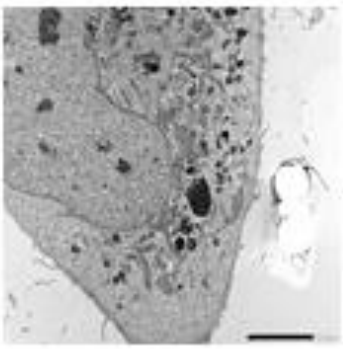

ER-22-240-C1-EVTGFB
Pub Images__13_1200X

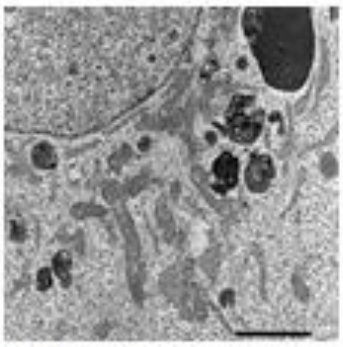

ER-22-240-C1-EVTGFB
Pub Images_14_4000X

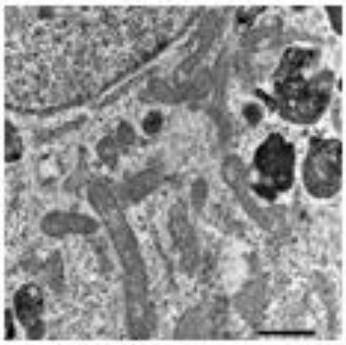

ER-22-240-C1-EVTGFB
Pub Images_15_6000X

B

RARRES-1
(Mitochondrial measurement)

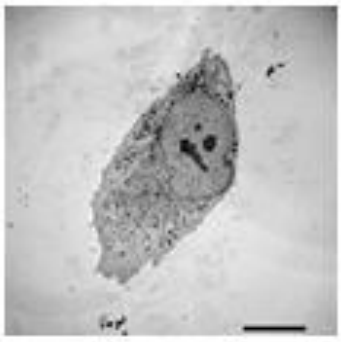

ER-22-240-D1-RPTGFB
Pub Images_43_500X

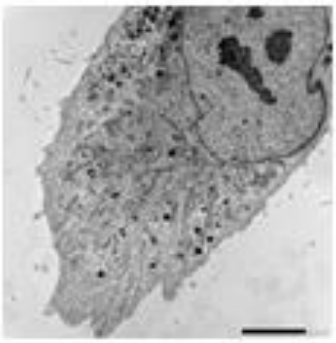

ER-22-240-D1-RPTGFB
Pub Images_47_1200X

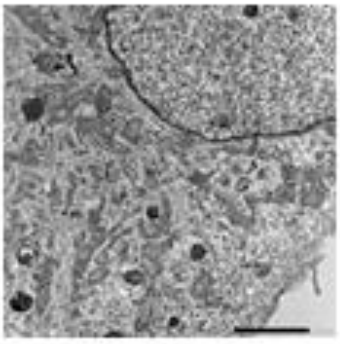

ER-22-240-D1-RPTGFB
Pub Images_48_4000X

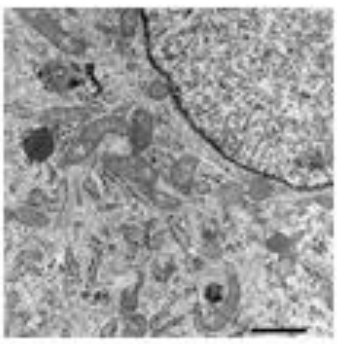

ER-22-240-D1-RPTGFB
Pub Images_50_6000X

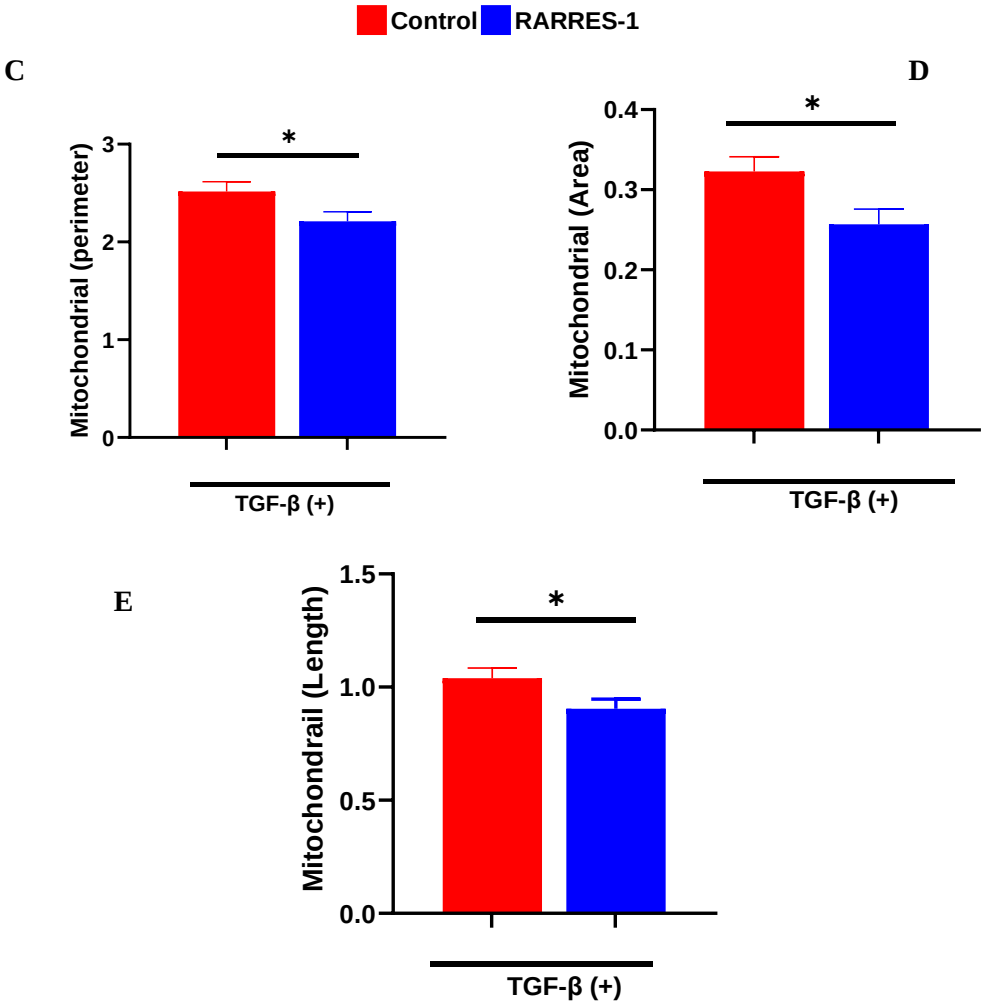

Figure 4.1: RARRES-1 activation regulates mitochondrial morphology in TGF-β stimulated HSCs. LX-2 cells transfected with RARRES-1 plasmid and control before challenging with TGFβ for 24 hours and TEM was undertaken to investigate the mitochondrial morphology. Representative images (scale bar 5.0µm) for **A)** control **B)** RARRES-1 transfected LX-2 cells. **C)** Quantification for mitochondrial perimeter. **D)** Quantification for mitochondrial Area. **E)** Quantification for mitochondrial Length. Mitochondrial measurements of perimeter, area and length were manually done by using free hand tool in the Jeol SightX image viewer software (n=231 and 283 in RARRES-1 transfected cells and control, respectively). Values are represented as mean ± SEM. Statistical difference between the groups was measured by one sample Wilcoxon test.*$p \leq 0.05$, **$p \leq 0.01$, ***$p \leq 0.001$, ****$p \leq 0.0001$.

4.2.2 RARRES-1 activation reduces the expression of mitochondrial importer protein

During fibrosis, disruption of mitochondrial quality control occurs [190]. After confirming that RARRES-1 activation regulates mitochondrial morphology, I moved to further investigate, if RARRES-1 regulates mitochondrial dynamics. The mitochondrial membrane consists of outer and inner membranes, separated by an intermembrane space [195]. The outer membrane is more permeable than the inner membrane. Translocase of the outer mitochondrial membrane 20 (TOM20) is a crucial part of the receptor complex that imports nuclear-encoded mitochondrial precursor proteins and is located in the outer membrane [9]. Disruptions in the import of mitochondrial proteins can have detrimental effects on mitochondrial function and survival [196-198].

To find the effect of RARRES-1 activation on the mitochondrial dynamics, firstly I investigated the effect of RARRES-1 activation on the expression of mitochondrial importer protein, namely TOM20. LX-2 cells were transfected with RARRES-1 for 48 hours, with and without TGF-β stimulation for 24 hours. Then I stained the cells with the antibody to Tomm20. Immunofluorescence was undertaken and analysis was confirmed using image J. Results has shown that RARRES-1 activation reduced the expression of the Tomm20 **(Figure 4.2A-B)**.

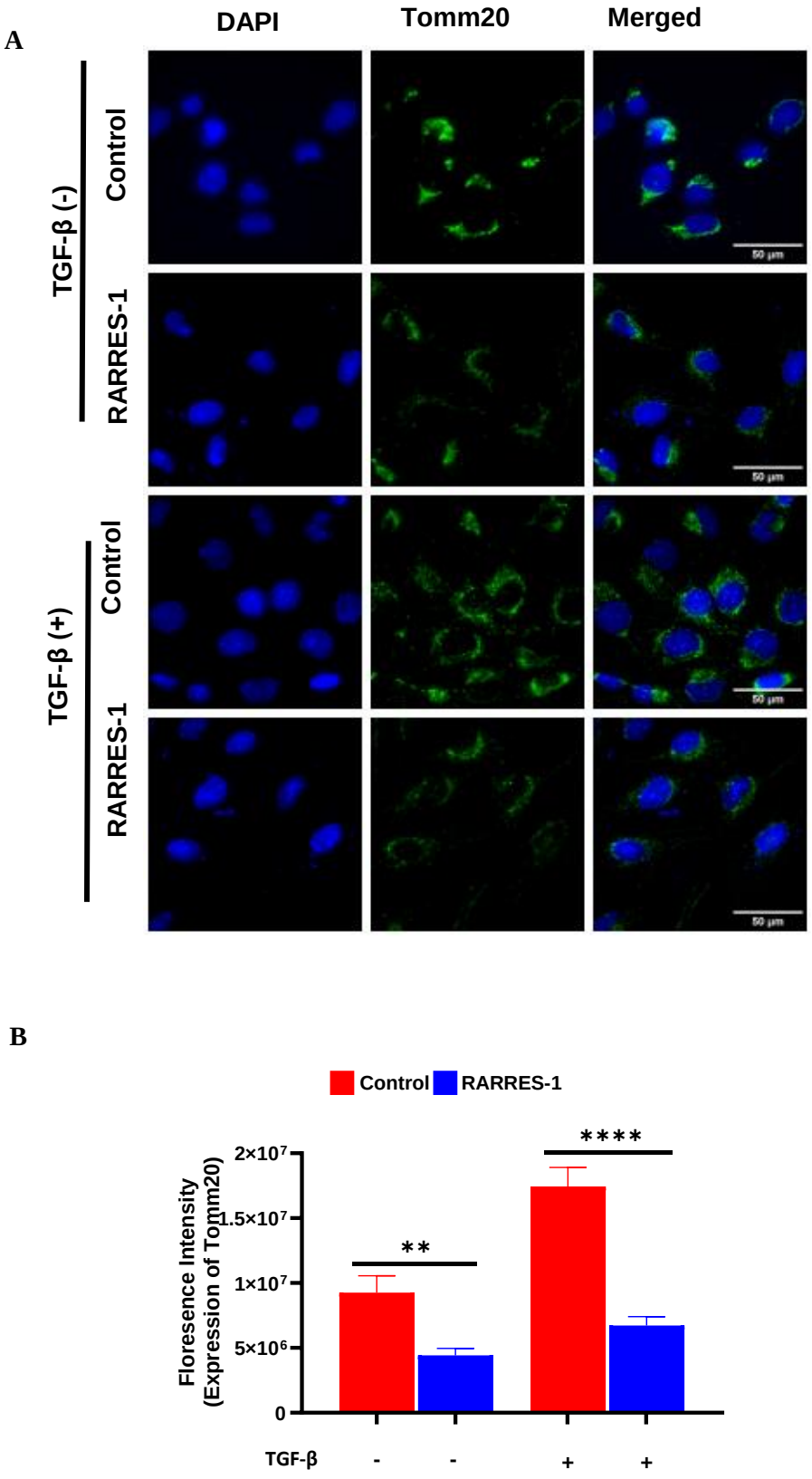

Figure 4.2: RARRES-1 activation reduces the expression of mitochondrial importer protein Tomm20. A) Representative images for the expression of Tomm20, with or without TGF-β stimulation (n=2). **B)** Quantification for the expression of Tomm20. Imaging was

undertaken using deltavision microscope and analysed using image J. Values are represented as mean ± SEM. Statistical difference between the groups was measured by 2- tailed Student's t test. *$p \leq 0.05$, **$p \leq 0.01$, ***$p \leq 0.001$A, ****$p \leq 0.0001$.

4.2.3 RARRES-1 activation regulates the expression of ATP synthase beta and metabolic reprogramming.

The activation of HSCs to myofibroblasts is accompanied by increased energy demand, which is supplemented by increased energy production in the form of ATP production [90]. The inner membrane of mitochondria is the site of oxidative phosphorylation and electron transport chain and contains synthase (ATP-β synthase) are involved in ATP production [199].

Next, I moved on to investigate if RARRES-1 activation will regulate genes controlling mitochondrial ATP production, namely ATP synthase beta. To investigate this, LX-2 cells were transfected with RARRES-1 plasmid for 48 hours and stimulated with TGF-β for 24 hours. Immunofluorescence was undertaken for ATP synthase beta expression.

Results have demonstrated that RARRES-1 activation reduces the expression of ATP synthase beta both at baseline and upon TGF-β stimulation **(Figure: 4.3A-B).**

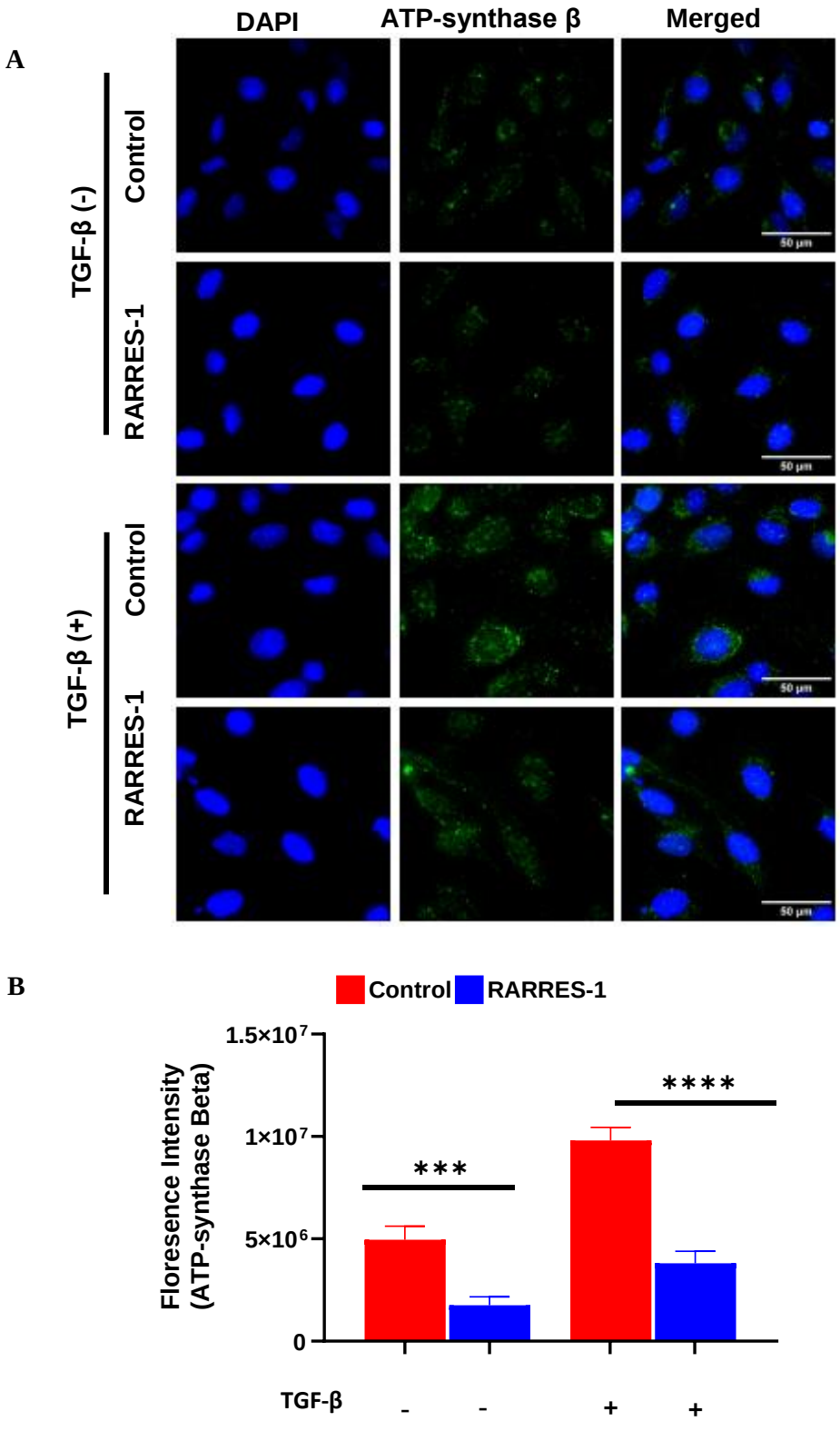

Figure 4.3: RARRES-1 activation reduces the expression of ATP synthase beta. A) Representative images for the expression of ATP synthase beta, with or without TGF-β stimulation (n=2). **B)** Quantification for the expression of ATP synthase beta. Imaging was

undertaken using deltavision microscope and analysed using image J. Values are represented as mean ± SEM. Statistical difference between the groups was measured by 2- tailed Student's t test. *$p \leq 0.05$, **$p \leq 0.01$, ***$p \leq 0.001$A, ****$p \leq 0.0001$.

4.2.4 RARRES-1 activation reduces the expression of fusion protein

During fibrosis, mitochondrial activty is increased to fulfil the energy demands of the cells and undergo continous changes in shape. Due to abnormal function of mitochondria, defective mitochondria will fuse and become elongated [200]. In an attempt to produce functional mitochondria, there will be increased expression of mitofusion protein (MFN1). That's why I further investigated if RARRES-1 activation will regulate the expression of MFN1.

To investigate it, LX-2 cells were transfected with RARRES-1 for 48 hours and stimulated with TGF-β for 24 hours. Immunofloresence was undertaken for the expression of MFN1. Results have shown that RARRES-1 activation reduces the expression of mitofusion protein, both at baseline and upon TGF-β stimulation **(Figure 4.4A-B)**.

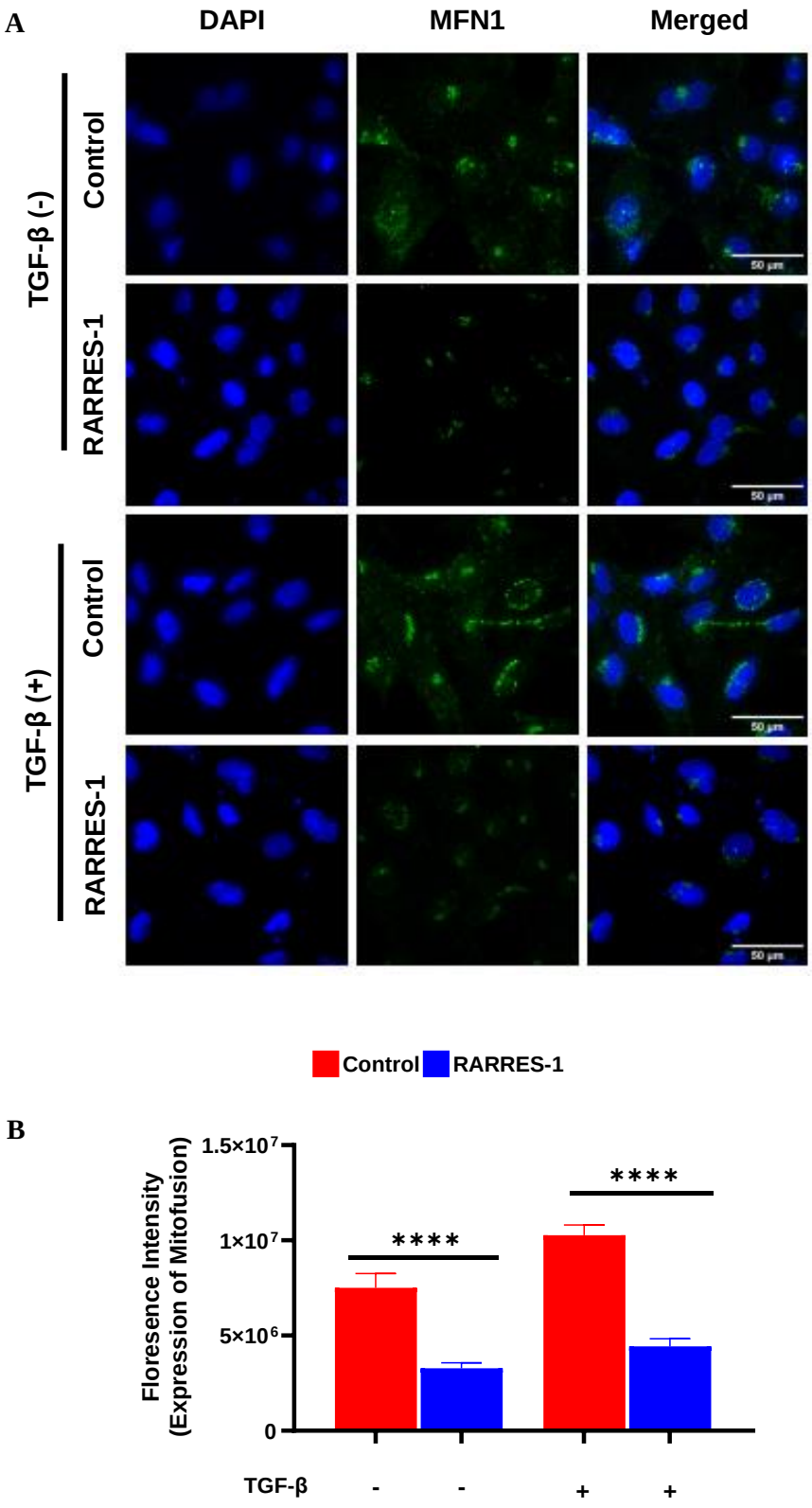

Figure 4.4: RARRES-1 activation reduces the expression of mitofusin protein. A) Representative images for the expression of MFN1, with or without TGF-β stimulation (n=2). **B)** Quantification for the expression of MFN1. Imaging was undertaken using Deltavision microscope and analysed using image J. Values are represented as mean ± SEM. Statistical

difference between the groups was measured by 2- tailed Student's t test. *$p \leq 0.05$, **$p \leq 0.01$, ***$p \leq 0.001$A, ****$p \leq 0.0001$.

4.2.5 RARRES-1 activation reduces mitochondrial membrane potential

Mitochondrial activity is indicated by mitochondrial membrane potential [201]. As I have demonstrated that RARRES1 regulates mitochondrial activity during HSCs activation, I further extended my investigation by exploring the impact of RARRES1 on mitochondrial membrane potential under fibrotic conditions.

To this end, LX-2 cells were transfected with RARRES-1 for 48 hours, with and without TGF-β stimulation for 24 hours. Then cells were stained with the red-orange, fluorescent dye TMRE (Tetramethylrhodamine, ethyl ester), a marker of the mitochondrial membrane potential (ψ). Live cell imaging was undertaken using deltavision microscope. Consistently, Results have shown that RARRES-1 activation reduced both baseline and TGF-β induced expression of mitochondrial membrane potential **(Figure 4.5A-B)**.

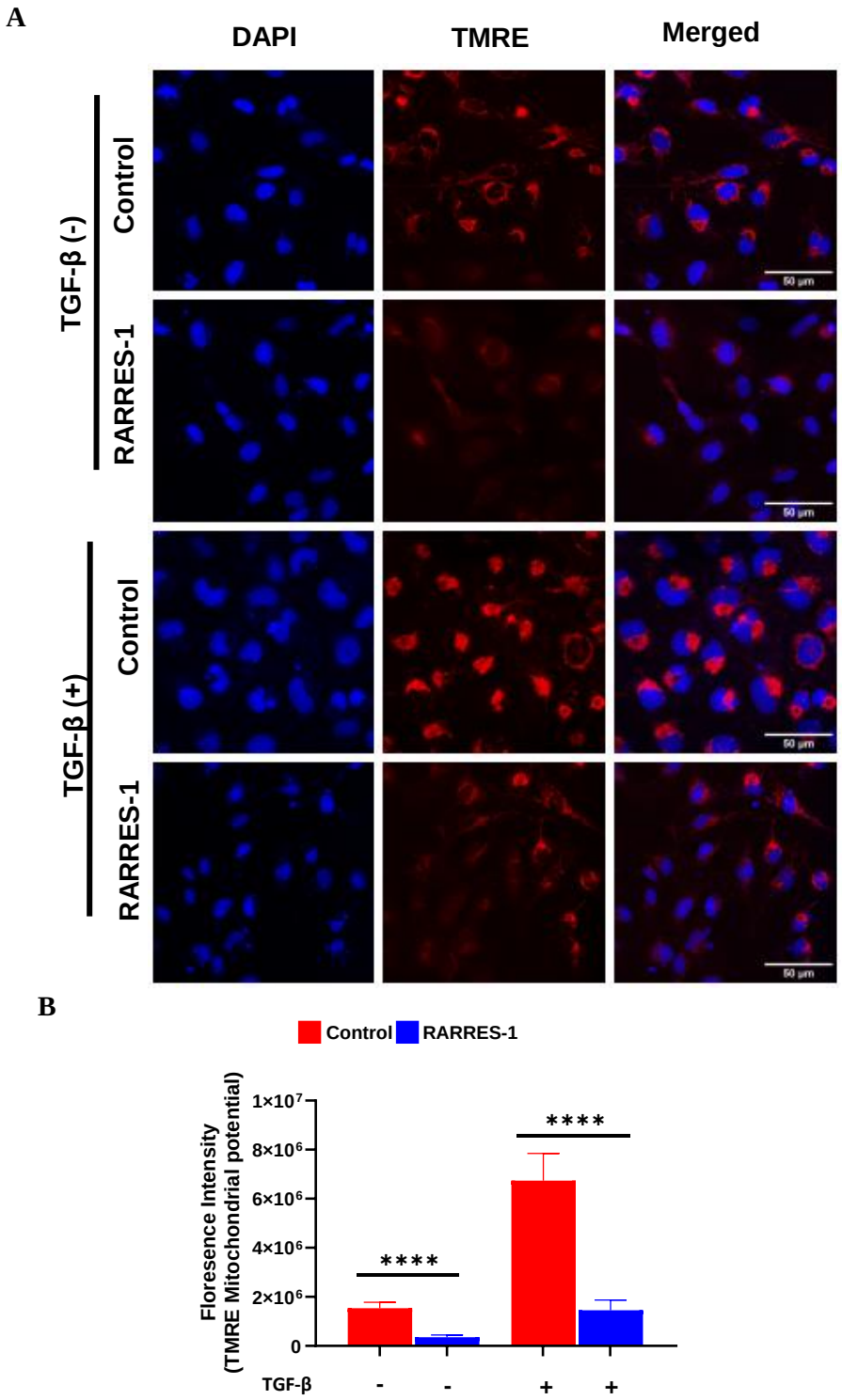

Figure 4.5: RARRES-1 activation reduces the mitochondrial membrane potential. A) Representative images for the expression of TMRE, with or without TGF-β stimulation (n=2). **B)** Quantification for the expression of TMRE. Imaging was undertaken using Deltavision microscope and analysed using image J. Values are represented as mean ± SEM. Statistical difference between the groups was measured by 2- tailed Student's t test. *$p \leq 0.05$, **$p \leq 0.01$, ***$p \leq 0.001$A, ****$p \leq 0.0001$.

4.2.6 RARRES-1 activation along with CCCP synergistically reduces the mitochondrial membrane potential

Having identified a role for RARRES-1 activation in modulating mitochondria dependent human HSCs activation, I questioned whether RARRES1 regulates fibrosis through these effects. Thus, I investigated the effect of carbonyl cyanide m-chlorophenyl hydrazone (CCCP), a mitochondrial membrane potential inhibitor on RARRES-1 anti-fibrotic effect.

To do that, I first examined the effect of the combined CCCP and RARRES-1 on mitochondrial membrane potential. LX-2 cells were transfected with RARRES-1 for 48 hours and treated with CCCP, 2 hours before challenging with or without TGF-β stimulation for 24 hours. LX-2 cells were stained with the mitochondrial membrane potential, TMRE. Live cell imaging was undertaken using Deltavision microscope.

Results confirmed that RARRES-1 activation along with carbonyl cyanide m-chlorophenyl hydrazone synergistically reduces the mitochondrial membrane potential both at baseline **(Figure 4.6A-B)** and upon TGF-β stimulation **(Figure 4.7A-B)**.

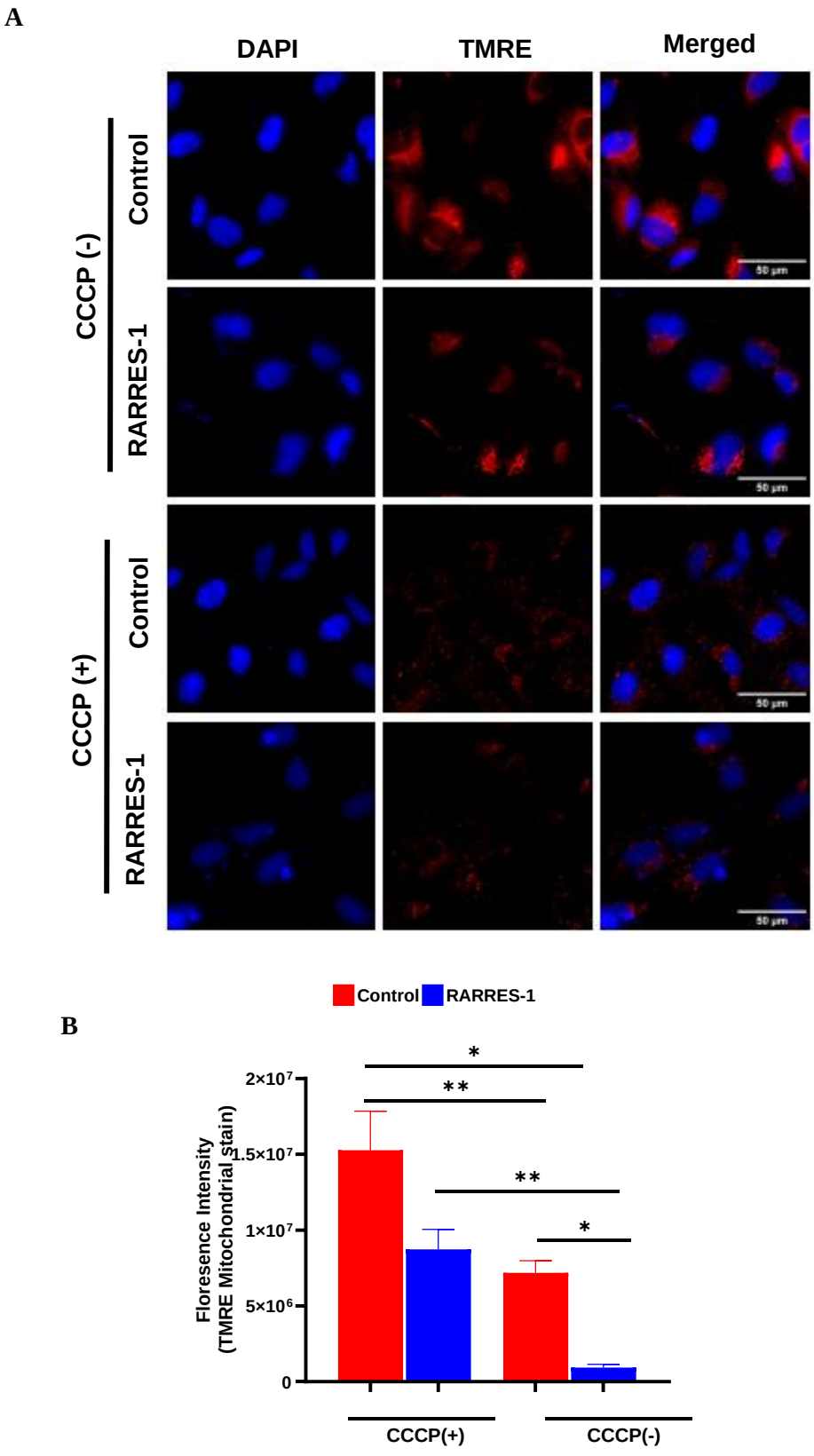

Figure 4.6: RARRES-1 activation along with CCCP synergistically reduces mitochondrial membrane potential in unstimulated HSCs. LX-2 cells transfected with RARRES-1 and treated with or without CCCP for 2 hours. **A)** Representative images for the

expression of TMRE. **B)** Quantification of TMRE at baseline. Live cell imaging was undertaken using Deltavision microscope and analysed using image J. Values are represented as mean ± SEM. Statistical difference between the groups was measured by one-way ANOVA; multiple comparisons were corrected by Boneferroni correction. *$p \leq 0.05$, **$p \leq 0.01$, ***$p \leq 0.001$A, ****$p \leq 0.0001$.

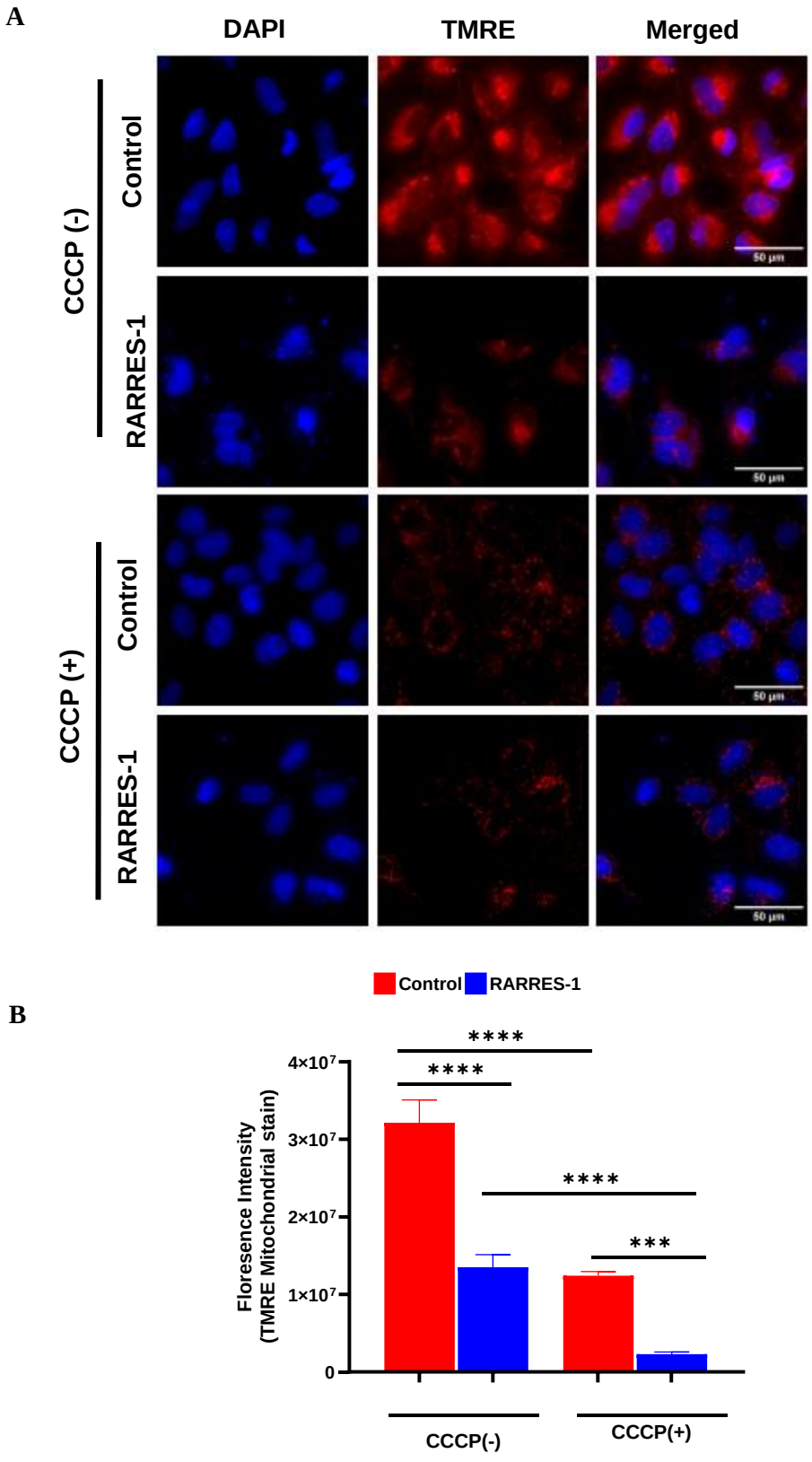

Figure 4.7: RARRES-1 activation along with CCCP synergistically reduce mitochondrial membrane potential in stimulated HSCs. LX-2 cells transfected with RARRES-1 and treated with or without CCCP for 2 hours, before challenging with TGF-β.

A) Representative images for the expression of TMRE. **B)** Quantification of TMRE upon stimulation with TGF-β. Live cell imaging was undertaken using Deltavision microscope and analysed using image J. Values are represented as mean ± SEM. Statistical difference between the groups was measured by one-way ANOVA; multiple comparisons were corrected by Boneferroni correction. *$p \leq 0.05$, **$p \leq 0.01$, ***$p \leq 0.001$A, ****$p \leq 0.0001$.

4.2.7 RARRES-1 activation along with CCCP synergistically reduces the generation of ROS

Then, I extended these studies and investigated the impact of RARRES-1 activation along with CCCP on the generation of ROS. To investigate this, LX-2 cells were transfected with RARRES-1 plasmid for 48 hours and treated with CCCP, 2 hours before challenging with TGF-β. Live cell imaging was undertaken for the expression of DCFDA stain, a marker of ROS. Results of analysis confirmed that RARRES-1 activation along with CCCP synergistically reduces the generation of ROS in LX-2 cells, both at baseline **(Figure: 4.8A-B)** and stimulated levels **(Figure: 4.9A-B)**.

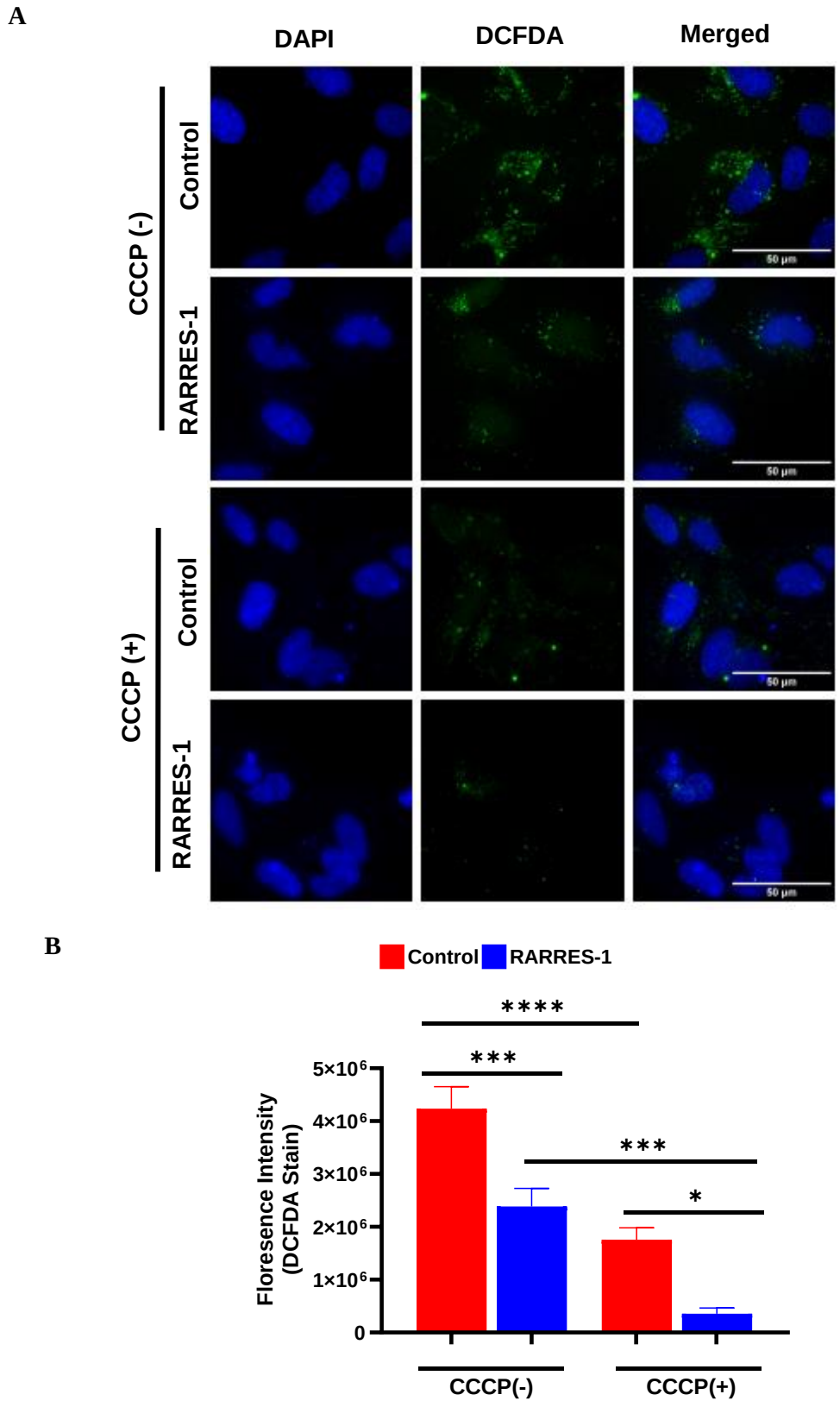

Figure 4.8: RARRES-1 activation along with CCCP synergistically reduce ROS generation in unstimulated HSCs. LX-2 cells transfected with RARRES-1 and treated with or without CCCP for 2 hours (n=2). **A)** Representative images for the expression of DCFDA.

B) Quantification of DCFDA at baseline. Live cell imaging was undertaken using Deltavision microscope and analysed using image J. Values are represented as mean ± SEM. Statistical difference between the groups was measured by one-way ANOVA; multiple comparisons were corrected by Bonferroni correction. *$p \leq 0.05$, **$p \leq 0.01$, ***$p \leq 0.001$A, ****$p \leq 0.0001$.

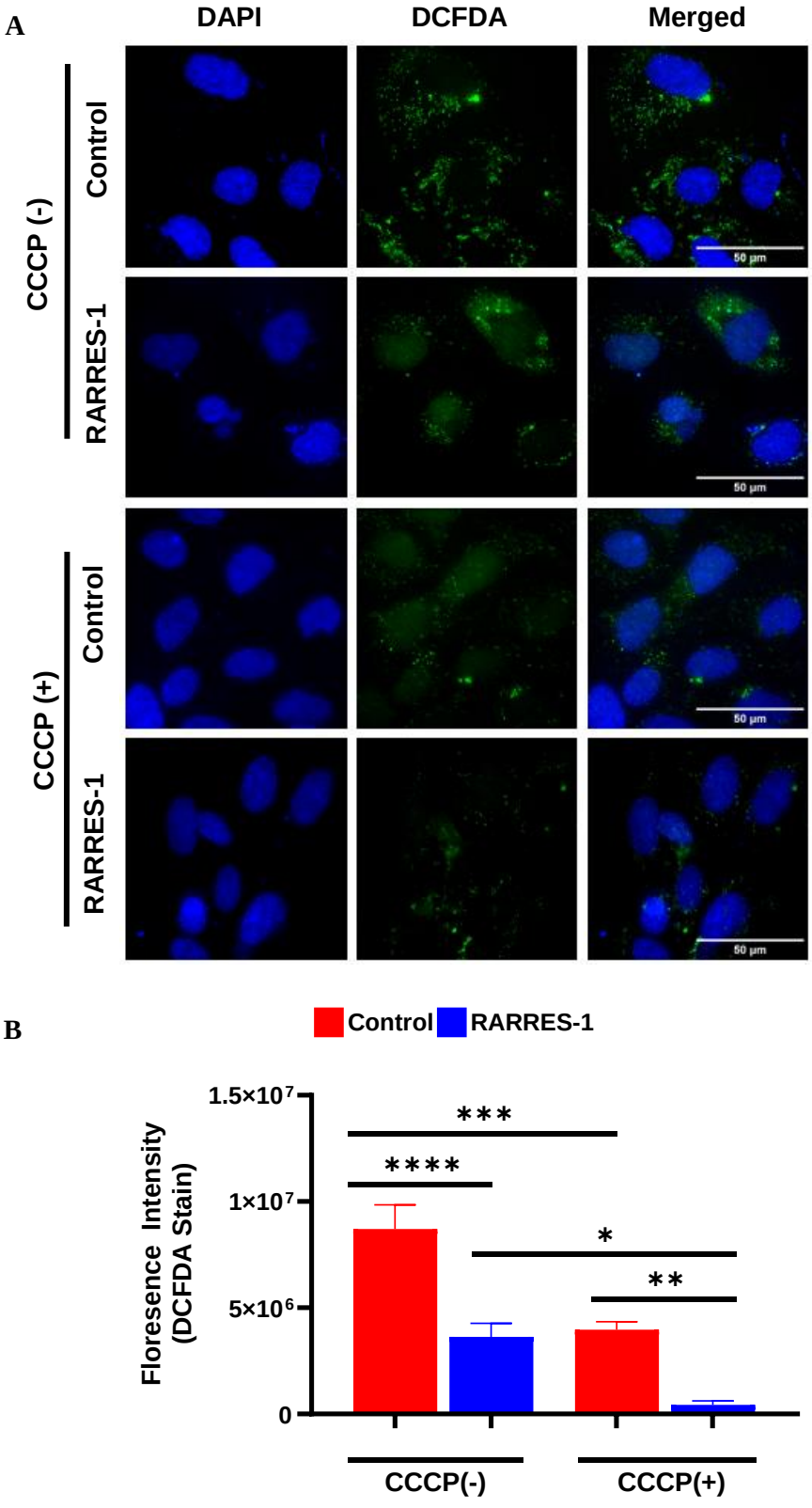

Figure 4.9: RARRES-1 activation along with CCCP synergistically reduce ROS generation in stimulated HSCs. LX-2 cells transfected with RARRES-1 and treated with or without CCCP for 2 hours, before challenging with TGF-β (n=2). **A)** Representative images

for the expression of DCFDA. **B)** Quantification of DCFDA upon stimulation with TGF-β. Live cell imaging was undertaken using deltavision microscope and analysed using image J. Values are represented as mean ± SEM. Statistical difference between the groups was measured by one-way ANOVA; multiple comparisons were corrected by Boneferroni correction. *$p \leq 0.05$, **$p \leq 0.01$, ***$p \leq 0.001$A, ****$p \leq 0.0001$.

4.2.8 RARRES-1 activation along with CCCP synergistically reduces the expression of fibrotic markers

In the previous experiments I confirmed that RARRES-1 activation accompanied with CCCP regulates the mitochondrial membrane potential and ROS generation. Next, I further want to explore if this regulation of mitochondrial activity is implicated in the anti-fibrotic effect of RARREs1.

To do that, LX-2 cells were transfected by either control or RARRES-1 plasmid for 48 hours and treated with CCCP for 2 hours before challenging with or without TGF-β stimulation. Immunofluorescence was undertaken for the expression of α-SMA.

The results have shown that RARRES-1 activation along with CCCP synergistically reduces the expression of fibrotic markers both at baseline **(Figure: 4.10A-B)** and upon TGF-β stimulation **(Figure: 4.11A-B)**.

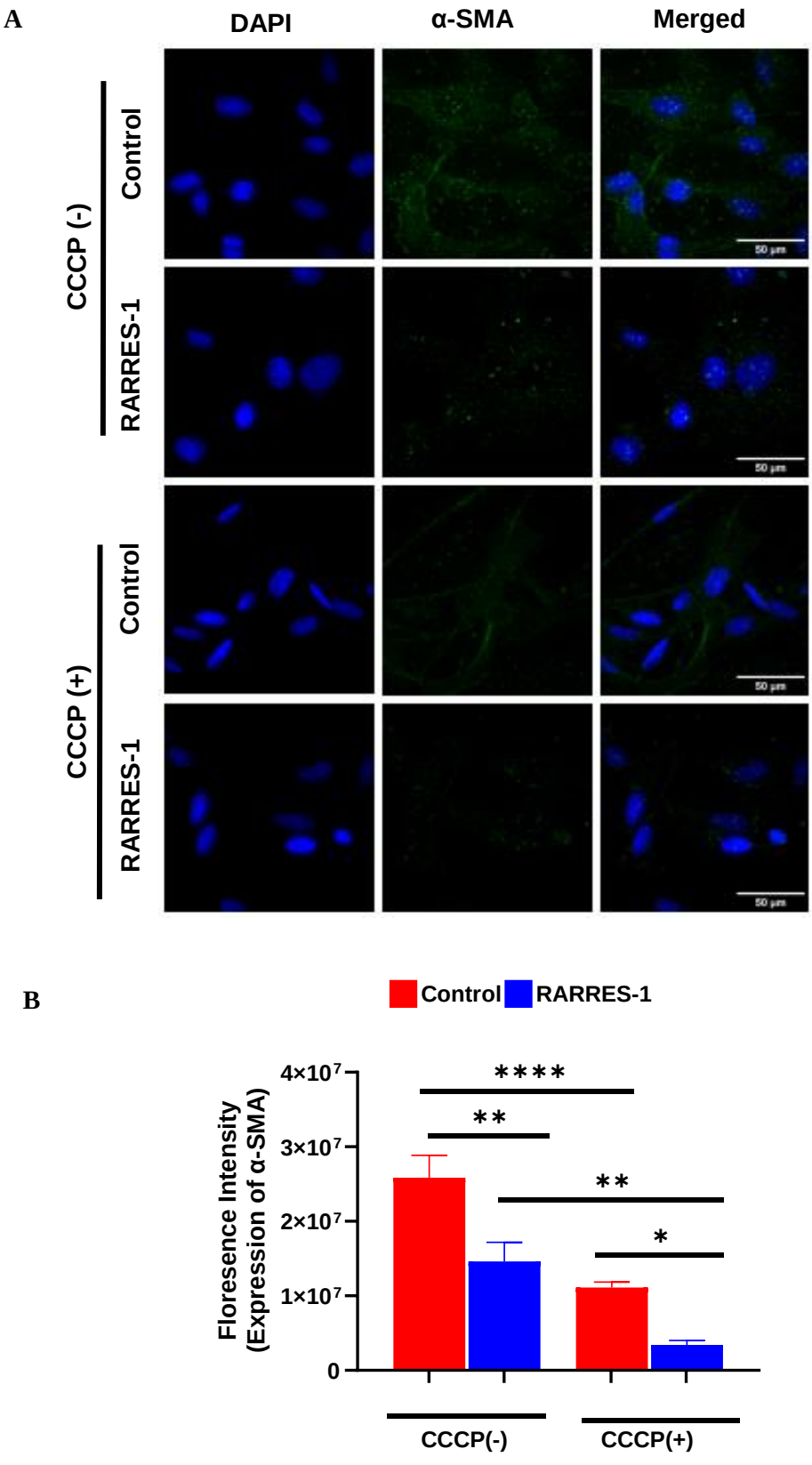

Figure 4.10: RARRES-1 activation along with CCCP synergistically reduces expression of fibrotic marker in unstimulated HSCs. LX-2 cells transfected with RARRES-1 and treated with or without CCCP for 2 hours. **A)** Representative images for the expression of α-

SMA. **B)** Quantification of α-SMA at baseline. Immunofluorescence was undertaken using deltavision microscope and analysed using image J. Values are represented as mean ± SEM. Statistical difference between the groups was measured by one-way ANOVA; multiple comparisons were corrected by Boneferroni correction. *$p \leq 0.05$, **$p \leq 0.01$, ***$p \leq$ 0.001A, ****$p \leq 0.0001$.

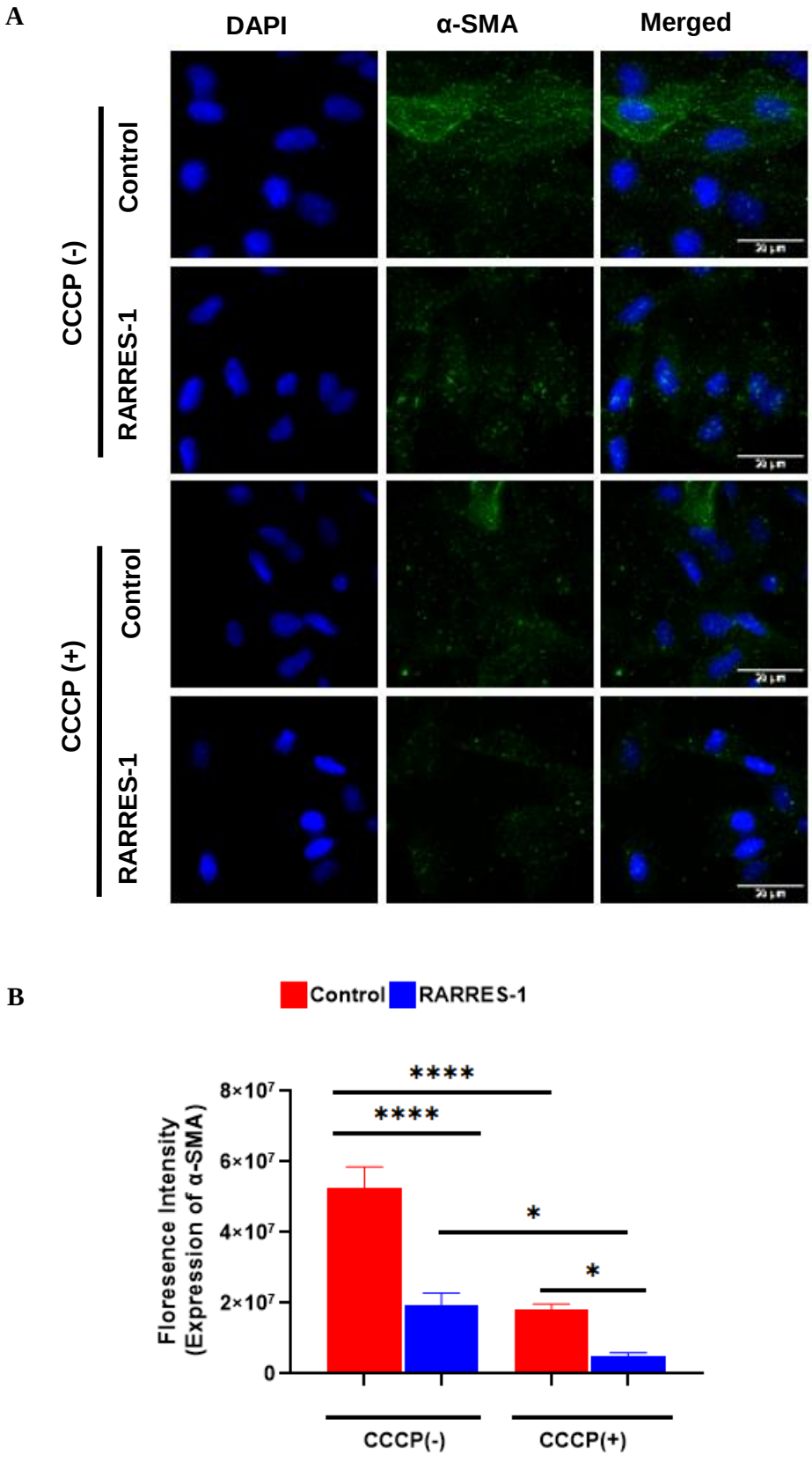

Figure 4.11: RARRES-1 activation along with CCCP synergistically reduce expression of fibrotic markers in stimulated HSCs. LX-2 cells transfected with RARRES-1 and treated with or without CCCP for 2 hours, before challenging with TGF-β. **A)** Representative

images for the expression of α-SMA. **B)** Quantification of α-SMA upon stimulation with TGF-β. Immunofluorescence was undertaken using deltavision microscope and analysed using image J. Values are represented as mean ± SEM. Statistical difference between the groups was measured by one-way ANOVA; multiple comparisons were corrected by Boneferroni correction. *$p \leq 0.05$, **$p \leq 0.01$, ***$p \leq 0.001$A, ****$p \leq 0.000$.

4.3 Discussion

In previous chapters, RARRES-1 was identified as a novel regulator of HSCs activation and liver fibrosis. I identified that the activation of RARRES-1 reduces the expression of fibrotic markers and has an antifibrotic effect. In this chapter, I extended my findings by confirming that the regulation of mitochondrial morphology and activity is one of the mechanisms underlying the antifibrotic effect of RARRES-1. These mechanisms are all interlinked, implying that the antifibrotic effect of RARRES-1 occurs via the regulation of energy release in activated HSCs.

TGF-β is a master cytokine that promotes fibrosis by exerting cytostatic and apoptotic effects [202, 203]. TGF-β has been shown to induce fibroblasts to differentiate into myofibroblasts by increasing the mitochondrial contents and respiration [204]. One of the mechanisms by which TGF-β promotes fibrosis involves direct effects on mitochondrial metabolism and mitochondrial ROS generation. These changes ultimately lead to increased mitochondrial permeability, osmotic pressure, swelling of mitochondria, apoptosis, and hence damage to mitochondria [205-207]. During liver fibrosis, mitochondrial permeability is altered due to fluctuations in mitochondrial importer proteins, which increase the mitochondrial membrane potential and ATP synthesis [208, 209]. Hence, all these processes damage mitochondrial morphology and initiate a vicious cycle [210]. I demonstrated that RARRES-1 breaks this vicious cycle and reduces the generation of mitochondrial ROS both at baseline and upon TGF-β stimulation. It also regulates mitochondrial import, ATP synthesis, mitochondrial fusion, the mitochondrial membrane potential, and mitochondrial morphology.

Elaborating on the results presented in this chapter, I showed that RARRES-1 activation regulates morphological changes in mitochondria under fibrotic conditions. Additionally, the data presented in this chapter confirmed that RARRES-1 activation reduces the expression of

mitochondrial importer proteins and ATP synthesis. This reduction in the expression of importer proteins might reduce electron transport in the mitochondria, which is needed for the increased phosphorylation of ADP to ATP and the subsequent increase in energy production to support fibrosis. RARRES-1 activation decreases the import of electrons; hence, ATP synthesis is reduced.

Moreover, this chapter also confirmed that RARRES-1 activation reduces the expression of mitochondrial fusion proteins, which are increased during fibrosis. RARRES-1 reduces the levels of these proteins and hence regulates mitochondrial quality control. These results further confirmed that RARRES-1 activation reduces the mitochondrial membrane potential. This change might be due to the reduction in the expression of importer proteins that interfere with the transport of ions and minerals inside the mitochondria. These results indicate that RARRES-1 activation regulates mitochondrial dynamics through a series of downstream events in the mitochondria.

In a series of experiments conducted with RARRES-1 and CCCP together, the results confirmed that CCCP, along with RARRES-1 activation, synergistically reduced the mitochondrial membrane potential. RARRES-1 activation and CCCP also reduced the generation of ROS and the expression of α-SMA, indicating that both CCCP and RARRES-1 might work through similar pathways to reduce fibrosis.

In conclusion, the overall results presented in this chapter confirmed that RARRES-1 activation exerts an antifibrotic effect by regulating mitochondrial activity in terms of the mitochondrial morphology, mitochondrial import, ATP synthesis, mitochondrial turnover, mitochondrial ROS production, and the mitochondrial membrane potential and ultimately reduces the expression of fibrotic markers. Therefore, RARRES-1 represses the profibrotic effect of TGF-β by regulating its effect on mitochondrial activity and structure. Therefore,

RARRES-1 represents an attractive therapeutic target that can be manipulated to restore normal mitochondrial function and reverse liver fibrosis.

Chapter Five: RARRES-1 regulates fibrosis by regulating ROS generation

5.1 Introduction

Hepatic stellate cells (HSCs) are the main cells responsible for producing excess matrix and collagen during liver fibrosis [211, 212]. These cells are located in the space of Disse, which is the space between hepatocytes and sinusoids in the liver. When the liver is injured, HSCs are activated and transformed into myofibroblasts, leading to the production of fibrous tissue [213]. The survival of activated HSCs contributes to fibrosis progression, and thus limiting the accumulation of activated HSCs in the injured liver could help treat fibrosis.

Quiescent HSCs are characterized by containing abundant lipid droplets composed mainly of retinyl esters, triglycerides and phospholipids. Their activation to cells that secrete fibrous tissue is an energy-dependent process. During this activation, free fatty acids are produced by the breakdown of triglycerides. These free fatty acids are then used in mitochondria to generate ATP, which is necessary for HSCs to acquire a myofibroblastic phenotype [90, 91, 214].

Altered mitochondrial activity has been observed in patients with cirrhosis and in activated HSCs [93, 215]. Mitochondria not only produce energy in the form of ATP but also generate about 90% of reactive oxygen species (ROS), which are responsible for oxidative stress [216]. Myofibroblast activation is an intense energy requiring process. Instead of focusing on cell signalling, as has previously been the case, targeting the energy demand of fibrosis thus represents a novel strategy to reverse fibrosis. This approach should minimally impact quiescent stellate cells.

In the previous chapters, I demonstrated that RARRES-1 activation can reduce HSCs activation and thereby fibrosis. I further showed that RARRES-1 has an antifibrotic effect by regulating mitochondrial morphology and mitochondrial activity and ultimately reduces the expression of fibrotic markers.

The mechanism by which RARRES-1 produces an antifibrotic effect is still unknown. I hypothesize that the increased TGF-β levels during fibrosis and subsequent RARRES-1 silencing might be responsible for increased energy release. Thus, RARRES-1 activation would reduce energy release during myofibroblast activation and thereby liver fibrosis.

This chapter focuses on investigating the possible mechanisms underlying the antifibrotic effect of RARRES-1, specifically by determining whether RARRES-1 regulates mitochondrial function and the release of ROS from HSCs and whether these mechanisms are responsible for the antifibrotic effect of RARRES-1.

5.2 Results

5.2.1 TGF-β induced ROS generation

During fibrosis, TGF-β produces ROS generation that could further promote fibrosis. To investigate if RARRES-1 produces antifibrotic effect by modulating ROS generation, I first, established time-dependent TGF-β induced ROS generation model. Human HSCs (LX-2 cells) were treated with TGF-β over different time points (0, 6 and 24 hours). Then production of ROS was measured by using 2'7'-dichlorofluorescin diacetate (DCFDA stain) fluorescent probe **(Figure 5.1)**. Maximum production of ROS was attained with 24 hours of TGF-β treatment. Hence, this time point was selected for further experiments.

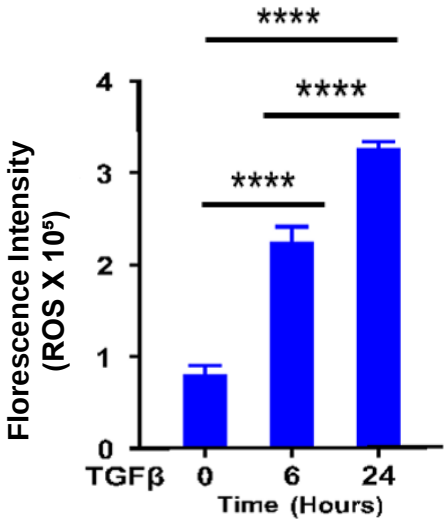

Figure 5.1: TGF-β induced ROS generation model in LX-2 cells. LX-2 cells were treated with TGF-β at 0, 6 and 24 hours. Total cellular ROS production was assessed using DCFDA stain upon TGF-β treatment. Values are represented as mean ± SEM. Statistical difference between the groups was measured by 2- tailed Student's t test. *$p \leq 0.05$, **$p \leq 0.01$, ***$p \leq$ 0.001A, ****$p \leq 0.0001$.

5.2.2 RARRES-1 activation modulates the generation of ROS

Then, I investigated if RARRES-1 activation modulates the generation of cellular ROS that is comprised of cytosolic and mitochondrial ROS upon TGF-β stimulation.

5.2.2.1 RARRES-1 modulates cytosolic ROS

First, to investigate if RARRES-1 activation regulates the generation of cytosolic ROS, LX-2 cells were transfected with RARRES-1 plasmid for 48 hours and stimulated with TGF-β for 24 hours. Live cell imaging was undertaken for the expression of DCFDA stain using Deltavision microscope. Image analysis has shown significant reduction in the expression of TGF-β induced ROS generation in LX-2 cells upon RARRES-1 activation **(Figure 5.2A-B)**.

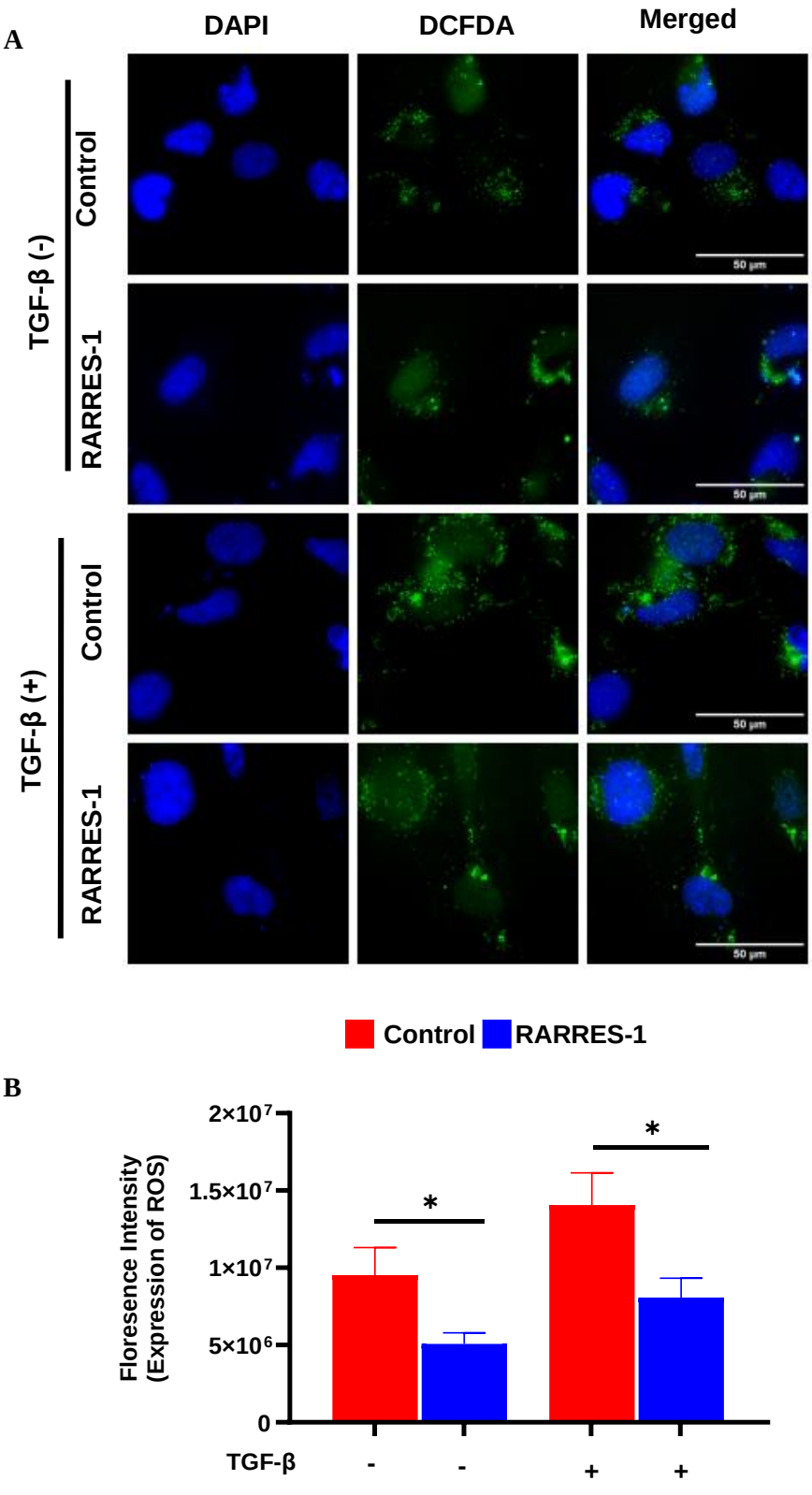

Figure 5.2: RARRES-1 activation regulates the generation of ROS. A) Representative images for the expression of DCFDA stain in LX-2 cells (n=2). **B)** Quantification of DCFDA stain. Live cell imaging was undertaken to investigate the generation of cytosolic ROS

measured by green fluorescent DCFDA dye and analysed using image J. Values are represented as mean ± SEM. Statistical difference between the groups was measured by 2-tailed Student's t test. *$p \leq 0.05$, **$p \leq 0.01$, ***$p \leq 0.001$A, ****$p \leq 0.0001$.

5.2.2.2 RARRES-1 activation modulates the generation of mitochondrial ROS

Mitochondria are the main source of cellular ROS and approximately 90% of cellular ROS is generated by mitochondria [217]. Next, I moved on to investigate if RARRES-1 activation regulates the generation of mitochondrial ROS. LX-2 cells were transfected with RARRES-1 plasmid for 48 hours and stimulated with TGF-β for 24 hours. Live cell imaging was undertaken for the measurement of mitochondrial ROS by using red fluorescent dye MitoSox. Image analysis has shown significant reduction in the expression of TGF-β induced mitochondrial ROS generation in LX-2 cells upon RARRES-1 activation **(Figure 5.3A-B)**.

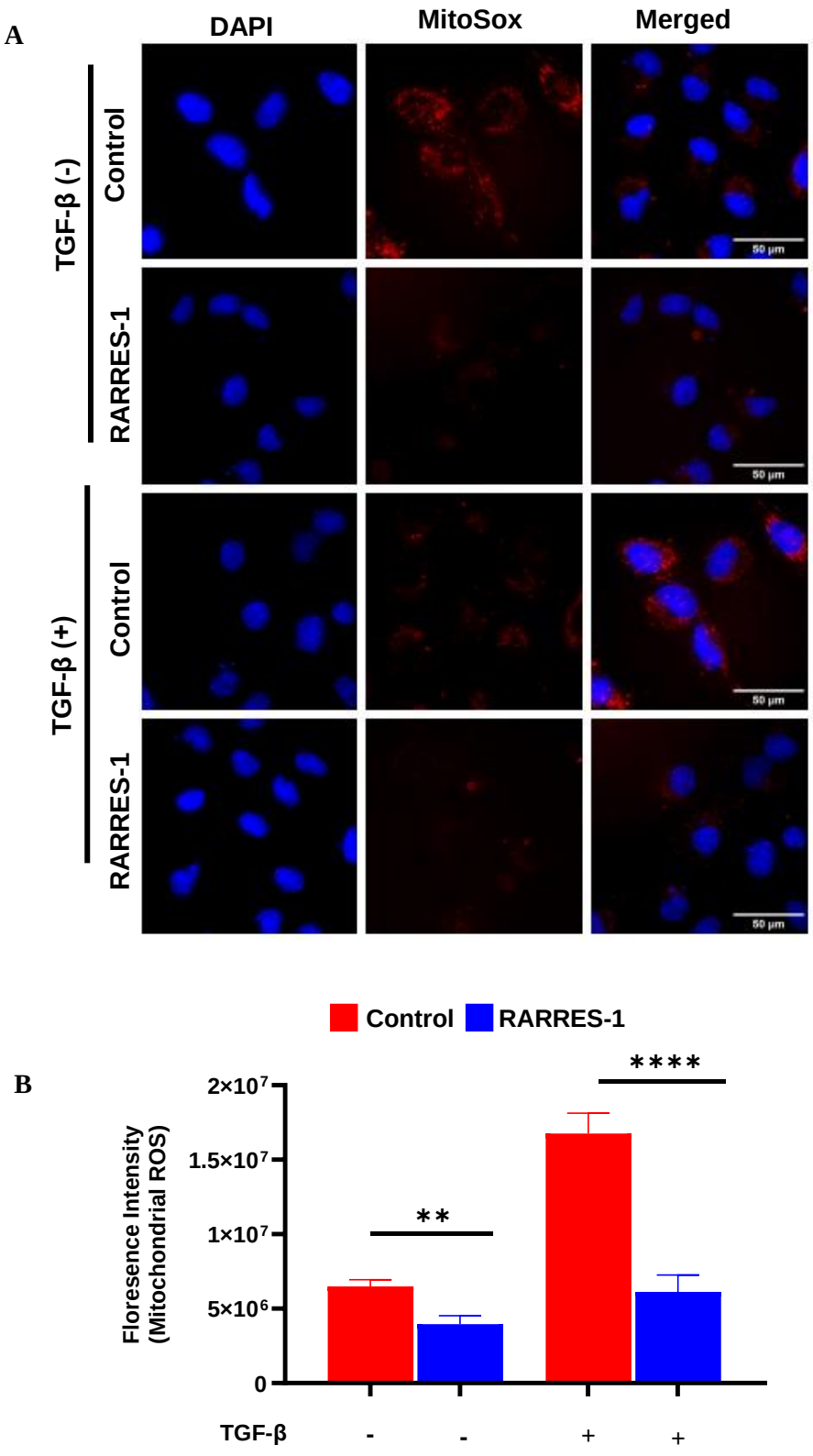

Figure 5.3: RARRES-1 activation regulates the generation of mitochondrial ROS. A) Representative images for the expression of red fluorescent dye MitoSox in LX-2 cells (n=2). **B)** Quantification of MitoSox. Live cell imaging was undertaken to investigate the generation of mitochondrial ROS (mROS), measured by the red fluorescent dye MitoSox and analysed

using image J. Values are represented as mean ± SEM. Statistical difference between the groups was measured by 2- tailed Student's t test. *$p \leq 0.05$, **$p \leq 0.01$, ***$p \leq 0.001$A, ****$p \leq 0.0001$.

5.2.3 ROS inducers reverse the antifibrotic effect of RARRES-1

After demonstrating that RARRES-1 activation reduces the generation of cellular ROS in activated HSCs. To explore if the mechanism involved in RARRES-1 antifibrotic effect is through modulation of ROS, I planned to investigate the impact of modulation of ROS levels on the RARRES-1 antifibrotic effect.

To evaluate this, I transfected LX-2 cells with RARRES-1 for 48 hours and treated with H_2O_2 (ROS inducer), 2 hours before challenging with or without TGF-β for 24 hours. Cells were then stained for α-SMA, as a robust marker of myofibroblast activation. Interestingly, while activation of RARRES-1 led to significant attenuation of α-SMA both at baseline **(Figure 5.4A-B)** and upon stimulation with TGF-β (**Figure 5.5 A-B)**, this effect was completely abolished upon treatment with H_2O_2.

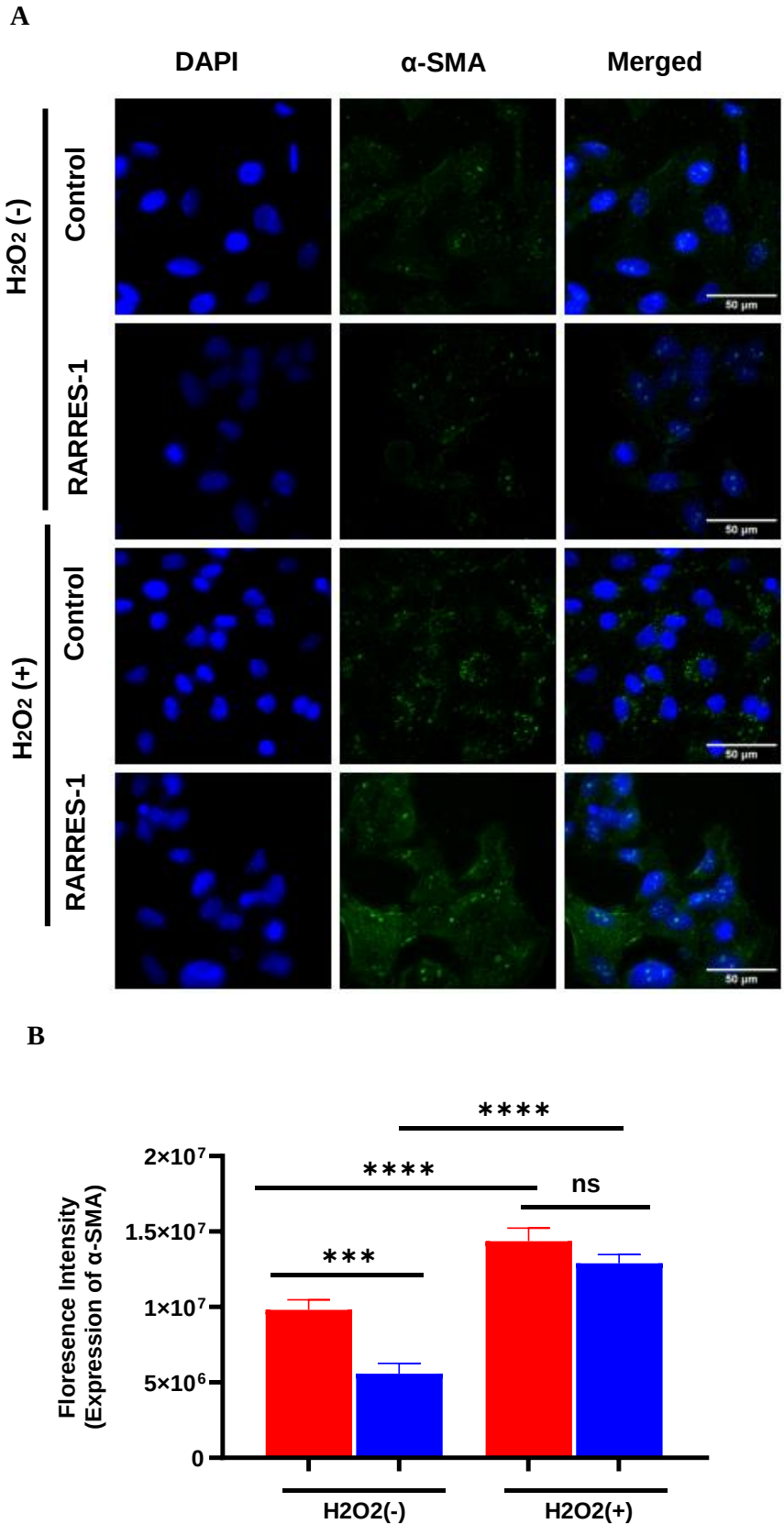

Figure 5.4: ROS inducers reverse the antifibrotic effect of RARRES-1 in unstimulated HSCs. LX-2 cells were transfected with RARRES-1 and treated with or without H2O2 for 2 hours and expression of α-SMA was assessed (n=2). **A)** Representative images for expression

of α-SMA. **B)** Quantification of α-SMA at baseline**.** Imaging was undertaken using deltavision microscope and analysed using image J. Values are represented as mean ± SEM. Statistical difference between the groups was measured by one-way ANOVA; multiple comparisons were corrected by Boneferroni correction. *$p \leq 0.05$, **$p \leq 0.01$, ***$p \leq$ 0.001A, ****$p \leq 0.0001$.

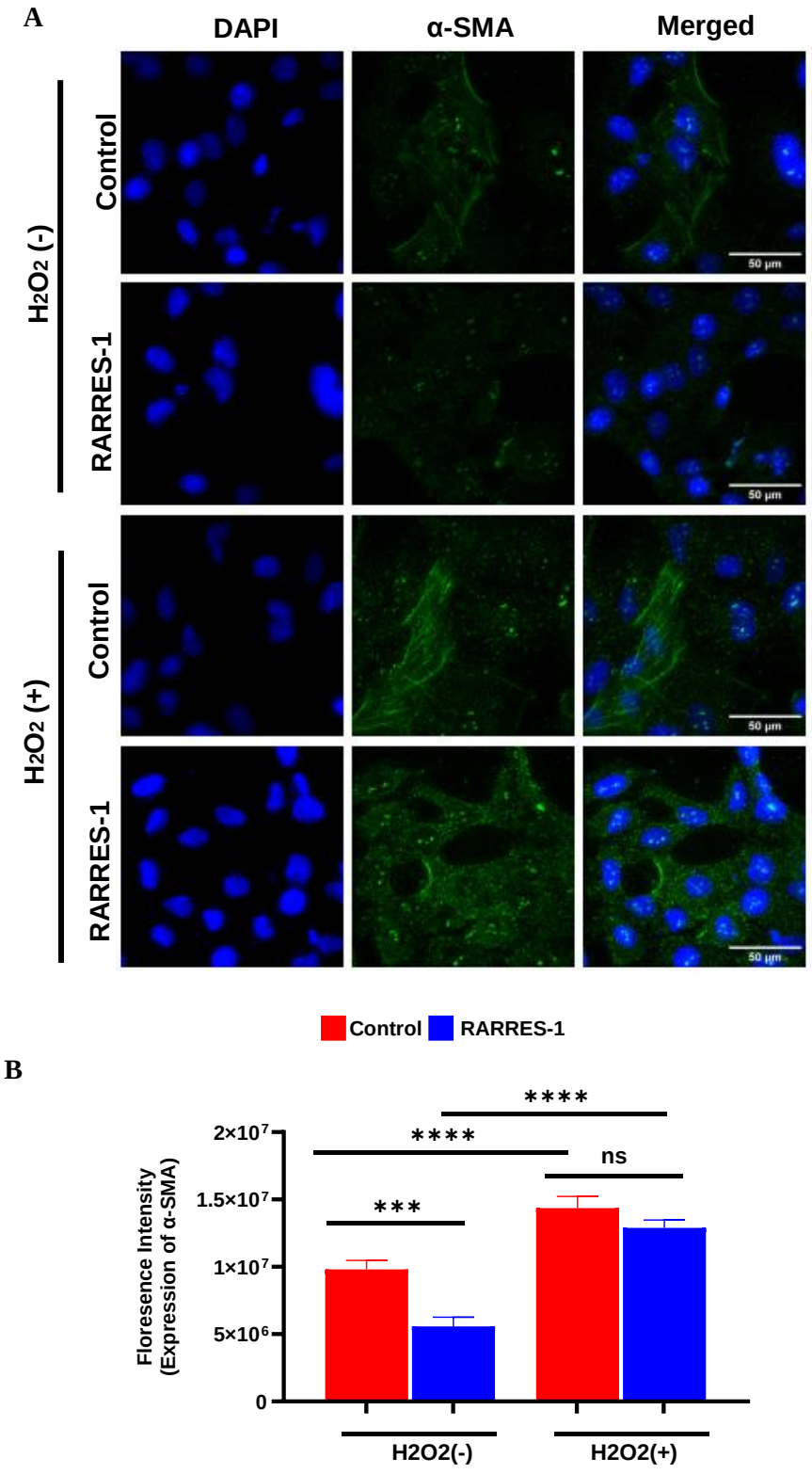

Figure 5.5: ROS inducers reverse the antifibrotic effect of RARRES-1 in TGF-β stimulated HSCs. LX-2 cells transfected with RARRES-1 plasmid and treated with or without H_2O_2 for 2 hours before challenging with TGF-β and expression of α-SMA was

assessed (n=2). **A)** Representative images for expression of α-SMA. **B)** Quantification of α-SMA upon stimulation with TGF-β. Imaging was undertaken using deltavision microscope and analysed using image J. Values are represented as mean ± SEM. Statistical difference between the groups was measured by one-way ANOVA; multiple comparisons were corrected by Boneferroni correction. *$p \leq 0.05$, **$p \leq 0.01$, ***$p \leq 0.001$A, ****$p \leq 0.0001$.

For further confirmation, I investigated if the similar effects would be discerned for the expression of another fibrotic marker, namely alpha-1-type I Collagen (COL1A1). Consistently, similar findings were obtained for the expression of COL1A1 at both baseline **(Figure 5.6A-B)** and upon stimulation with TGF-β **(Figure 5.7 A-B).**

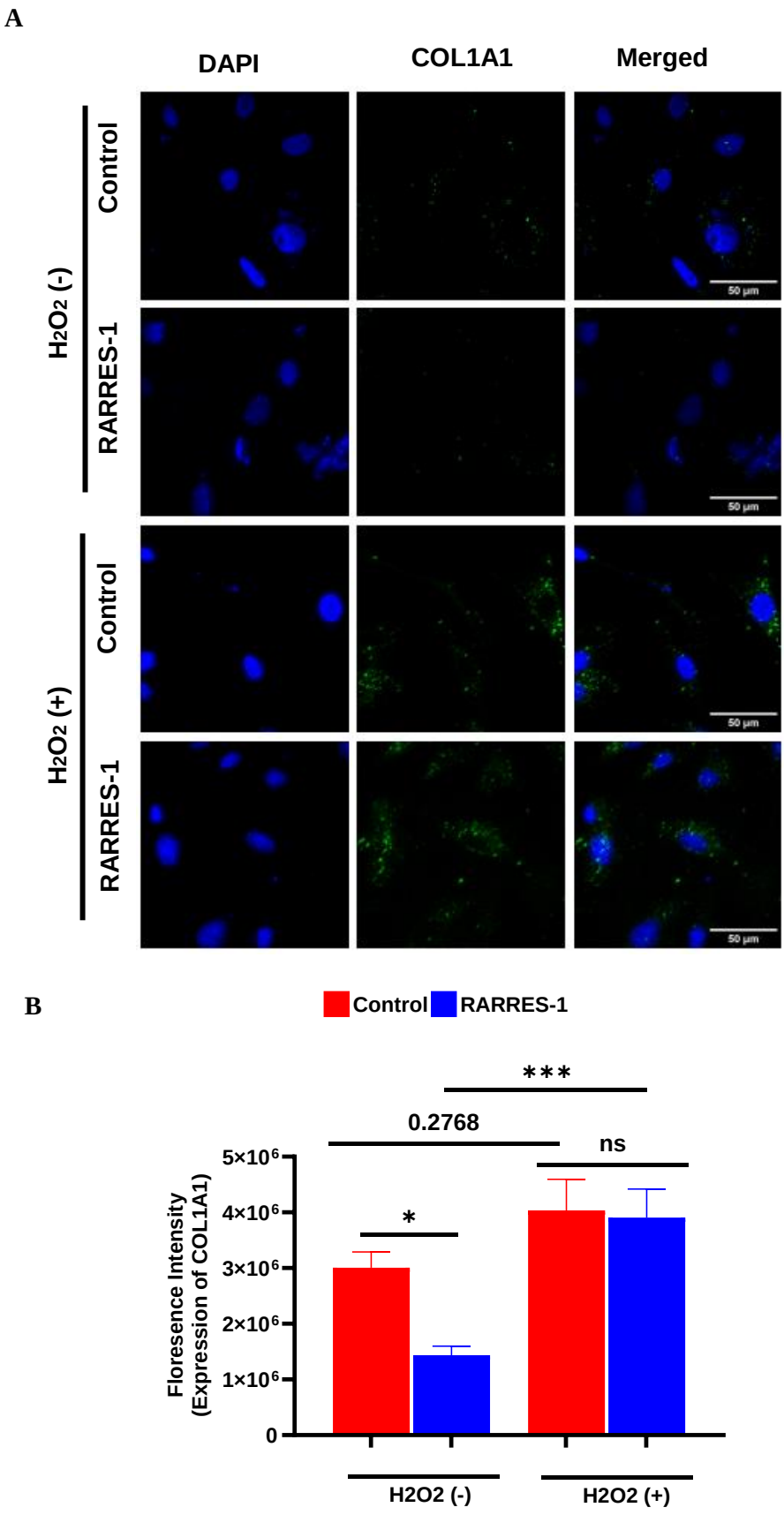

Figure 5.6: ROS inducers reverse the antifibrotic effect of RARRES-1 in unstimulated HSCs. LX-2 cells transfected with RARRES-1 and treated with or without H2O2 for 2 hours

and expression of COL1A1was assessed (n=2). **A)** Representative images for expression of COL1A1. **B)** Quantification of COL1A1 at baseline. Imaging was undertaken using deltavision microscope and analysed using image J. Values are represented as mean ± SEM. Statistical difference between the groups was measured by one-way ANOVA; multiple comparisons were corrected by Boneferroni correction. *$p \leq 0.05$, **$p \leq 0.01$, ***$p \leq$ 0.001A, ****$p \leq 0.0001$.

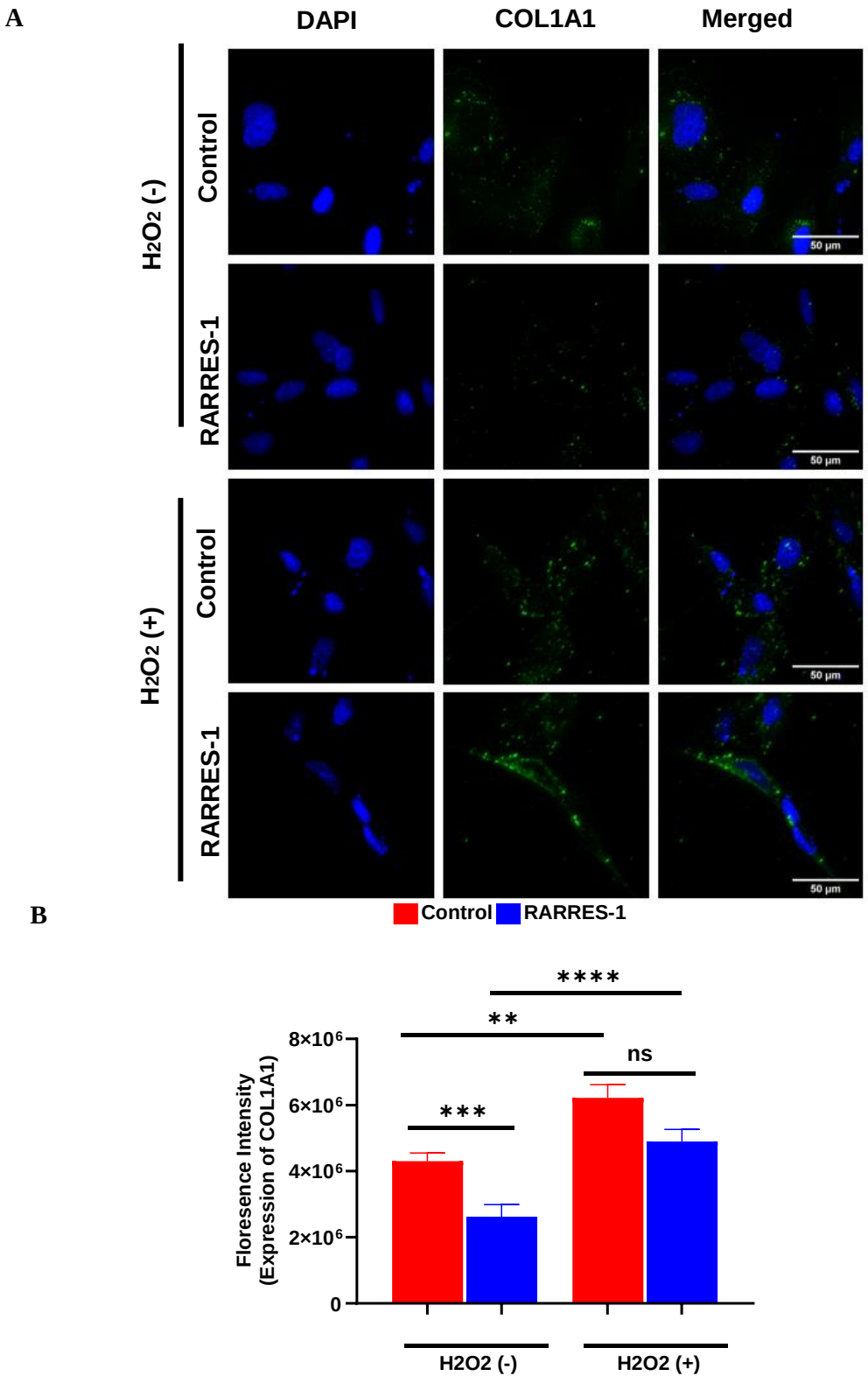

Figure 5.7: ROS inducers reverse the antifibrotic effect of in TGF-β stimulated HSCs. LX-2 cells transfected with RARRES-1 plasmid and treated with or without H_2O_2 for 2 hours before challenging with TGF-β and expression of COL1A1 was assessed (n=2). **A)**

Representative images for expression of COL1A1. **B)** Quantification of COL1A1 upon stimulation with TGF-β. Imaging was undertaken using deltavision microscope and analysed using image J. Values are represented as mean ± SEM. Statistical difference between the groups was measured by one-way ANOVA; multiple comparisons were corrected by Boneferroni correction. *$p \leq 0.05$, **$p \leq 0.01$, ***$p \leq 0.001$A, ****$p \leq 0.0001$.

5.2.4 ROS inhibitors synergize the antifibrotic effect of RARRES-1

For further confirmation that the antifibrotic effect of RARRES-1 is via regulation of ROS generation level, I opted to investigate the reverse approach and test effect of ROS inhibitors on the RARRES1 anti-fibrotic effect. To this end, Lx2 cells were transfected with RARRES-1 as described above, and cells were treated with different ROS inhibitors, namely glutathione (detoxify free radicals), Mito-TEMPO (mitochondrial targeted antioxidant that specifically scavenges mitochondrial ROS) and 4μ8C (IREA1 inhibitor that prevent splicing of XBP1 mRNA and reduce ROS generation), 2 hours before challenging with or without TGFβ for 24 hours. The expression of α-SMA was measured by immunofluorescence. Results confirmed synergistic inhibition of α-SMA in LX-2 cells transfected with RARRES-1 and treated with ROS inhibitors: glutathione **(Figure 5.8** and **Figure 5.9)**, Mito-TEMPO **(Figure 5.10** and **Figure 5.11)** and 4μ8C **(Figure 5.12** and **Figure 5.13)**.

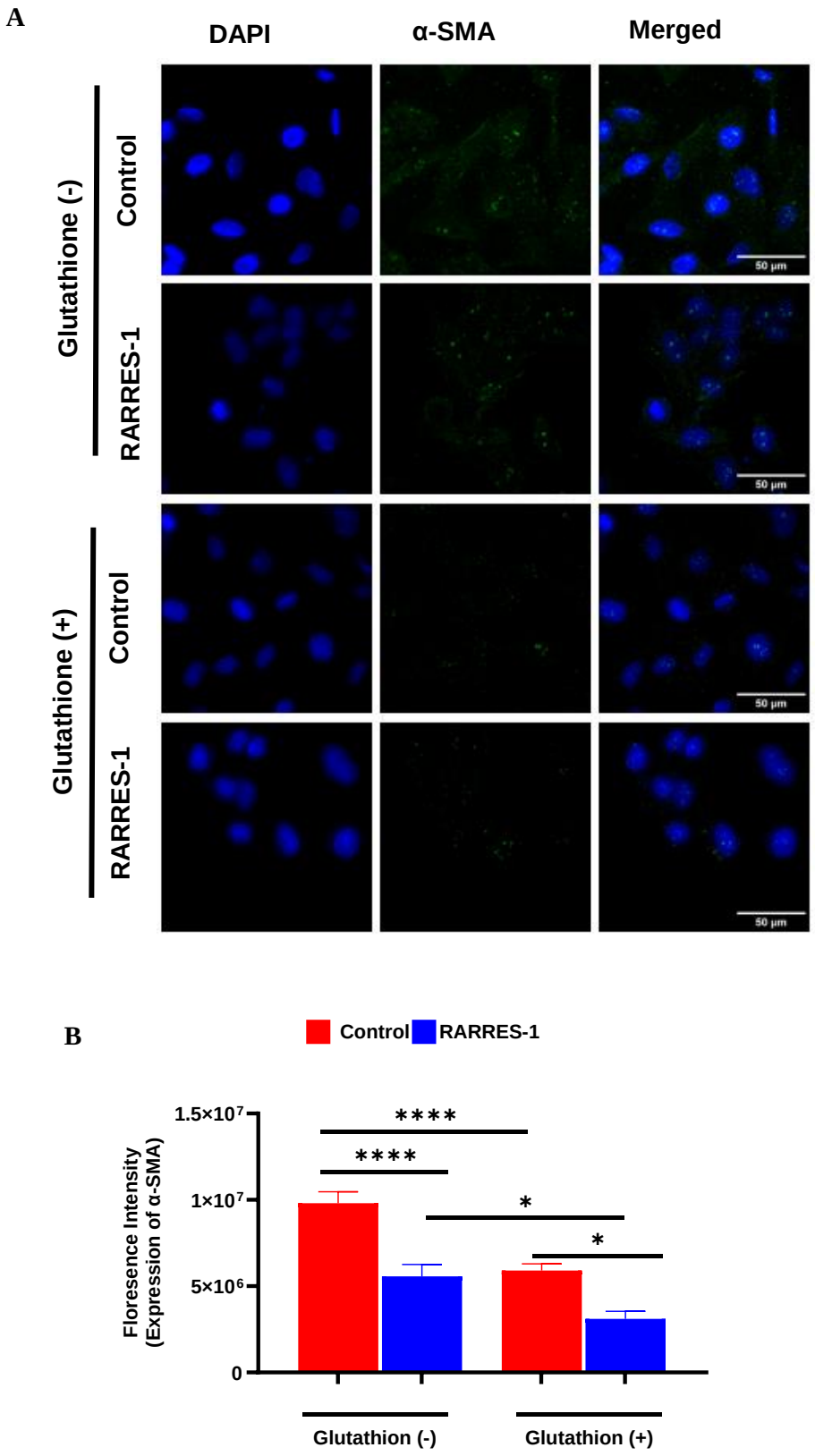

Figure 5.8: ROS inhibitors synergise the antifibrotic effect of RARRES-1 in unstimulated HSCs. LX-2 cells were transfected with RARRES-1 plasmid and treated with glutathione for 2 hours and expression of α-SMA was assessed (n=2). **A)** Representative

images for expression of α-SMA. **B)** Quantification of α-SMA at baseline. Imaging was undertaken using deltavision microscope and analysed using image J. Values are represented as mean ± SEM. Statistical difference between the groups was measured by one-way ANOVA; multiple comparisons were corrected by Boneferroni correction. *$p \leq 0.05$, **$p \leq 0.01$, ***$p \leq 0.001$A, ****$p \leq 0.0001$.

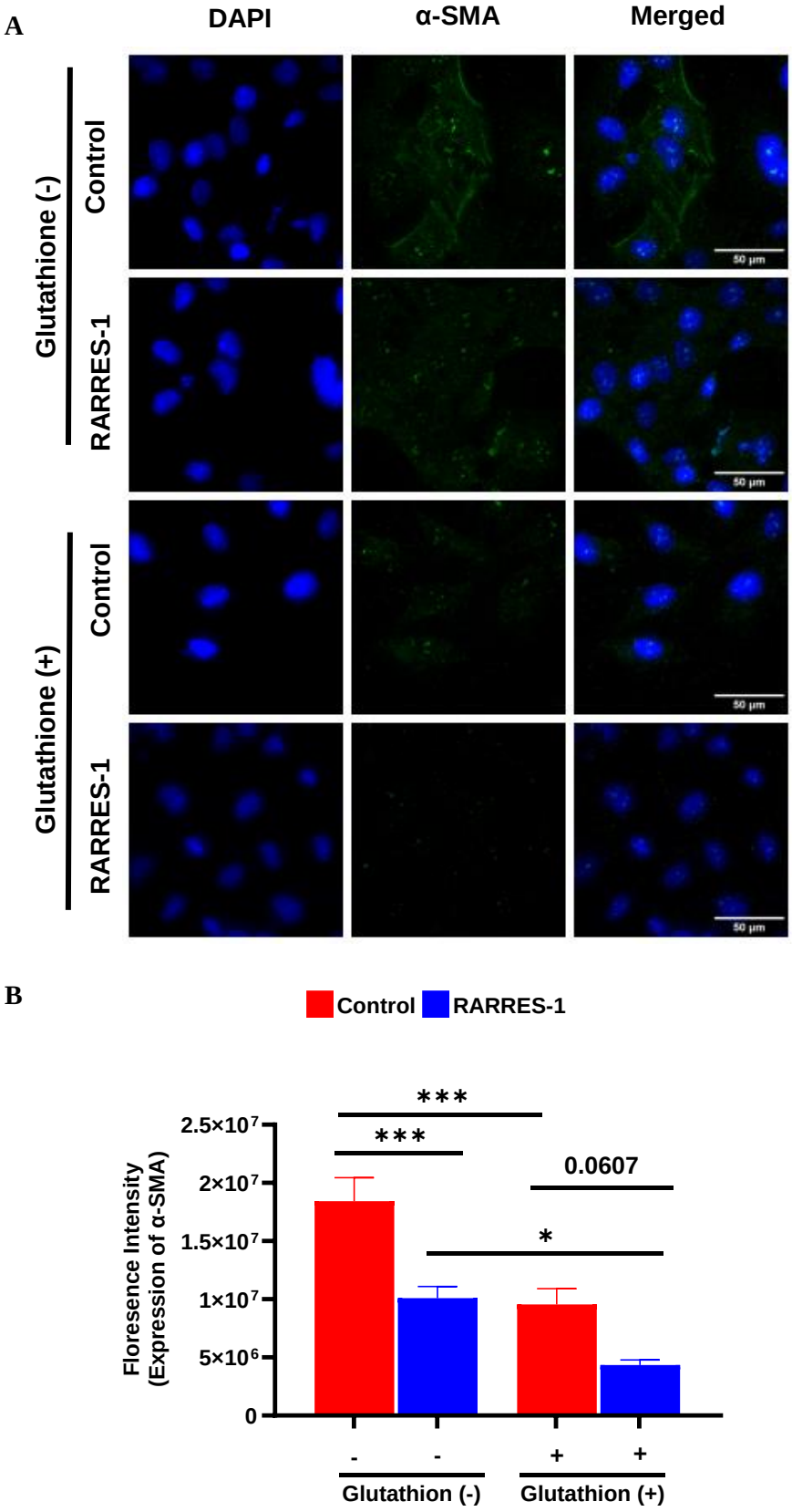

Figure 5.9: ROS inhibitors synergise the antifibrotic effect of RARRES-1 in TGF-β stimulated HSCs. LX-2 cells were transfected with RARRES-1 and treated with glutathione for 2 hours before challenging with TGFβ and expression of α-SMA was assessed (n=2). **A)**

Representative images for expression of α-SMA. **B)** Quantification of α-SMA upon stimulation with TGF-β. Imaging was undertaken using deltavision microscope and analysed using image J. Values are represented as mean ± SEM. Statistical difference between the groups was measured by one-way ANOVA; multiple comparisons were corrected by Boneferroni correction. $*p \leq 0.05$, $**p \leq 0.01$, $***p \leq 0.001$A, $****p \leq 0.0001$.

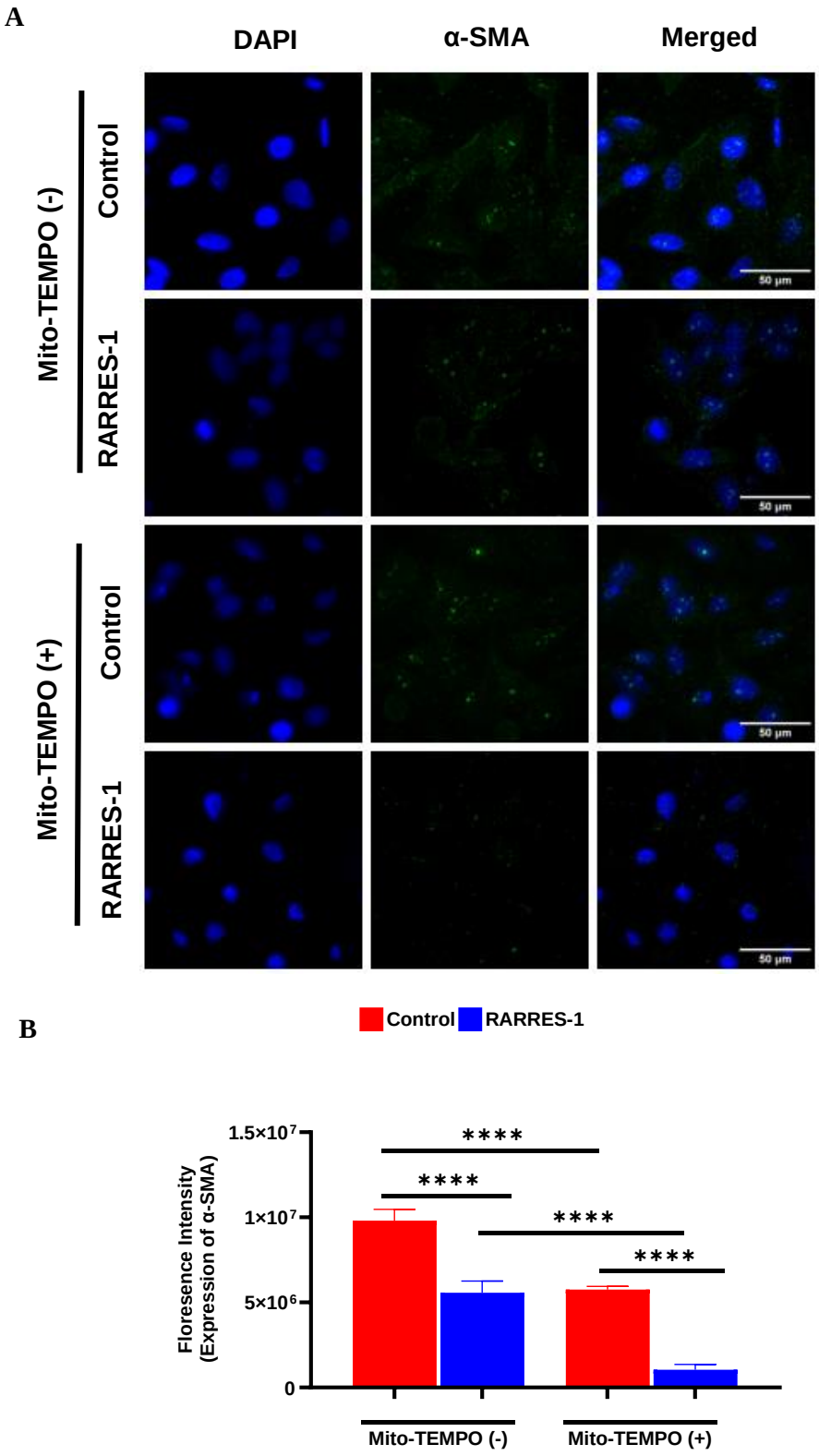

Figure 5.10: ROS inhibitors synergise the antifibrotic effect of RARRES-1 in unstimulated HSCs. LX-2 cells transfected with RARRES-1 plasmid and treated with Mito-TEMPO for 2 hours and expression of α-SMA was assessed (n=2). **A)** Representative images for expression of α-SMA. **B)** Quantification of α-SMA at baseline. Imaging was undertaken

using Deltavision microscope and analysed using image J. Values are represented as mean ± SEM. Statistical difference between the groups was measured by one-way ANOVA; multiple comparisons were corrected by Boneferroni correction.*$p \leq 0.05$, **$p \leq 0.01$, ***$p \leq 0.001$A, ****$p \leq 0.0001$.

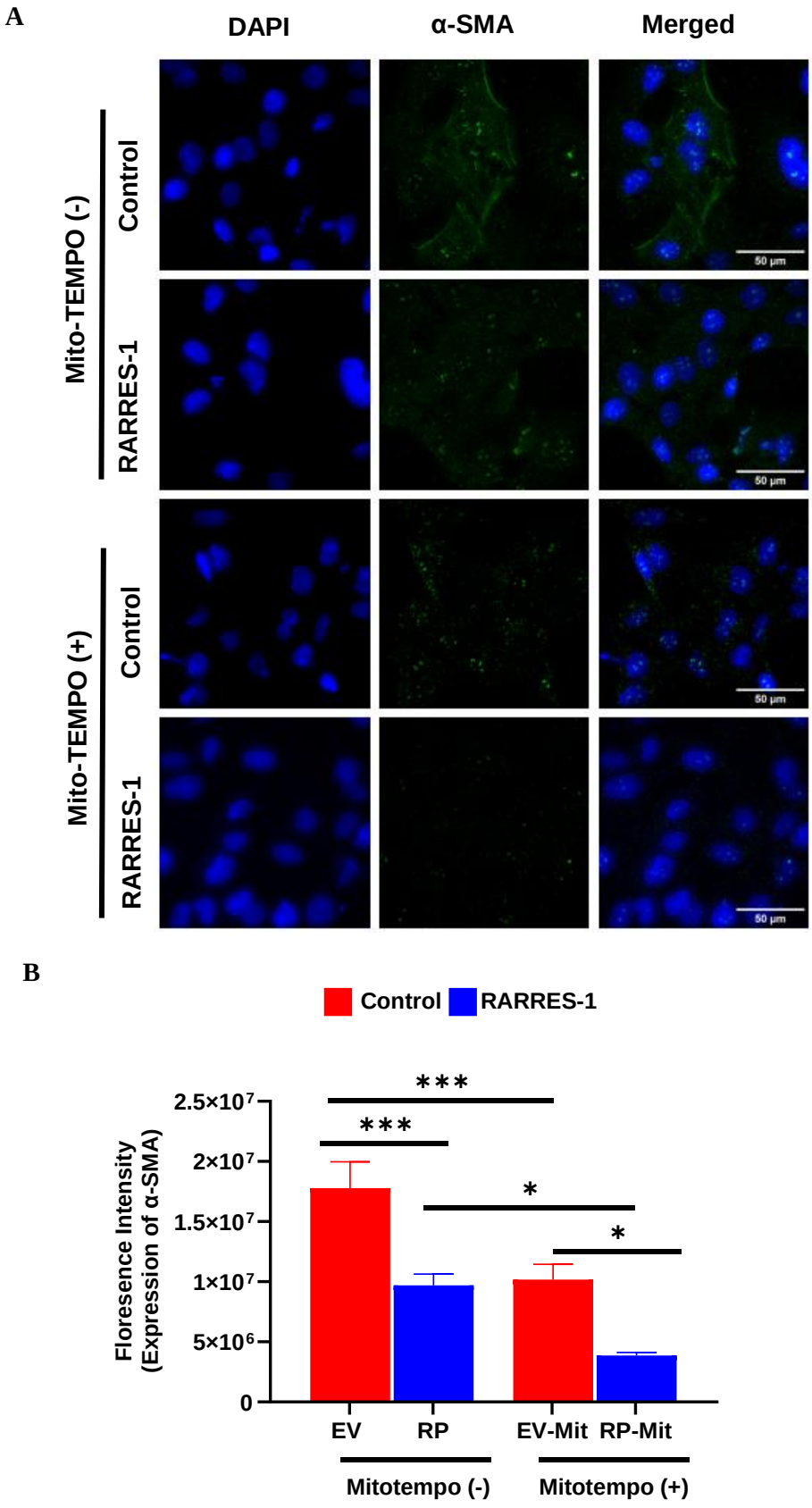

Figure 5.11: ROS inhibitors synergise the antifibrotic effect of RARRES-1 in TGF-β stimulated HSCs. LX-2 cells were transfected with RARRES-1 and treated with Mito-

TEMPO for 2 hours before challenging with TGF-β and expression of α-SMA was assessed (n=2). **A)** Representative images for expression of α-SMA. **B)** Quantification of α-SMA upon stimulation with TGF-β. Imaging was undertaken using Deltavision microscope and analysed using image J. Values are represented as mean ± SEM. Statistical difference between the groups was measured by one-way ANOVA; multiple comparisons were corrected by Boneferroni correction. *$p \leq 0.05$, **$p \leq 0.01$, ***$p \leq 0.001$A, ****$p \leq 0.0001$.

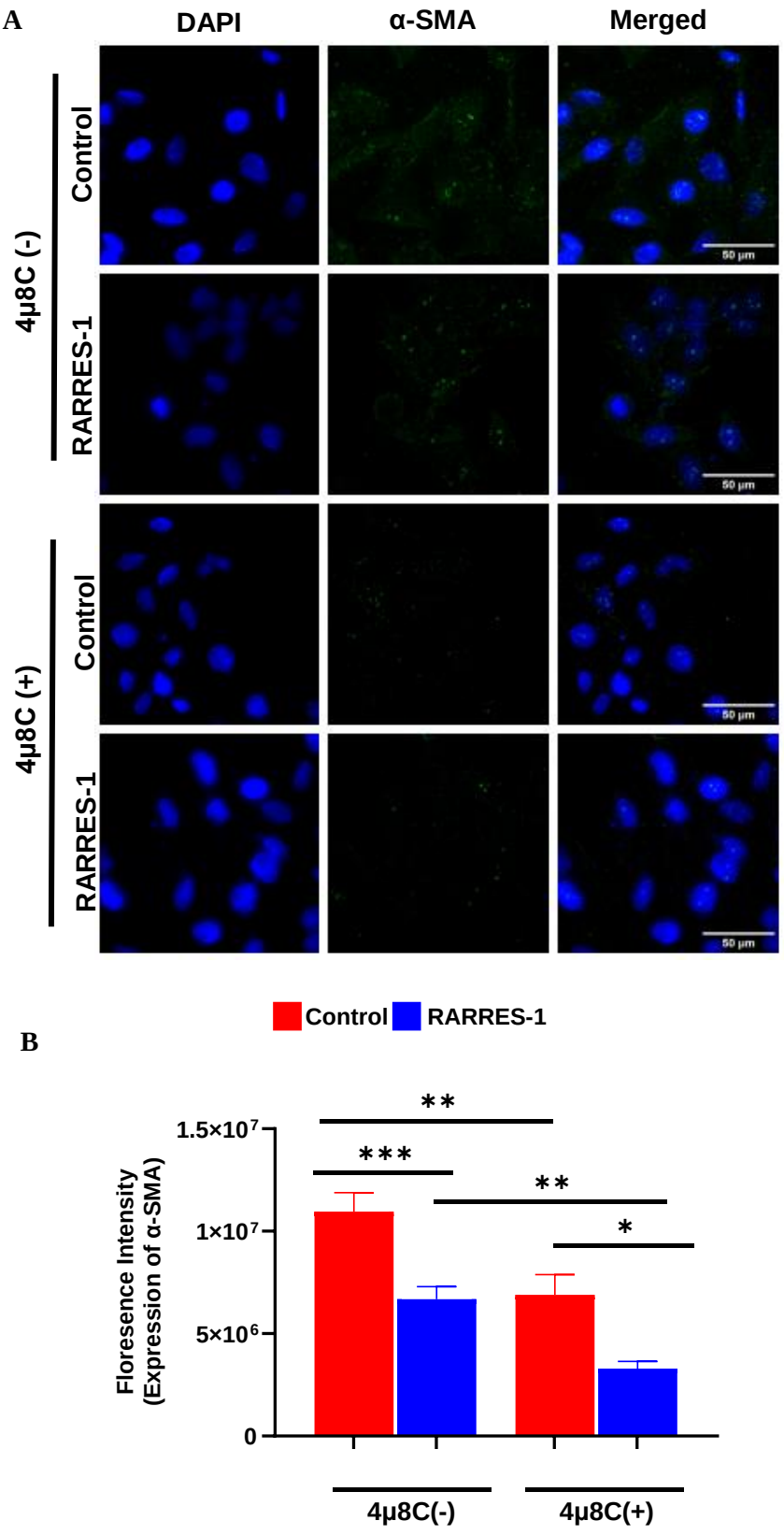

Figure 5.12: ROS inhibitors synergise the antifibrotic effect of RARRES-1 in unstimulated HSCs. LX-2 cells were transfected with RARRES-1 plasmid and treated with 4µ8C for 2 hours and expression of α-SMA was assessed (n=2). **A)** Representative images for

expression of α-SMA at baseline. **B)** Quantification of α-SMA at baseline. Imaging was undertaken using Deltavision microscope and analysed using image J. Values are represented as mean ± SEM. Statistical difference between the groups was measured by one-way ANOVA; multiple comparisons were corrected by Boneferroni correction. *$p \leq 0.05$, **$p \leq 0.01$, ***$p \leq 0.001$A, ****$p \leq 0.0001$.

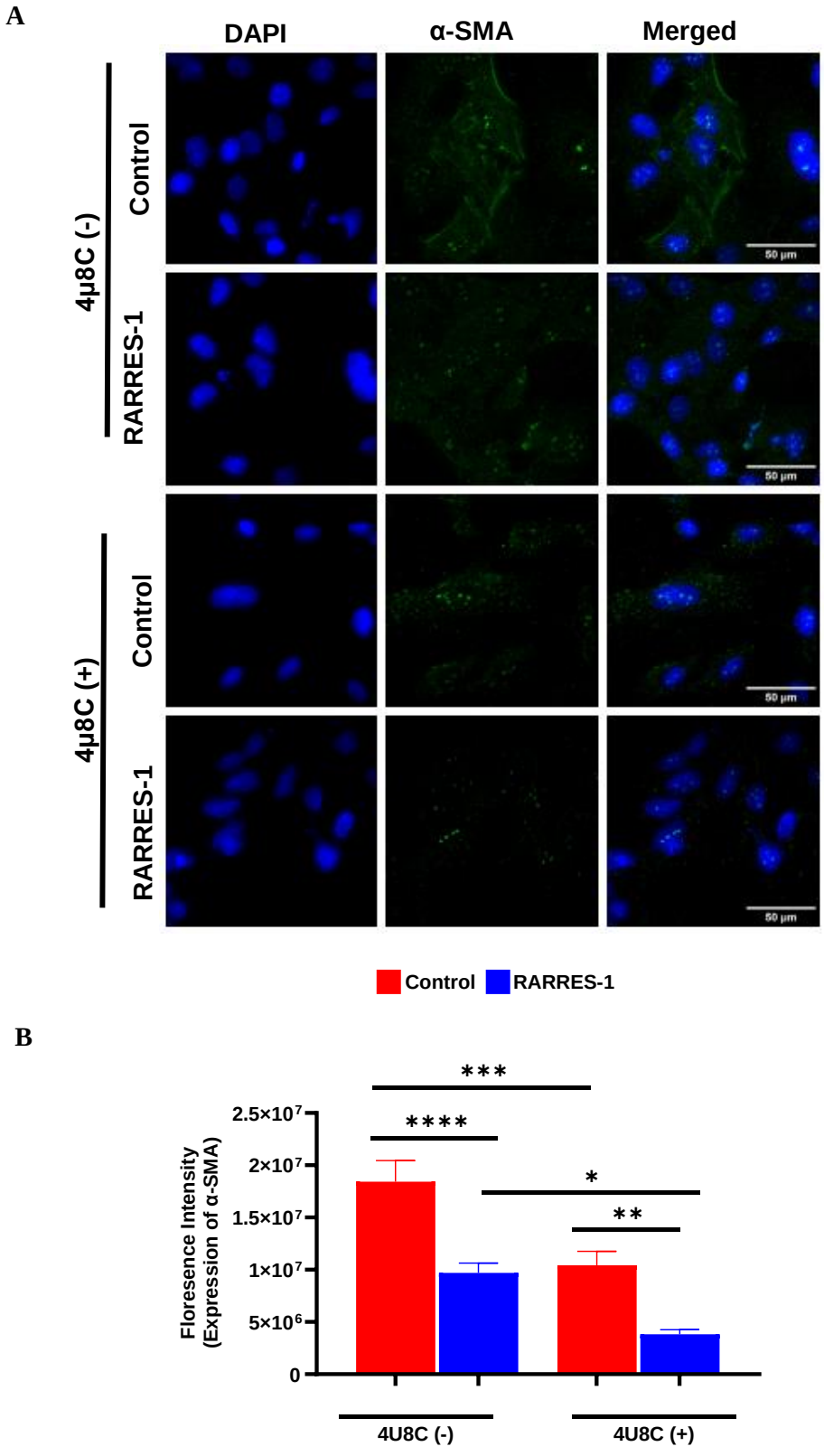

Figure 5.13: ROS inhibitors synergise the antifibrotic effect of RARRES-1 in TGF-β stimulated HSCs. LX-2 cells were transfected with RARRES-1 and treated with 4µ8C for 2 hours before challenging with TGFβ and expression of α-SMA was assessed (n=2). **A)**

Representative images for expression of α-SMA. **B)** Quantification of α-SMA upon stimulation with TGF-β. Imaging was undertaken using Deltavision microscope and analysed using image J. Values are represented as mean ± SEM. Statistical difference between the groups was measured by one-way ANOVA; multiple comparisons were corrected by Boneferroni correction. *$p \leq 0.05$, **$p \leq 0.01$, ***$p \leq 0.001$A, ****$p \leq 0.0001$.

For further confirmation, the expression of another fibrotic marker; COL1A1 was also assessed. To do this, Lx2 cells were transfected with RARRES-1 and treated with ROS inhibitors as described above. The expression of COL1A1 was measured by immunofluorescence. Consistently, similar results were obtained upon treatment with various ROS inhibitors: glutathione **(Figure 5.14-Figure 5.15)**, Mito-TEMPO **(Figure 5.16-Figure 5.17)** and 4μ8C **(Figure 5.18-Figure 5.19).**

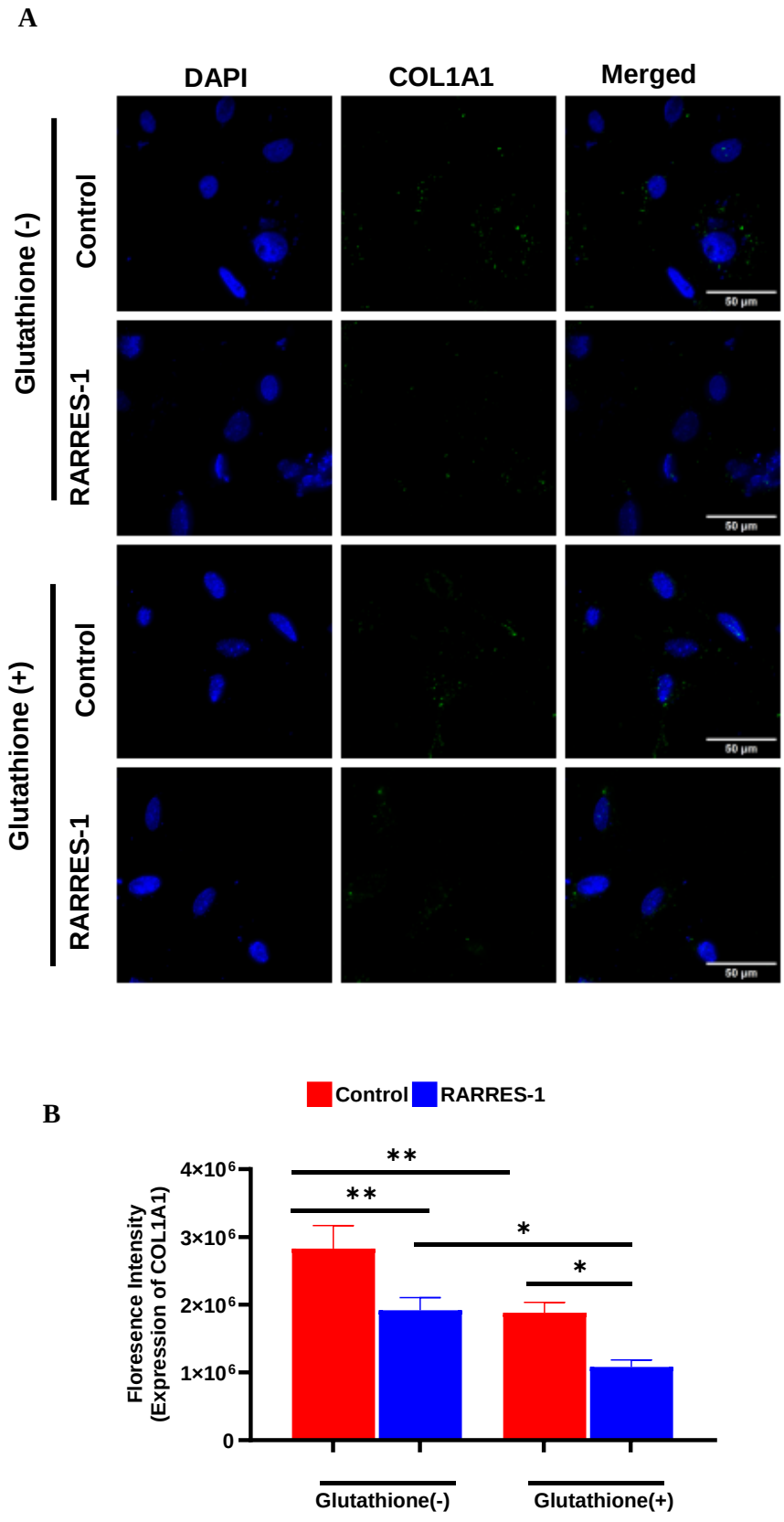

Figure 5.14: ROS inhibitors synergise the antifibrotic effect of RARRES-1 in unstimulated HSCs. LX-2 cells were transfected with RARRES-1 plasmid and treated with

glutathione for 2 hours and expression of COL1A1 was assessed (n=2). **A)** Representative images for expression of COL1A1. **B)** Quantification of COL1A1 at baseline. Imaging was undertaken using Deltavision microscope and analysed using image J. Values are represented as mean ± SEM. Statistical difference between the groups was measured by one-way ANOVA; multiple comparisons were corrected by Boneferroni correction. *$p \leq 0.05$, **$p \leq 0.01$, ***$p \leq 0.001$A, ****$p \leq 0.0001$.

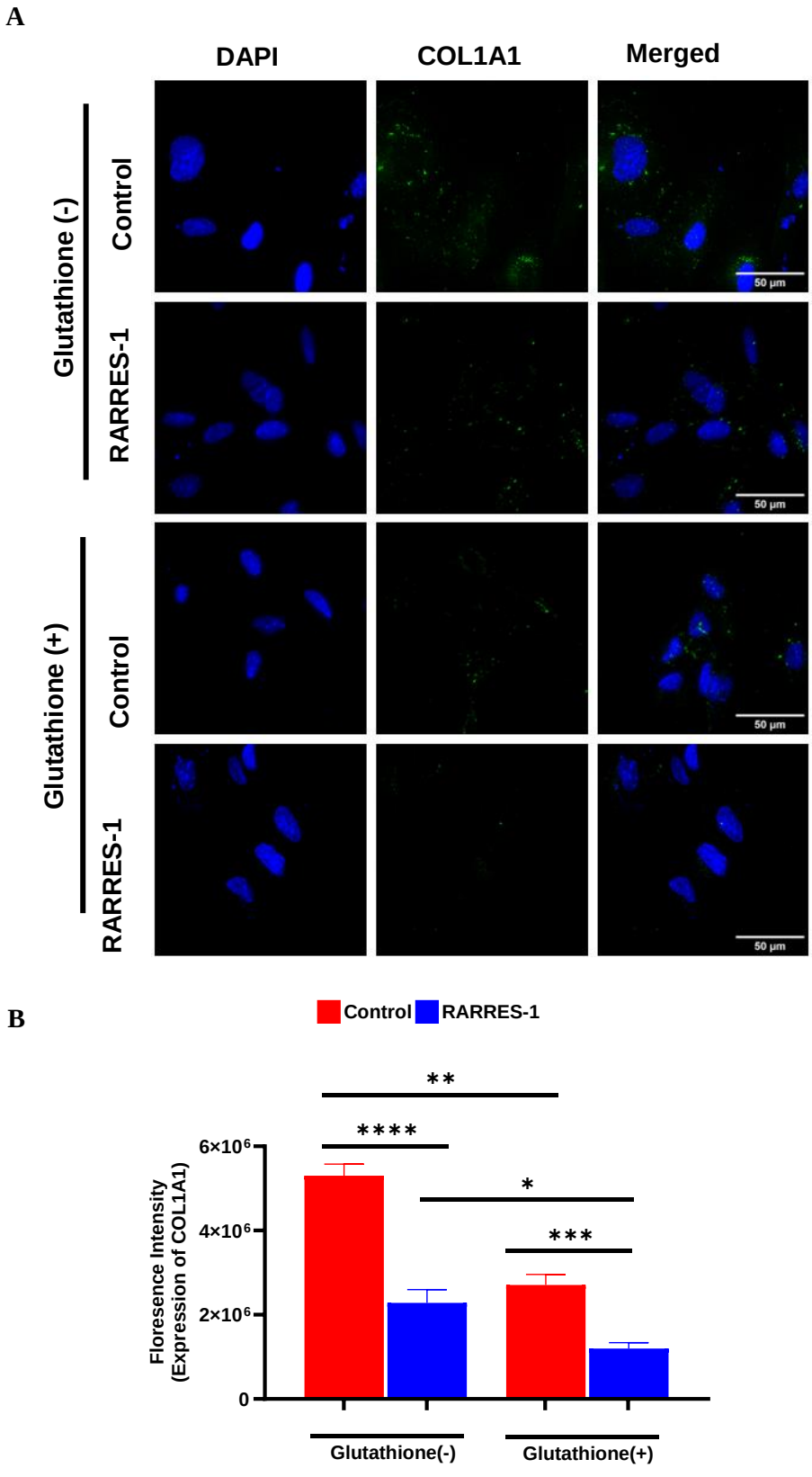

Figure 5.15: ROS inhibitors synergise the antifibrotic effect of RARRES-1 in TGF-β stimulated HSCs. LX-2 cells were transfected with RARRES-1 and treated with glutathione for 2 hours before challenging with TGFβ and expression of COL1A1 was assessed (n=2). **A)**

Representative images for expression of COL1A1. **B)** Quantification of COL1A1 upon stimulation with TGF-β. Imaging was undertaken using deltavision microscope and analysed using image J. Values are represented as mean ± SEM. Statistical difference between the groups was measured by one-way ANOVA; multiple comparisons were corrected by Boneferroni correction.*$p \leq 0.05$, **$p \leq 0.01$, ***$p \leq 0.001$A, ****$p \leq 0.0001$.

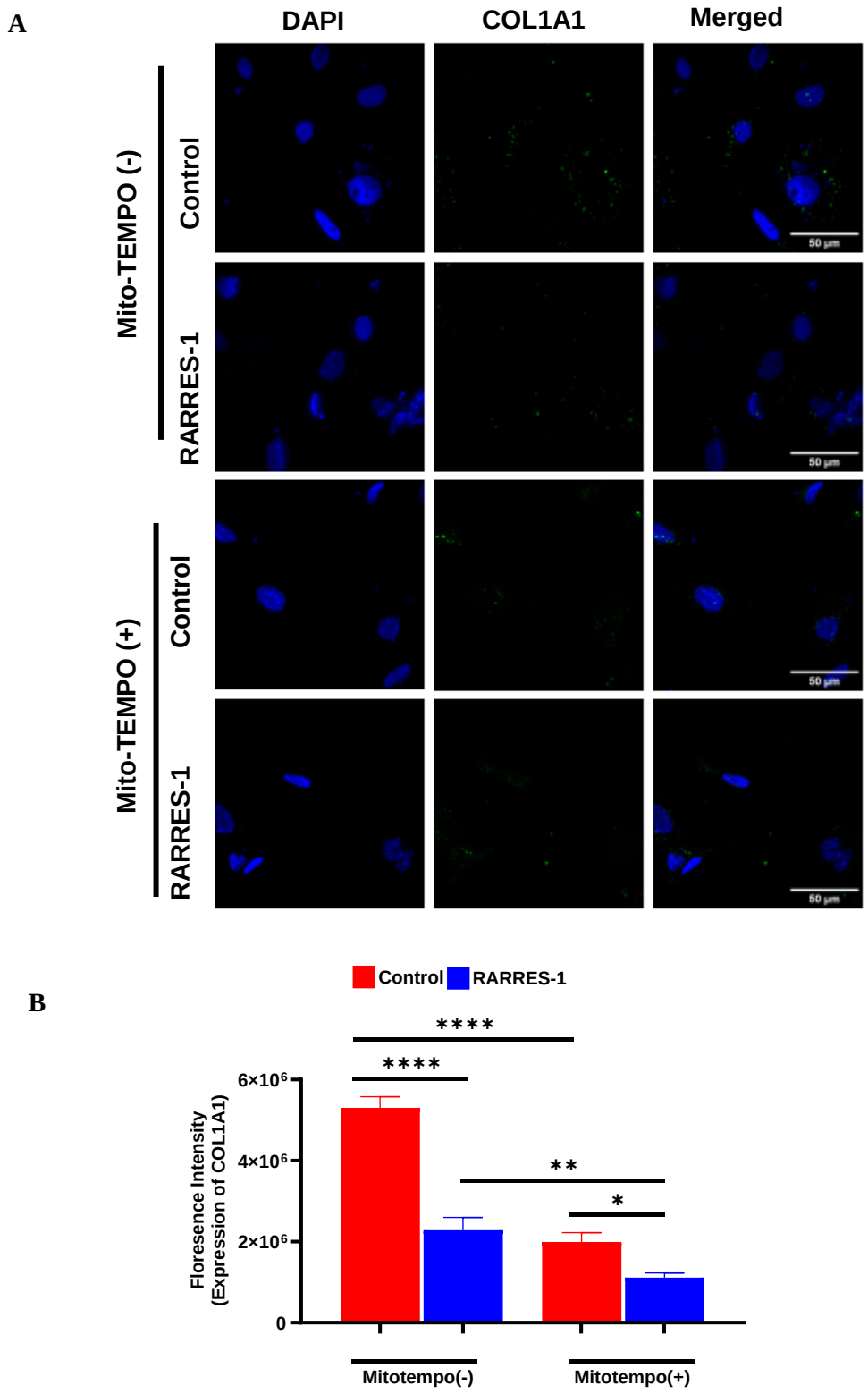

Figure 5.16: ROS inhibitors synergise the antifibrotic effect of RARRES-1 in unstimulated HSCs. LX-2 cells were transfected with RARRES-1 and treated with Mito-TEMPO for 2 hours and expression of COL1A1 was assessed (n=2). **A)** Representative images for expression of COL1A1. **B)** Quantification of COL1A1 at baseline. Imaging was

undertaken using Deltavision microscope and analysed using image J. Values are represented as mean ± SEM. Statistical difference between the groups was measured by one-way ANOVA; multiple comparisons were corrected by Boneferroni correction. *$p \leq 0.05$, **$p \leq 0.01$, ***$p \leq 0.001$A, ****$p \leq 0.0001$.

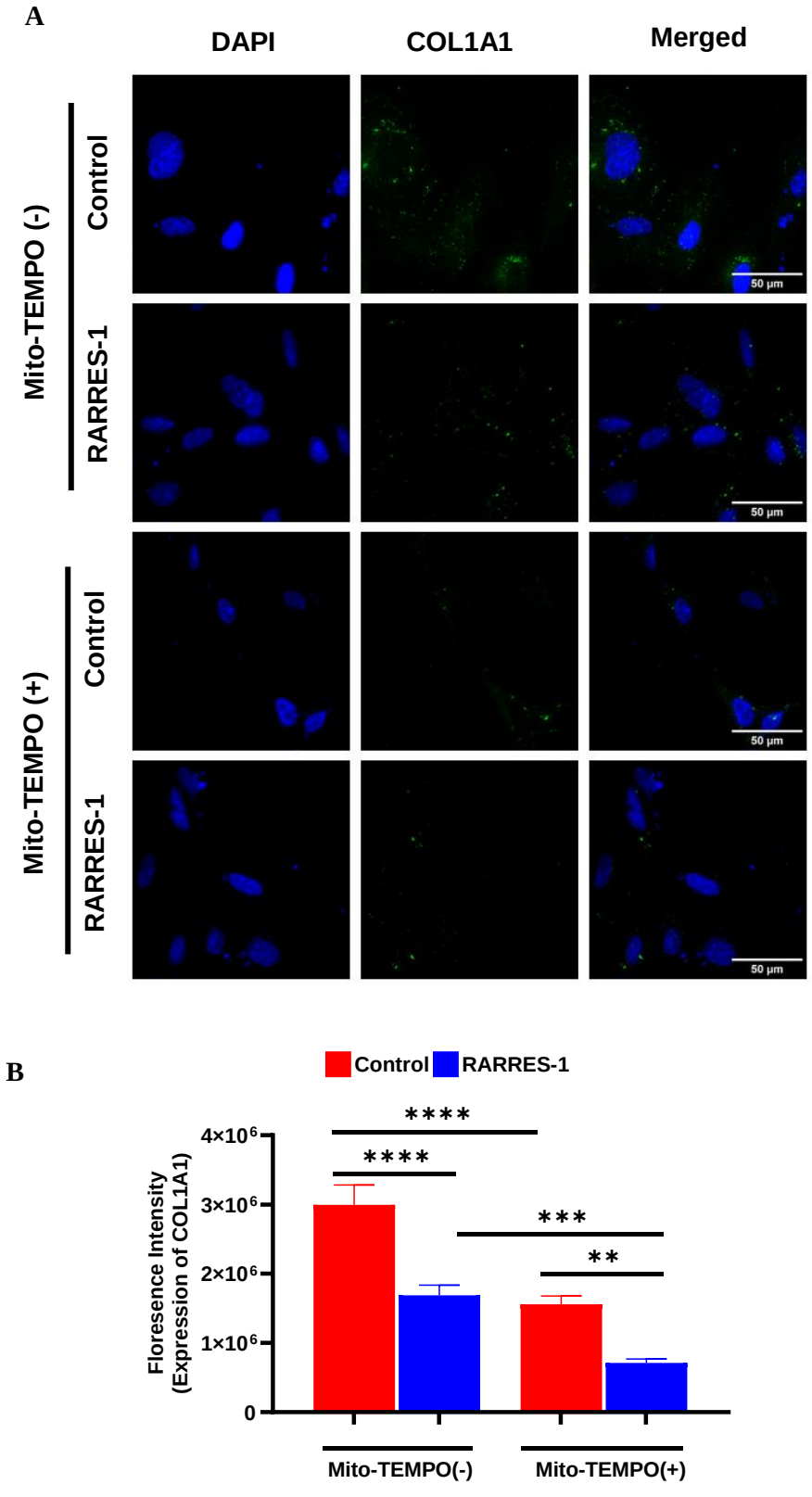

Figure 5.17: ROS inhibitors synergise the antifibrotic effect of RARRES-1 in TGF-β stimulated HSCs. LX-2 cells were transfected with RARRES-1 and treated with Mito-TEMPO for 2 hours before challenging with TGF-β and expression of COL1A1 was assessed

(n=2). **A)** Representative images for expression of COL1A1. **B)** Quantification of COL1A1 upon stimulation with TGF-β. Imaging was undertaken using deltavision microscope and analysed using image J. Values are represented as mean ± SEM. Statistical difference between the groups was measured by one-way ANOVA; multiple comparisons were corrected by Boneferroni correction. *$p \leq 0.05$, **$p \leq 0.01$, ***$p \leq 0.001$A, ****$p \leq 0.0001$.

A

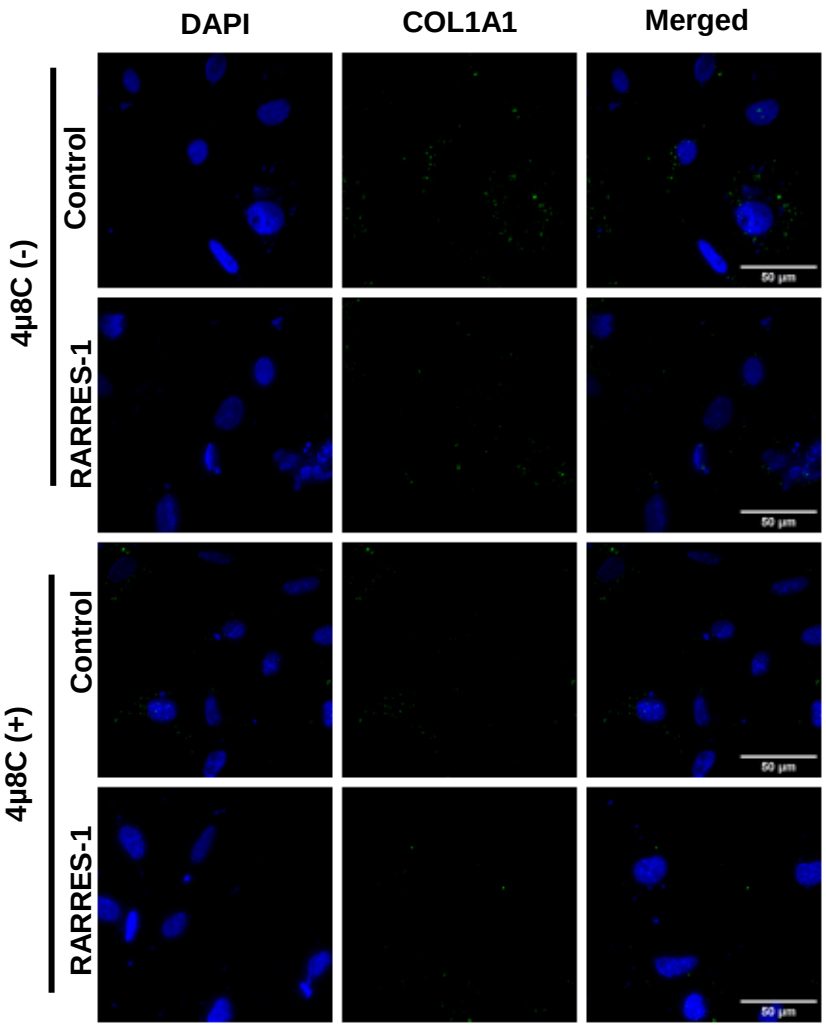

B

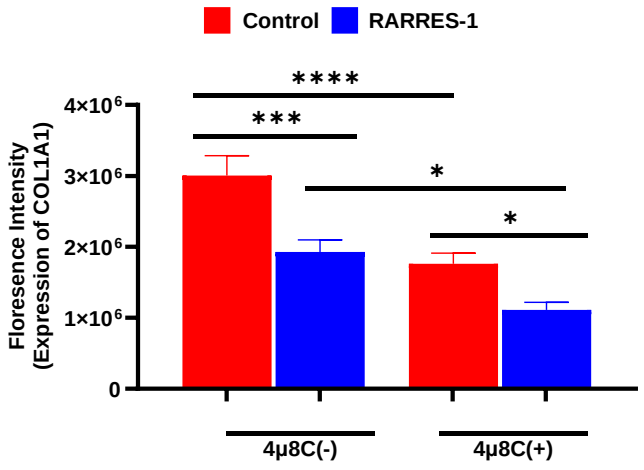

Figure 5.18: ROS inhibitors synergise the antifibrotic effect of RARRES-1in unstimulated HSCs. LX-2 cells transfected with RARRES-1 and treated with 4µ8C for 2 hours and expression of COL1A1 was assessed (n=2). **A)** Representative images for

expression of COL1A1. **B)** Quantification of COL1A1 at baseline. Imaging was undertaken using Deltavision microscope and analysed using image J. Values are represented as mean ± SEM. Statistical difference between the groups was measured by one-way ANOVA; multiple comparisons were corrected by Boneferroni correction. *$p \leq 0.05$, **$p \leq 0.01$, ***$p \leq$ 0.001A, ****$p \leq 0.0001$.

A

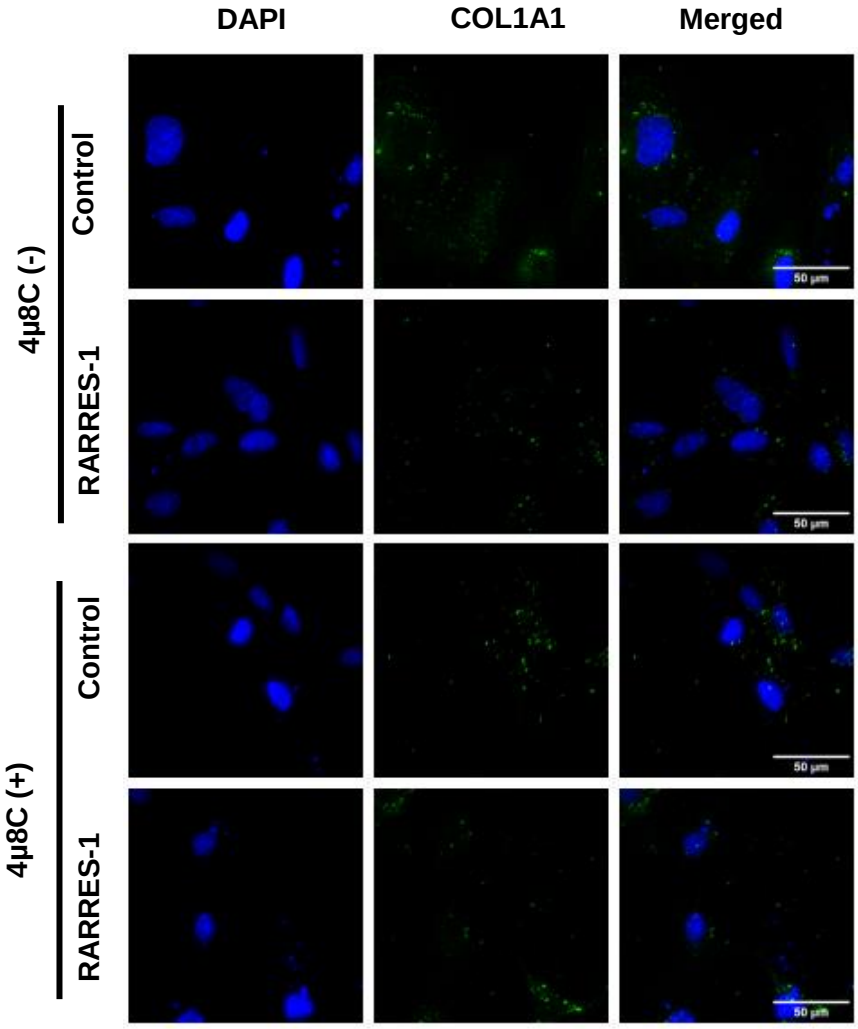

B

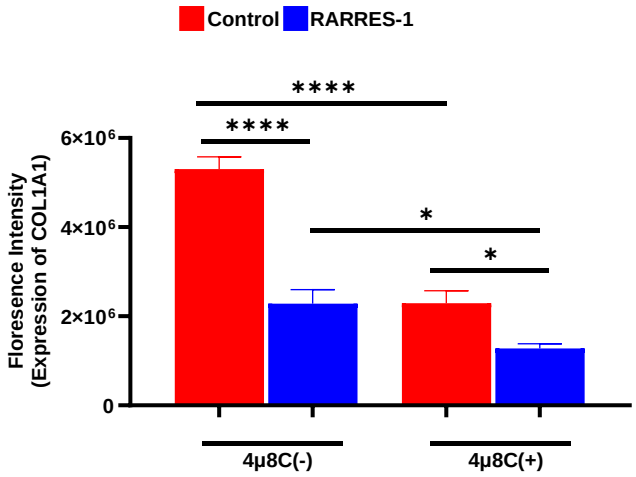

Figure 5.19: ROS inhibitors synergise the antifibrotic effect of RARRES-1 in TGF-β stimulated HSCs. LX-2 cells were transfected with RARRES-1 and treated with 4µ8C for 2 hours before challenging with TGF-β and expression of COL1A1 was assessed (n=2). **A)**

Representative images for expression of COL1A1. **B)** Quantification of COL1A1 upon stimulation with TGF-β. Imaging was undertaken using deltavision microscope and analysed using image J. Values are represented as mean ± SEM. Statistical difference between the groups was measured by one-way ANOVA; multiple comparisons were corrected by Boneferroni correction. *$p \leq 0.05$, **$p \leq 0.01$, ***$p \leq 0.001$A, ****$p \leq 0.0001$.

5.2.5 NOX4 siRNA synergises the antifibrotic effect of RARRES-1

I have demonstrated the synergistic impact of various ROS inhibitors on the antifibrotic effect of RARRES-1. However, these drugs might have also some unspecific effects rather than ROS inhibition. NOX4 is a nicotinamide adenine dinucleotide phosphate (NADPH) oxidase. NADPH is a key source of ROS production [218-220]. Thus, for further confirmation of the specificity of the findings I noticed, I then used NOX4 siRNA to investigate how genetic ROS inhibition modulates the antifibrotic effect of RARRES-1.

To this end, LX-2 cells were double transfected with both RARRES-1 plasmid and NOX4 siRNA for 48 hours and treated with or without TGF-β for 24 hours. Consistently, silencing of NOX4 augmented the reducing effect of RARRES-1 on α-SMA expression both at baseline **(Figure 5.20A-B)** and upon TGF-β stimulation **(Figure 5.21A-B)**.

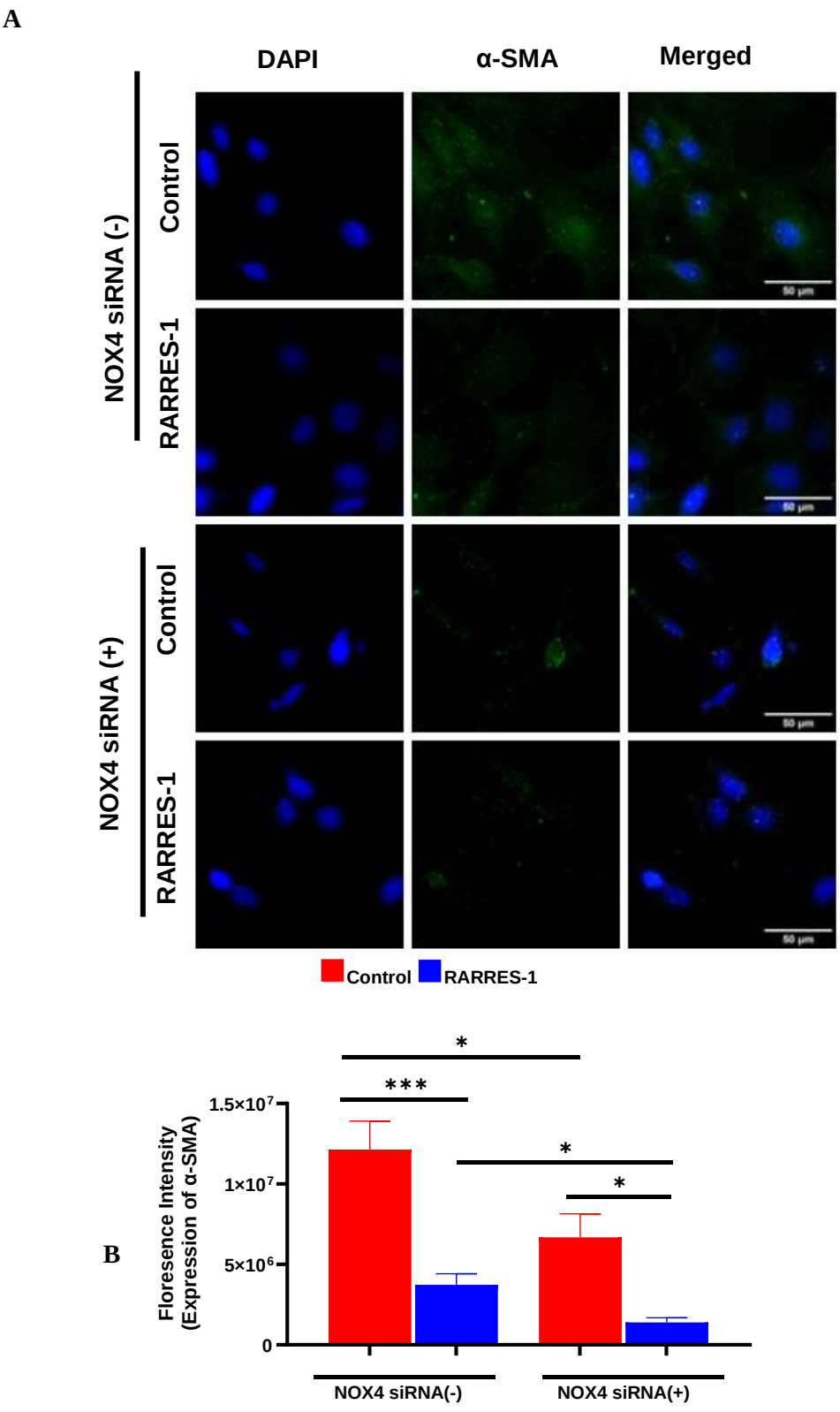

Figure 5.20: NOX4 silencing synergizes the antifibrotic effect of RARRES-1 in unstimulated HSCs. LX-2 cells were transfected with RARRES-1 and NOX4 siRNA for 2 hours and expression of α-SMA was assessed (n=2). **A)** Representative images for expression

of α-SMA. **B)** Quantification of α-SMA in baseline. Imaging was undertaken using deltavision microscope and analysed using image J. Values are represented as mean ± SEM. Statistical difference between the groups was measured by one-way ANOVA; multiple comparisons were corrected by Boneferroni correction. *$p \leq 0.05$, **$p \leq 0.01$, ***$p \leq$ 0.001A, ****$p \leq 0.0001$.

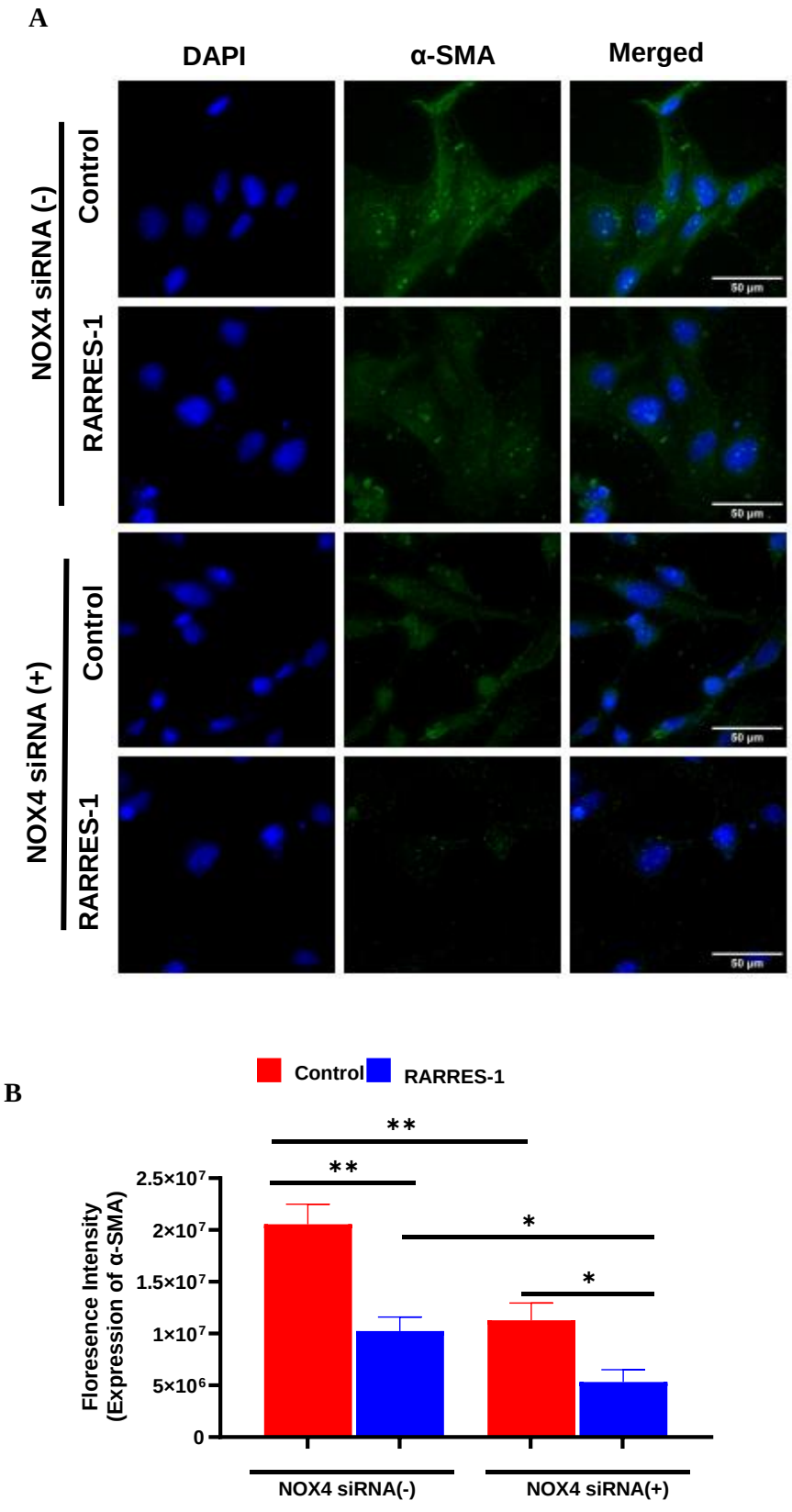

Figure 5.21: NOX4 silencing synergizes the antifibrotic effect of RARRES-1 in TGF-β stimulated HSCs. LX-2 cells were transfected with RARRES-1 and NOX4 siRNA before challenging with TGF-β and expression of α-SMA was assessed (n=2). **A)** Representative

images for expression of α-SMA **B)** Quantification of α-SMA upon stimulation with TGF-β. Imaging was undertaken using deltavision microscope and analysed using image J. Values are represented as mean ± SEM. Statistical difference between the groups was measured by one-way ANOVA; multiple comparisons were corrected by Boneferroni correction. *$p \leq 0.05$, **$p \leq 0.01$, ***$p \leq 0.001$A, ****$p \leq 0.0001$.

Moving further, I investigated if the similar effect could be discerned on the expression of COL1A1. Undertaking similar experiment as described above and measuring the expression of COL1A1 using immunofluorescence. Similar results were obtained at baseline **(Figure 5.22A-B)** and upon TGF-β stimulation **(Figure 5.23A-B)**.

Collectively these findings indicate that RARRES-1 produces its antifibrotic effect, at least partially through regulation of ROS production.

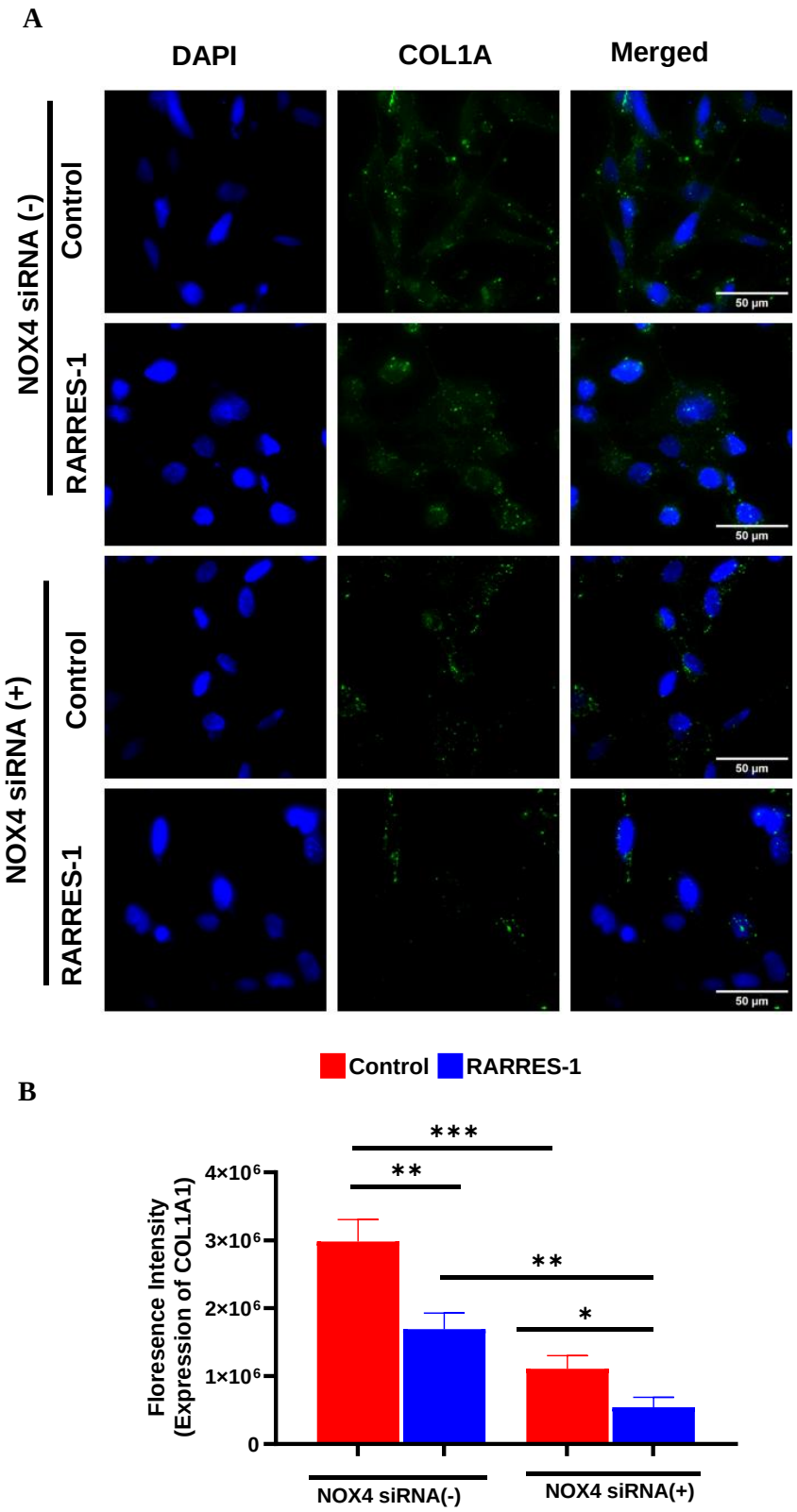

Figure 5.22: NOX4 siRNA synergizes the antifibrotic effect of RARRES-1 in unstimulated HSCs. LX-2 cells were transfected with RARRES-1 and NOX4 siRNA for 2 hours and expression of COL1A1 was assessed (n=2). **A)** Representative images for

expression of COL1A1. **B)** Quantification of COL1A1 at baseline. Imaging was undertaken using deltavision microscope and analysed using image J. Values are represented as mean ± SEM. Statistical difference between the groups was measured by one-way ANOVA; multiple comparisons were corrected by Boneferroni correction. *$p \leq 0.05$, **$p \leq 0.01$, ***$p \leq$ 0.001A, ****$p \leq 0.0001$.

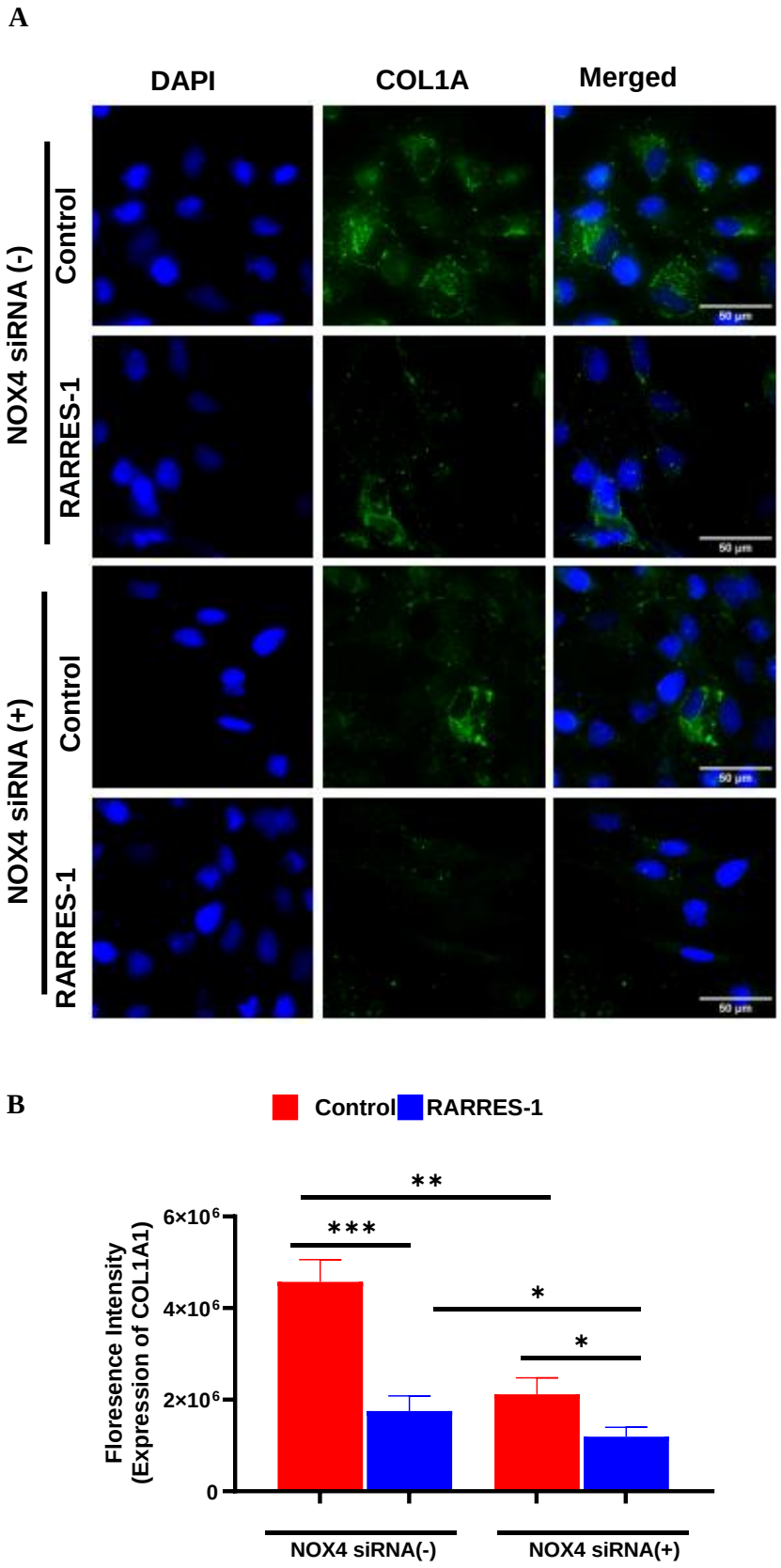

Figure 5.23: NOX4 siRNA synergizes the antifibrotic effect of RARRES-1 in TGF-β stimulated HSCs. LX-2 cells transfected with RARRES-1 and NOX4 siRNA before challenging with TGF-β and expression of COL1A1 was assessed (n=2). **A)** Representative

images for expression of COL1A1. **B)** Quantification of COL1A1 upon stimulation with TGF-β. Imaging was undertaken using Deltavision microscope and analysed using image J. Values are represented as mean ± SEM. Statistical difference between the groups was measured by one-way ANOVA; multiple comparisons were corrected by Boneferroni correction. *$p \leq 0.05$, **$p \leq 0.01$, ***$p \leq 0.001$A, ****$p \leq 0.0001$.

5.3 Discussion

In the previous chapter, I reported that RARRES1 produces antifibrotic effect by regulating mitochondrial activity in terms of mitochondrial morphology, mitochondrial import, ATP synthesis, mitochondrial turnover, mitochondrial ROS production, and the mitochondrial membrane potential and ultimately reduces the expression of fibrotic markers. In this chapter, I extended these findings and revealed that the underlying mechanism of the antifibrotic effect of RARRES-1 is at least partially mediated by the regulation of ROS production.

To elaborate further, the results presented in this chapter indicated that RARRES-1 activation reduces the generation of both cytoplasmic and mitochondrial ROS. Additionally, the data presented in this chapter confirmed that the antifibrotic effect of RARRES-1 is reversed by ROS inducers. This phenomenon might mocking the pathophysiological context that occurs during liver fibrosis when a constant source of liver injury results in the loss of all protective barriers and may cause uncontrolled ROS generation [221-223], attenuating RARRES1 expression, which ultimately causes further HSCs activation and liver fibrosis progression.

Interestingly, my results confirmed that RARRES-1 activation along with ROS inhibitors synergistically reduced HSCs activation, as evidenced by the expression of various fibrotic markers. This effect was confirmed using a multipronged approach involving the administration of multiple pharmacological ROS inhibitors (glutathione, Mito-TEMPO and 4μ8C) and complemented by genetic inhibitors (NOX4 siRNA).

TGF-β, which a key pro-fibrogenic cytokine promotes fibrosis via multiple mechanisms. One of these effects is to increase the generation of ROS via regulation of NOX4 signalling pathway [224] and to supress the antioxidant enzymes that develop redox imbalance. Increased ROS cause liver damage, initiate fibrosis and disrupts oxidative stress. This oxidative stress damages cellular proteins, lipids and DNA ultimately inducing inflammatory

responses, apoptosis, and necrosis [225]. This ROS in turn activates TGF-β and hence form a vicious cycle [226].

Herein, I demonstrated that RARRES1 breaks this vicious cycle as it reduces the ROS generation in HSCs at both baseline and upon TGF-β stimulation. Additionally, it attenuates the pro-fibrotic effect of TGF-β and the synergistic effect of ROS on the pro-fibrotic effect of TGF-β. Therefore, RARRES-1 represents an attractive therapeutic target for liver fibrosis that can restore normal redox balance in cells and thereby halt liver fibrosis.

In conclusion, the results presented in this chapter indicated that RARRES-1 activation has an antifibrotic effect that is at least partially mediated by the regulation of ROS generation. However, whether other pathways and mechanisms might be involved in the anti-fibrotic effect of RARRES-1 activation has yet to be determined, which I will explore in the next chapters.

Chapter Six: RARRES-1 regulates fibrosis by regulating autophagy

6.1 Introduction

Hepatic stellate cells (HSCs) are the primary cells involved in fibrosis. In the quiescent phase, lipid droplets are normally present. During the activation phase, HSCs lose lipids [227], as lipid droplets are used as energy for HSC activation and fibrosis. Both mitochondrial metabolism and autophagy produce energy during fibrosis, which are closely linked processes [228, 229].

Autophagy is a highly regulated catabolic pathway that maintains cellular homeostasis under normal physiological conditions. However, during cellular stress, autophagy induces the degradation of intracellular lipid droplets (LDs) through a process called lipophagy [101, 230].

Autophagy facilitates liver fibrosis by providing the energy required to activate myofibroblasts and fuel the pathways of cell proliferation, extracellular matrix secretion, and cellular contractility via lipid droplet mobilization, free fatty acid release, and mitochondrial β-oxidation [101, 144, 230-233].

During fibrosis, TGF-β1 activates autophagy-related proteins that promote HSCs to initiate autophagy and accelerate liver fibrosis [234]. Similarly, in an *in vivo* mouse model, liver fibrosis was shown to be associated with increased formation of autophagosomes and autophagic vacuoles and increased autophagic flux [101]. Consequently, various autophagy inhibitors have been found to reduce HSC activation and liver fibrosis [235].

The process of autophagy involves different stages, including phagophore formation, nucleation, elongation, autophagosome formation (sequestration) and autolysosome formation (degradation). Mitochondria and autophagy have bidirectional connections, and both processes are sources of energy. Mitochondria produce energy and are also the main source of ROS [194, 236]. However, ROS generation initiates autophagy and increases

autophagic flux during liver fibrosis [237, 238]. Autophagy determines the mitochondrial number and function through mitophagy. Mitophagy selectively degrades mitochondria [239]. Autophagy degrades lipids to produce free fatty acids. Mitochondria oxidize fatty acids to produce energy [229].

In the previous chapters, I showed that RARRES-1 regulates the mitochondrial metabolism and the generation of ROS during HSCs activation. Therefore, I hypothesize that the activation of RARRES-1 might also regulate autophagy. This regulation of autophagy could subsequently preserve lipid droplets, leading to a reduction in energy release and ultimately resulting in the observed anti-fibrotic effect of RARRES-1. In this chapter, I will investigate whether RARRES-1 activation regulates autophagy and, if so, whether RARRES-1 activation is one of the mechanisms underlying the antifibrotic effect of RARRES-1.

Therefore, I will investigate the effects of RARRES1 on the different stages of autophagy, as depicted in **Figure 6.1,** as follows:

- Impact of RARRES-1 on autophagosomal morphology
- Impact of RARRES-1 on the various stages of
    1. Autophagy initiation
    2. Autophagy nucleation
    3. Autophagy elongation
    4. Autophagy sequestration
    5. Autophagy degradation

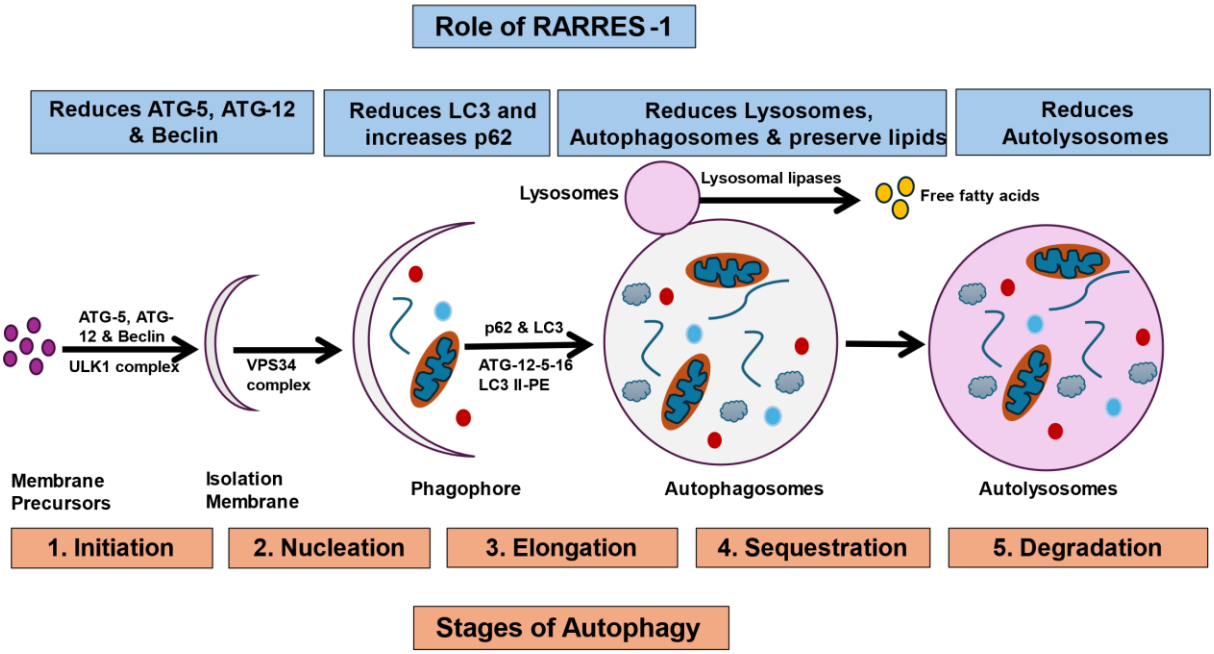

Figure 6.1 Schematic model of the design of experiments in this chapter exploring the effect of RARRES1 on the different stages of autophagy.

6.2 Results

6.2.1 RARRES-1 activation modulates autophagosomal morphology

During HSCs activation and liver fibrosis, HSCs undergo increased state of autophagy [235] and autophagosomal changes including increased formation of doubled membrane autophagosomes during liver fibrosis [240, 241].

To investigate the impact of RARRES-1 activation on autophagosomal morphology. LX-2 cells were transfected with RARRES-1 for 48 hours and stimulated with TGF-β for 24 hours. Analysis was then undertaken using transmission electron microscope. Formation of double membraned autophagosomes is observed upon TGF-β stimulation **(Figure 6.2A-E)**. Images obtained from TEM has shown that RARRES-1 reversed the TGF-β induced increase in autophagosomal perimeter, area, and length. The analysis suggested that RARRES-1 regulates autophagosomal morphology.

A

Control (EV)
Autophagosomes

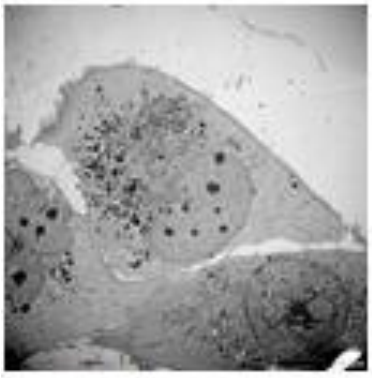

ER-22-240-C1-EVTGFB
Pub Images_18_500X

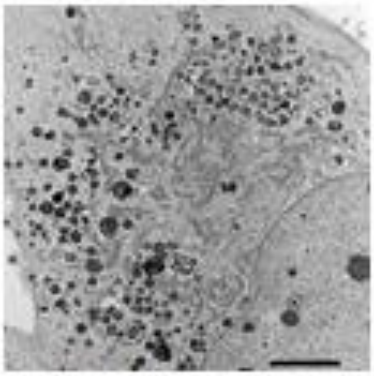

ER-22-240-C1-EVTGFB
Pub Images__19_1200X

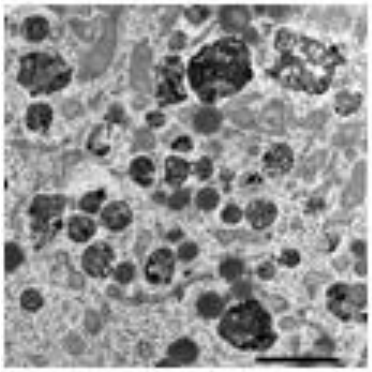

ER-22-240-C1-EVTGFB
Pub Images_25_4000X

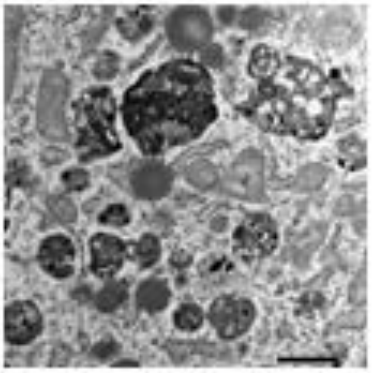

ER-22-240-C1-EVTGFB
Pub Images_26_6000X

B

RARRES-1
Autophagosomes

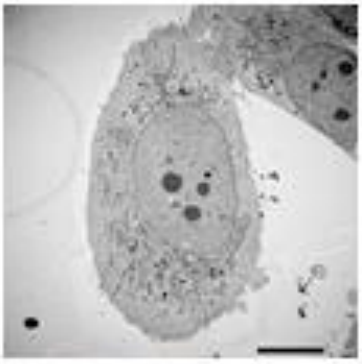

ER-22-240-D1-RPTGFB
Pub Images_27_500X

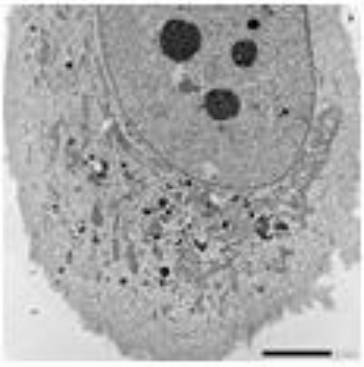

ER-22-240-D1-RPTGFB
Pub Images_28_1200X

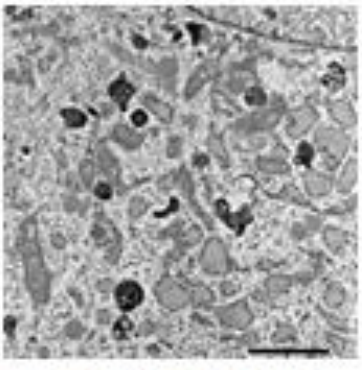

ER-22-240-D1-RPTGFB
Pub Images_29_4000X

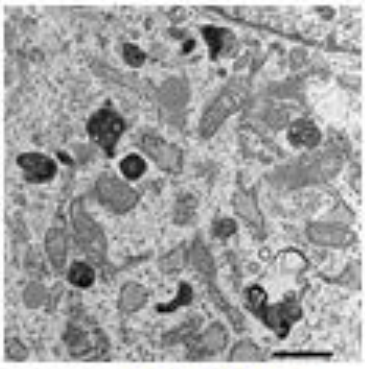

ER-22-240-D1-RPTGFB
Pub Images_30_6000X

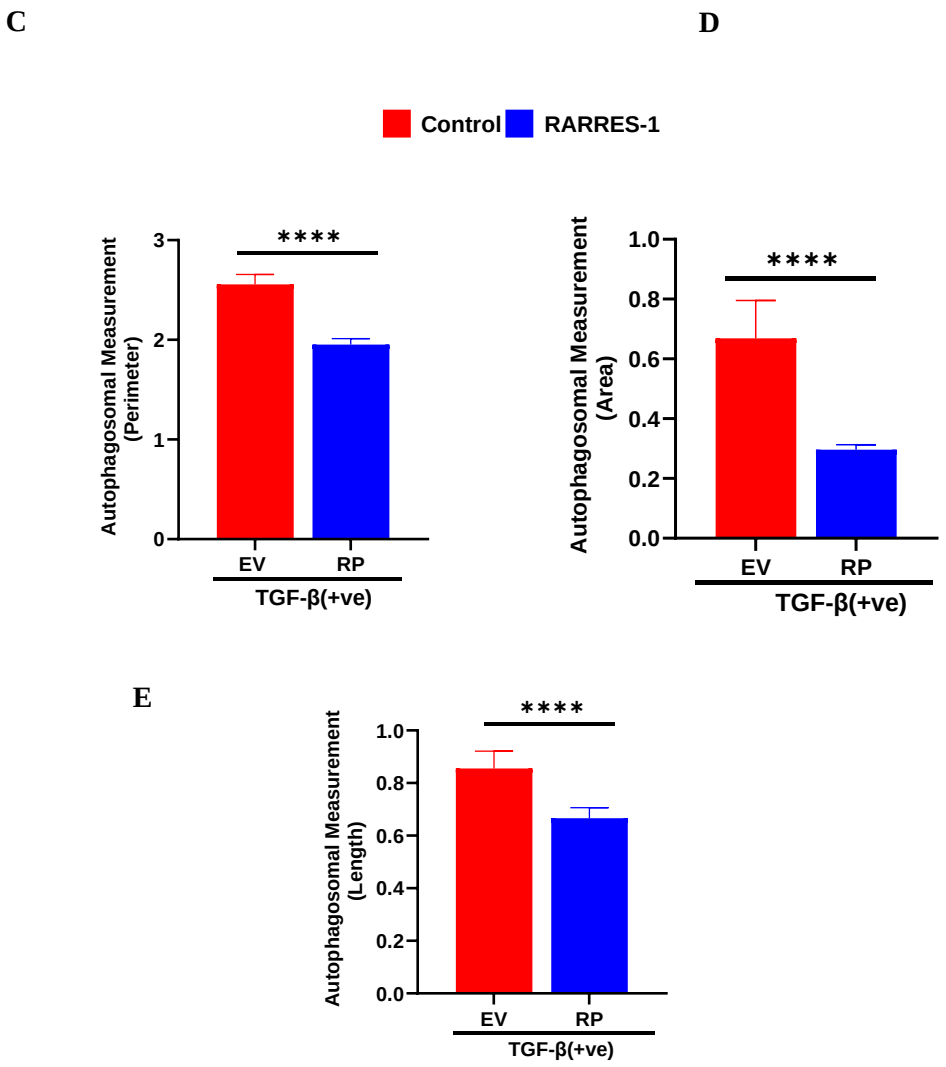

Figure 6.2: RARRES-1 activation preserves autophagosomal morphology in TGF-β stimulated HSCs. LX-2 cells transfected with RARRES-1 plasmid and control before challenging with TGF-β for 24 hours and TEM was undertaken to investigate the autophagosomal morphology. Representative images (Scale bar 5.0µm) for **A)** control **B)** RARRES-1 transfected LX-2 cells. Quantification for **C)** autophagosomal perimeter, **D)** autophagosomal Area and **E)** autophagosomal Length. Measurements were undertaken using the Jeol SightX image viewer software (n=162 and 507 in RARRES-1 transfected cells and control, respectively). Values are represented as mean ± SEM. Statistical difference between the groups was measured by one sample Wilcoxon test.*$p \leq 0.05$, **$p \leq 0.01$, ***$p \leq 0.001$, ****$p \leq 0.0001$.

6.2.2 RARRES-1 activation reduces the autophagy initiation in HSCs

During HSC activation, TGF-β increases the expression of autophagy [242]. To investigate if RARRES-1 regulates the different stages of autophagy. I started with the investigation of the impact of RARRES-1 on the initiation phase of autophagy by measuring the expression level of ATG-5, ATG-12, LC3 & beclin (well-established autophagy markers).

LX-2 cells were transfected with RARRES-1 for 48 hours, with and without TGF-β stimulation for 24 hours. Immunofluorescence was undertaken to assess the expression level of these markers. Results have shown that RARRES-1 activation consistently decreases the expression of these four autophagy markers: ATG-5 **(Figure 6.3A-B)**, ATG-12 **(Figure 6.4A-B)**, LC3 **(Figure 6.5A-B)** and Beclin **(Figure 6.6A-B)** both at baseline and upon stimulation with TGFβ.

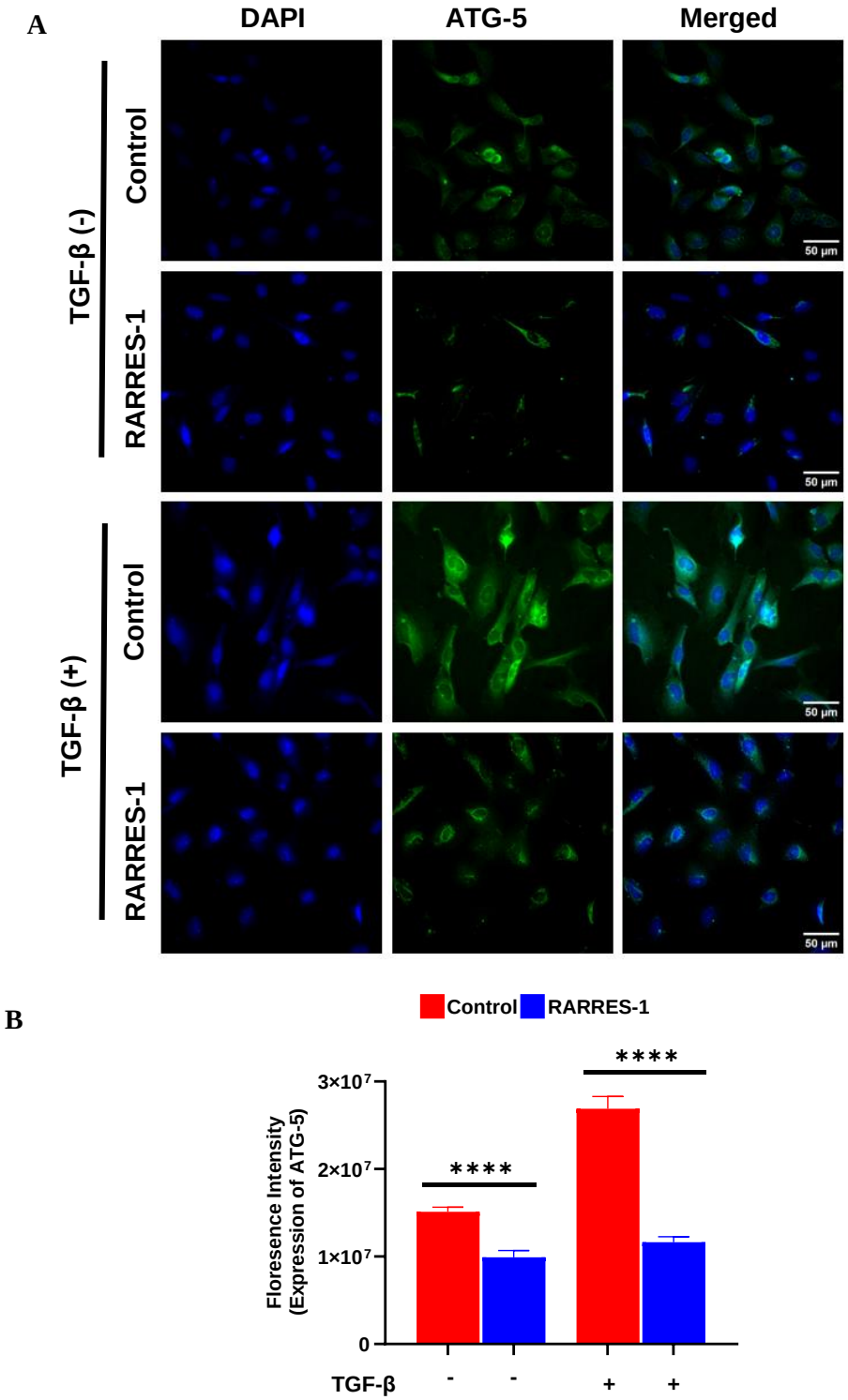

Figure 6.3: RARRES-1 activation reduces the expression of ATG-5. **A)** Representative images for the expression of ATG-5, with or without TGF-β stimulation (n=2). **B)** Quantification for the expression of ATG-5. Imaging was undertaken using deltavision microscope and analysed using image J. Values are represented as mean ± SEM. Statistical difference between the groups was measured by 2- tailed Student's t test. *$p \leq 0.05$, **$p \leq 0.01$, ***$p \leq 0.001$A, ****$p \leq 0.0001$

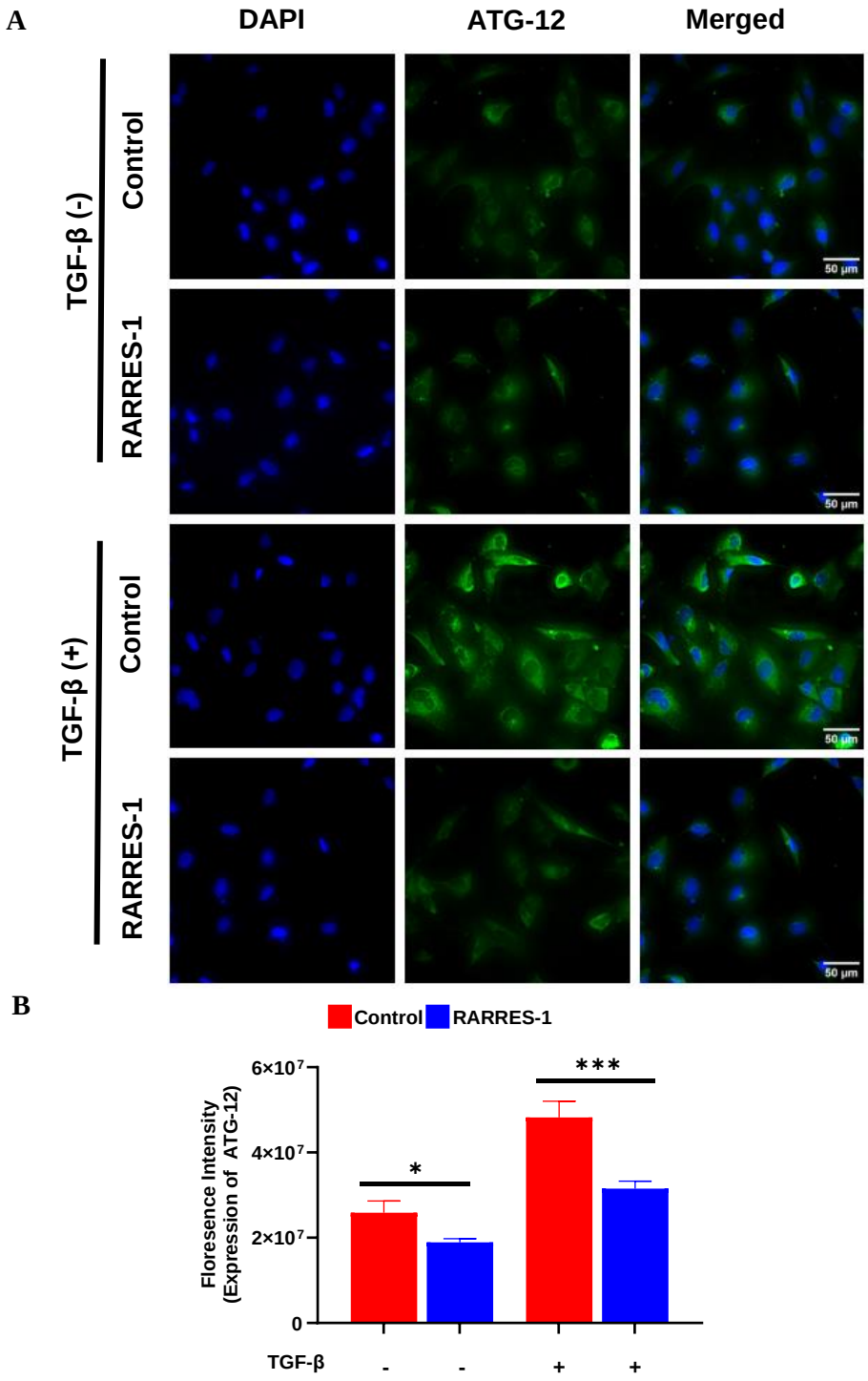

Figure 6.4: RARRES-1 activation reduces the expression of ATG-12. **A)** Representative images for the expression of ATG-12, with or without TGF-β stimulation (n=2). **B)** Quantification for the expression of ATG-12. Imaging was undertaken using Deltavision microscope and analysed using image J. Values are represented as mean ± SEM. Statistical difference between the groups was measured by 2- tailed Student's t test. *$p \leq 0.05$, **$p \leq 0.01$, ***$p \leq 0.001$A, ****$p \leq 0.0001$.

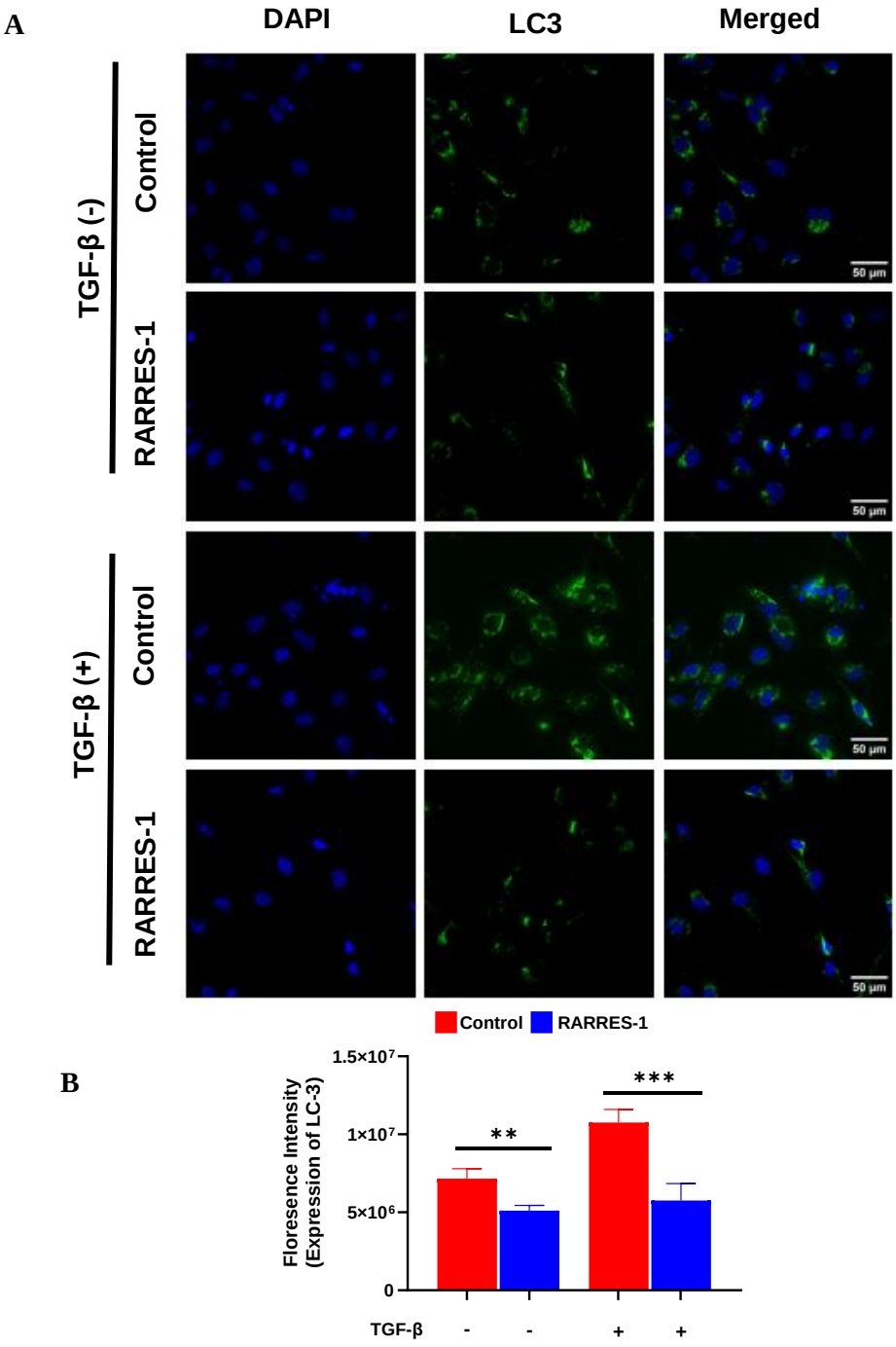

Figure 6.5: RARRES-1 activation reduces the expression of LC3. **A)** Representative images for the expression of LC3, with or without TGF-β stimulation (n=2). **B)** Quantification for the expression of LC3. Imaging was undertaken using Deltavision microscope and analysed using image J. Values are represented as mean ± SEM. Statistical difference between the groups was measured by 2- tailed Student's t test. *$p \leq 0.05$, **$p \leq 0.01$, ***$p \leq 0.001$A, ****$p \leq 0.0001$.

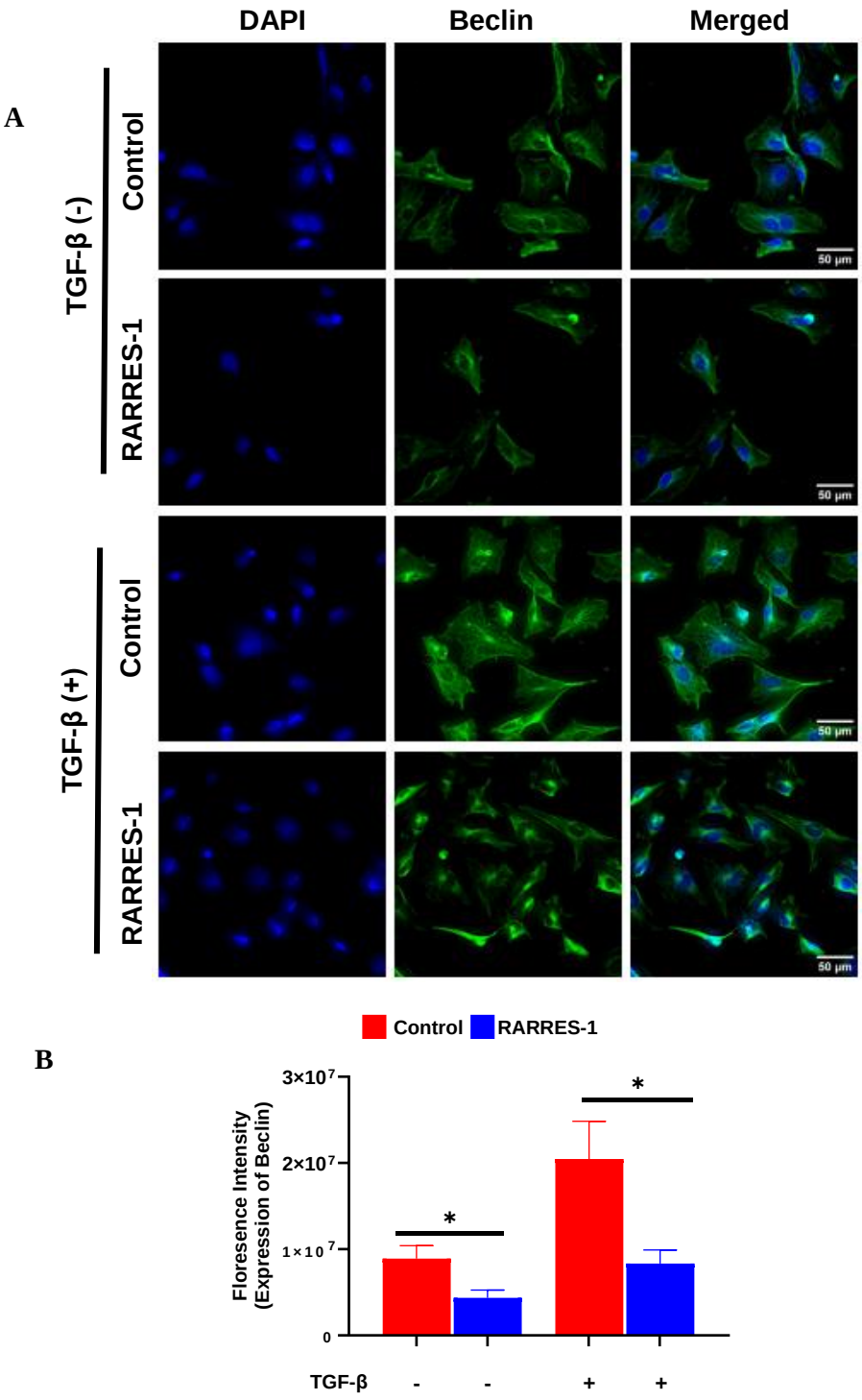

Figure 6.6: RARRES-1 activation reduces the expression of Beclin. **A)** Representative images for the expression of Beclin, with or without TGF-β stimulation (n=2). **B)** Quantification for the expression of Beclin. Imaging was undertaken using deltavision microscope and analysed using image J. Values are represented as mean ± SEM. Statistical difference between the groups was measured by 2- tailed Student's t test. *$p \leq 0.05$, **$p \leq 0.01$, ***$p \leq 0.001$A, ****$p \leq 0.000$

6.2.3 RARRES-1 activation reduces the autophagic flux

I next investigated the effect of RARRES-1 on autophagy flux. The p62 protein plays a role in breaking down misfolded proteins. It directly binds to LC3 and transports the misfolded proteins for degradation through autophagy. Additionally, p62 itself is degraded through this process and is considered as a marker of autophagic flux [243, 244].

Thus, I next investigated the effect of RARRES-1 activation on the expression of p62 protein through Enzyme linked immunosorbent Assay (ELISA). A significant increase in the expression of p62 proteins as compared to control was observed, which implies that RARRES-1 preserves p62 protein and correspondence decrease in autophagy should occur (**Figure 6.7)**.

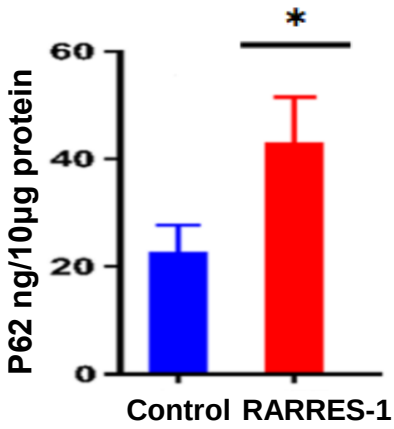

Figure: 6.7 RARRES-1 activation preserves p62 protein. LX-2 cells were transfected with RARRES-1 and control for 48 hours. Supernatant was tested for the expression of p62 proteins using manufacturer's protocol for enzyme-linked immunosorbent assay (ELISA). *$p \leq 0.05$, **$p \leq 0.01$, ***$p \leq 0.001$A, ****$p \leq 0.0001$.

To further confirm the effect of RARRES-1 on the modulation of autophagic flux (Formation of autophagosomes and autolysosomes), I next used Premo autophagy tandem sensor RFP-GFP-LC3B kit, which utilises BacMem virus that matures autophagosomes to lysosomes and increases the delivery of LC3 to autolysosomes. Then, I undertook a tandem fluorescent-tagged LC3 assay based on the difference in pKa values between red fluorescent protein (RFP) and green fluorescent protein (GFP) to distinguish non-degradative(GFP+RFP+) and degradative (GFP−RFP+) autophagic structures. Image analysis has shown that RARRES-1 activation significantly reduces the formation of autophagosomes and autolysosomes **(Figure 6.8A-C)**. However, this effect was observed to be more pronounced on formation of autolysosomes than autophagosomes.

A

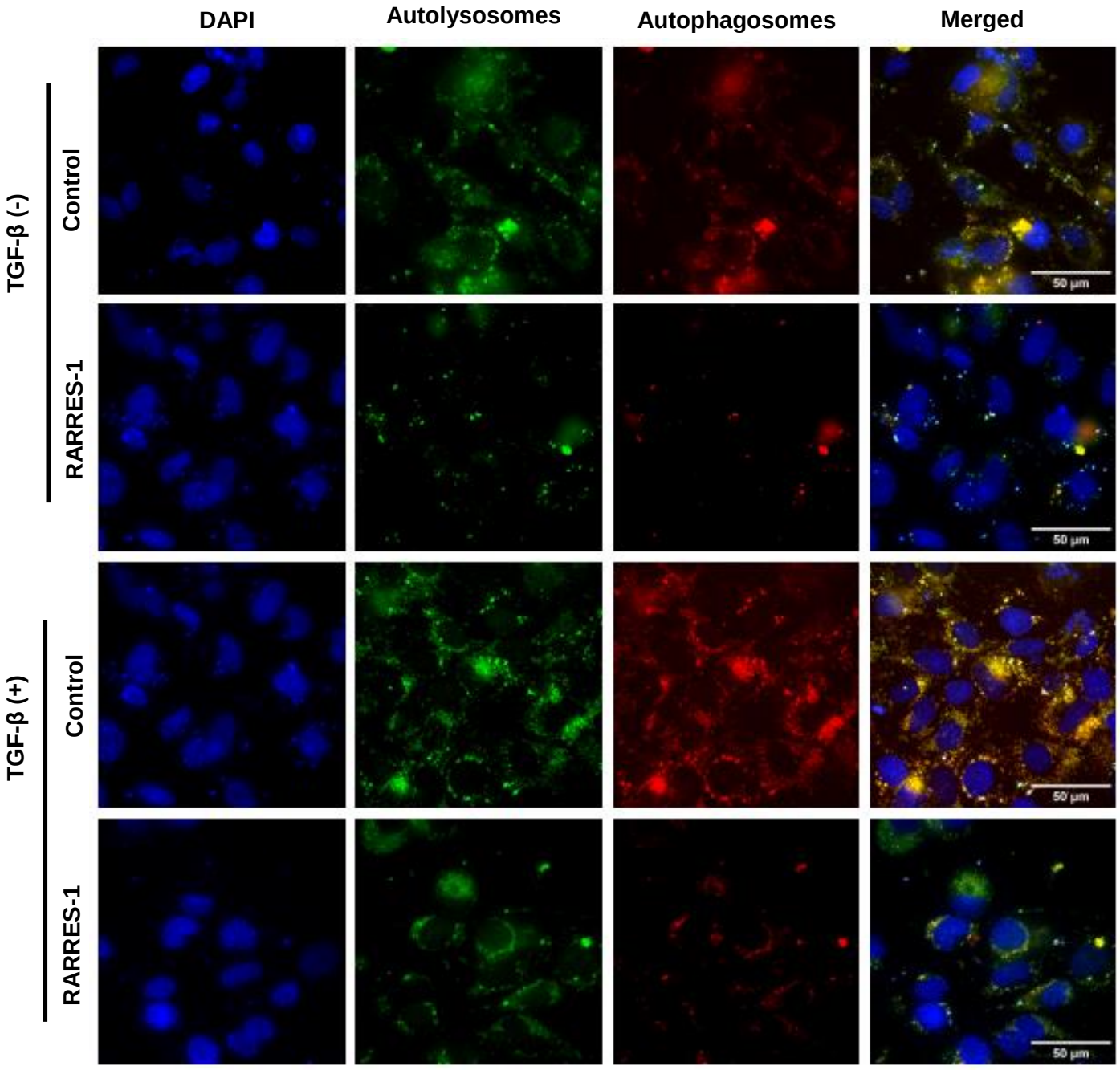
DAPI
Autolysosomes
Autophagosomes
Merged
TGF-β (-)
Control
RARRES-1
TGF-β (+)
Control
RARRES-1
50 μm

B

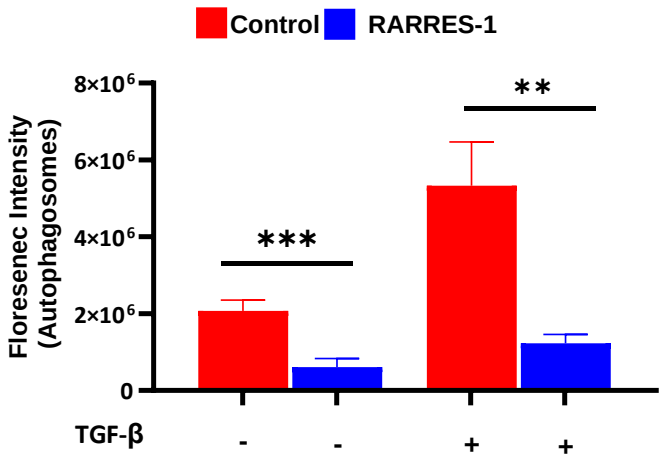
Control
RARRES-1
Floresenec Intensity (Autophagosomes)
8×10⁶
6×10⁶
4×10⁶
2×10⁶
0
***
**
TGF-β
-
-
+
+

C

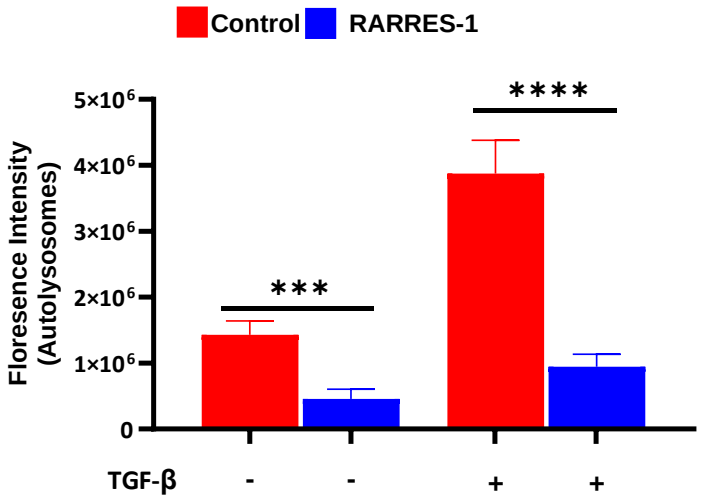

Figure 6.8: RARRES-1 modulates autophagic flux in HSCs. **A)** Representative images for the expression of autophagosomes and autolysosomes (n=2). **B)** Quantification for the formation of autophagosomes with or without TGF-β stimulation. **C)** Quantification for the formation of autolysosomes with or without TGF-β stimulation. Immunofluorescence using deltavision microscope was undertaken. Image analysis was done using image J. Values are represented as mean ± SEM. Statistical difference between the groups was measured by 2-tailed Student's t test. *$p \leq 0.05$, **$p \leq 0.01$, ***$p \leq 0.001$A, ****$p \leq 0.0001$.

6.2.4 RARRES-1 activation reduces the formation of lysosomes.

To investigate further if RARRES activation regulates other stages of autophagy as well, I then investigated the effect of RARRES-1 activation on lysosomes formation. LX-2 cells were transfected with RARRES-1 plasmid for 48 hours and stimulated with TGF-β for 24 hours. Live cell imaging using deltavision microscope was undertaken to investigate the formation of lysosomes using red fluorescent dye Lysotracker^{TM} Red DND-99. Image analysis has confirmed that RARRES-1 activation in LX-2 cells significantly reduces the formation of lysosomes **(Figure 6.9 A-B)**.

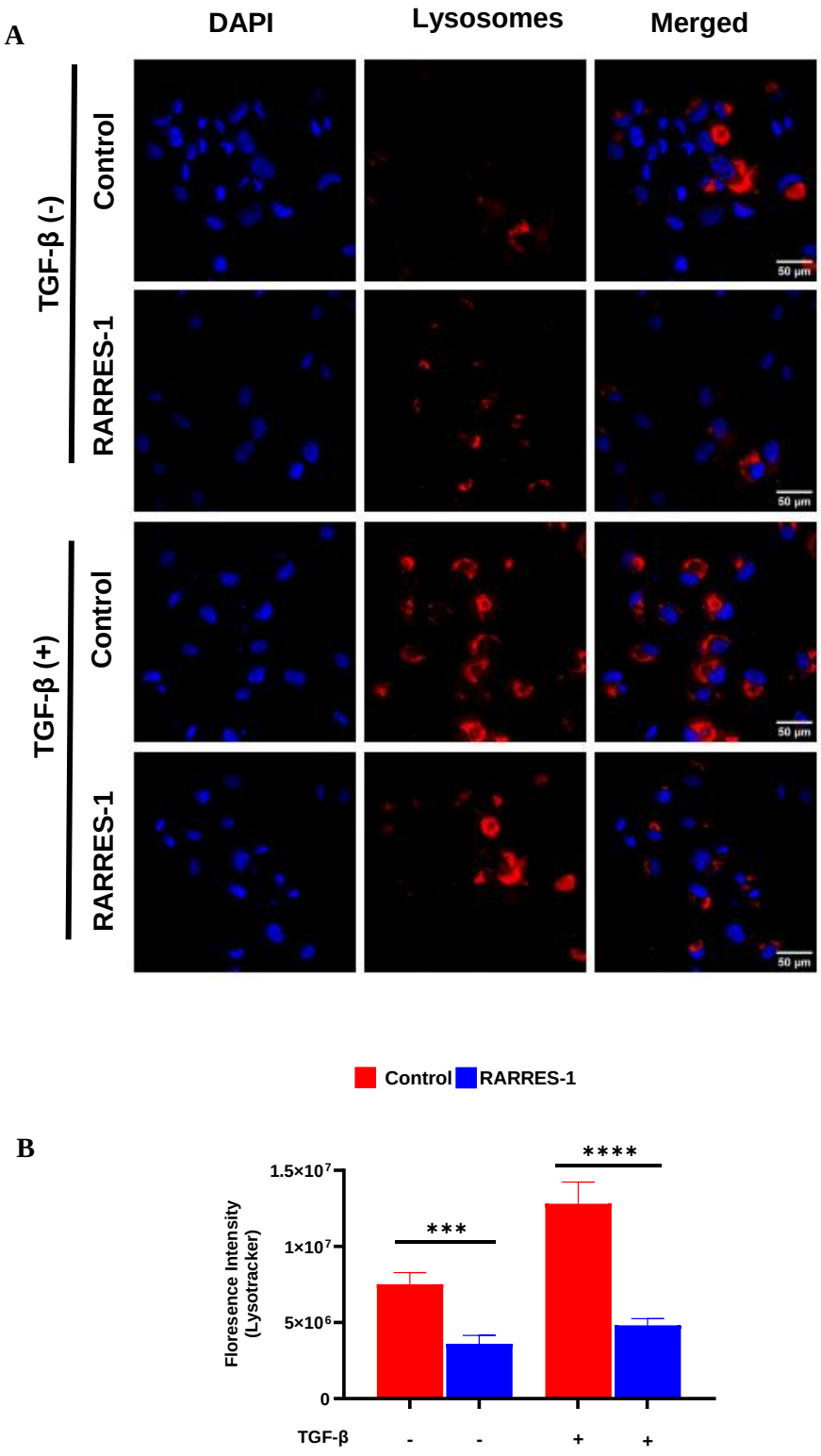

Figure 6.9: **RARRES-1 activation reduces the formation of lysosomes**. **A)** Representative images for the expression of lysotracker, with or without stimulation with TGF-β (n=2). **B)** Quantification for the expression of lysosomes. Image analysis was undertaken using image J. Values are represented as mean ± SEM. Statistical difference between the groups was measured by 2- tailed Student's t test. *$p \leq 0.05$, **$p \leq 0.01$, ***$p \leq 0.001$A, ****$p \leq 0.0001$.

6.2.5 RARRES-1 activation regulates the formation of lysosomes and autophagy.

Moving further, I opted to investigate if RARRES-1 activation simultaneously attenuates more than one stages of autophagy. To investigate it, I have undertaken immunofluorescence double staining for lysotracker and LC3. LX-2 cells were transfected with RARRES-1 for 48 hours and stimulated with TGF-β for 24 hours. At the end of final treatment, LX-2 cells were stained with LC3 antibody (for the expression of autophagy) and lysotracker stain (for the formation of lysosomes). Image analysis has shown that RARRES-1 activation reduces not only the formation of lysosomes but also decreases the expression of LC3, both at baseline **(Figure 6.10A-B)** and upon TGF-β stimulation **(Figure 6.11)**.

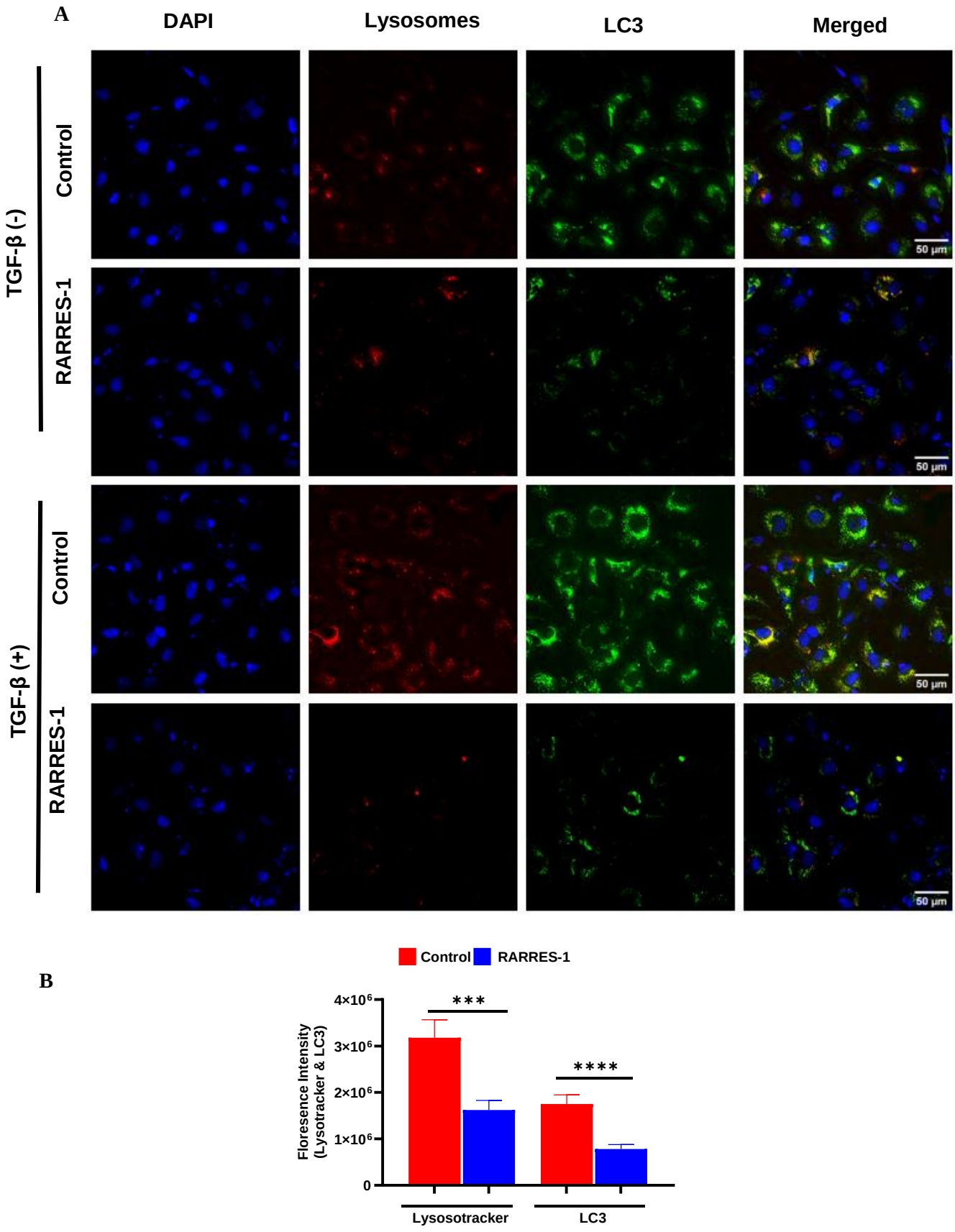

Figure 6.10: RARRES-1 activation reduces the formation of lysosomes and autophagy in unstimulated HSCs. LX-2 cells were transfected with RARRES-1 for 48 hours and

expression of lysotracker and LC3 was assessed (n=2). **A)** Representative images for the expression of lysotracker (red fluorescence) and LC3 (green fluorescence). **B)** Quantification of lysotracker and LC3 at baseline. Image analysis was undertaken using image J. Values are represented as mean ± SEM. Statistical difference between the groups was measured by 2-tailed Student's t test. *$p \leq 0.05$, **$p \leq 0.01$, ***$p \leq 0.001$A, ****$p \leq 0.0001$.

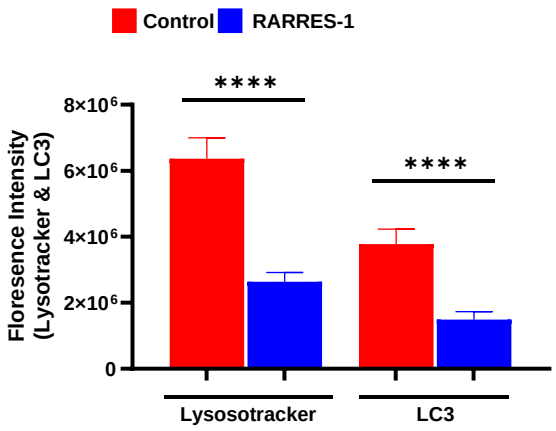

Figure 6.11: RARRES-1 activation reduces the formation of lysosomes and autophagy in TGF-β stimulated HSCs. LX-2 cells were transfected with RARRES-1 for 48 hours and treated with TGF-β for 24 hours (n=2). Quantification of lysotracker (red fluorescence) and LC3 (green fluorescence) upon stimulation with TGF-β. Image analysis was undertaken using image J. Values are represented as mean ± SEM. Statistical difference between the groups was measured by 2- tailed Student's t test. *$p \leq 0.05$, **$p \leq 0.01$, ***$p \leq 0.001$A, ****$p \leq 0.0001$.

6.2.6 RARRES-1 activation preserves cell lipids

Myofibroblast activation is an intense energy requiring process. During fibrosis, HSCs lose lipid droplets to fuel HSCs activation [245]. Autophagy causes loss of lipid droplets [101]. Therefore, I further investigated the effect of RARRES-1 activation on preservation of HSCs lipids. LX-2 cells were transfected with RARRES-1 for 48 hours and stimulated with TGF-β for 24 hours. Two different stains BODIPY and Oil red (markers of cell lipid) were used in two independent experiments. RARRES-1 activation significantly increases the preservation of lipid droplets which is manifested by the expression of BODIPY **(Figure 6.12A-B**) and Oil red **(Figure 6.13A-B)**.

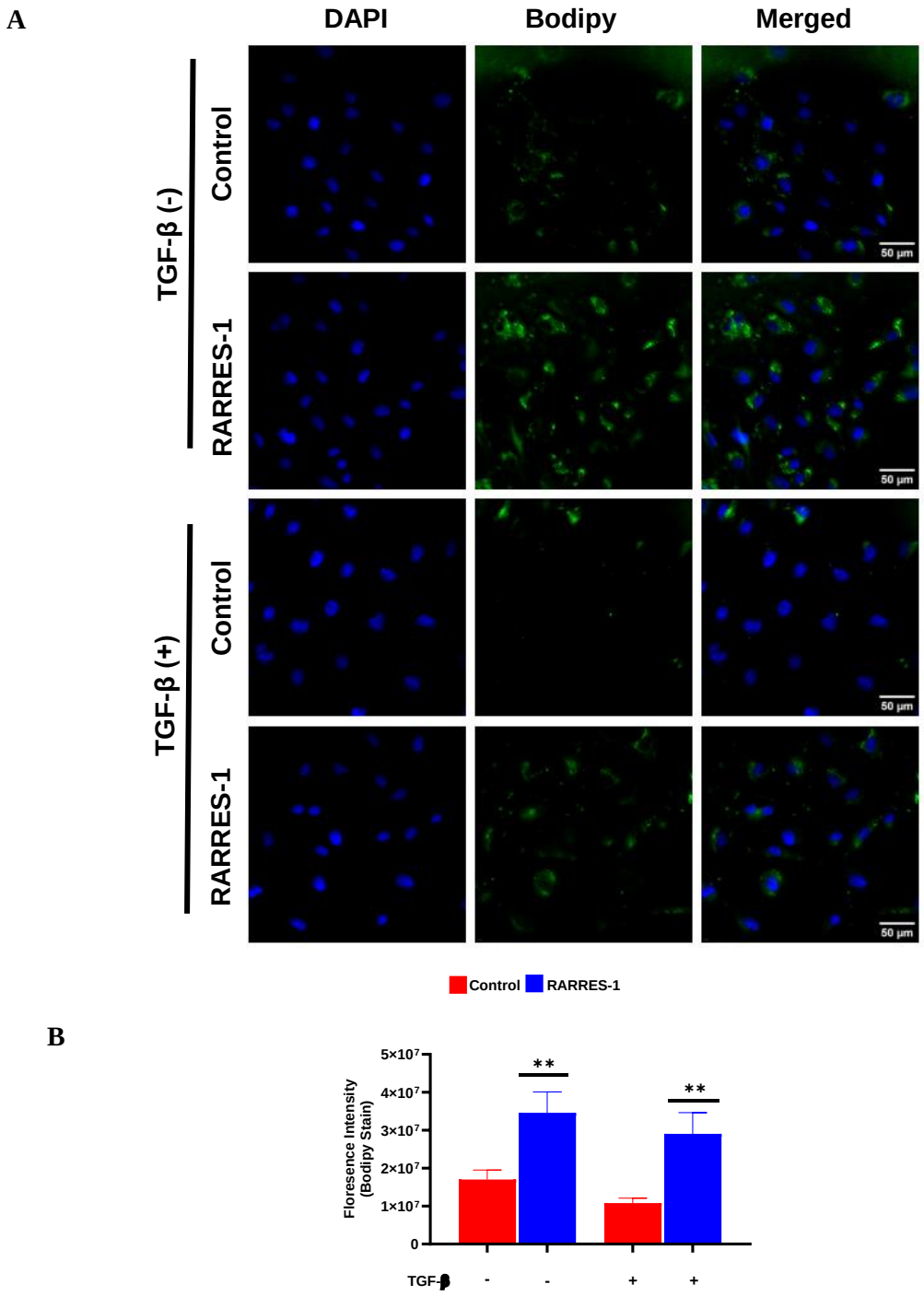

Figure 6.12: RARRES-1 activation preserves the expression of Bodipy (n=2). A) Representative images for expression of BODIPY in RARRES-1 transfected LX-2 cells, with or without TGF-β stimulation. **B)** Quantification for BODIPY. Image analysis was undertaken using image J. Values are represented as mean ± SEM. Statistical difference between the groups was measured by 2- tailed Student's t test. *$p \leq 0.05$, **$p \leq 0.01$, ***$p \leq$ 0.001A, ****$p \leq 0.0001$.

A

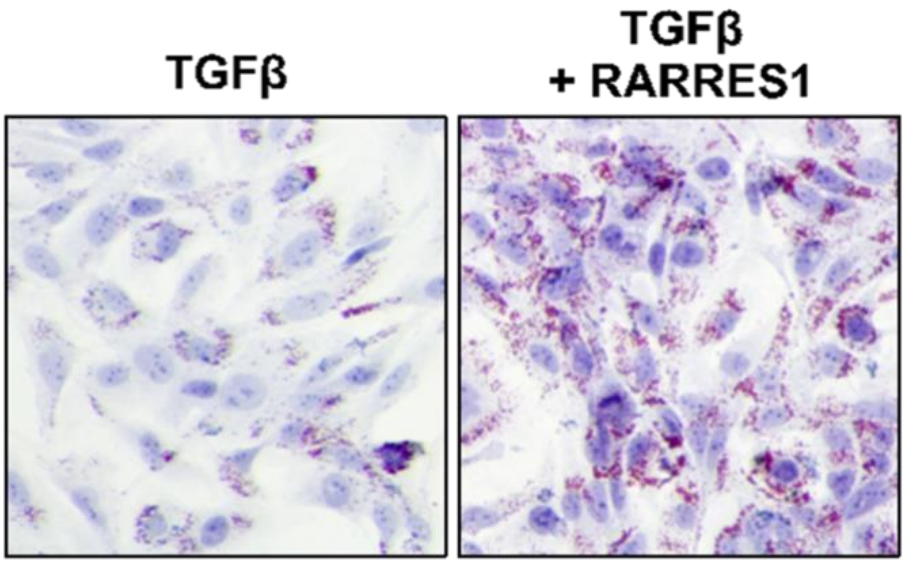

B

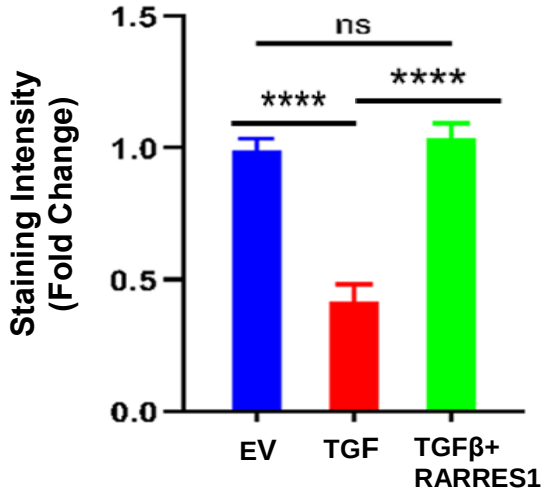

Figure 6.13: RARRES-1 activation preserves the expression of oil red. **A)** Representative images for expression of oil red, with or without TGF-β stimulation. **B)** Quantification for oil red. Image analysis was undertaken using image J. Values are represented as mean ± SEM. Statistical difference between the groups was measured by 2- tailed Student's t test. *$p \leq$ 0.05, **$p \leq 0.01$, ***$p \leq 0.001$A, ****$p \leq 0.0001$.

6.2.7 RARRES-1 activation preserves cell lipids and reduce autophagy

After confirming RARRES-1 activation preserves cell lipid, I further investigated if this preservation of cell lipids is due to inhibition of autophagy. To investigate that, I transfected LX-2 cells with RARRES-1 plasmid for 48 hours and treated with TGF-β for 24 hours. Cells were washed, and double staining was done to investigate co-localization of BODIPY (a marker of cell lipids) with LC3 (indicator of autophagy). RARRES-1 activation not only preserved lipid droplets, but it also reduced the expression of LC3 **(Figure 6.14A-B)** at baseline and upon stimulation with TGF-β **(Figure 6.15)**. Which indicates that this preservation of lipid droplet is via the inhibition of autophagy.

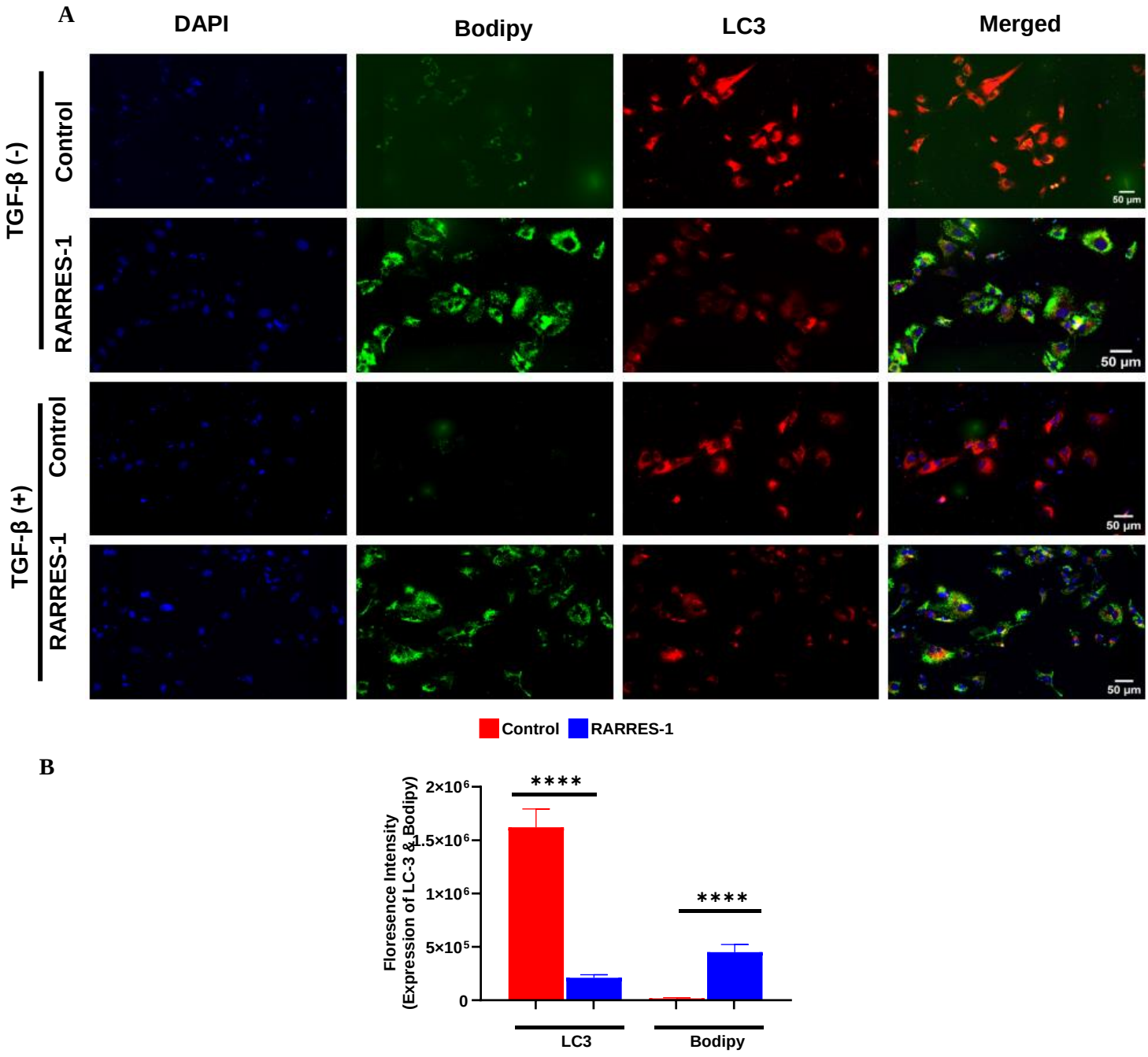

Figure 6.14: RARRES-1 activation attenuates the expression of cell lipids and LC3 in unstimulated HSCs (n=2). **A)** Representative images for the expression of BODIPY (green fluorescence) and LC3 (Red fluorescence). **B)** Quantification for the expression of BODIPY and LC3. Values are represented as mean ± SEM. Statistical difference between the groups was measured by 2- tailed Student's t test. *$p \leq 0.05$, **$p \leq 0.01$, ***$p \leq 0.001$A, ****$p \leq 0.0001$.

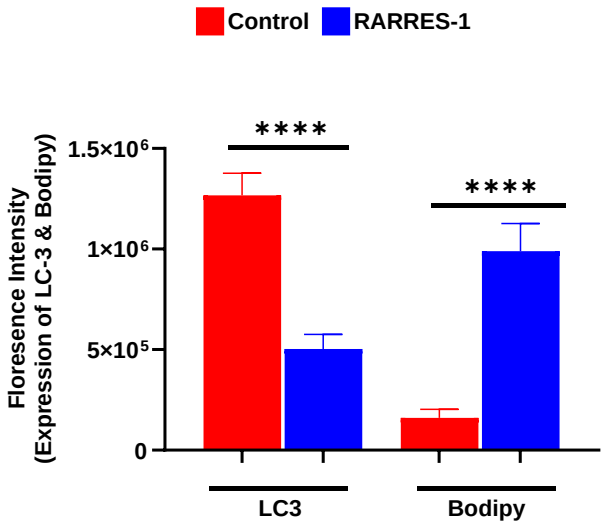

Figure 6.15: RARRES-1 activation attenuates the expression of cell lipids and LC3 in TGF-β stimulated HSCs. Quantification for the expression of bodipy and LC3 upon TGF-β stimulation (n=2). Values are represented as mean ± SEM. Statistical difference between the groups was measured by 2- tailed Student's t test. *$p \leq 0.05$, **$p \leq 0.01$, ***$p \leq 0.001$A, ****$p \leq 0.0001$.

6.2.8 Effect of autophagy modulation on antifibrotic effect of RARRES-1

After confirming that RARRES-1 activation has a regulatory effect on different stages of autophagy in activated HSCs and attenuates autophagy-induced HSC's lipid loss, I further investigated whether these effects could be one of the mechanisms antifibrotic effects of RARRES-1's. To evaluate this, I designed a series of experiments to examine RARRES-1's antifibrotic effect upon modulation of autophagy levels by either inducers or and inhibitors.

6.2.8.1 Autophagy inducers reverse the antifibrotic effect of RARRES-1

To induce autophagy, two specific plasmids ATG-12 and LC3 were used and their impact on the antifibrotic effect of RARRES-1 in HSCs cells were evaluated, as depicted in **Figure 6.16**.

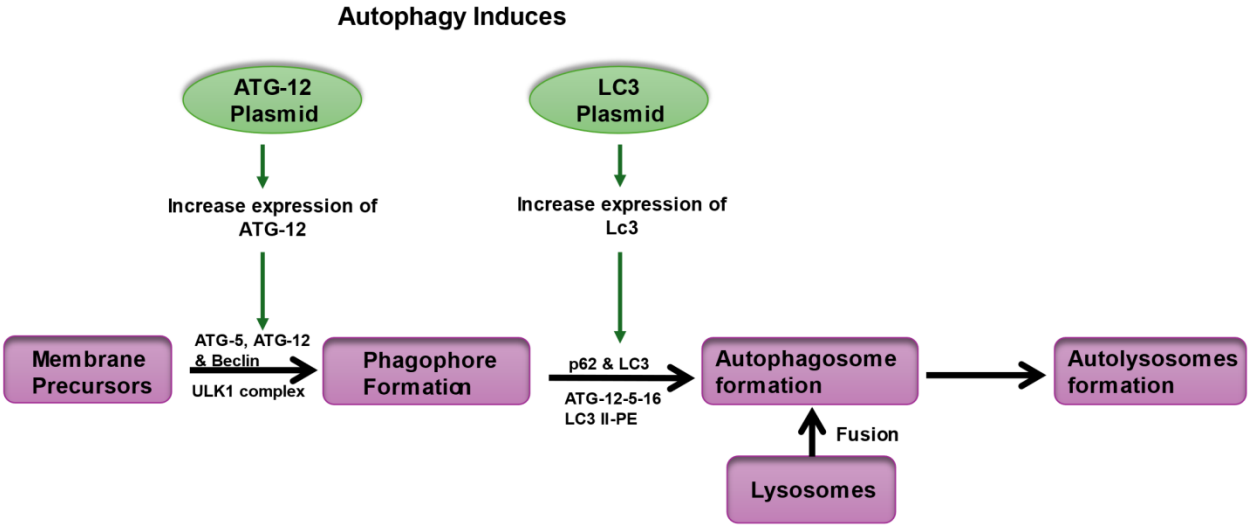

Figure 6.16: Schematic diagram of the autophagy inducers experiments.

6.2.8.1.1 LC3 plasmid reverses the antifibrotic effect of RARRES-1

To investigate the effect of LC3 activation on the antifibrotic effect of RARRES-1, I have undertaken a double transfection of LX-2 cells with RARRES-1 plasmid and LC3 plasmid for 48 hours with or without TGF-β treatment for 24 hours. Cells were then stained for the expression of α-SMA, a robust fibrotic marker. Image analysis has shown that as expected RARRES-1 activation led to a significant attenuation of α-SMA expression, an effect was reversed by LC3 activation both at baseline **(Figure 6.17A-B)** and upon stimulation with TGF-β **(Figure 6.18A-B)**.

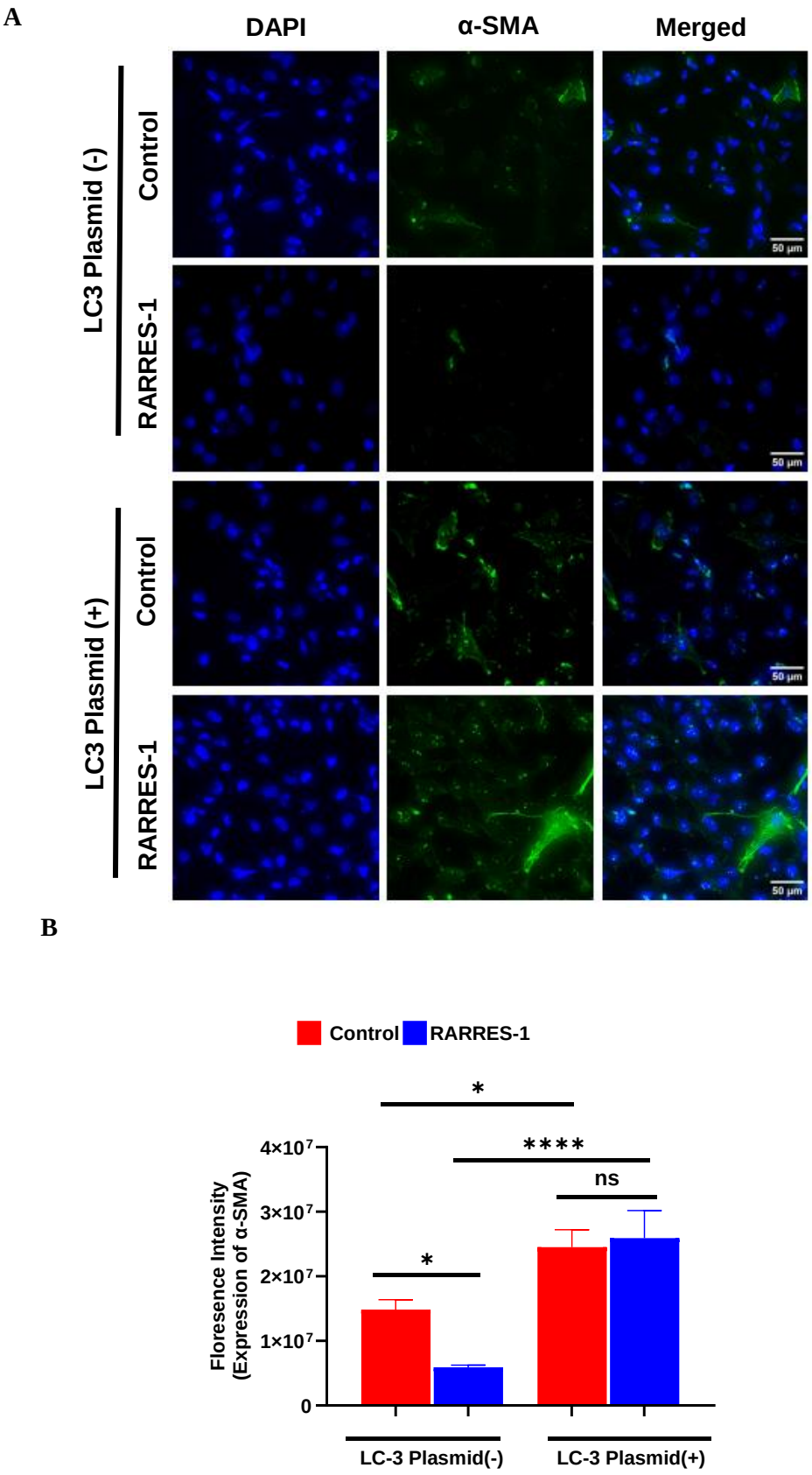

Figure 6.17: LC3 plasmid reverse the antifibrotic effect of RARRES-1 in unstimulated HSCs. LX-2 cells transfected with RARRES-1 plasmid and LC3 plasmid for 48 and

expression of LC3 was assessed (n=2). **A)** Representative images for expression of α-SMA. **B)** Quantification of α-SMA at baseline. Imaging was undertaken using deltavision microscope and analysed using image J. Values are represented as mean ± SEM. Statistical difference between the groups was measured by one-way ANOVA; multiple comparisons were corrected by Boneferroni correction. *$p \leq 0.05$, **$p \leq 0.01$, ***$p \leq 0.001$A, ****$p \leq 0.0001$.

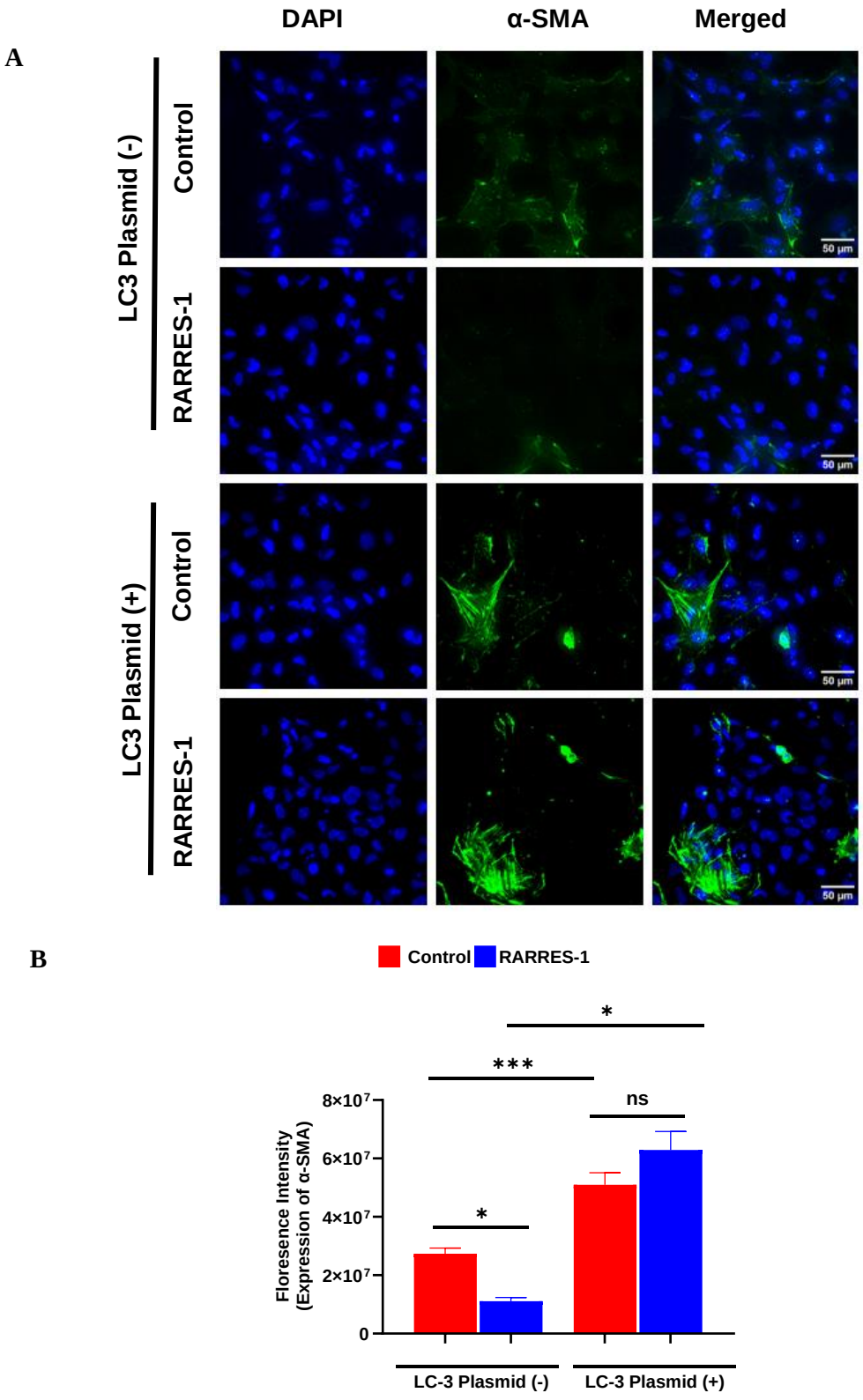

Figure 6.18: LC3 plasmid reverse the antifibrotic effect of RARRES-1 in TGF-β stimulated HSCs. LX-2 cells transfected with RARRES-1 plasmid and LC3 plasmid for 48 and treated with TGF-β for 24 hours. Expression of LC3 was assessed (n=2). **A)** Representative images for expression of α-SMA. **B)** Quantification of α-SMA upon TGF-β

stimulation. Imaging was undertaken using deltavision microscope and analysed using image J. Values are represented as mean ± SEM. Statistical difference between the groups was measured by one-way ANOVA; multiple comparisons were corrected by Boneferroni correction. *$p \leq 0.05$, **$p \leq 0.01$, ***$p \leq 0.001$A, ****$p \leq 0.0001$.

6.2.8.1.2 ATG-12 plasmid will reverse the antifibrotic effect of RARRES-1

For further confirmation that autophagy inducers reverse the antifibrotic effect of RARRES-1, I have used another autophagy plasmid, namely ATG-12. I have undertaken double transfection of LX-2 cells with RARRES-1 plasmid and ATG-12 plasmid for 48 hours, with or without TGF-β treatment for 24 hours. Image analysis was undertaken using immunofluorescence and image J. Consistent results were obtained both at baseline **(Figure 6.19A-B)** and upon stimulation with TGF-β **(Figure 6.20A-B)**.

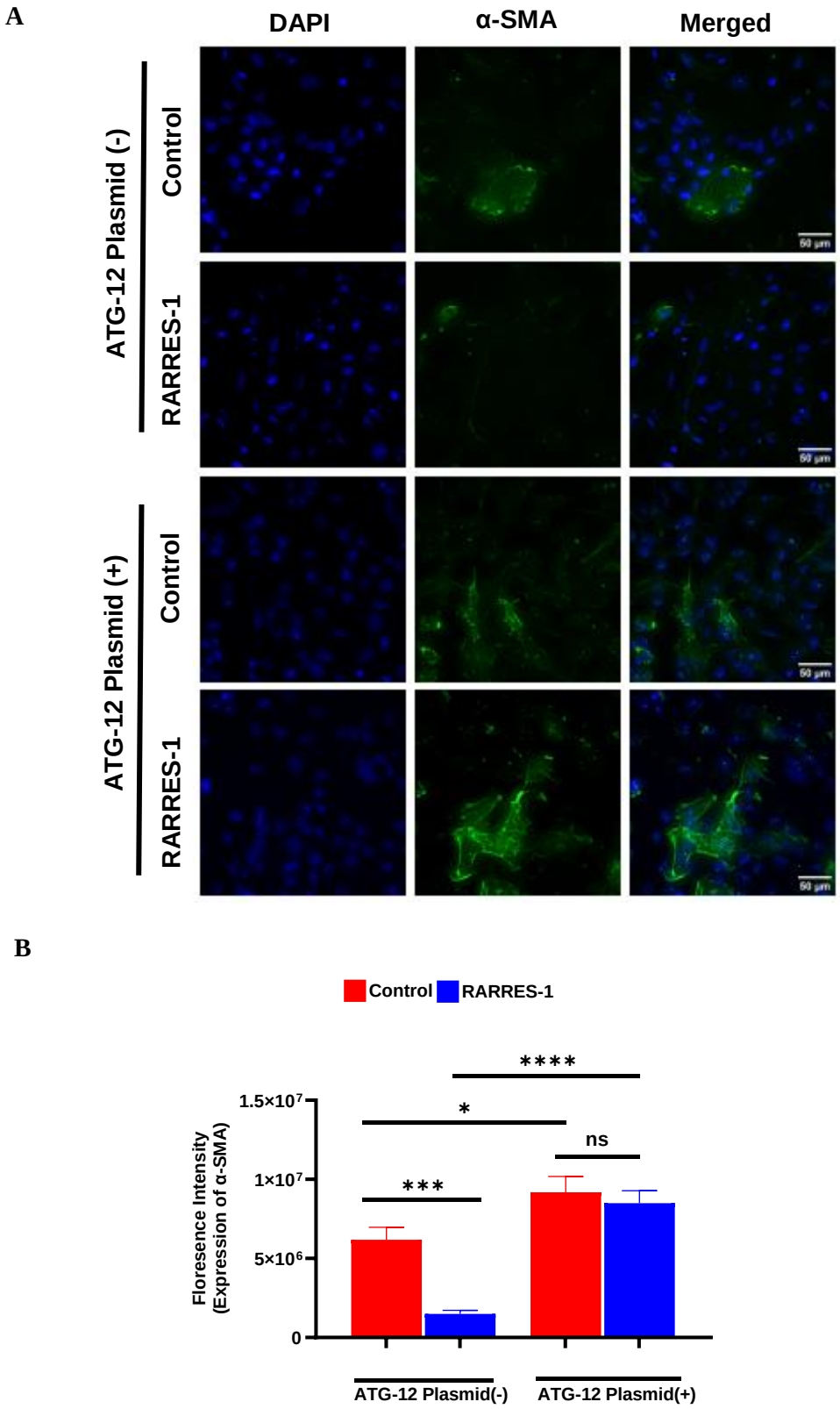

Figure 6.19: ATG-12 plasmid reverses the antifibrotic effect of RARRES-1 in unstimulated HSCs. LX-2 cells transfected with RARRES-1 plasmid and ATG-12 plasmid for 48 and expression of α-SMA was assessed (n=2). **A)** Representative images for

expression of α-SMA. **B)** Quantification of α-SMA at baseline. Imaging was undertaken using deltavision microscope and analysed using image J. Values are represented as mean ± SEM. Statistical difference between the groups was measured by one-way ANOVA; multiple comparisons were corrected by Boneferroni correction. *$p \leq 0.05$, **$p \leq 0.01$, ***$p \leq$ 0.001A, ****$p \leq 0.0001$.

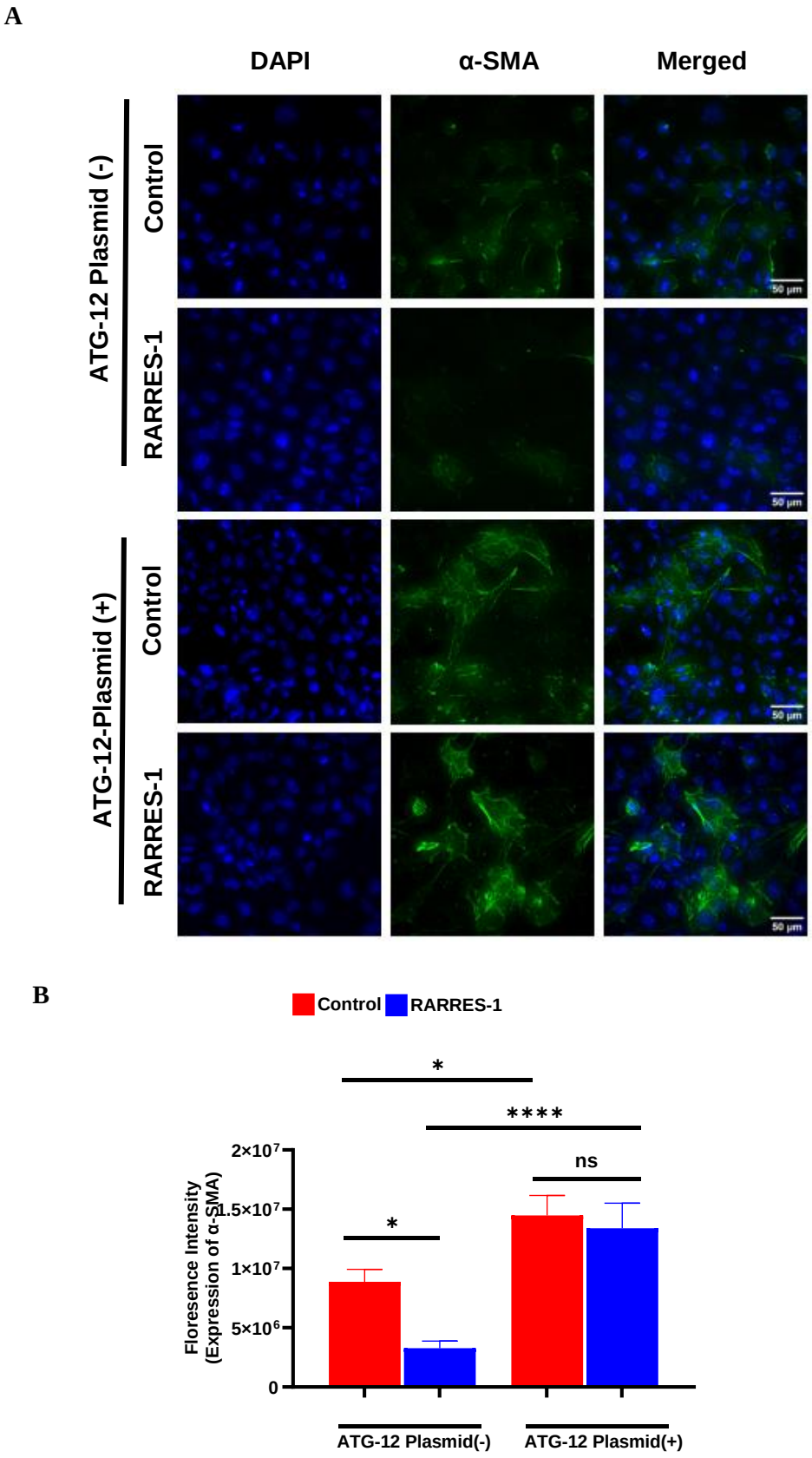

Figure 6.20: ATG-12 plasmid reverses the antifibrotic effect of RARRES-1 in TGF-β stimulated HSCs. LX-2 cells transfected with RARRES-1 plasmid and ATG-12 plasmid for

48 and treated with TGF-β for 24 hours. Expression of α-SMA was assessed (n=2). **A)** Representative images for expression of α-SMA. **B)** Quantification of α-SMA upon TGF-β stimulation. Imaging was undertaken using deltavision microscope and analysed using image J. Values are represented as mean ± SEM. Statistical difference between the groups was measured by one-way ANOVA; multiple comparisons were corrected by Boneferroni correction. *$p \leq 0.05$, **$p \leq 0.01$, ***$p \leq 0.001$A, ****$p \leq 0.0001$.

6.2.8.2 Autophagy inhibitors synergise the antifibrotic effect of RARRES-1

For further confirmation that the antifibrotic effect of RARRES-1 is via regulation of autophagy, I opted to investigate the reverse approach and evaluated how autophagy inhibitors modulate the antifibrotic effect of RARRES-1. To this end, different autophagy inhibitors (both chemical and genetic inhibitors of autophagy) have been used to test this hypothesis, as depicted in **Figure 6.21**.

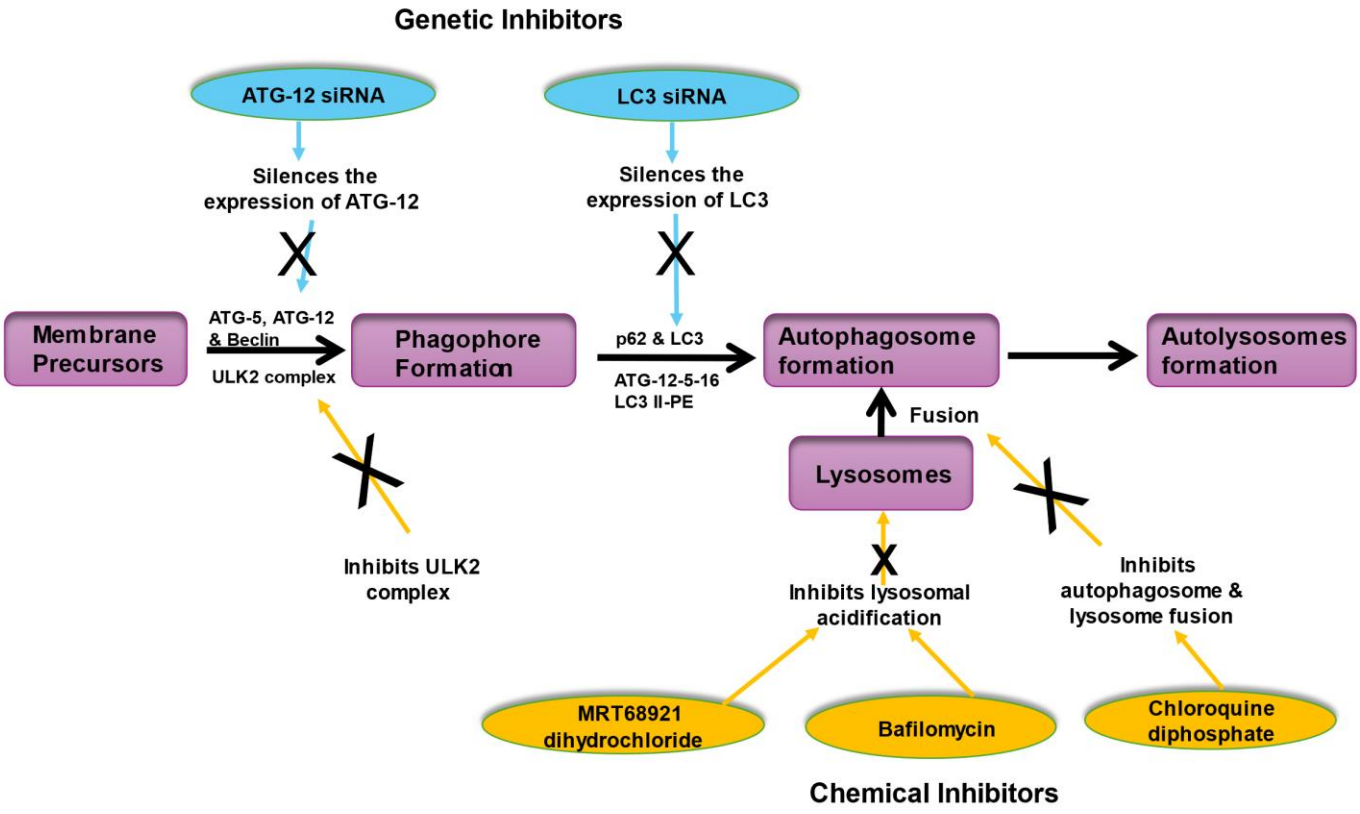

Figure 6.21: Schematic diagram of the autophagy inhibitors experiments.

6.2.8.2.1 Chemical Inhibitors

First, I investigated the effect of autophagy inhibitors or the antifibrotic effect of RARRES-1. For this I transfected LX-2 cells with the RARRES-1 plasmid for 48 hours and treated with different autophagy inhibitors, namely chloroquine diphosphate (autophagosome and lysosomes fusion inhibitor) [246], MRT68921 dihydrochloride (ULK1 and ULK2 kinase inhibitor) [247] and Bafilomycin (lysosomal acidification inhibitor) [248], 2 hours before challenging with or without TGF-β. The expression of LC3 was measured by immunofluorescence, to confirm the inhibition of autophagy. Consistently, all used autophagy inhibitors: chloroquine diphosphate **(Figure 6.22** and **Figure 6.23)**, MRT68921 dihydrochloride **(Figure 6.24** and **Figure 6.25)** and Bafilomycin **(Figure 6.26** and **Figure 6.27)** led to the expected reduction in the expression of LC3 both in the presence and absence of RARRES1 transfection.

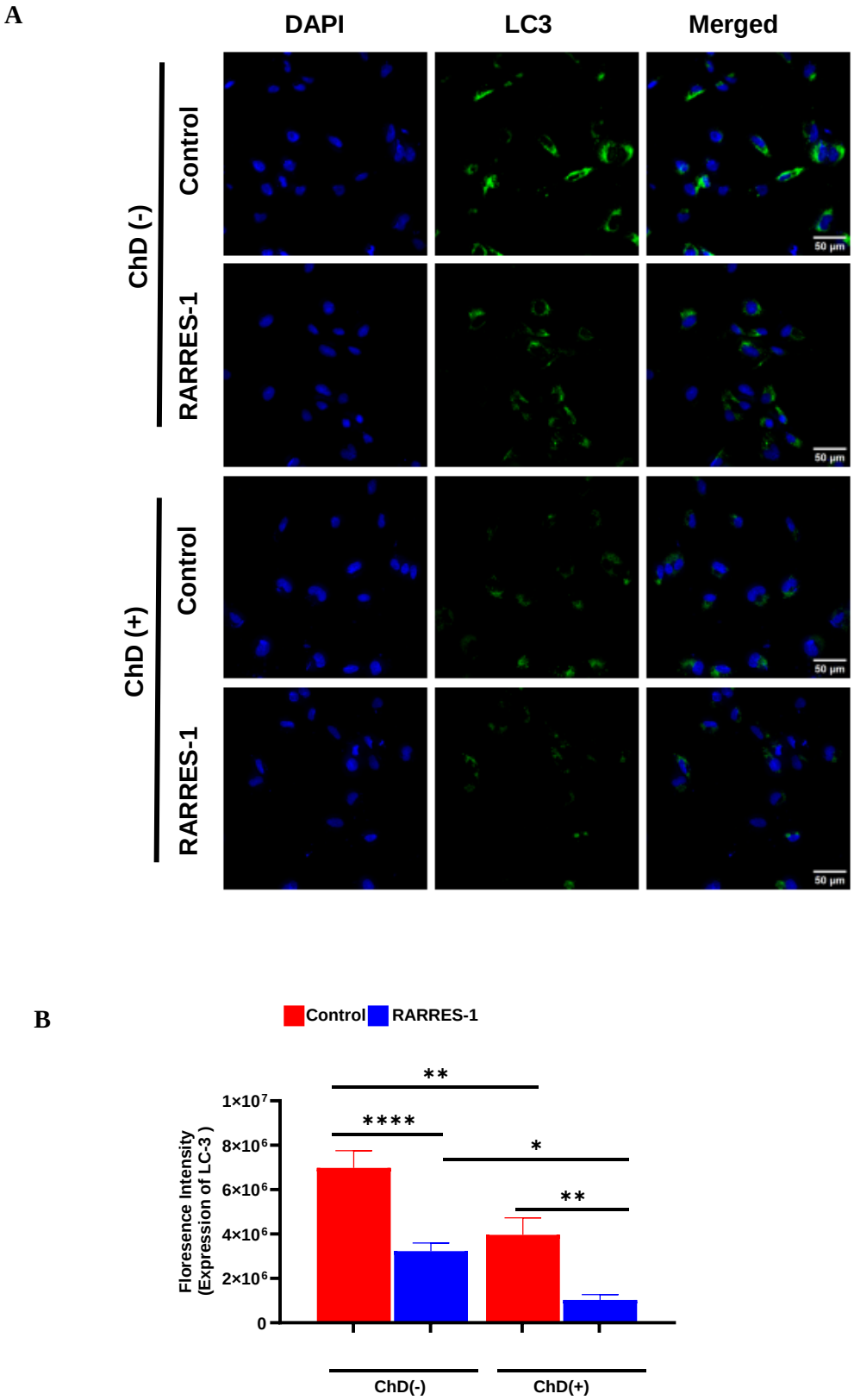

Figure 6.22: Chloroquine diphosphate synergises the antifibrotic effect of RARRES-1 in unstimulated HSCs. LX-2 cells transfected with RARRES-1 plasmid and treated with chloroquine diphosphate for 2 hours and expression of LC3 was assessed (n=2). **A)**

Representative images for expression of LC3. **B)** Quantification of LC3 at baseline. Imaging was undertaken using deltavision microscope and analysed using image J. Values are represented as mean ± SEM. Statistical difference between the groups was measured by one-way ANOVA; multiple comparisons were corrected by Boneferroni correction. *$p \leq 0.05$, **$p \leq 0.01$, ***$p \leq 0.001$A, ****$p \leq 0.0001$.

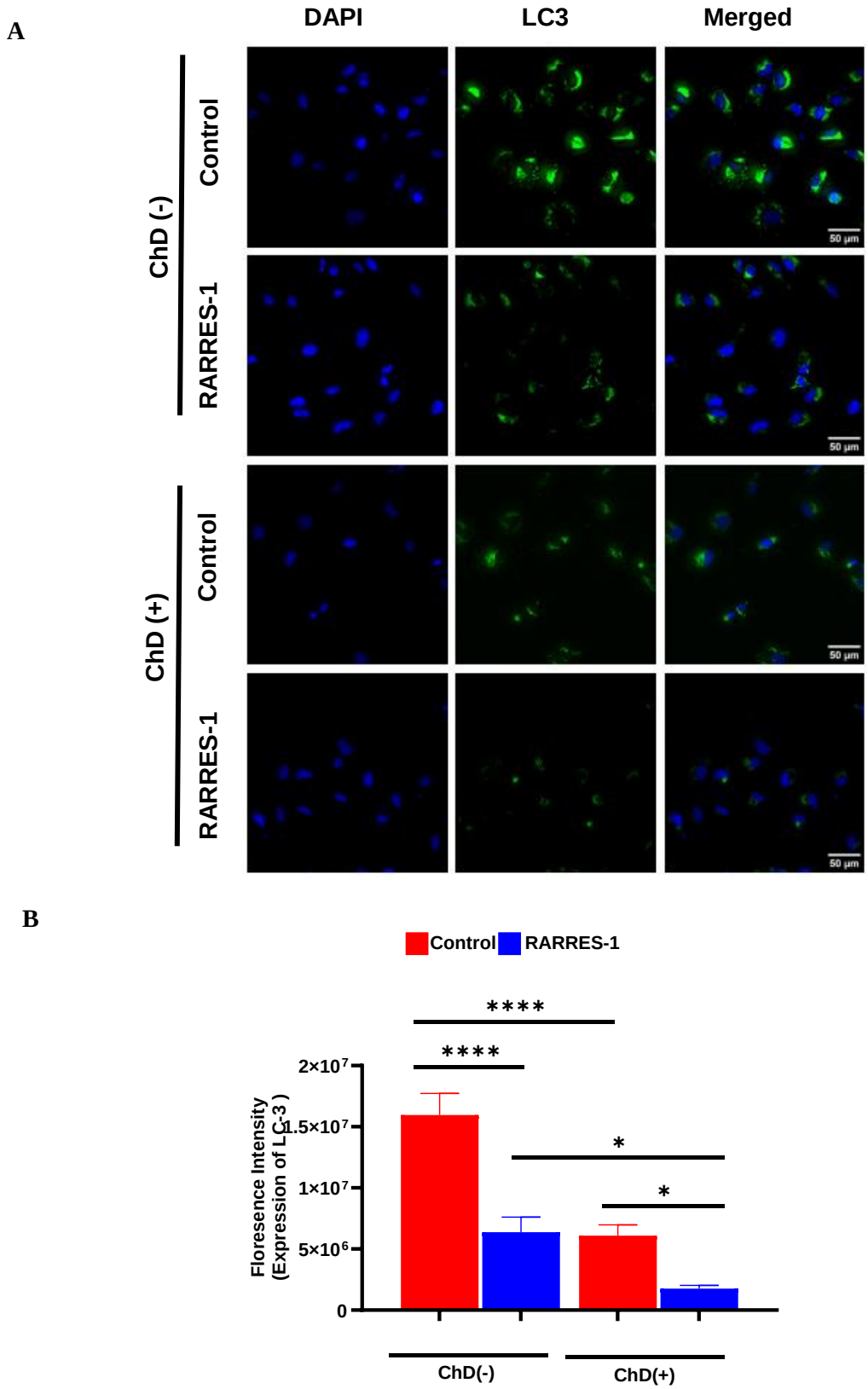

Figure 6.23: Chloroquine diphosphate synergises the antifibrotic effect of RARRES-1 in stimulated HSCs. LX-2 cells transfected with RARRES-1 and treated with chloroquine

diphosphate for 2 hours before challenging with TGF-β and expression of LC3 was assessed (n=2). **A)** Representative images for expression of LC3. **B)** Quantification of LC3 upon stimulation with TGF-β. Imaging was undertaken using deltavision microscope and analysed using image J. Values are represented as mean ± SEM. Statistical difference between the groups was measured by one-way ANOVA; multiple comparisons were corrected by Boneferroni correction. *$p \leq 0.05$, **$p \leq 0.01$, ***$p \leq 0.001$A, ****$p \leq 0.0001$.

A

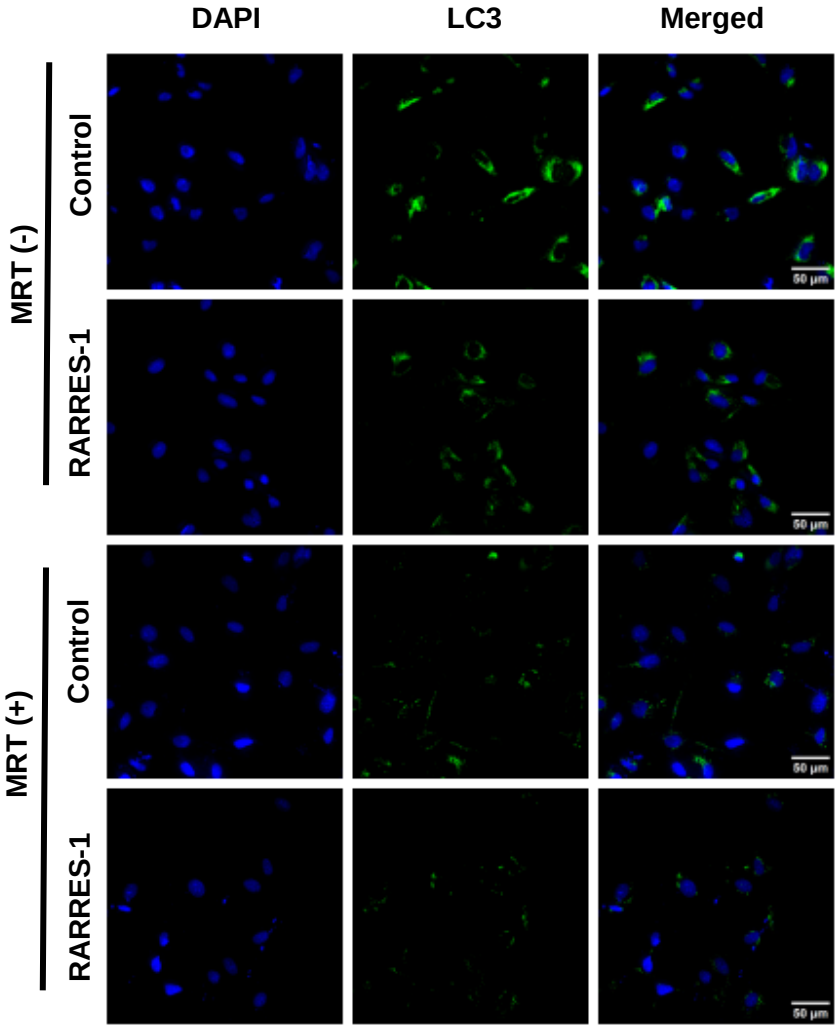

B

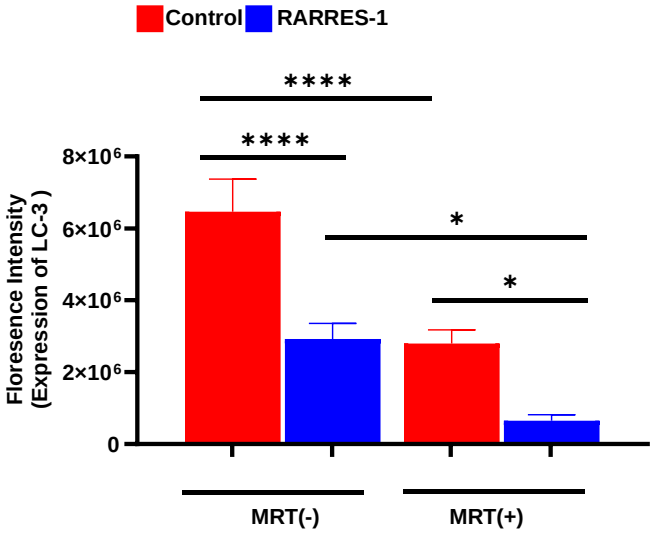

Figure 6.24: MRT68921 dihydrochloride synergises the antifibrotic effect of RARRES-1 in unstimulated HSCs. LX-2 cells transfected with RARRES-1 plasmid and treated with

MRT68921 dihydrochloride for 2 hours and expression of LC3 was assessed (n=2). **A)** Representative images for expression of LC3. **B)** Quantification of LC3 at baseline. Imaging was undertaken using deltavision microscope and analysed using image J. Values are represented as mean ± SEM. Statistical difference between the groups was measured by one-way ANOVA; multiple comparisons were corrected by Boneferroni correction. *$p \leq 0.05$, **$p \leq 0.01$, ***$p \leq 0.001$A, ****$p \leq 0.0001$.

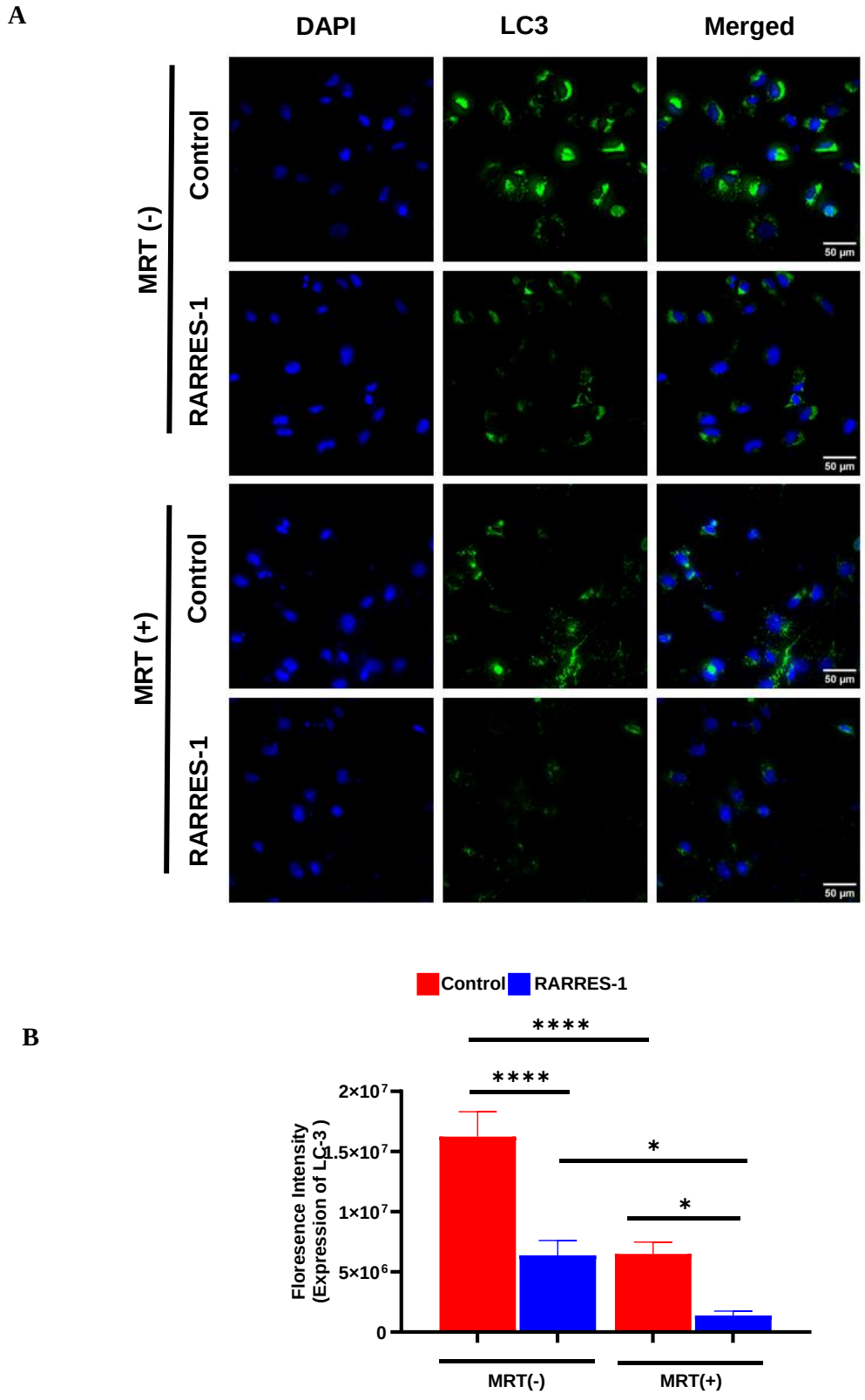

Figure 6.25: MRT68921 dihydrochloride synergises the antifibrotic effect of RARRES-1 in stimulated HSCs. LX-2 cells transfected with RARRES-1 and treated with MRT68921 dihydrochloride for 2 hours before challenging with TGF-β and expression of LC3 was

assessed (n=2). **A)** Representative images for expression of LC3. **B)** Quantification of LC3 upon stimulation with TGF-β. Imaging was undertaken using deltavision microscope and analysed using image J. Values are represented as mean ± SEM. Statistical difference between the groups was measured by one-way ANOVA; multiple comparisons were corrected by Boneferroni correction. *$p \leq 0.05$, **$p \leq 0.01$, ***$p \leq 0.001$A, ****$p \leq 0.0001$.

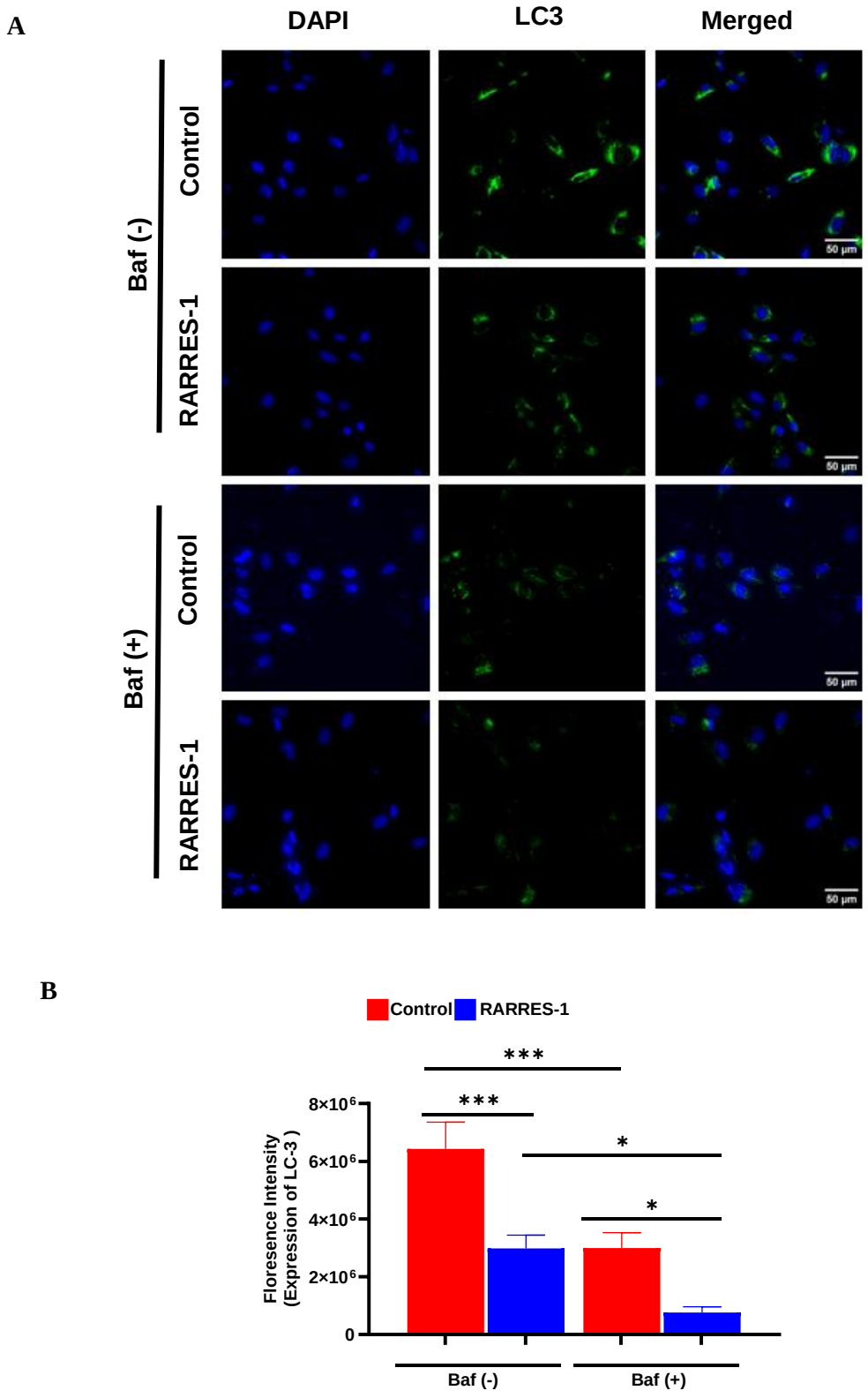

Figure 6.26: Bafilomycin synergises the antifibrotic effect of RARRES-1 in unstimulated HSCs. LX-2 cells transfected with RARRES-1 plasmid and treated with MRT68921 dihydrochloride for 2 hours and expression of LC3 was assessed (n=2). **A)**

Representative images for expression of LC3. **B)** Quantification of LC3 at baseline. Imaging was undertaken using deltavision microscope and analysed using image J. Values are represented as mean ± SEM. Statistical difference between the groups was measured by one-way ANOVA; multiple comparisons were corrected by Boneferroni correction. *$p \leq 0.05$, **$p \leq 0.01$, ***$p \leq 0.001$A, ****$p \leq 0.0001$.

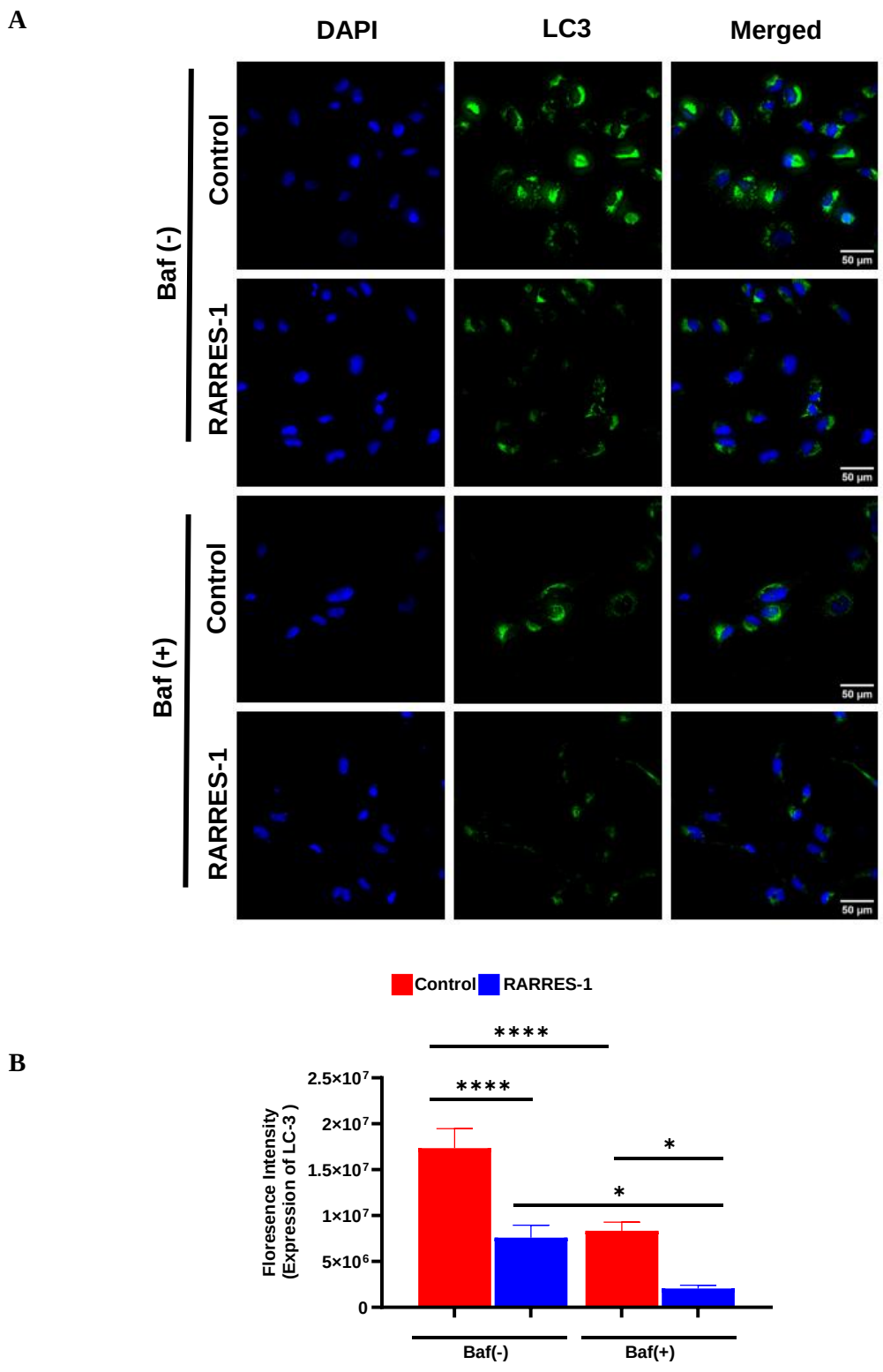

Figure 6.27: Bafilomycin synergises the antifibrotic effect of RARRES-1 in stimulated HSCs. LX-2 cells transfected with RARRES-1 and treated with bafilomycin for 2 hours before challenging with TGF-β and expression of LC3 was assessed (n=2). **A)** Representative

images for expression of LC3. **B)** Quantification of LC3 upon stimulation with TGF-β. Imaging was undertaken using deltavision microscope and analysed using image J. Values are represented as mean ± SEM. Statistical difference between the groups was measured by one-way ANOVA; multiple comparisons were corrected by Boneferroni correction. *$p \leq 0.05$, **$p \leq 0.01$, ***$p \leq 0.001$A, ****$p \leq 0.0001$.

After confirmation the effect of autophagy inhibitors on the attenuation of autophagy, I next investigated their impact on the antifibrotic effect of RARRES-1. LX-2 cells were transfected with RARRES-1 for 48 hours and treated with autophagy inhibitors (chloroquine diphosphate, MRT68921 dihydrochloride and Bafilomycin) for 2 hours before challenging with or without TGF-β for 24 hours and the expression of α-SMA was measured.

Results has shown a synergistic reduction in the expression of α-SMA in LX-2 cells transfected with RARRES-1 and treated with chloroquine diphosphate **(Figure 6.28** and **Figure 6.29)**, MRT68921 dihydrochloride **(Figure 6.30** and **Figure 6.31)** and Bafilomycin **(Figure 6.32** and **Figure 6.33)**.

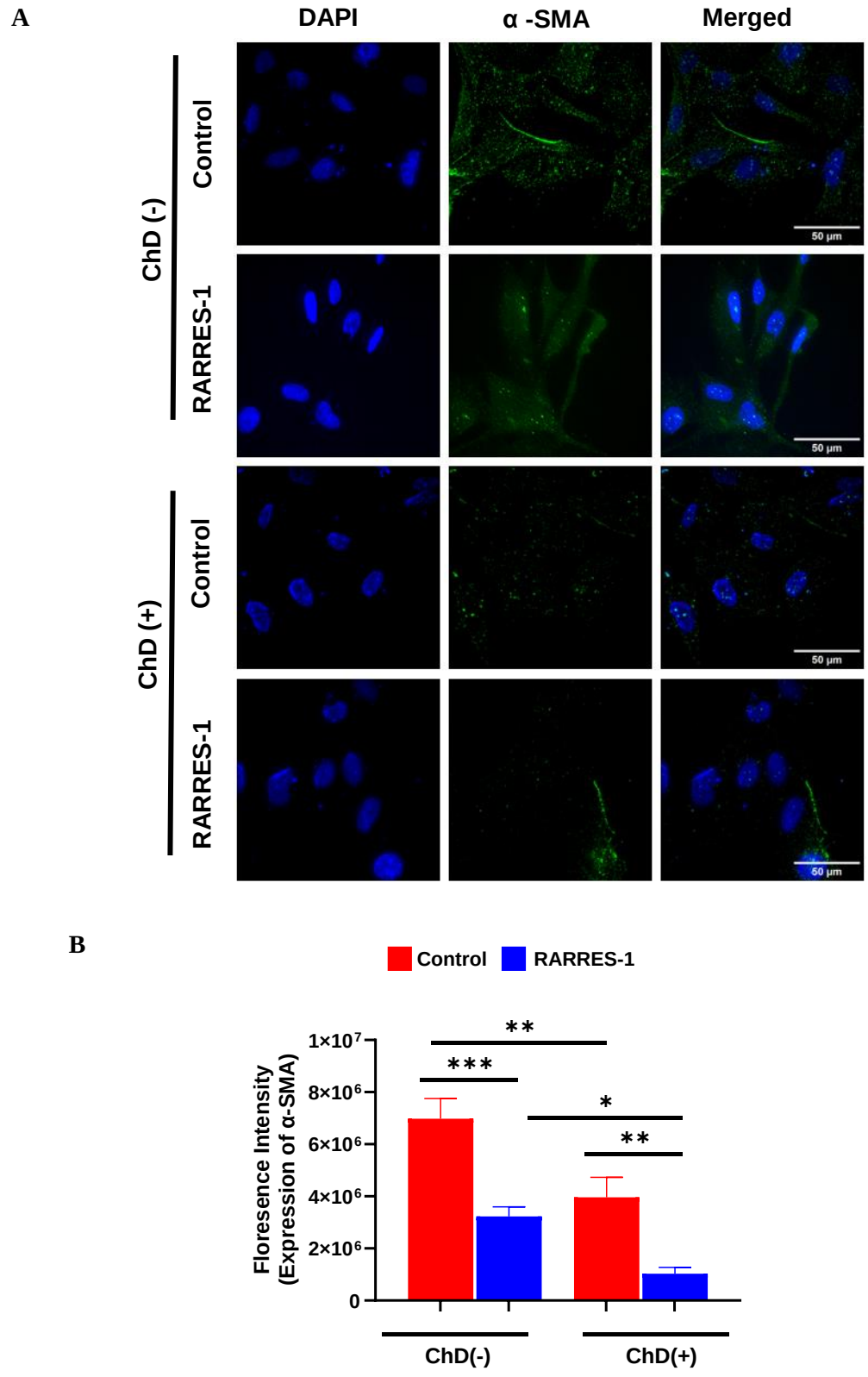

Figure 6.28: Chloroquine diphosphate synergises the antifibrotic effect of RARRES-1 in unstimulated HSCs. LX-2 cells transfected with RARRES-1 plasmid and treated with chloroquine diphosphate for 2 hours and expression of α-SMA was assessed (n=2). **A)**

Representative images for expression of α-SMA. **B)** Quantification of α-SMA at baseline. Imaging was undertaken using deltavision microscope and analysed using image J. Values are represented as mean ± SEM. Statistical difference between the groups was measured by one-way ANOVA; multiple comparisons were corrected by Boneferroni correction. *$p \leq 0.05$, **$p \leq 0.01$, ***$p \leq 0.001$A, ****$p \leq 0.0001$.

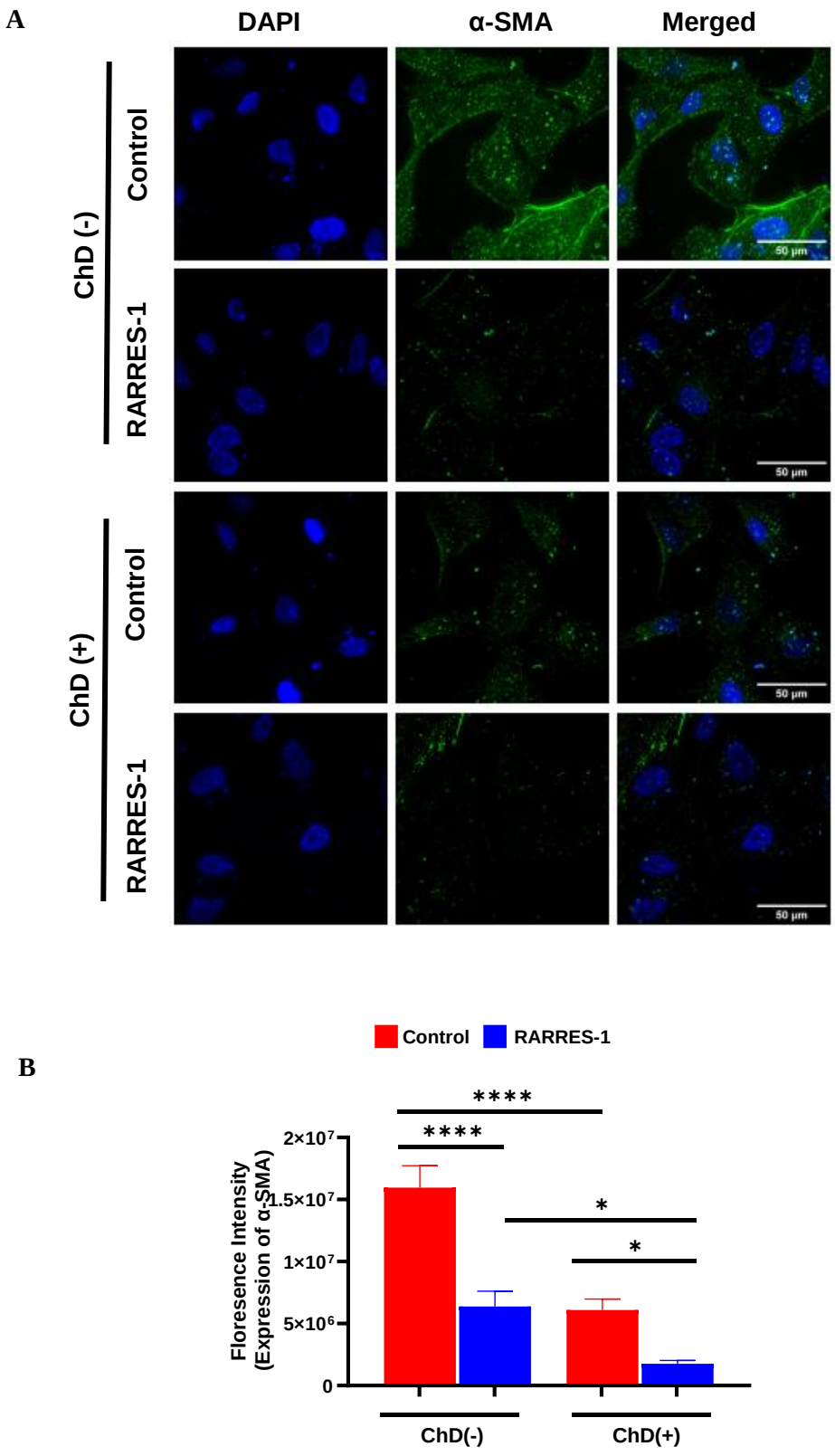

Figure 6.29: Chloroquine diphosphate synergises the antifibrotic effect of RARRES-1 in stimulated HSCs. LX-2 cells transfected with RARRES-1 and treated with chloroquine

diphosphate for 2 hours before challenging with TGF-β and expression of α-SMA was assessed (n=2). **A)** Representative images for expression of α-SMA. **B)** Quantification of α-SMA upon stimulation with TGF-β. Imaging was undertaken using deltavision microscope and analysed using image J. Values are represented as mean ± SEM. Statistical difference between the groups was measured by one-way ANOVA; multiple comparisons were corrected by Boneferroni correction. *$p \leq 0.05$, **$p \leq 0.01$, ***$p \leq 0.001$A, ****$p \leq 0.0001$.

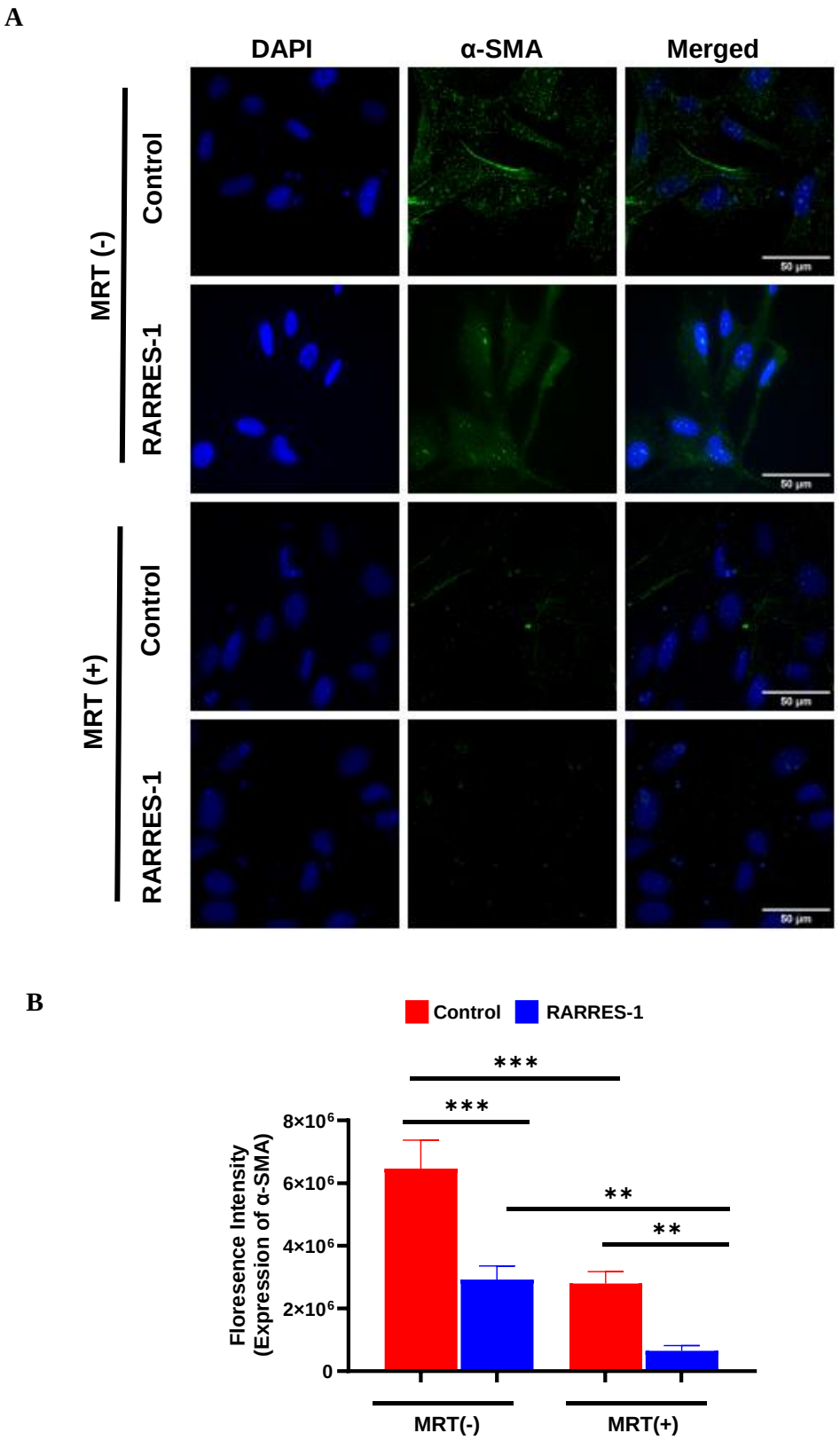

Figure 6.30: MRT68921 dihydrochloride synergises the antifibrotic effect of RARRES-1 in unstimulated HSCs. LX-2 cells transfected with RARRES-1 plasmid and treated with MRT68921 dihydrochloride for 2 hours and expression of α-SMA was assessed (n=2). **A)**

Representative images for expression of α-SMA. **B)** Quantification of α-SMA at baseline. Imaging was undertaken using deltavision microscope and analysed using image J. Values are represented as mean ± SEM. Statistical difference between the groups was measured by one-way ANOVA; multiple comparisons were corrected by Boneferroni correction. *$p \leq 0.05$, **$p \leq 0.01$, ***$p \leq 0.001$A, ****$p \leq 0.0001$.

A

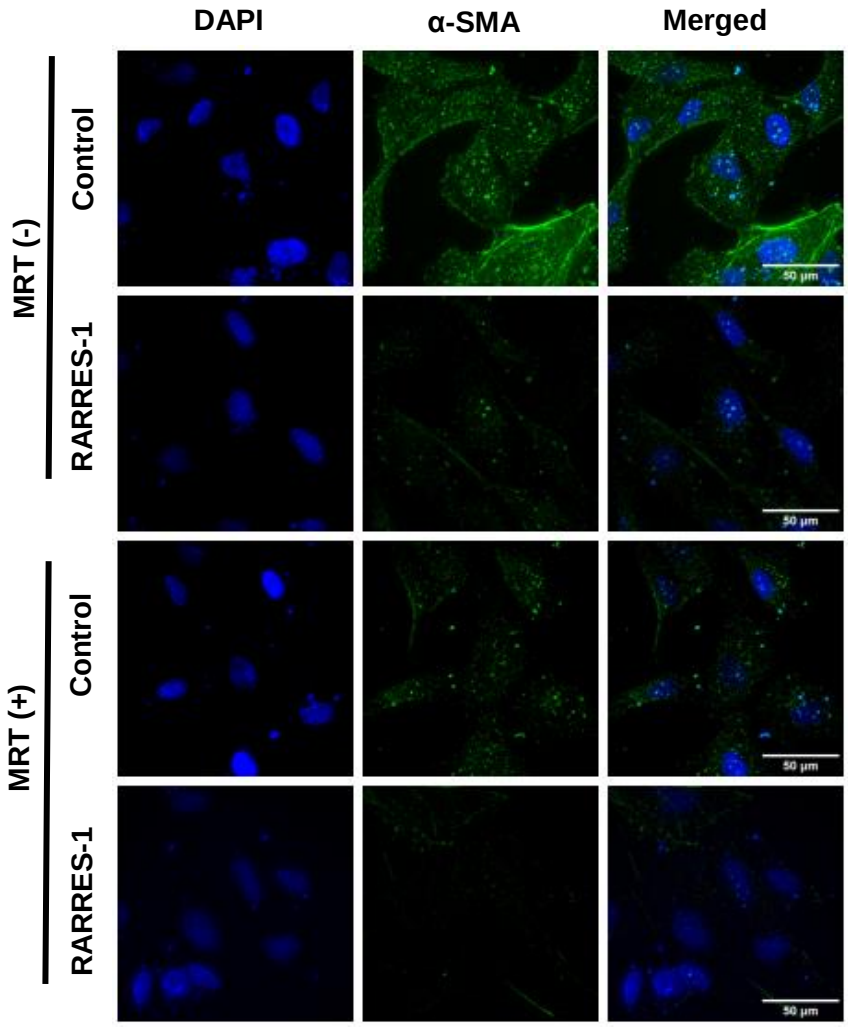

B

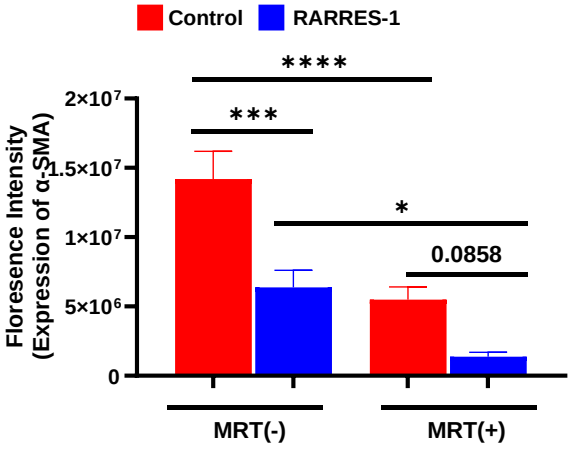

Figure 6.31: MRT68921 dihydrochloride synergises the antifibrotic effect of RARRES-1 in stimulated HSCs. LX-2 cells transfected with RARRES-1 and treated with MRT68921 dihydrochloride for 2 hours before challenging with TGF-β and expression of α-SMA was

assessed (n=2). **A)** Representative images for expression of α-SMA. **B)** Quantification of α-SMA upon stimulation with TGF-β. Imaging was undertaken using deltavision microscope and analysed using image J. Values are represented as mean ± SEM. Statistical difference between the groups was measured by one-way ANOVA; multiple comparisons were corrected by Boneferroni correction. *$p \leq 0.05$, **$p \leq 0.01$, ***$p \leq 0.001$A, ****$p \leq 0.0001$.

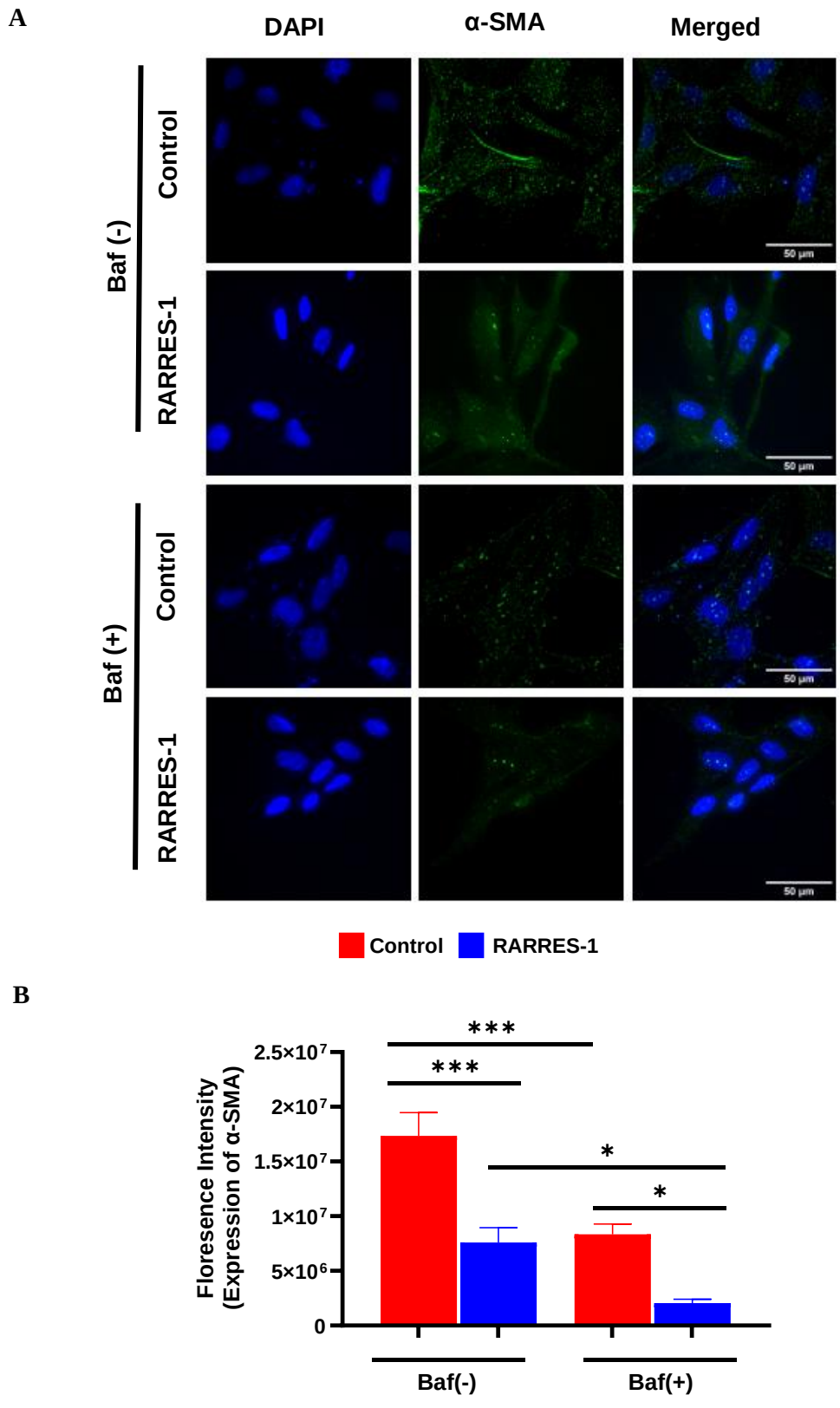

Figure 6.32: Bafilomycin synergises the antifibrotic effect of RARRES-1 in unstimulated HSCs. LX-2 cells transfected with RARRES-1 plasmid and treated with bafilomycin for 2 hours and expression of α-SMA was assessed (n=2). **A)** Representative

images for expression of α-SMA. **B)** Quantification of α-SMA at baseline. Imaging was undertaken using deltavision microscope and analysed using image J. Values are represented as mean ± SEM. Statistical difference between the groups was measured by one-way ANOVA; multiple comparisons were corrected by Boneferroni correction. *$p \leq 0.05$, **$p \leq 0.01$, ***$p \leq 0.001$A, ****$p \leq 0.0001$.

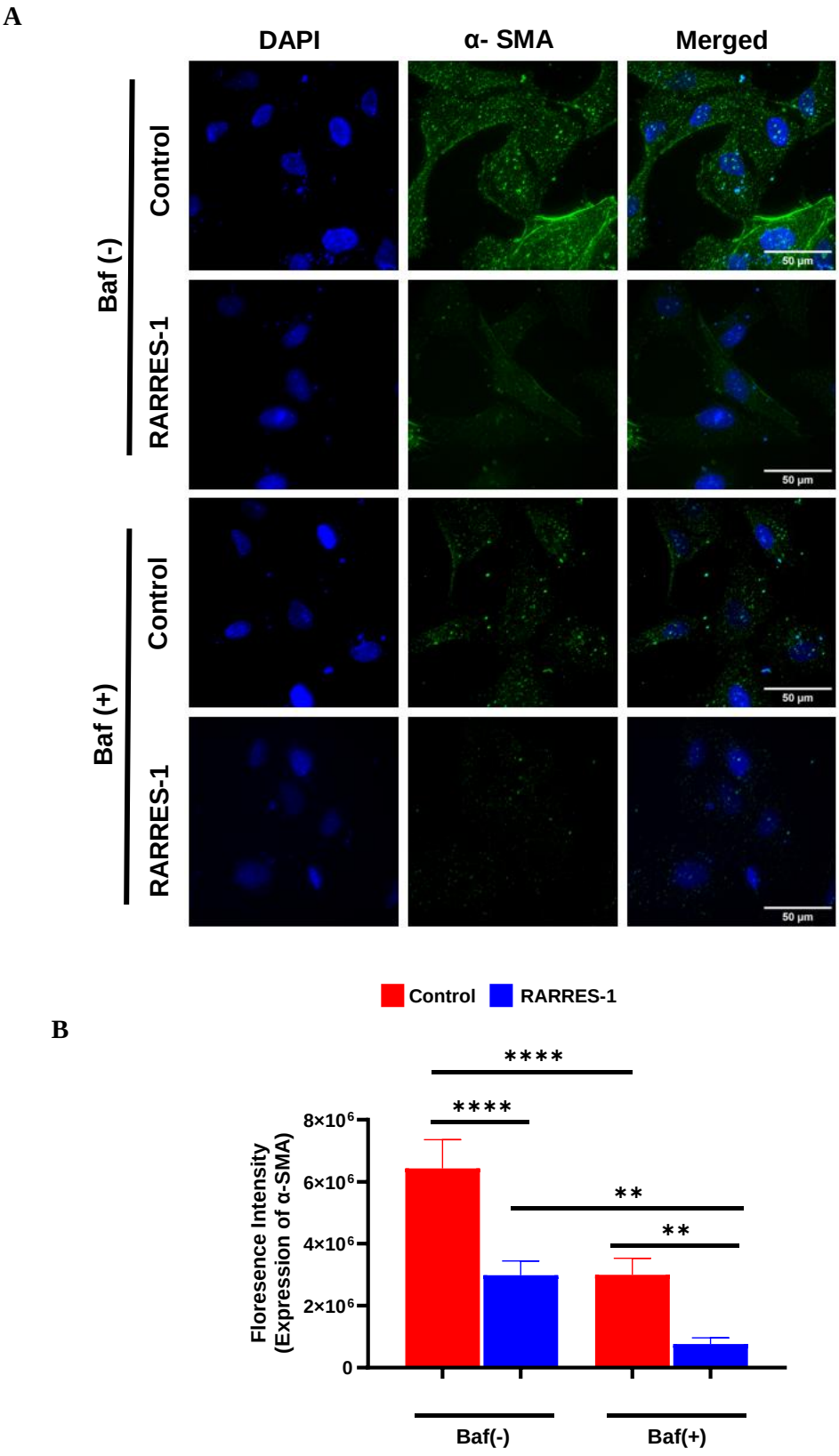

Figure 6.33: Bafilomycin synergises the antifibrotic effect of RARRES-1 in stimulated HSCs. LX-2 cells transfected with RARRES-1 and treated with bafilomycin for 2 hours before challenging with TGF-β and expression of α-SMA was assessed (n=2). **A)** Representative images for expression of α-SMA. **B)** Quantification of α-SMA upon

stimulation with TGF-β. Imaging was undertaken using deltavision microscope and analysed using image J. Values are represented as mean ± SEM. Statistical difference between the groups was measured by one-way ANOVA; multiple comparisons were corrected by Boneferroni correction. *$p \leq 0.05$, **$p \leq 0.01$, ***$p \leq 0.001$A, ****$p \leq 0.0001$.

6.2.8.2.2 Autophagy genetic inhibitors

I have demonstrated that chemical inhibitor of autophagy synergises the antifibrotic effect of RARRES-1. Since these drugs may have nonspecific effects other than autophagy inhibition, for further confirmation I used genetic inhibitors, namely LC3 siRNA and ATG-12 siRNA, to further confirm the specificity of the inhibition of autophagy. I have done double transfection with RARRES-1 and LC3 siRNA for 48 hours, with or without TGF-β stimulation for 24 hours. The analysis of my experiment confirmed that RARRES-1 activation accompanied with LC3 silencing have a synergistic antifibrotic effect, as shown by reducing the expression of α-SMA both at **(Figure 6.34A-B)** and upon TGF-β stimulation **(Figure 6.35A-B)**.

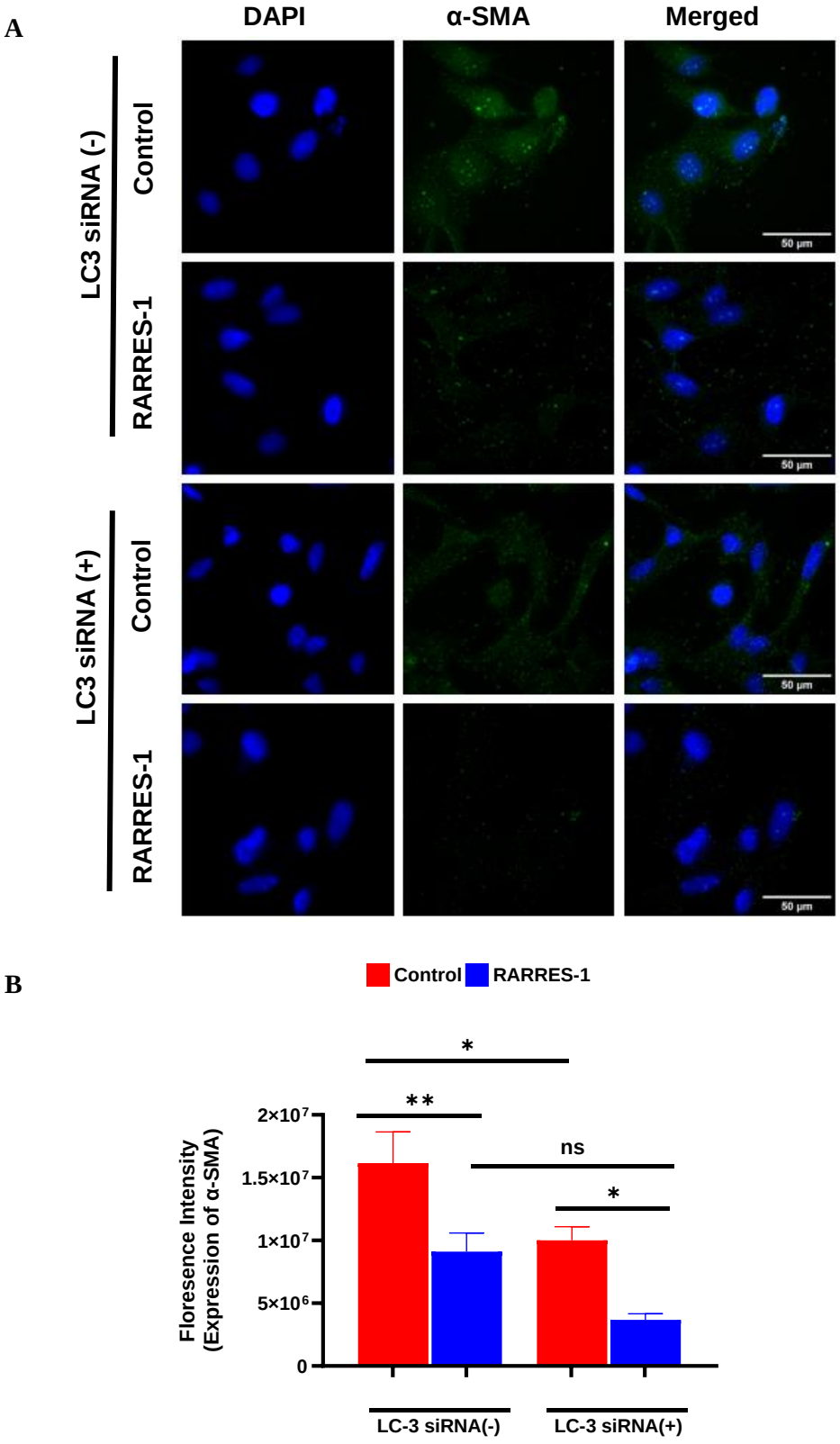

Figure 6.34: LC3 silencing synergizes the antifibrotic effect of RARRES-1 in unstimulated HSCs. LX-2 cells were transfected with RARRES-1 and LC3 siRNA for 2 hours and expression of α-SMA was assessed (n=2). **A)** Representative images for expression

of α-SMA. **B)** Quantification of α-SMA at baseline. Imaging was undertaken using deltavision microscope and analysed using image J. Values are represented as mean ± SEM. Statistical difference between the groups was measured by one-way ANOVA; multiple comparisons were corrected by Boneferroni correction. *$p \leq 0.05$, **$p \leq 0.01$, ***$p \leq$ 0.001A, ****$p \leq 0.0001$.

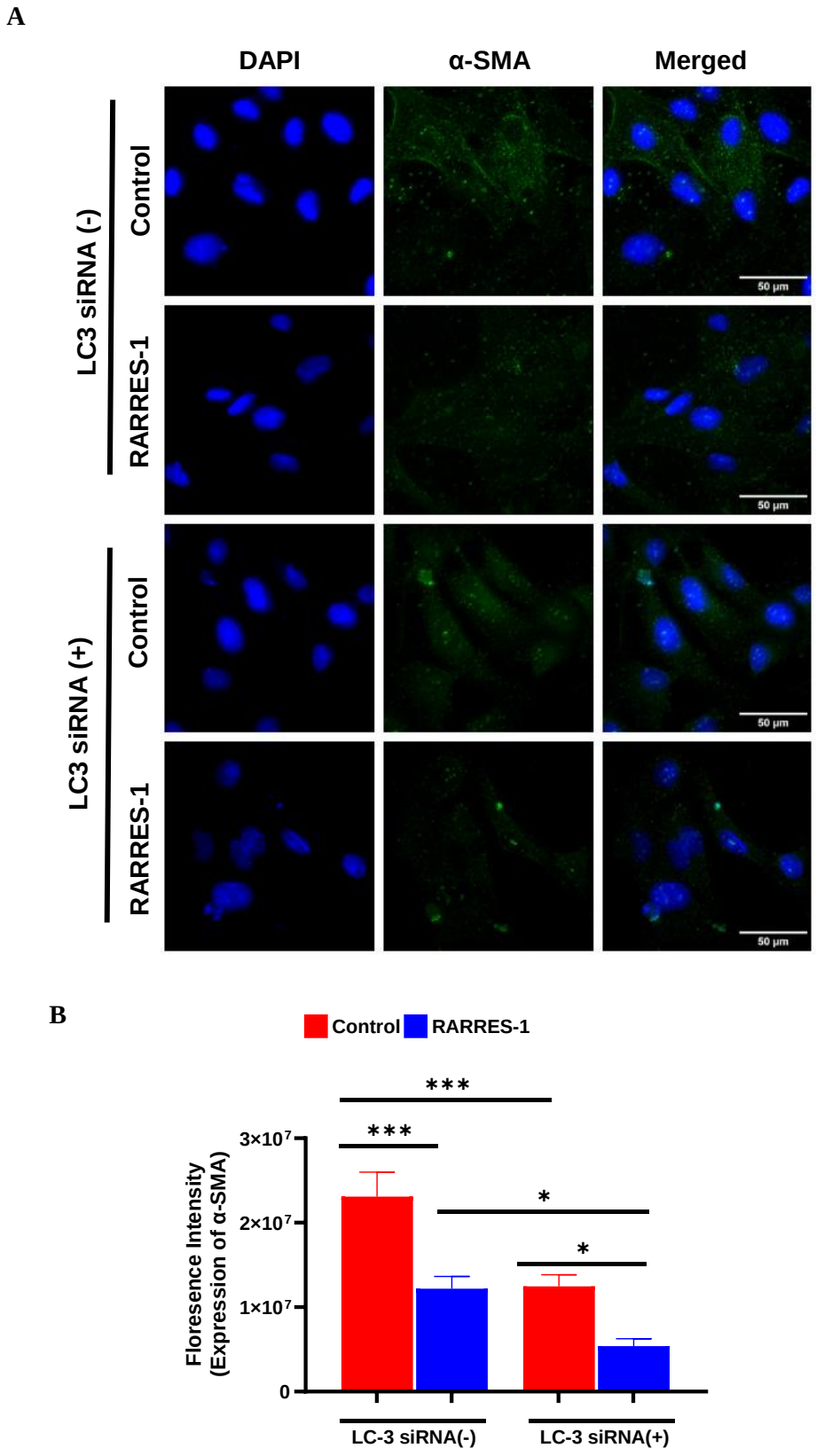

Figure 6.35: LC3 silencing synergizes the antifibrotic effect of RARRES-1 in TGF-β stimulated HSCs. LX-2 cells were transfected with RARRES-1 and LC3 siRNA before

challenging with TGF-β and expression of α-SMA was assessed (n=2). **A)** Representative images for expression of α-SMA. **B)** Quantification of α-SMA upon stimulation with TGF-β. Imaging was undertaken using deltavision microscope and analysed using image J. Values are represented as mean ± SEM. Statistical difference between the groups was measured by one-way ANOVA; multiple comparisons were corrected by Boneferroni correction. *$p \leq 0.05$, **$p \leq 0.01$, ***$p \leq 0.001$A, ****$p \leq 0.0001$.

For further confirmation that the discerned effect is not gene or siRNA specific, I used another one, ATG-12 siRNA. For this, LX-2 cells were double transfected with both RARRES-1 plasmid and ATG-12 siRNA for 48 hours and treated with or without TGF-β for 24 hours. Consistently, RARRES-1 activation reduces the expression of α-SMA (antifibrotic marker) both at baseline and upon TGF-β stimulation. However, the double transfection of RARRES-1 and ATG-12 siRNA produces synergistic inhibition in the expression of α-SMA both at baseline **(Figure 6.36A-B)** and upon TGF-β stimulation **(Figure 6.37A-B)**. Collectively these findings indicate that RARRES-1 produces its antifibrotic effect through the regulation of autophagy at various stages.

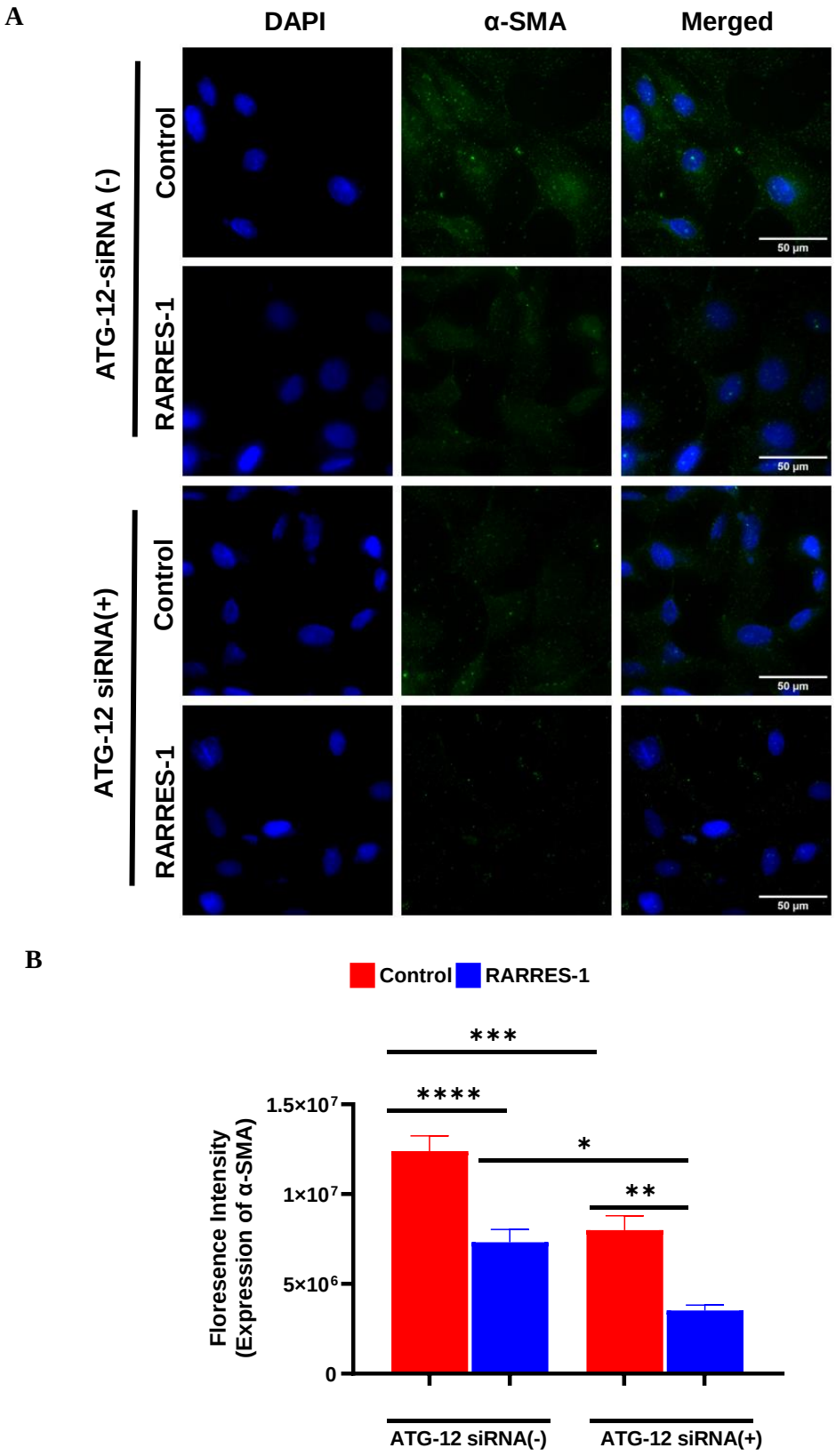

Figure 6.36: ATG-12 silencing synergizes the antifibrotic effect of RARRES-1 in unstimulated HSCs. LX-2 cells were transfected with RARRES-1 and ATG-12 siRNA for 2

hours and expression of α-SMA was assessed (n=2). **A)** Representative images for expression of α-SMA. **B)** Quantification of α-SMA in baseline. Imaging was undertaken using deltavision microscope and analysed using image J. Values are represented as mean ± SEM. Statistical difference between the groups was measured by one-way ANOVA; multiple comparisons were corrected by Boneferroni correction. *$p \leq 0.05$, **$p \leq 0.01$, ***$p \leq$ 0.001A, ****$p \leq 0.0001$.

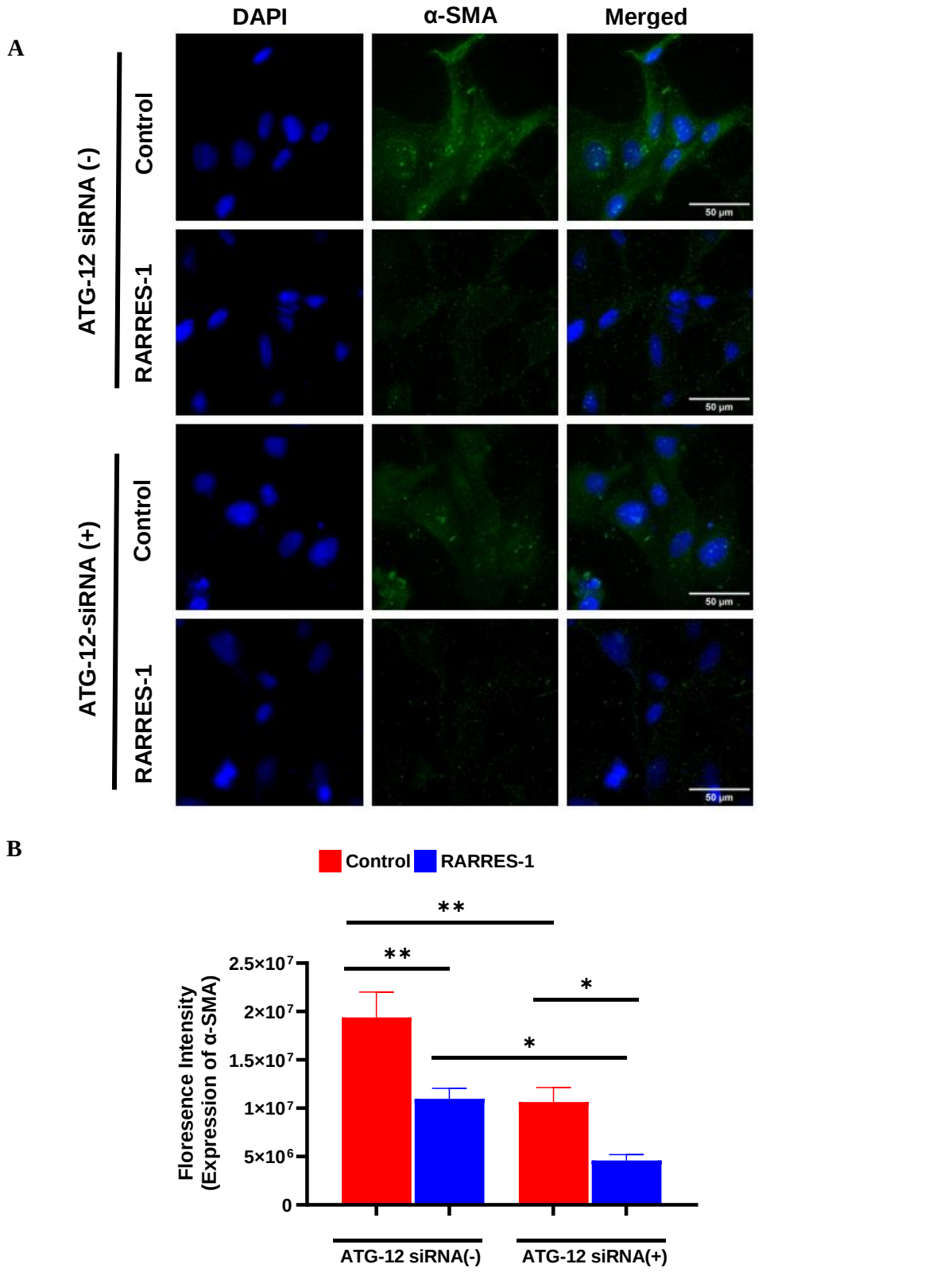

Figure 6.37: ATG-12 silencing synergizes the antifibrotic effect of RARRES-1 in TGF-β stimulated HSCs. LX-2 cells were transfected with RARRES-1 and ATG-12 siRNA before challenging with TGF-β and expression of α-SMA was assessed (n=2). **A)** Representative

images for expression of α-SMA. **B)** Quantification of α-SMA upon stimulation with TGF-β. Imaging was undertaken using deltavision microscope and analysed using image J. Values are represented as mean ± SEM. Statistical difference between the groups was measured by one-way ANOVA; multiple comparisons were corrected by Boneferroni correction. *$p \leq 0.05$, **$p \leq 0.01$, ***$p \leq 0.001$A, ****$p \leq 0.0001$.

6.3 Discussion

In the previous chapters, I reported that RARRES-1 exerts antifibrotic effects by reducing mitochondrial activity and the generation of ROS. In this chapter, I extended these findings and confirmed that RARRES-1 regulates autophagy and its downstream pathways. Overall, I showed that RARRES-1 reduces fibrosis by regulating two key processes involved in energy release, a key prerequisite for HSC activation and liver fibrosis progression.

An intertwined and bidirectional interaction exists between autophagy and mitochondrial function, which is implicated in HSCs activation. Various studies of human and animal models have shown that TGF-β increases autophagy [242]. TGF-β has been reported to increase the expression of LC-II/I in HSCs [249] and increase the generation of ROS that further induce autophagy, which promotes HSCs activation and liver fibrosis [237, 250]. On the other hand, autophagy has been reported to increase mitochondrial ROS generation [251, 252]. Additionally, autophagy promotes liver fibrosis directly by inducing the loss of lipid droplets in HSCs to fuel myofibroblast activation and increase the energy demand of the cells [253]. Here, I showed that RARRES-1 activation disrupts this vicious cycle and reverses the activation of HSCs.

In this chapter, the data confirmed that RARRES-1 activation represses the process of autophagy at various levels. It regulates the morphological changes in autophagosomes under fibrotic conditions. Additionally, RARRES-1 activation reduces the expression of the autophagy-related proteins ATG-5, ATG-12, LC3, and Beclin, which are involved in initiating the process of autophagy. These results also indicate that RARRES-1 activation preserves the p62 protein, which indicates a reduction in autophagy. Furthermore, RARRES-1 activation regulates autophagic flux by reducing the formation of autophagosomes and autolysosomes.

The findings also confirmed that RARRES-1 activation regulates the formation of lysosomes during fibrosis. The expanded work using double staining revealed that RARRES-1 activation collectively reduces the formation of lysosomes and the expression of the LC3 marker, indicating parallel stages during autophagy.

Additionally, the data presented in this chapter confirmed that RARRES-1 activation preserves lipid droplets and by utilizing a double-staining approach, I further confirmed that this preservation of lipid droplets is due to the inhibition of autophagy.

These findings further confirmed that the antifibrotic effect of RARRES-1 is reversed upon treatment with autophagy inducers. This phenomenon might illuminate the pathophysiological context that occurs during liver fibrosis when a constant source of injury masks some of the regulatory protective nodes, leading to uncontrolled autophagy and attenuated RARRES-1 expression, which subsequently causes HSC activation, ROS generation, autophagy acceleration [249] and the progression of liver fibrosis.

Interestingly, my results further confirmed that RARRES-1 activation along with autophagy inhibitor synergistically reduced HSCs activation, as evidenced by the expression of various fibrotic markers. This effect was confirmed using genetic (ATG-12 siRNA and LC-3 siRNA) and chemical (chloroquine diphosphate, MRT 68921 dihydrochloride and bafilomycin) inhibitors [254-256]. RARRES-1 activation, along with autophagy inhibitors, synergistically repressed the expression of autophagy markers and fibrotic markers.

In conclusion, the results presented in this chapter confirm that activating RARRES-1 produces an antifibrotic effect, partially by regulating autophagy and preserving lipid droplets. Therefore, RARRES-1 activation is an attractive therapeutic target that can be used to regulate autophagy, maintain normal homeostasis, and reverse liver fibrosis.

Chapter Seven: Summary and future direction

7.1 Summary of future challenges and open questions

Liver disease is the 5th most common cause of death in Australia, with a financial cost estimated at $5.4 billion [5]. The main histological determinant of liver disease outcomes is the development of liver fibrosis and ultimately cirrhosis. Virtually all liver disease-related morbidity and mortality are due to fibrosis, which culminates in liver failure or cancer [257]. Currently, no therapeutic options are available to cure liver fibrosis, and liver transplantation is the only option for survival in patients with end-stage liver disease [90]. Since no drugs are available to reverse fibrosis, new approaches to drug development are needed [16, 152, 258].

In this work, I discovered a novel strategy for antifibrotic drug development that involves targeting the retinoic acid receptor responder 1 (RARRES-1) to regulate the interplay between epigenetics and energy metabolism.

Epigenetics can be avenue to find novel therapeutic targets for liver fibrosis. Epigenetics is a heritable phenotype changes that donot involve alterations in the DNA sequence. DNA methylation is important epigenetic process, that plays role in HSCs differentiation and extracellular matrix accumulation during liver fibrosis [177]. Epigenome-wide association study identified increased methylation at the Retinoic acid receptor responder protein 1 gene (RARRES-1) locus was found as the top hit associated with advanced fibrosis. Aberrant DNA hypermethylation of RARRES-1 expression has been demonstrated in various cancers. However the role of RARRES-1 in liver fibrosis is still largely unknown [182].

In this thesis, I opted to investigate the effect RARRES-1 activation as a treatment option for liver fibrosis. To investigate it in detail, I hypothesized that RARRES-1 is inactivated in liver fibrosis and restoring RARRES1 expression would reverse liver fibrosis through downregulation of energy release. I tested my hypothesis through the following aims:

I. Explored if RARRES-1 attenuates liver fibrosis in activated hepatic stellate cells

II. Explored if RARRES-1 regulates fibrosis by regulating mitochondrial function

III. Explored if RARRES-1 regulates fibrosis by regulating ROS generation

IV. Explored if RARRES-1 regulates fibrosis by regulating autophagy

7.2 Summary of findings

In Chapter 3, I reported that RARRES-1 is expressed in various tissues and liver subsets. Within the liver, it is highly expressed in HSCs. I also find that RARRES1 expression is attenuated with fibrosis in human, mouse, and *in vitro* models. While restoring RARRES-1 expression showed anti-fibrotic effects.

In Chapter 4, I demonstrated that RARRES-1 activation produces an antifibrotic effect by regulating mitochondrial activity in terms of mitochondrial morphology, mitochondrial import, ATP synthesis, mitochondrial turnover, mitochondrial ROS production, mitochondrial membrane potential, and ultimately reduces the expression of fibrotic markers.

In Chapter 5, I showed that RARRES-1 activation produces antifibrotic effect that is at least partially mediated by the regulation of ROS generation. I found that RARRES-1 activation reduces the generation of both cytoplasmic and mitochondrial ROS. I also confirmed that the antifibrotic effect of RARRES-1 is altered through the modulation of ROS production via both induction and inhibition.

In Chapter 6, I confirmed that activating RARRES-1 produces an antifibrotic effect, partially by regulating different stages of autophagy and preserving lipid droplets. I also confirmed that autophagy inducers reverse the antifibrotic effect of RARRES-1 and that autophagy inhibitors synergies the antifibrotic effect of RARRES-1.

Therefore, collectively RARRES-1 is a promising therapeutic target that can be extrapolated as a therapeutic option for liver fibrosis.

7.3 Significance of the findings

Using human, mouse and cell-based models, I have demonstrated that RARRES-1 silencing is responsible for the progression of liver fibrosis. This study has specifically confirmed that under the conditions of consistent injury, the profibrotic regulator TGF-β causes the transcriptional silencing of RARRES-1, which activates downstream mechanisms to develop fibrosis.

Mechanistically, I propose **(Figure 7.1)** that fibrosis is regulated by RARRES-1 activation. TGF-β is a key regulator of fibrosis through the activation of various pathways, which involves mitochondrial dysfunction that ultimately increases the generation of ROS, increases autophagy, and decreases lipid droplets and hence increases the energy release to support myofibroblast activation and liver fibrosis.

This study confirms that RARRES-1 activation will reduce fibrosis by regulating metabolic reprogramming, especially by reducing energy production through mitochondria and ROS release. I further confirmed that RARRES-1 activation inhibits autophagy, decreases the expression of autophagy markers, reduces the formation of double-membrane autophagosomes, reduces autophagic flux and consequently preserves lipid droplets. This regulation of autophagy by RARRES-1 ultimately reduces energy release, which supports HSCs activation and liver fibrosis.

Taken together, these findings confirmed that RARRES-1 activation can be exploited to reverse liver fibrosis.

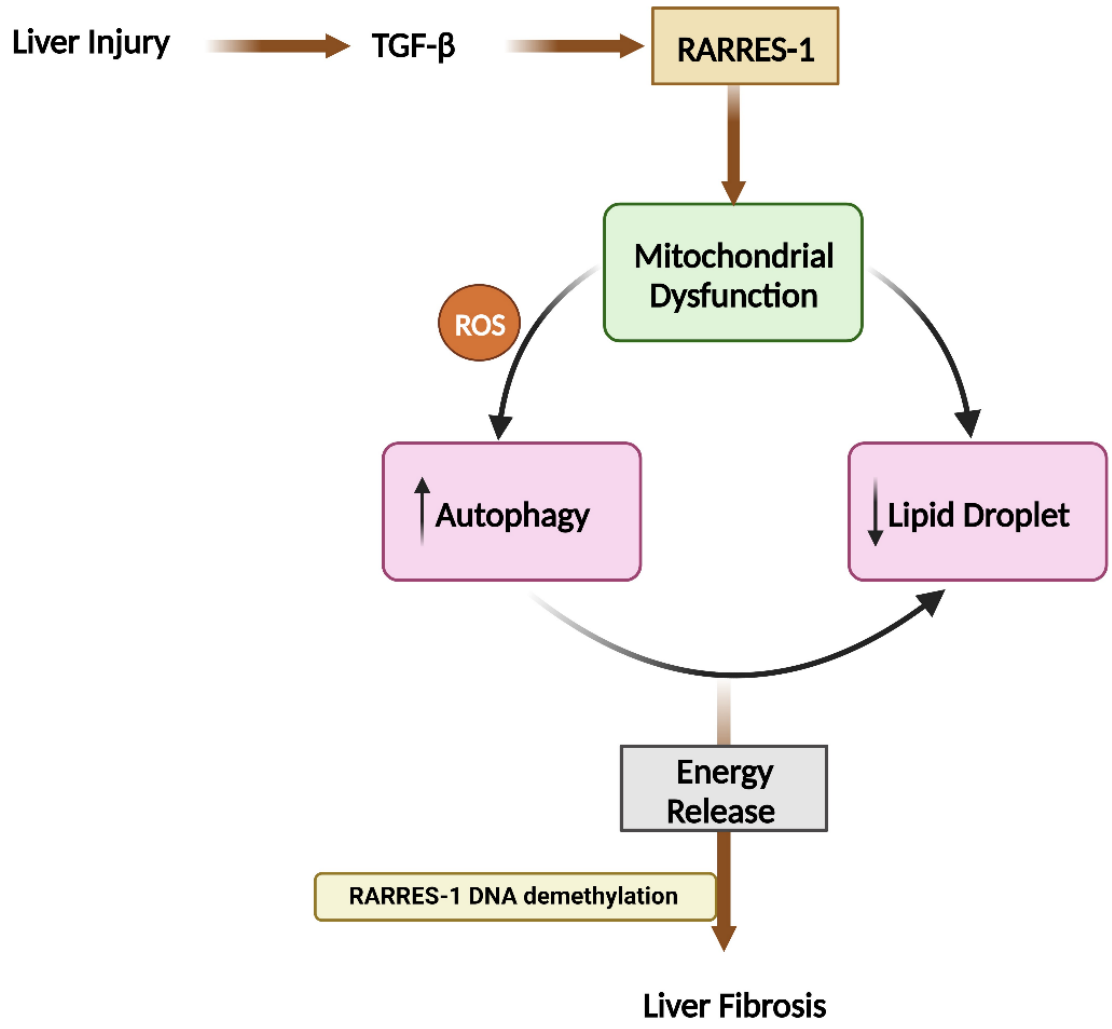

Figure 7.1 Model of RARRES-1 mechanisms for regulation of TGF-β induced fibrotic pathways in liver fibrosis

7.4 Future directions

7.4.1 Determining whether RARRES-1 activation limits fibrosis progression *in vivo*

After confirming the anti-fibrotic effect of RARRES1 *in vitro*, it would be interesting in future studies to extend my findings and test the role of RARRES-1 in liver fibrosis in *in vivo*.

7.4.2 Determining whether RARRES-1 activation accelerates fibrosis resolution *in-vivo*.

In practice, patients present with established fibrosis and the aim of therapy is to limit progression, and ideally to hasten resolution. Thus, it would be also interested to test if RARRES-1 activation can accelerate fibrosis resolution in *in vivo*.

7.4.3 Developing CRISPR Cas9 epigenetic editing tool

Conventional drugs are limited in their ability to reverse epigenetic changes. Thus, future approaches are needed to target the epigenome and restore the healthy epigenetic landscape [259]. To reverse epigenetic changes occurred in fibrosis, future studies should include developing epigenome editing tool (CRISPR Cas9) that will cause DNA demethylation to restore RARRES-1 transcription and investigate if targeted DNA demethylation of RARRES-1 through administration of CRISPR Cas9 reduces fibrosis in LX-2, human hepatic stellate cells *in vitro* and *in vivo* experimental models.

For HSC targeted gene delivery, CRISPR Cas9 could be generated by a validated lentiviral system [260, 261] harbouring dCas9- TET1CD-Rarres1-sgRNA4 or dCas9-TET1CD-LacZ-scramble gRNA (as a control), cloned downstream of the α-SMA promoter.

7.5 Conclusion

Liver fibrosis is an unmet clinical health challenge that requires novel therapeutic approaches. Taken together, the results of this study support RARRES-1 as a potential therapeutic target to cure liver fibrosis. Designing CRISPR Cas9, as epigenome editing tool for specific DNA demethylation of RARRES-1 may constitute a first-in-class treatment to reverse liver fibrosis. This approach can restore the homeostatic balance between the epigenome and metabolism. However, long term effects of RARRES-1 activation may need to be considered.

References

1. Yang, H., et al., *COX-2 in liver fibrosis.* Clinica chimica acta, 2020. **506**: p. 196-203.
2. Zhao, J., Y.-F. Qi, and Y.-R. Yu, *STAT3: A key regulator in liver fibrosis.* Annals of Hepatology, 2021. **21**: p. 100224.
3. Devarbhavi, H., et al., *Global burden of liver disease: 2023 update.* Journal of hepatology, 2023. **79**(2): p. 516-537.
4. Lan, Y., et al., *The burden of liver cirrhosis and underlying etiologies: results from the Global Burden of Disease Study 2019.* Hepatology Communications, 2023. **7**(2): p. e0026.
5. Sarin, S.K., et al., *Liver diseases in the Asia-Pacific region: a lancet gastroenterology & hepatology commission.* The lancet Gastroenterology & hepatology, 2020. **5**(2): p. 167-228.
6. Economics, D.A., *The economic cost and health burden of liver diseases in Australia.* Kingston: The Gastroenterological Society of Australia/Australian Liver Association, 2013.
7. Calzadilla-Bertot, L., et al., *Increasing incidence of nonalcoholic steatohepatitis as an indication for liver transplantation in Australia and New Zealand.* Liver Transplantation, 2019. **25**(1): p. 25-34.
8. Li, H., et al., *Interplays of liver fibrosis-associated microRNAs: Molecular mechanisms and implications in diagnosis and therapy.* Genes Dis, 2023. **10**(4): p. 1457-1469.
9. Hernandez-Gea, V. and S.L. Friedman, *Pathogenesis of liver fibrosis.* Annual review of pathology: mechanisms of disease, 2011. **6**: p. 425-456.
10. Estes, C., et al., *Modeling the epidemic of nonalcoholic fatty liver disease demonstrates an exponential increase in burden of disease.* Hepatology, 2018. **67**(1): p. 123-133.
11. Sangro, P., et al., *Metabolic dysfunction–associated fatty liver disease (MAFLD): an update of the recent advances in pharmacological treatment.* Journal of physiology and biochemistry, 2023. **79**(4): p. 869-879.
12. Poynard, T., et al., *Prevalence of liver fibrosis and risk factors in a general population using non-invasive biomarkers (FibroTest).* BMC Gastroenterol, 2010. **10**: p. 40.
13. Clark, J.M. and A.M. Diehl, *Nonalcoholic fatty liver disease: an underrecognized cause of cryptogenic cirrhosis.* Jama, 2003. **289**(22): p. 3000-3004.
14. Loomba, R. and L.A. Adams, *The 20% Rule of NASH Progression: The Natural History of Advanced Fibrosis and Cirrhosis Caused by NASH.* Hepatology, 2019. **70**(6).
15. Gastaldelli, A., *Fatty liver disease: the hepatic manifestation of metabolic syndrome.* Hypertension Research, 2010. **33**(6): p. 546-547.
16. Eslam, M. and J. George, *Genetic contributions to NAFLD: leveraging shared genetics to uncover systems biology.* Nature reviews Gastroenterology & hepatology, 2020. **17**(1): p. 40-52.
17. Zhang, C.-Y., S. Liu, and M. Yang, *Treatment of liver fibrosis: Past, current, and future.* World Journal of Hepatology, 2023. **15**(6): p. 755.
18. Cheng, J.Y.-K. and G.L.-H. Wong, *Advances in the diagnosis and treatment of liver fibrosis.* Hepatoma Res, 2017. **3**(8): p. 156-69.
19. Bedossa, P., K. Patel, and L. Castera, *Histologic and noninvasive estimates of liver fibrosis.* Clinical liver disease, 2015. **6**(1): p. 5.
20. Tapper, E.B., et al., *Simple non-invasive biomarkers of advanced fibrosis in the evaluation of non-alcoholic fatty liver disease.* Gastroenterology report, 2014. **2**(4): p. 276-280.

21. Nascimbeni, F., et al., *Clinical validation of the FLIP algorithm and the SAF score in patients with non-alcoholic fatty liver disease.* Journal of hepatology, 2020. **72**(5): p. 828-838.
22. Parikh, P., J.D. Ryan, and E.A. Tsochatzis, *Fibrosis assessment in patients with chronic hepatitis B virus (HBV) infection.* Annals of translational medicine, 2017. **5**(3).
23. Afdhal, N.H. and D. Nunes, *Evaluation of liver fibrosis: a concise review.* Official journal of the American College of Gastroenterology| ACG, 2004. **99**(6): p. 1160-1174.
24. Gara, N., et al., *Discordance among transient elastography, aspartate aminotransferase to platelet ratio index, and histologic assessments of liver fibrosis in patients with chronic hepatitis C.* Clinical Gastroenterology and Hepatology, 2013. **11**(3): p. 303-308. e1.
25. Cequera, A. and M.G. de Leon Mendez, *Biomarkers for liver fibrosis: advances, advantages and disadvantages.* Revista de Gastroenterología de México (English Edition), 2014. **79**(3): p. 187-199.
26. Nallagangula, K.S., et al., *Liver fibrosis: a compilation on the biomarkers status and their significance during disease progression.* Future science OA, 2018. **4**(1): p. FSO250.
27. Gokcen, P., et al., *Liver Fatty Acid Binding Protein: Is it an early diagnostic and prognostic marker in liver damage?* Medical Science and Discovery, 2021. **8**(4): p. 213-218.
28. Parikh, P., J.D. Ryan, and E.A. Tsochatzis, *Fibrosis assessment in patients with chronic hepatitis B virus (HBV) infection.* Ann Transl Med, 2017. **5**(3): p. 40.
29. Adams, L.A., et al., *Hepascore: an accurate validated predictor of liver fibrosis in chronic hepatitis C infection.* Clinical chemistry, 2005. **51**(10): p. 1867-1873.
30. Koda, M., et al., *FibroIndex, a practical index for predicting significant fibrosis in patients with chronic hepatitis C.* Hepatology, 2007. **45**(2): p. 297-306.
31. Forns, X., et al., *Identification of chronic hepatitis C patients without hepatic fibrosis by a simple predictive model.* Hepatology, 2002. **36**(4): p. 986-992.
32. Wai, C.-T., et al., *A simple noninvasive index can predict both significant fibrosis and cirrhosis in patients with chronic hepatitis C.* Hepatology, 2003. **38**(2): p. 518-526.
33. Rosenberg, W.M., et al., *Serum markers detect the presence of liver fibrosis: a cohort study.* Gastroenterology, 2004. **127**(6): p. 1704-13.
34. Angulo, P., et al., *The NAFLD fibrosis score: a noninvasive system that identifies liver fibrosis in patients with NAFLD.* Hepatology, 2007. **45**(4): p. 846-854.
35. Daniels, S.J., et al., *ADAPT: An Algorithm Incorporating PRO-C3 Accurately Identifies Patients With NAFLD and Advanced Fibrosis.* Hepatology, 2019. **69**(3): p. 1075-1086.
36. Daniels, S.J., et al., *ADAPT: An Algorithm Incorporating PRO‐C3 Accurately Identifies Patients With NAFLD and Advanced Fibrosis.* Hepatology, 2019. **69**(3): p. 1075-1086.
37. Patel, K., et al., *Evaluation of a panel of non-invasive serum markers to differentiate mild from moderate-to-advanced liver fibrosis in chronic hepatitis C patients.* J Hepatol, 2004. **41**(6): p. 935-42.
38. Mehta, P., et al., *Diagnostic accuracy of serum hyaluronic acid, FIBROSpect II, and YKL-40 for discriminating fibrosis stages in chronic hepatitis C.* Official journal of the American College of Gastroenterology| ACG, 2008. **103**(4): p. 928-936.
39. Sterling, R.K., et al., *Development of a simple noninvasive index to predict significant fibrosis in patients with HIV/HCV coinfection.* Hepatology, 2006. **43**(6): p. 1317-1325.
40. Treeprasertsuk, S., et al., *NAFLD fibrosis score: a prognostic predictor for mortality and liver complications among NAFLD patients.* World journal of gastroenterology: WJG, 2013. **19**(8): p. 1219.
41. Teshale, E., et al., *APRI and FIB‐4 are good predictors of the stage of liver fibrosis in chronic hepatitis B: the Chronic Hepatitis Cohort Study (CH e CS).* Journal of viral hepatitis, 2014. **21**(12): p. 917-920.

42. Saarinen, K., et al., *Enhanced liver Fibrosis® test predicts liver-related outcomes in the general population.* JHEP reports, 2023. **5**(7): p. 100765.
43. Vali, Y., et al., *Enhanced liver fibrosis test for the non-invasive diagnosis of fibrosis in patients with NAFLD: a systematic review and meta-analysis.* Journal of hepatology, 2020. **73**(2): p. 252-262.
44. Berumen, J., et al., *Liver fibrosis: Pathophysiology and clinical implications.* WIREs mechanisms of disease, 2021. **13**(1): p. e1499.
45. Dhar, D., et al., *Mechanisms of liver fibrosis and its role in liver cancer.* Experimental Biology and Medicine, 2020. **245**(2): p. 96-108.
46. Bataller, R. and D.A. Brenner, *Liver fibrosis.* The Journal of clinical investigation, 2005. **115**(2): p. 209-218.
47. Liu, X., et al., *Reversibility of liver fibrosis and inactivation of fibrogenic myofibroblasts.* Current pathobiology reports, 2013. **1**(3): p. 209-214.
48. Troeger, J.S., et al., *Deactivation of hepatic stellate cells during liver fibrosis resolution in mice.* Gastroenterology, 2012. **143**(4): p. 1073-1083. e22.
49. Kisseleva, T., et al., *Myofibroblasts revert to an inactive phenotype during regression of liver fibrosis.* Proceedings of the National Academy of Sciences, 2012. **109**(24): p. 9448-9453.
50. Kim, H.Y., et al., *The origin and fate of liver myofibroblasts.* Cellular and Molecular Gastroenterology and Hepatology, 2024. **17**(1): p. 93-106.
51. Ghiassi-Nejad, Z. and S.L. Friedman, *Advances in antifibrotic therapy.* Expert review of gastroenterology & hepatology, 2008. **2**(6): p. 803-816.
52. Tsuchida, T. and S.L. Friedman, *Mechanisms of hepatic stellate cell activation.* Nature reviews Gastroenterology & hepatology, 2017. **14**(7): p. 397-411.
53. Melton, A.C. and H.F. Yee, *Hepatic stellate cell protrusions couple platelet-derived growth factor-BB to chemotaxis.* Hepatology, 2007. **45**(6): p. 1446-1453.
54. Gao, R. and D.R. Brigstock, *Connective tissue growth factor (CCN2) induces adhesion of rat activated hepatic stellate cells by binding of its C-terminal domain to integrin αvβ3 and heparan sulfate proteoglycan.* Journal of Biological Chemistry, 2004. **279**(10): p. 8848-8855.
55. Reynaert, H., et al., *Hepatic stellate cells: role in microcirculation and pathophysiology of portal hypertension.* Gut, 2002. **50**(4): p. 571-581.
56. Herbst, H., et al., *Tissue inhibitor of metalloproteinase-1 and-2 RNA expression in rat and human liver fibrosis.* The American journal of pathology, 1997. **150**(5): p. 1647.
57. El Sharkawy, R., *MERTK receptor tyrosine kinase: A novel therapeutic target for liver fibrosis*. 2020, University of Sydney.
58. Schulze, R.J., et al., *The cell biology of the hepatocyte: A membrane trafficking machine.* Journal of Cell Biology, 2019. **218**(7): p. 2096-2112.
59. Zeisberg, M., et al., *Fibroblasts derive from hepatocytes in liver fibrosis via epithelial to mesenchymal transition.* Journal of Biological Chemistry, 2007. **282**(32): p. 23337-23347.
60. Yang, J., et al., *Guidelines and definitions for research on epithelial–mesenchymal transition.* Nature reviews Molecular cell biology, 2020. **21**(6): p. 341-352.
61. Jiang, J.X., et al., *Apoptotic body engulfment by hepatic stellate cells promotes their survival by the JAK/STAT and Akt/NF-κB-dependent pathways.* Journal of hepatology, 2009. **51**(1): p. 139-148.
62. Acharya, P., et al., *Cellular mechanisms of liver fibrosis.* Frontiers in Pharmacology, 2021. **12**: p. 671640.
63. Xie, W., et al., *Base-resolution analyses of sequence and parent-of-origin dependent DNA methylation in the mouse genome.* Cell, 2012. **148**(4): p. 816-831.
64. DeLeve, L.D., *Liver sinusoidal endothelial cells in hepatic fibrosis.* Hepatology, 2015. **61**(5): p. 1740-1746.
65. Seki, E. and R.F. Schwabe, *Hepatic inflammation and fibrosis: functional links and key pathways.* Hepatology, 2015. **61**(3): p. 1066-1079.

66. Dooley, S. and P. Ten Dijke, *TGF-β in progression of liver disease.* Cell and tissue research, 2012. **347**(1): p. 245-256.
67. Liu, X., et al., *Identification of lineage-specific transcription factors that prevent activation of hepatic stellate cells and promote fibrosis resolution.* Gastroenterology, 2020. **158**(6): p. 1728-1744. e14.
68. Moon, H., et al. *High Risk of Hepatocellular Carcinoma Development in Fibrotic Liver: Role of the Hippo-YAP/TAZ Signaling Pathway*. International Journal of Molecular Sciences, 2019. **20**, DOI: 10.3390/ijms20030581.
69. Moon, H., et al., *High risk of hepatocellular carcinoma development in fibrotic liver: role of the hippo-YAP/TAZ signaling pathway.* International journal of molecular sciences, 2019. **20**(3): p. 581.
70. Biernacka, A., M. Dobaczewski, and N.G. Frangogiannis, *TGF-β signaling in fibrosis.* Growth factors, 2011. **29**(5): p. 196-202.
71. Schiller, M., D. Javelaud, and A. Mauviel, *TGF-β-induced SMAD signaling and gene regulation: consequences for extracellular matrix remodeling and wound healing.* Journal of dermatological science, 2004. **35**(2): p. 83-92.
72. Derynck, R. and E.H. Budi, *Specificity, versatility, and control of TGF-β family signaling.* Science signaling, 2019. **12**(570).
73. Schuster, N. and K. Krieglstein, *Mechanisms of TGF-β-mediated apoptosis.* Cell and tissue research, 2002. **307**(1): p. 1-14.
74. Kolios, G., V. Valatas, and E. Kouroumalis, *Role of Kupffer cells in the pathogenesis of liver disease.* World J Gastroenterol, 2006. **12**(46): p. 7413-20.
75. Guo, X. and S.-Y. Chen, *Transforming growth factor-β and smooth muscle differentiation.* World journal of biological chemistry, 2012. **3**(3): p. 41.
76. Li, H., et al., *Hepatic macrophages in liver fibrosis: pathogenesis and potential therapeutic targets.* BMJ open gastroenterology, 2016. **3**(1): p. e000079.
77. Breitkopf, K., et al., *TGF-β/Smad signaling in the injured liver.* Zeitschrift für Gastroenterologie, 2006. **44**(01): p. 57-66.
78. Teixeira, A.F., P. Ten Dijke, and H.-J. Zhu, *On-target anti-TGF-β therapies are not succeeding in clinical cancer treatments: what are remaining challenges?* Frontiers in cell and developmental biology, 2020. **8**: p. 605.
79. Zhu, H., et al., *A novel TGFβ trap blocks chemotherapeutics-induced TGFβ1 signaling and enhances their anticancer activity in gynecologic cancers.* Clinical Cancer Research, 2018. **24**(12): p. 2780-2793.
80. Bhola, N.E., et al., *TGF-β inhibition enhances chemotherapy action against triple-negative breast cancer.* The Journal of clinical investigation, 2013. **123**(3): p. 1348-1358.
81. Earl, L.A., S. Bi, and L.G. Baum, *Galectin multimerization and lattice formation are regulated by linker region structure.* Glycobiology, 2011. **21**(1): p. 6-12.
82. Wang, Y., et al., *Notch signaling mediated by TGF-β/Smad pathway in concanavalin A-induced liver fibrosis in rats.* World journal of gastroenterology, 2017. **23**(13): p. 2330.
83. Dewidar, B., C. Meyer, and S. Dooley, *TGF-β in hepatic stellate cell activation and liver fibrogenesis—updated 2019.* Cells, 2019. **8**(11): p. 1419.
84. Dewidar, B., et al., *TGF-β in Hepatic Stellate Cell Activation and Liver Fibrogenesis-Updated 2019.* Cells, 2019. **8**(11).
85. Galluzzi, L., et al., *Metabolic Control of Autophagy.* Cell, 2014. **159**(6): p. 1263-1276.
86. Yang, J., H. Ueharu, and Y. Mishina, *Energy metabolism: A newly emerging target of BMP signaling in bone homeostasis.* Bone, 2020. **138**: p. 115467.
87. Yakupova, E.I., D.B. Zorov, and E.Y. Plotnikov, *Bioenergetics of the Fibrosis.* Biochemistry (Moscow), 2021. **86**: p. 1599-1606.
88. Dewidar, B., et al., *Alterations of hepatic energy metabolism in murine models of obesity, diabetes and fatty liver diseases.* EBioMedicine, 2023. **94**.
89. Mesmin, B., *Mitochondrial lipid transport and biosynthesis: a complex balance.* Journal of Cell Biology, 2016. **214**(1): p. 9-11.

90. Friedman, S.L., et al., *Therapy for fibrotic diseases: nearing the starting line.* Science translational medicine, 2013. **5**(167): p. 167sr1-167sr1.
91. Bernard, K., et al., *Metabolic reprogramming is required for myofibroblast contractility and differentiation.* Journal of Biological Chemistry, 2015. **290**(42): p. 25427-25438.
92. Gajendiran, P., et al., *Elevated mitochondrial activity distinguishes fibrogenic hepatic stellate cells and sensitizes for selective inhibition by mitotropic doxorubicin.* Journal of Cellular and Molecular Medicine, 2018. **22**(4): p. 2210-2219.
93. Nishikawa, T., et al., *A switch in the source of ATP production and a loss in capacity to perform glycolysis are hallmarks of hepatocyte failure in advance liver disease.* Journal of Hepatology, 2014. **60**(6): p. 1203-1211.
94. Sunny, N.E., et al., *Excessive hepatic mitochondrial TCA cycle and gluconeogenesis in humans with nonalcoholic fatty liver disease.* Cell metabolism, 2011. **14**(6): p. 804-810.
95. Karthikeyan, S., et al., *Deregulation of energy metabolism promotes antifibrotic effects in human hepatic stellate cells and prevents liver fibrosis in a mouse model.* Biochemical and Biophysical Research Communications, 2016. **469**(3): p. 463-469.
96. Hailey, D.W., et al., *Mitochondria supply membranes for autophagosome biogenesis during starvation.* Cell, 2010. **141**(4): p. 656-667.
97. Graef, M. and J. Nunnari, *Mitochondria regulate autophagy by conserved signalling pathways.* The EMBO journal, 2011. **30**(11): p. 2101-2114.
98. Zhang, Z., et al., *Autophagy regulates turnover of lipid droplets via ROS-dependent Rab25 activation in hepatic stellate cell.* Redox biology, 2017. **11**: p. 322-334.
99. Field, C.S., et al., *Mitochondrial Integrity Regulated by Lipid Metabolism Is a Cell-Intrinsic Checkpoint for Treg Suppressive Function.* Cell Metabolism, 2020. **31**(2): p. 422-437.e5.
100. Roca-Agujetas, V., et al., *Recent Insights into the Mitochondrial Role in Autophagy and Its Regulation by Oxidative Stress.* Oxidative Medicine and Cellular Longevity, 2019. **2019**: p. 3809308.
101. Hernández–Gea, V., et al., *Autophagy releases lipid that promotes fibrogenesis by activated hepatic stellate cells in mice and in human tissues.* Gastroenterology, 2012. **142**(4): p. 938-946.
102. Heaton, N.S., et al., *Dengue virus nonstructural protein 3 redistributes fatty acid synthase to sites of viral replication and increases cellular fatty acid synthesis.* Proceedings of the National Academy of Sciences, 2010. **107**(40): p. 17345-17350.
103. Singh, R., et al., *Autophagy regulates lipid metabolism.* Nature, 2009. **458**(7242): p. 1131-1135.
104. Higashi, T., S.L. Friedman, and Y. Hoshida, *Hepatic stellate cells as key target in liver fibrosis.* Advanced drug delivery reviews, 2017. **121**: p. 27-42.
105. Zhang, J., et al., *TGF-β1-induced autophagy activates hepatic stellate cells via the ERK and JNK signaling pathways.* Int J Mol Med, 2021. **47**(1): p. 256-266.
106. Blaner, W.S., et al., *Hepatic stellate cell lipid droplets: A specialized lipid droplet for retinoid storage.* Biochimica et Biophysica Acta (BBA) - Molecular and Cell Biology of Lipids, 2009. **1791**(6): p. 467-473.
107. Casalena, G., I. Daehn, and E. Bottinger, *Transforming growth factor-β, bioenergetics, and mitochondria in renal disease.* Semin Nephrol, 2012. **32**(3): p. 295-303.
108. Liu, H. and Y.-G. Chen, *The interplay between TGF-β signaling and cell metabolism.* Frontiers in Cell and Developmental Biology, 2022. **10**: p. 846723.
109. Boengler, K., et al., *Mitochondria and ageing: role in heart, skeletal muscle and adipose tissue.* Journal of Cachexia, Sarcopenia and Muscle, 2017. **8**(3): p. 349-369.
110. Topf, U., L. Wrobel, and A. Chacinska, *Chatty Mitochondria: Keeping Balance in Cellular Protein Homeostasis.* Trends in Cell Biology, 2016. **26**(8): p. 577-586.
111. He, T., et al., *Resveratrol inhibits renal interstitial fibrosis in diabetic nephropathy by regulating AMPK/NOX4/ROS pathway.* Journal of Molecular Medicine, 2016. **94**(12): p. 1359-1371.

112. Cao, Q., D.C. Harris, and Y. Wang, *Macrophages in kidney injury, inflammation, and fibrosis.* Physiology, 2015. **30**(3): p. 183-194.
113. Prasun, P., I. Ginevic, and K. Oishi, *Mitochondrial dysfunction in nonalcoholic fatty liver disease and alcohol related liver disease.* Translational gastroenterology and hepatology, 2021. **6**.
114. Zhao, R.Z., et al., *Mitochondrial electron transport chain, ROS generation and uncoupling.* International journal of molecular medicine, 2019. **44**(1): p. 3-15.
115. Zerihun, M., S. Sukumaran, and N. Qvit, *The Drp1-mediated mitochondrial fission protein interactome as an emerging core player in mitochondrial dynamics and cardiovascular disease therapy.* International Journal of Molecular Sciences, 2023. **24**(6): p. 5785.
116. Geng, N., et al., *Nuclear receptor Nur77 protects against oxidative stress by maintaining mitochondrial homeostasis via regulating mitochondrial fission and mitophagy in smooth muscle cell.* Journal of Molecular and Cellular Cardiology, 2022. **170**: p. 22-33.
117. Jia, L., et al., *Mitochondrial quality control in liver fibrosis: Epigenetic hallmarks and therapeutic strategies.* Cellular Signalling, 2024. **115**: p. 111035.
118. Zhou, Y., et al., *Oxidative stress-mediated mitochondrial fission promotes hepatic stellate cell activation via stimulating oxidative phosphorylation.* Cell Death & Disease, 2022. **13**(8): p. 689.
119. Liang, H. and W.F. Ward, *PGC-1alpha: a key regulator of energy metabolism.* Adv Physiol Educ, 2006. **30**(4): p. 145-51.
120. Li, X., et al., *Mitochondrial dysfunction in fibrotic diseases.* Cell death discovery, 2020. **6**(1): p. 80.
121. Legaki, A.-I., et al., *Hepatocyte mitochondrial dynamics and bioenergetics in obesity-related non-alcoholic fatty liver disease.* Current obesity reports, 2022. **11**(3): p. 126-143.
122. Liu, R.-M. and L.P. Desai, *Reciprocal regulation of TGF-β and reactive oxygen species: A perverse cycle for fibrosis.* Redox biology, 2015. **6**: p. 565-577.
123. Picard, M., et al., *Mitochondrial function in permeabilized cardiomyocytes is largely preserved in the senescent rat myocardium.* 2012.
124. Pickrell, A.M. and R.J. Youle, *The roles of PINK1, parkin, and mitochondrial fidelity in Parkinson's disease.* Neuron, 2015. **85**(2): p. 257-273.
125. Guimarães, E.L., et al., *Mitochondrial uncouplers inhibit hepatic stellate cell activation.* BMC Gastroenterology, 2012. **12**(1): p. 68.
126. Li, Y., et al., *BNIP3L/NIX-mediated mitophagy: molecular mechanisms and implications for human disease.* Cell Death & Disease, 2021. **13**(1): p. 14.
127. Kaur, J. and J. Debnath, *Autophagy at the crossroads of catabolism and anabolism.* Nature Reviews Molecular Cell Biology, 2015. **16**(8): p. 461-472.
128. Lamming, D.W. and L. Bar-Peled, *Lysosome: The metabolic signaling hub.* Traffic, 2019. **20**(1): p. 27-38.
129. Czaja, M.J., *Function of Autophagy in Nonalcoholic Fatty Liver Disease.* Digestive Diseases and Sciences, 2016. **61**(5): p. 1304-1313.
130. An, L., et al., *Metabolic role of autophagy in the pathogenesis and development of NAFLD.* Metabolites, 2023. **13**(1): p. 101.
131. Friedman, S.L., *Hepatic stellate cells: protean, multifunctional, and enigmatic cells of the liver.* Physiological reviews, 2008. **88**(1): p. 125-172.
132. Friedman, S.L., S. Wei, and W.S. Blaner, *Retinol release by activated rat hepatic lipocytes: regulation by Kupffer cell-conditioned medium and PDGF.* American Journal of Physiology-Gastrointestinal and Liver Physiology, 1993. **264**(5): p. G947-G952.
133. Meijer, A.J. and P. Codogno, *Regulation and role of autophagy in mammalian cells.* The international journal of biochemistry & cell biology, 2004. **36**(12): p. 2445-2462.
134. Xu, F., et al., *Modulation of Autophagy: A Novel "Rejuvenation" Strategy for the Aging Liver.* Oxidative Medicine and Cellular Longevity, 2021. **2021**.

135. Bjørkøy, G., et al., *p62/SQSTM1 forms protein aggregates degraded by autophagy and has a protective effect on huntingtin-induced cell death.* The Journal of cell biology, 2005. **171**(4): p. 603-614.
136. Pugsley, H.R., *Assessing Autophagic Flux by Measuring LC3, p62, and LAMP1 Co-localization Using Multispectral Imaging Flow Cytometry.* J Vis Exp, 2017(125).
137. Umemura, A., et al., *p62, Upregulated during Preneoplasia, Induces Hepatocellular Carcinogenesis by Maintaining Survival of Stressed HCC-Initiating Cells.* Cancer Cell, 2016. **29**(6): p. 935-948.
138. Deng, J., et al., *Hypoxia-inducible factor-1alpha regulates autophagy to activate hepatic stellate cells.* Biochemical and Biophysical Research Communications, 2014. **454**(2): p. 328-334.
139. Fu, M.Y., et al., *Transforming growth factor-β1 reduces apoptosis via autophagy activation in hepatic stellate cells.* Mol Med Rep, 2014. **10**(3): p. 1282-8.
140. Sun, M., L. Tan, and M. Hu, *The role of autophagy in hepatic fibrosis.* Am J Transl Res, 2021. **13**(6): p. 5747-5757.
141. Thoen, L.F.R., et al., *A role for autophagy during hepatic stellate cell activation.* Journal of Hepatology, 2011. **55**(6): p. 1353-1360.
142. He, W., et al., *Chloroquine improved carbon tetrachloride-induced liver fibrosis through its inhibition of the activation of hepatic stellate cells: role of autophagy.* Biol Pharm Bull, 2014. **37**(9): p. 1505-9.
143. Kwanten, W.J., et al., *Role of autophagy in the pathophysiology of nonalcoholic fatty liver disease: a controversial issue.* World J Gastroenterol, 2014. **20**(23): p. 7325-38.
144. Song, Y., et al., *Autophagy in hepatic fibrosis.* Biomed Res Int, 2014. **2014**: p. 436242.
145. Miyamae, Y., et al., *Tetrandrine induces lipid accumulation through blockade of autophagy in a hepatic stellate cell line.* Biochem Biophys Res Commun, 2016. **477**(1): p. 40-46.
146. Polderman, T.J., et al., *Meta-analysis of the heritability of human traits based on fifty years of twin studies.* Nat Genet, 2015. **47**(7): p. 702-9.
147. Fraga, M.F., et al., *Epigenetic differences arise during the lifetime of monozygotic twins.* Proc Natl Acad Sci U S A, 2005. **102**(30): p. 10604-9.
148. Eslam, M., L. Valenti, and S. Romeo, *Genetics and epigenetics of NAFLD and NASH: Clinical impact.* J Hepatol, 2018. **68**(2): p. 268-279.
149. Bayoumi, A., et al., *The Epigenetic Drug Discovery Landscape for Metabolic-associated Fatty Liver Disease.* Trends Genet, 2020. **36**(6): p. 429-441.
150. Mann, D.A., *Epigenetics in liver disease.* Hepatology, 2014. **60**(4): p. 1418-1425.
151. El Taghdouini, A. and L.A. van Grunsven, *Epigenetic regulation of hepatic stellate cell activation and liver fibrosis.* Expert review of gastroenterology & hepatology, 2016. **10**(12): p. 1397-1408.
152. Bayoumi, A., et al., *The epigenetic drug discovery landscape for metabolic-associated fatty liver disease.* Trends in Genetics, 2020. **36**(6): p. 429-441.
153. Crispo, F., et al., *Metabolic Dysregulations and Epigenetics: A Bidirectional Interplay that Drives Tumor Progression.* Cells, 2019. **8**(8).
154. Montellier, E. and J. Gaucher, *Targeting the interplay between metabolism and epigenetics in cancer.* Curr Opin Oncol, 2019. **31**(2): p. 92-99.
155. Leung, J.Y., et al., *Interweaving Tumor Heterogeneity into the Cancer Epigenetic/Metabolic Axis.* Antioxid Redox Signal, 2020. **33**(13): p. 946-965.
156. Yang, Z., et al., *Control of Hematopoietic Stem and Progenitor Cell Function through Epigenetic Regulation of Energy Metabolism and Genome Integrity.* Stem Cell Reports, 2019. **13**(1): p. 61-75.
157. Liu, M., et al., *RARRES1 identified by comprehensive bioinformatic analysis and experimental validation as a promising biomarker in Skin Cutaneous Melanoma.* Scientific Reports, 2024. **14**(1): p. 14113.
158. *Genecard.*

159. Wu, C.-C., et al., *RARRES1 expression is significantly related to tumour differentiation and staging in colorectal adenocarcinoma.* European Journal of Cancer, 2006. **42**(4): p. 557-565.
160. Chen, G., S. Weiskirchen, and R. Weiskirchen, *Vitamin A: too good to be bad?* Frontiers in Pharmacology, 2023. **14**: p. 1186336.
161. Zhang, R., et al., *Transcriptional factors mediating retinoic acid signals in the control of energy metabolism.* International journal of molecular sciences, 2015. **16**(6): p. 14210-14244.
162. Semba, R.D., *On the 'discovery'of vitamin A.* Annals of nutrition and metabolism, 2012. **61**(3): p. 192-198.
163. Lamb, T.D. and E.N. Pugh, *Phototransduction, dark adaptation, and rhodopsin regeneration the proctor lecture.* Investigative ophthalmology & visual science, 2006. **47**(12): p. 5138-5152.
164. Benbrook, D.M., et al., *History of retinoic acid receptors.* The Biochemistry of Retinoic Acid Receptors I: Structure, Activation, and Function at the Molecular Level, 2014: p. 1-20.
165. Bayoumi, A., *Mistranslation drives alterations in protein levels and the effects of a synonymous variant at the FGF21 locus.* 2020.
166. Pan, Z., et al., *Exportin 4 DNA promoter methylation in liver fibrosis.* Plos one, 2024. **19**(5): p. e0302786.
167. El Sharkawy, R., *MERTK receptor tyrosine kinase: A novel therapeutic target for liver fibrosis.* 2020.
168. Pan, Z., *MerTK inhibition for the treatment of organ fibrosis*. 2023.
169. Alharthi, J., et al., *A metabolic associated fatty liver disease risk variant in MBOAT7 regulates toll like receptor induced outcomes.* Nature Communications, 2022. **13**(1): p. 7430.
170. Iredale, J.P., *Models of liver fibrosis: exploring the dynamic nature of inflammation and repair in a solid organ.* J Clin Invest, 2007. **117**(3): p. 539-48.
171. Roehlen, N., E. Crouchet, and T.F. Baumert, *Liver Fibrosis: Mechanistic Concepts and Therapeutic Perspectives.* Cells, 2020. **9**(4).
172. Tan, Z., et al., *Liver Fibrosis: Therapeutic Targets and Advances in Drug Therapy.* Front Cell Dev Biol, 2021. **9**: p. 730176.
173. Shan, L., et al., *New Drugs for Hepatic Fibrosis.* Front Pharmacol, 2022. **13**: p. 874408.
174. Bataller, R. and D.A. Brenner, *Liver fibrosis.* J Clin Invest, 2005. **115**(2): p. 209-18.
175. Iredale, J.P., et al., *Mechanisms of spontaneous resolution of rat liver fibrosis. Hepatic stellate cell apoptosis and reduced hepatic expression of metalloproteinase inhibitors.* J Clin Invest, 1998. **102**(3): p. 538-49.
176. Issa, R., et al., *Apoptosis of hepatic stellate cells: involvement in resolution of biliary fibrosis and regulation by soluble growth factors.* Gut, 2001. **48**(4): p. 548-57.
177. Liu, R., et al., *Epigenetic modification in liver fibrosis: Promising therapeutic direction with significant challenges ahead.* Acta Pharmaceutica Sinica B, 2023.
178. Zeybel, M., et al., *A proof-of-concept for epigenetic therapy of tissue fibrosis: inhibition of liver fibrosis progression by 3-deazaneplanocin A.* Molecular Therapy, 2017. **25**(1): p. 218-231.
179. Bian, E.-B., et al., *DNA methylation: New therapeutic implications for hepatic fibrosis.* Cellular Signalling, 2013. **25**(1): p. 355-358.
180. Campagna, M.P., et al., *Epigenome-wide association studies: current knowledge, strategies and recommendations.* Clinical epigenetics, 2021. **13**: p. 1-24.
181. Birney, E., G.D. Smith, and J.M. Greally, *Epigenome-wide association studies and the interpretation of disease-omics.* PLoS genetics, 2016. **12**(6): p. e1006105.
182. Peng, Z., et al., *Epigenetic repression of RARRES1 is mediated by methylation of a proximal promoter and a loss of CTCF binding.* PLoS One, 2012. **7**(5): p. e36891.
183. M Amann, P., et al., *Regulation of gene expression by retinoids.* Current medicinal chemistry, 2011. **18**(9): p. 1405-1412.

184. Fabregat, I. and D. Caballero-Díaz, *Transforming growth factor-β-induced cell plasticity in liver fibrosis and hepatocarcinogenesis.* Frontiers in oncology, 2018. **8**: p. 357.
185. Brenner, D.A., *Molecular pathogenesis of liver fibrosis.* Transactions of the American clinical and Climatological Association, 2009. **120**: p. 361.
186. Nakano, Y., et al., *A deactivation factor of fibrogenic hepatic stellate cells induces regression of liver fibrosis in mice.* Hepatology, 2020. **71**(4): p. 1437-1452.
187. Schuppan, D. and Y.O. Kim, *Evolving therapies for liver fibrosis.* The Journal of clinical investigation, 2013. **123**(5): p. 1887-1901.
188. Hu, H.-H., et al., *New insights into TGF-β/Smad signaling in tissue fibrosis.* Chemico-biological interactions, 2018. **292**: p. 76-83.
189. Topf, U., L. Wrobel, and A. Chacinska, *Chatty Mitochondria: Keeping Balance in Cellular Protein Homeostasis.* Trends Cell Biol, 2016. **26**(8): p. 577-586.
190. Jia, L., et al., *Mitochondrial quality control in liver fibrosis: Epigenetic hallmarks and therapeutic strategies.* Cellular Signalling, 2024: p. 111035.
191. Gajendiran, P., et al., *Elevated mitochondrial activity distinguishes fibrogenic hepatic stellate cells and sensitizes for selective inhibition by mitotropic doxorubicin.* Journal of Cellular and Molecular Medicine, 2018. **22**(4): p. 2210-2219.
192. Moon, J.S., et al., *NOX4-dependent fatty acid oxidation promotes NLRP3 inflammasome activation in macrophages.* Nat Med, 2016. **22**(9): p. 1002-12.
193. Krähenbühl, S., *Alterations in mitochondrial function and morphology in chronic liver disease: pathogenesis and potential for therapeutic intervention.* Pharmacology & therapeutics, 1993. **60**(1): p. 1-38.
194. Murphy, M.P., *How mitochondria produce reactive oxygen species.* Biochemical journal, 2009. **417**(1): p. 1-13.
195. Vajrala, V., et al., *Effects of oscillatory electric fields on internal membranes: an analytical model.* Biophys J, 2008. **94**(6): p. 2043-52.
196. Mårtensson, C.U., et al., *Mitochondrial protein translocation-associated degradation.* Nature, 2019. **569**(7758): p. 679-683.
197. Weidberg, H. and A. Amon, *MitoCPR—A surveillance pathway that protects mitochondria in response to protein import stress.* Science, 2018. **360**(6385): p. eaan4146.
198. Lenkiewicz, A.M., M. Krakowczyk, and P. Bragoszewski, *Cytosolic quality control of mitochondrial protein precursors—the early stages of the organelle biogenesis.* International Journal of Molecular Sciences, 2021. **23**(1): p. 7.
199. Kirkinezos, I.G., et al., *Cytochrome c association with the inner mitochondrial membrane is impaired in the CNS of G93A-SOD1 mice.* J Neurosci, 2005. **25**(1): p. 164-72.
200. Al Ojaimi, M., A. Salah, and A.W. El-Hattab, *Mitochondrial fission and fusion: molecular mechanisms, biological functions, and related disorders.* Membranes, 2022. **12**(9): p. 893.
201. Lee, Y.-X., et al., *Mitochondria Research in Human Reproduction*, in *The ovary*. 2019, Elsevier. p. 327-335.
202. Manoury, B., et al., *The absence of reactive oxygen species production protects mice against bleomycin-induced pulmonary fibrosis.* Respiratory research, 2005. **6**: p. 1-12.
203. Giannelli, G., et al., *TGF-beta inhibitor.*
204. Negmadjanov, U., et al., *TGF-β1-mediated differentiation of fibroblasts is associated with increased mitochondrial content and cellular respiration.* PloS one, 2015. **10**(4): p. e0123046.
205. Weinberg, S.E., L.A. Sena, and N.S. Chandel, *Mitochondria in the regulation of innate and adaptive immunity.* Immunity, 2015. **42**(3): p. 406-417.
206. Beutner, G., et al., *The Mitochondrial Permeability Transition Pore and ATP Synthase.* Handb Exp Pharmacol, 2017. **240**: p. 21-46.

207. Ghezzi, D. and M. Zeviani, *Assembly factors of human mitochondrial respiratory chain complexes: physiology and pathophysiology.* Mitochondrial Oxidative Phosphorylation: Nuclear-Encoded Genes, Enzyme Regulation, and Pathophysiology, 2012: p. 65-106.
208. Shiota, T., et al., *Molecular architecture of the active mitochondrial protein gate.* Science, 2015. **349**(6255): p. 1544-1548.
209. Jackson, T.D., C.S. Palmer, and D. Stojanovski, *Mitochondrial diseases caused by dysfunctional mitochondrial protein import.* Biochemical society transactions, 2018. **46**(5): p. 1225-1238.
210. Zorova, L.D., et al., *Mitochondrial membrane potential.* Anal Biochem, 2018. **552**: p. 50-59.
211. Omar, R., et al., *Hepatic stellate cells in liver fibrosis and siRNA-based therapy.* Reviews of Physiology, Biochemistry and Pharmacology, Vol. 172, 2016: p. 1-37.
212. Xu, J., et al., *The types of hepatic myofibroblasts contributing to liver fibrosis of different etiologies.* Frontiers in pharmacology, 2014. **5**: p. 167.
213. Iwaisako, K., D.A. Brenner, and T. Kisseleva, *What's new in liver fibrosis? The origin of myofibroblasts in liver fibrosis.* Journal of gastroenterology and hepatology, 2012. **27**: p. 65-68.
214. Bobowski-Gerard, M., et al., *Retinoids issued from hepatic stellate cell lipid droplet loss as potential signaling molecules orchestrating a multicellular liver injury response.* Cells, 2018. **7**(9): p. 137.
215. Gajendiran, P., et al., *Elevated mitochondrial activity distinguishes fibrogenic hepatic stellate cells and sensitizes for selective inhibition by mitotropic doxorubicin.* J Cell Mol Med, 2018. **22**(4): p. 2210-2219.
216. Tirichen, H., et al., *Mitochondrial reactive oxygen species and their contribution in chronic kidney disease progression through oxidative stress.* Frontiers in physiology, 2021. **12**: p. 398.
217. Zhang, W., et al., *Mitochondria-specific drug release and reactive oxygen species burst induced by polyprodrug nanoreactors can enhance chemotherapy.* Nature communications, 2019. **10**(1): p. 1704.
218. Mortezaee, K., *Nicotinamide adenine dinucleotide phosphate (NADPH) oxidase (NOX) and liver fibrosis: A review.* Cell Biochemistry and function, 2018. **36**(6): p. 292-302.
219. Laurindo, F.R., T.L. Araujo, and T.B. Abrahao, *Nox NADPH oxidases and the endoplasmic reticulum.* Antioxidants & redox signaling, 2014. **20**(17): p. 2755-2775.
220. Szanto, I., *NADPH Oxidase 4 (NOX4) in cancer: linking redox signals to oncogenic metabolic adaptation.* International Journal of Molecular Sciences, 2022. **23**(5): p. 2702.
221. Sies, H., *Oxidative stress: oxidants and antioxidants.* Experimental Physiology: Translation and Integration, 1997. **82**(2): p. 291-295.
222. Allameh, A., et al., *Oxidative stress in liver pathophysiology and disease.* Antioxidants, 2023. **12**(9): p. 1653.
223. Liu, M., et al., *Harnessing reactive oxygen/nitrogen species and inflammation: Nanodrugs for liver injury.* Materials Today Bio, 2022. **13**: p. 100215.
224. Boudreau, H.E., et al., *Nox4 involvement in TGF-beta and SMAD3-driven induction of the epithelial-to-mesenchymal transition and migration of breast epithelial cells.* Free Radical Biology and Medicine, 2012. **53**(7): p. 1489-1499.
225. Sánchez-Valle, V., et al., *Role of oxidative stress and molecular changes in liver fibrosis: a review.* Current medicinal chemistry, 2012. **19**(28): p. 4850-4860.
226. Liu, R.M. and L.P. Desai, *Reciprocal regulation of TGF-β and reactive oxygen species: A perverse cycle for fibrosis.* Redox Biol, 2015. **6**: p. 565-577.
227. Onal, G., et al., *Lipid droplets in health and disease.* Lipids in health and disease, 2017. **16**(1): p. 1-15.
228. Li, A., et al., *Mitochondrial autophagy: molecular mechanisms and implications for cardiovascular disease.* Cell death & disease, 2022. **13**(5): p. 444.

229. Yang, J., R. Zhou, and Z. Ma, *Autophagy and energy metabolism.* Autophagy: Biology and Diseases: Basic Science, 2019: p. 329-357.
230. Mao, Y.-Q. and X.-M. Fan, *Autophagy: A new therapeutic target for liver fibrosis.* World journal of hepatology, 2015. **7**(16): p. 1982.
231. Lucantoni, F., et al., *Implication of autophagy in the antifibrogenic effect of Rilpivirine: when more is less.* Cell Death & Disease, 2022. **13**(4): p. 385.
232. Levine, B. and G. Kroemer, *Autophagy in the pathogenesis of disease.* Cell, 2008. **132**(1): p. 27-42.
233. Mochida, K., et al., *Receptor-mediated selective autophagy degrades the endoplasmic reticulum and the nucleus.* Nature, 2015. **522**(7556): p. 359-362.
234. Panieri, E. and M.M. Santoro, *ROS homeostasis and metabolism: a dangerous liason in cancer cells.* Cell Death Dis, 2016. **7**(6): p. e2253.
235. Lucantoni, F., et al., *Understanding the implication of autophagy in the activation of hepatic stellate cells in liver fibrosis: are we there yet?* The Journal of Pathology, 2021. **254**(3): p. 216-228.
236. García-Miranda, A., et al., *Regulation of mitochondrial metabolism by autophagy supports leptin-induced cell migration.* Scientific Reports, 2024. **14**(1): p. 1408.
237. Chang, K.-C., et al., *The interplay of autophagy and oxidative stress in the pathogenesis and therapy of retinal degenerative diseases.* Cell & bioscience, 2022. **12**: p. 1-20.
238. Gual, P., H. Gilgenkrantz, and S. Lotersztajn, *Autophagy in chronic liver diseases: the two faces of Janus.* Am J Physiol Cell Physiol, 2017. **312**(3): p. C263-C273.
239. Rambold, A.S. and J. Lippincott-Schwartz, *Mechanisms of mitochondria and autophagy crosstalk.* Cell cycle, 2011. **10**(23): p. 4032-4038.
240. Murugan, S. and R.K. Amaravadi, *Methods for studying autophagy within the tumor microenvironment.* Tumor Microenvironment: Study Protocols, 2016: p. 145-166.
241. Meng, D., et al., *Carvedilol attenuates liver fibrosis by suppressing autophagy and promoting apoptosis in hepatic stellate cells.* Biomedicine & Pharmacotherapy, 2018. **108**: p. 1617-1627.
242. Ding, Y. and M.E. Choi. *Regulation of autophagy by TGF-β: emerging role in kidney fibrosis*. in *Seminars in nephrology*. 2014. Elsevier.
243. Kumar, A.V., J. Mills, and L.R. Lapierre, *Selective autophagy receptor p62/SQSTM1, a pivotal player in stress and aging.* Frontiers in cell and developmental biology, 2022. **10**: p. 793328.
244. Pugsley, H.R., *Assessing autophagic flux by measuring LC3, p62, and LAMP1 co-localization using multispectral imaging flow cytometry.* JoVE (Journal of Visualized Experiments), 2017(125): p. e55637.
245. Mak, K.M., C. Wu, and C.P. Cheng, *Lipid droplets, the Holy Grail of hepatic stellate cells: In health and hepatic fibrosis.* The Anatomical Record, 2023. **306**(5): p. 983-1010.
246. Mauthe, M., et al., *Chloroquine inhibits autophagic flux by decreasing autophagosome-lysosome fusion.* Autophagy, 2018. **14**(8): p. 1435-1455.
247. Petherick, K.J., et al., *Pharmacological inhibition of ULK1 kinase blocks mammalian target of rapamycin (mTOR)-dependent autophagy.* Journal of Biological Chemistry, 2015. **290**(18): p. 11376-11383.
248. Mauvezin, C. and T.P. Neufeld, *Bafilomycin A1 disrupts autophagic flux by inhibiting both V-ATPase-dependent acidification and Ca-P60A/SERCA-dependent autophagosome-lysosome fusion.* Autophagy, 2015. **11**(8): p. 1437-1438.
249. Sun, M., L. Tan, and M. Hu, *The role of autophagy in hepatic fibrosis.* American journal of translational research, 2021. **13**(6): p. 5747.
250. Jain, M., et al., *Mitochondrial reactive oxygen species regulate transforming growth factor-β signaling.* Journal of Biological Chemistry, 2013. **288**(2): p. 770-777.
251. Yu, L., et al., *Autophagic programmed cell death by selective catalase degradation.* Proceedings of the national academy of sciences, 2006. **103**(13): p. 4952-4957.

252. Hasan, A., et al., *Crosstalk between ROS and autophagy in tumorigenesis: understanding the multifaceted paradox.* Frontiers in Oncology, 2022. **12**: p. 852424.
253. Hernández-Gea, V., et al., *Autophagy releases lipid that promotes fibrogenesis by activated hepatic stellate cells in mice and in human tissues.* Gastroenterology, 2012. **142**(4): p. 938-46.
254. Jiang, B., et al., *Combination of chloroquine diphosphate and salidroside induces human liver cell apoptosis via regulation of mitochondrial dysfunction and autophagy.* Mol Med Rep, 2023. **27**(2).
255. Petherick, K.J., et al., *Pharmacological inhibition of ULK1 kinase blocks mammalian target of rapamycin (mTOR)-dependent autophagy.* J Biol Chem, 2015. **290**(18): p. 11376-83.
256. Mauvezin, C. and T.P. Neufeld, *Bafilomycin A1 disrupts autophagic flux by inhibiting both V-ATPase-dependent acidification and Ca-P60A/SERCA-dependent autophagosome-lysosome fusion.* Autophagy, 2015. **11**(8): p. 1437-8.
257. Iredale, J.P., *Models of liver fibrosis: exploring the dynamic nature of inflammation and repair in a solid organ.* The Journal of clinical investigation, 2007. **117**(3): p. 539-548.
258. Eslam, M. and J. George, *Genetic insights for drug development in NAFLD.* Trends in pharmacological sciences, 2019. **40**(7): p. 506-516.
259. Kato, M. and R. Natarajan, *Epigenetics and epigenomics in diabetic kidney disease and metabolic memory.* Nature Reviews Nephrology, 2019. **15**(6): p. 327-345.
260. Koo, J.H., et al., *Endoplasmic reticulum stress in hepatic stellate cells promotes liver fibrosis via PERK-mediated degradation of HNRNPA1 and up-regulation of SMAD2.* Gastroenterology, 2016. **150**(1): p. 181-193. e8.
261. Kim, K.M., et al., *Gα12 overexpression induced by miR-16 dysregulation contributes to liver fibrosis by promoting autophagy in hepatic stellate cells.* Journal of hepatology, 2018. **68**(3): p. 493-504.